260
Topics in Current Chemistry

Topics in Current Chemistry

Recently Published and Forthcoming Volumes

Molecular Machines
Volume Editor: Kelly, T. R.
Vol. 262, 2006

Immobilisation of DNA on Chips II
Volume Editor: Wittmann, C.
Vol. 261, 2005

Immobilisation of DNA on Chips I
Volume Editor: Wittmann, C.
Vol. 260, 2005

Prebiotic Chemistry
From Simple Amphiphiles to Protocell Models
Volume Editor: Walde, P.
Vol. 259, 2005

Supramolecular Dye Chemistry
Volume Editor: Würthner, F.
Vol. 258, 2005

Molecular Wires
From Design to Properties
Volume Editor: De Cola, L.
Vol. 257, 2005

Low Molecular Mass Gelators
Design, Self-Assembly, Function
Volume Editor: Fages, F.
Vol. 256, 2005

Anion Sensing
Volume Editor: Stibor, I.
Vol. 255, 2005

Organic Solid State Reactions
Volume Editor: Toda, F.
Vol. 254, 2005

DNA Binders and Related Subjects
Volume Editors:Waring, M. J., Chaires, J. B.
Vol. 253, 2005

Contrast Agents III
Volume Editor: Krause,W.
Vol. 252, 2005

Chalcogenocarboxylic Acid Derivatives
Volume Editor: Kato, S.
Vol. 251, 2005

New Aspects in Phosphorus Chemistry V
Volume Editor: Majoral, J.-P.
Vol. 250, 2005

Templates in Chemistry II
Volume Editors: Schalley, C. A.,Vögtle, F., Dötz, K. H.
Vol. 249, 2005

Templates in Chemistry I
Volume Editors: Schalley, C. A.,Vögtle, F., Dötz, K. H.
Vol. 248, 2004

Collagen
Volume Editors: Brinckmann, J., Notbohm, H., Müller, P. K.
Vol. 247, 2005

New Techniques in Solid-State NMR
Volume Editor: Klinowski, J.
Vol. 246, 2005

Functional Molecular Nanostructures
Volume Editor: Schlüter, A. D.
Vol. 245, 2005

Natural Product Synthesis II
Volume Editor: Mulzer, J.
Vol. 244, 2005

Natural Product Synthesis I
Volume Editor: Mulzer, J.
Vol. 243, 2005

Immobilisation of DNA on Chips I

Volume Editor: Christine Wittmann

With contributions by

S. Alegret · I. J. Bruce · A. del Campo · A. Guiseppi-Elie
T. Kawasaki · L. Lingerfelt · F. Luderer · Y. Okahata · D. V. Nicolau
M. I. Pividori · P. D. Sawant · U. Walschus

Springer

The series *Topics in Current Chemistry* presents critical reviews of the present and future trends in polymer and biopolymer science including chemistry, physical chemistry, physics and material science. It is adressed to all scientists at universities and in industry who wish to keep abreast of advances in the topics covered.
As a rule, contributions are specially commissioned. The editors and publishers will, however, always be pleased to receive suggestions and supplementary information. Papers are accepted for *Topics in Current Chemistry* in English.
In references *Topics in Current Chemistry* is abbreviated *Top Curr Chem* and is cited as a journal.

Springer WWW home page: http://www.springeronline.com
Visit the TCC content at http://www.springerlink.com/

ISSN 0340-1022
ISBN-10 3-540-28437-0 Springer Berlin Heidelberg New York
ISBN-13 978-3-540-28437-6 Springer Berlin Heidelberg New York
DOI 10.1007/b105173

Springer is a part of Springer Science+Business Media

springeronline.com

Printed in Germany

Cover design: *Design & Production* GmbH, Heidelberg
Typesetting and Production: LE-TEX Jelonek, Schmidt & Vöckler GbR, Leipzig

Printed on acid-free paper 02/3141 YL – 5 4 3 2 1 0

Volume Editor

Prof. Dr. Christine Wittmann

FH Neubrandenburg
Fachbereich Technologie
Brodaer Straße 2
17033 Neubrandenburg, Germany
wittmann@fh-nb.de

Editorial Board

Topics in Current Chemistry
Also Available Electronically

For all customers who have a standing order to Topics in Current Chemistry, we offer the electronic version via SpringerLink free of charge. Please contact your librarian who can receive a password or free access to the full articles by registering at:

springerlink.com

If you do not have a subscription, you can still view the tables of contents of the volumes and the abstract of each article by going to the SpringerLink Homepage, clicking on "Browse by Online Libraries", then "Chemical Sciences", and finally choose Topics in Current Chemistry.

You will find information about the

- Editorial Board
- Aims and Scope
- Instructions for Authors
- Sample Contribution

at springeronline.com using the search function.

Preface

DNA chips are gaining increasing importance in different fields ranging from medicine to analytical chemistry with applications in the latter in food safety and food quality issues as well as in environmental protection. In the medical field, DNA chips are frequently used in arrays for gene expression studies (e.g. to identify diseased cells due to over- or under-expression of certain genes, to follow the response of drug treatments, or to grade cancers), for genotyping of individuals, for the detection of single nucleotide polymorphisms, point mutations, and short tandem reports, or moreover for genome and transcriptome analyses in the quasi post-genomic sequencing era. Furthermore, due to some unique properties of DNA molecules, self-assembled layers of DNA are promising candidates in the field of molecular electronics.

One crucial and hence central step in the design, fabrication and operation of DNA chips, DNA microarrays, genosensors and further DNA-based systems described here (e.g. nanometer-sized DNA crafted beads in microfluidic networks) is the immobilization of DNA on different solid supports. Therefore, the main focus of these two volumes is on the immobilization chemistry, considering the various aspects of the immobilization process itself, since different types of nucleic acids, support materials, surface activation chemistries and patterning tools are of key concern.

Immobilization techniques described so far include two main strategies: (1) The direct on-surface synthesis of DNA via photolithography or ink-jet methods by photoactivatable chemistries or standard phosphoramidite chemistries, and (2) The immobilization or automated deposition of prefabricated DNA onto chemically activated surfaces. In applying these two main strategies, different types of nucleic acids or their analogues have to be selected for immobilization depending on the final purpose. In several chapters immobilization regimes are described for different types of nucleic acid probes as, e.g. complementary DNA, oligonucleotides and peptide nucleic acids, with one chapter focussing on nucleic acids modified for special purposes (e.g. aptamers, catalytic nucleic acids or nucleozymes, native protein binding sequences, and nanoscale scaffolds). The quality of DNA arrays is highly dependent on the support material and in subsequence on its surface chemistry as the manifold surface types employed also dictate, in most cases, the appropriate detection method (i.e. optical or electrochemical detection with both

principles being discussed in some of the chapters). Solid supports reported as transducing materials for electrochemical analytical devices focus on conducting metal substrates (e.g. platinum, gold, indium-tin oxide, copper solid amalgam, and mercury) but as described in some chapters engineered carbons as graphite, glassy carbon, carbon-film and more recently carbon nanotubes have also been successfully used. The majority of DNA-based microdevices employing optical detection principles is manufactured from glass or silica as support materials. Further surface types used and described in several chapters are oxidized silicon, polymers, and hydrogels. To study DNA immobilized on surfaces, to characterize the immobilized DNA layers, and finally to decide for a suitable surface and coupling chemistry advanced microscopy techniques are required. As a representative example, atomic force microscopy (AFM) was chosen and its versatility discussed in the respective chapter. In some chapters there is also a brief overview given about the different techniques used to pattern (e.g. photolithographic techniques, ink-jetting, printing, dip-pen nanolithography and nanografting) the solid support surface for DNA array fabrication.

However, the focus of the major part of the chapters lies on the coupling chemistry used for DNA immobilization. Successful immobilization techniques for DNA appear to either involve a multi-site attachment of DNA (preferentially by electrochemical and/or physical adsorption) or a single-point attachment of DNA (mainly by surface activation and covalent immobilization or (strept)avidin-biotin linkage). Immobilization methods described here comprise physical or electrochemical adsorption, cross-linking or entrapment in polymeric films, (strept)avidin-biotin complexation, a surface activation via self-assembled monolayers using thiol linker chemistry or silanization procedures, and finally covalent coupling strategies.

Physical or electrochemical adsorption uses non-covalent forces to affix the nucleic acid to the solid support and represents a relatively simple mechanism for attachment that is easy to automate. Adsorption was favoured and described in some chapters as suitable immobilization technique when multisite attachment of DNA is needed to exploit the intrinsic DNA oxidation signal in hybridization reactions. Dendrimers such as polyamidoamine with a high density of terminal amino groups have been reported to increase the surface coverage of physically adsorbed DNA to the surface. Furthermore, electrochemical adsorption is described as a useful immobilization strategy for electrochemical genosensor fabrication.

Another coupling method, i.e. cross-linking or entrapment in polymeric films, which has been used to create a more permanent nucleic acid surface, is described in some chapters (e.g. conductive electroactive polymers for DNA immobilization and self-assembly DNA-conjugated polymers). One chapter reviews the basic characteristics of the biotin-(strept)avidin system laying the emphasis on nucleic acids applications. The biotin-(strept)avidin system can be also used for rapid prototyping to test a large number of protocols and

molecules, which is one major advantage. In some chapters the use of thiol linkers and silanization as two methods of surface preparation or activation strategy is compared and discussed. In the case of the thiol linker the nucleic acid can be constructed with a thiol group that can be used to directly complex to gold surfaces. In the case of silanization many organosilanes have been used to create functionalized surfaces on glasses, silicas, optical fibres, silicon and metal oxides. The silanes hydrolyze onto the surface to form a robust siloxane bond with surface silanols, and also crosslink themselves to further increase adhesion. Silanized surfaces, i.e. surfaces modified with some type of adhesion agent, can be used for covalent coupling processes in a next step. An overview of coupling strategies leading to covalent and therefore stable bonds is indicated in more than one chapter as it is desirable to fix the nucleic acid covalently to the surface by a linker attached to one of the ends of the nucleic acid chain. By doing so, the nucleic acid probe should remain quite free to change its conformation in a way that hybridization can take place, yet in such a way that the covalently coupled probe cannot be displaced from the solid support. There is a large variety of potential reagents and methods for covalent coupling with one of the earliest attempts being based on attaching the 3′-hydroxyl or phosphate group of the DNA molecule to different kinds of modified celluloses.

To give the reader an idea of the practical effort of the immobilization strategies discussed, applications of these DNA chips are also included, e.g. with one chapter describing the immobilization step included in a "short oligonucleotide ligation assay on DNA chip" (SOLAC) to identify mutations in a gene of *Mycobacterium tuberculosis* in clinic isolates indicating rifampin resistance.

Neubrandenburg, August 2005 Christine Wittmann

Contents

Contents of Volume 261

Immobilisation of DNA on Chips II

Volume Editor: Christine Wittmann
ISBN: 3-540-28436-2

Top Curr Chem (2005) 260: 1–36
DOI 10.1007/b136064

Published online: 6 September 2005

DNA Adsorption on Carbonaceous Materials

María Isabel Pividori (✉) · Salvador Alegret

Grup de Sensors i Biosensors, Departament de Química,
Universitat Autónoma de Barcelona, Barcelona, Spain
Isabel.Pividori@uab.es

Abstract The immobilization of DNA on different solid supports has become an important issue in different fields ranging from medicine to analytical chemistry and, more recently, molecular electronics. Among the different immobilization procedures, adsorption is the simplest and the easiest to automate, avoiding the use of procedures based on previous activation/modification of the substrate and subsequent immobilization, which are tedious, expensive and time-consuming. Carbon-based materials are widely used for this task due to their electrochemical, physical and mechanical properties, their commercial availability, and their compatibility with modern microchip fabrication technology.

Moreover, carbonaceous materials are widely used as transducers for electrochemical sensors. The knowledge of the adsorbed DNA morphology on carbon surfaces can be used to develop stable and functional DNA layers for their use in DNA analytical devices with improved properties.

Presented here is a concise description of surface immobilization of DNA, oligonucleotides, and DNA derivatives by adsorption onto carbonaceous materials, and the properties of the DNA layer adsorbed on carbonaceous solid phase.

Keywords DNA · Adsorption · Materials · Graphite · Carbon · Composite · Nanotube · Electrochemical sensing

Abbreviations

A	Adenine
ABS	Acetate buffer solution
AFM	Atomic force microscopy
BDD	Boron-doped diamond
BLM	Bilayer lipid membrane
C	Cytosine
CNT	Carbon nanotube
CNTP	Carbon nanotube paste
CP	Carbon paste
dsDNA	Double-stranded DNA or native DNA
G	Guanine
GC	Glassy carbon
$GC_{(ox)}$	Anodized glassy carbon
GEC	Graphite epoxy composite
HOPG	Highly ordered pyrolytic graphite
MWCNT	Multi-wall carbon nanotube
ODN	Oligodeoxynucleotide
PBS	Phosphate buffer solution
PG	Pyrolytic graphite
SCE	Saturated calomel electrode
ssDNA	Single-stranded DNA or denatured DNA
SWCNT	Single-wall carbon nanotube
T	Thymine

1 Introduction

The growing demand for genetic information in an increasingly broad range of disciplines has led to research into the development of new techniques for genetic analysis. The Human Genome Project (HGP) [1] has stimulated the development of analytical methods that yield genetic information quickly and reliably. Examples of this development are the DNA chips [2–4] and lab-on-a-chips based on micro fluidic techniques [5]. Additionally, the knowledge

obtained from the HGP has expanded the market that requires genetic devices, hence generating new applications. However, this expanding market would obviously benefit from simple, cheap and easy to use analytical devices, especially for industrial applications.

Therefore, the development of new methodologies possessing the convenience of solid-phase reaction, along with advantages of rapid response, sensitivity and ease of multiplexing is now a challenge in the development of new biochemical diagnostic tools. Electrochemical biosensors and chips can meet these demands, offering considerable promise for obtaining sequence-specific information in a faster, simpler and cheaper manner than traditional hybridization assays. Such devices possess great potential for numerous applications, ranging from decentralized clinical testing, to environmental monitoring, food safety and forensic investigations.

The use of nucleic acids recognition layers is a new and exciting area in analytical chemistry which requires extensive research.

To prepare electroanalytical devices based on DNA, the immobilization of the biological species must be carefully considered. The most successful immobilization techniques for DNA appear to be those involving multi-site attachment (either electrochemical or physical adsorption) or single-point attachment (mainly covalent immobilization or strept(avidin)/biotin linkage) [6]. Single-point attachment is beneficial to hybridization kinetics, especially if a spacer arm is used. However, among the different DNA immobilization procedures reported, multi-site adsorption is the simplest and most easily automated technique, avoiding the use of pre-treatment procedures based on previous activation/modification of the surface transducer and subsequent DNA immobilization. Such pre-treatment steps are known to be tedious, expensive and time-consuming. Furthermore, the adsorption properties of DNA on various supports (e.g., nylon, nitrocellulose) have been known for a long time [7].

Electrochemical detection of successful DNA hybridization events should be also considered. Although it is based mostly on external electrochemical markers, such as electroactive indicators or enzymes, the exploitation of the intrinsic DNA oxidation signal requires a multi-site attachment such as adsorption as the immobilization technique.

The direct electrochemical detection of DNA was initially proposed by Paleček [8, 9], who recognized the capability of both DNA and RNA to yield reduction and oxidation signals after being adsorbed. The DNA oxidation was shown to be strongly dependent on the DNA adsorption on the substrate; it requires meticulous control of the DNA-adsorbed layer.

While immobilization and detection are important features, the choice of a suitable electrochemical substrate is also of great significance in determining the overall performance of the analytical electrochemical-based device, especially regarding the immobilization efficiency of DNA.

The development of new transducing materials for DNA analysis is a key issue in the current research efforts in electrochemical-based DNA analytical devices. The use of platinum, gold, indium–tin oxide, copper solid amalgam, mercury and other continuous conducting metal substrates has been reported [6]. However, this chapter is focused on carbon-based materials and their properties for immobilizing DNA by simple adsorption procedures.

2 Carbonaceous Materials

The extraordinary ability of carbon to combine with itself and other chemical elements in different ways is the basis of organic chemistry. As a consequence, there is a rich diversity of structural forms of solid carbon because it can exist as any of several allotropes. It is found abundantly in nature as coal, as natural graphite and also in much less abundant form as diamond.

Engineered carbons [10] are the product of the carbonization process of a carbon-containing material, conducted in an oxygen-free atmosphere. Depending on the starting precursor material (hydrocarbon gases, petroleum-derived products, coals, polymers, biomass), the product of a carbonization process will have different properties, including the adsorption capability. Traditional engineered carbons can take many forms, such as coke, graphite, carbon and graphite fiber, carbon monoliths, glassy carbon (GC), carbon black, carbon film, and diamond-like film [10]. More recently, a promising new carbon-based material—carbon nanotubes—has been developed using the vapor deposition technique.

Engineered carbons have found intensive use as adsorbents because of their porous and highly developed internal surface areas as well as their complex chemical structures.

As with the majority of organic molecules, DNA can be easily adsorbed on carbon-based material. Adsorption processes can be driven in both liquid and gaseous media by physical forces. The porous structure and the chemical nature of the carbon surface are significantly related to its crystalline constitution. The crystal structure of graphite consists of parallel layers of condensed, regular hexagonal rings. The in-plane C – C distance is intermediate between the Csp^3–Csp^3 and the Csp^2 = Csp^2 bond lengths (Fig. 1).

The pore structure and surface area of carbon-based materials determine their physical characteristics, while the surface chemical structure affects interactions with polar and nonpolar molecules due to the presence of chemically reactive functional groups. Active sites—edges, dislocations, and discontinuities—determine the reactivity of the carbon surface. As shown in Fig. 1, graphitic materials have at least two distinct types of surface sites, namely, the basal-plane and edge-plane sites [11]. It is generally considered

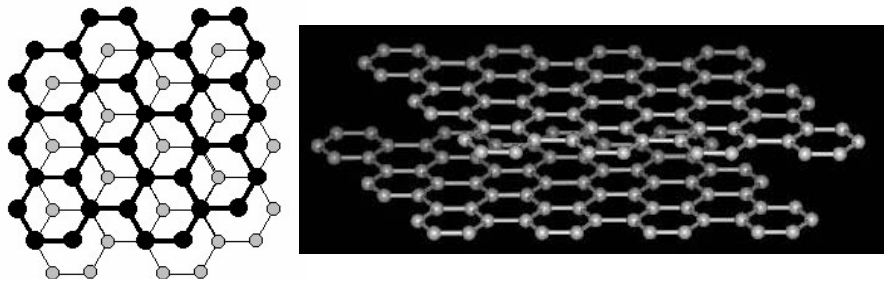

Fig. 1 Positional relationship between two identical graphene planes. Graphite structure can be described as an alternate succession of these basal planes. The *right panel* was taken from the image gallery of Prof. R. Smalley (to be found at http://smalley.rice.edu/ and reprinted with his kind permission

that the active sites for electrochemical reactions are associated with the edge-plane sites, while the basal plane is mostly inactive.

Heteroatoms (usually oxygen) play an important role in the chemical nature of the carbon "active" surface [10]. The adsorption process is thus strongly dependent on the type, quantity, and bonding of these functional groups in the structure. Heteroatoms distributed randomly in the core of the carbon matrix may be non-reactive due to their inaccessibility. However, the heteroatoms can be also concentrated at the exposed surface of carbons or presented as an "active" dislocation of the microcrystalline structure. Much of the research being carried out is focused on the identification and characterization of oxygen-containing functional groups in oxidized carbon surfaces, such as carboxyl, phenolic, quinonic, and lactones, but also in the changes that take place in the carbon surface under different oxidation treatments.

The electrochemical oxidation pretreatment was found to improve the electrochemical behavior by introducing more active edge sites on the treated carbon surface. The effect of oxidation on the chemical composition is related to the increased concentration of strong and weak acidic groups found upon electrochemical oxidation of the graphite surface [12]. The acidity of carboxylic groups on the oxidized carbon surface could be stronger than that of a carboxylic resin. The weight increase after electrochemical pretreatment was attributed to the formation of the oxidized graphite and the intercalation of solvent molecules and anions into graphitic material. A model of a fragment of oxidized carbon surface illustrating the general chemical character of the oxidized carbon surface is shown in Fig. 2.

Among the different carbonaceous materials, GC and pyrolytic graphite (PG) and the graphite-powder-based composites such as carbon paste (CP) are the most popular choices as electrochemical transducer materials.

GC is made by heating a high molecular weight carbonaceous polymer to 600–800 °C. Most of the non-carbon elements are volatilized, but the backbone is not degraded. Regions of hexagonal sp^2 carbon are formed during

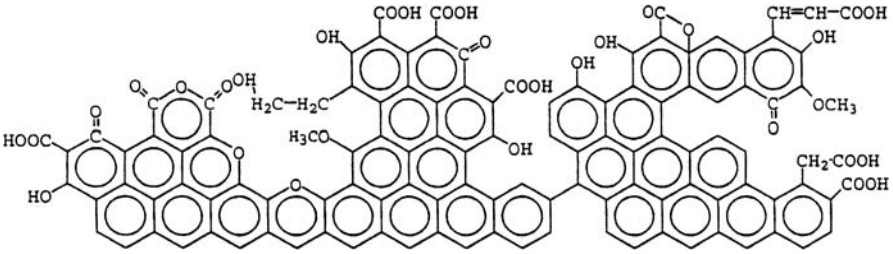

Fig. 2 Hypothetical fragment of an oxidized carbon surface. The figure was taken from [10] with kind permission from Prof. M. Streat

this treatment, but they are unable to form extensive graphitic domains without breaking the original polymer chain. GC is impermeable to liquid, so porosity is not an issue [13]. Pretreated GC has been obtained by (1) polishing and/or ultrasonication, (2) chemical oxidation or (3) electrochemical anodization treatments [14]. These surface treatments have been extensively used to improve the electrochemical performance of GC [15]. Suggested reasons for activation have been the removal of contaminants from the surface, and the increase in the surface area due to the roughening of the surface or the exposure of fresh carbon edges, microparticles and defects that may be sites for electron transfer. On the other hand, the increase in surface functional groups that may act as electron transfer mediators could play a role. While some of these factors are related to improvements in the electrochemical performance, others are related to both electrochemical and physical features. As an example, the increment in the surface roughness can cause enhancement of the heterogeneous electron transfer rates as the effective area for electron transfer is greater than the geometric area, but can also improve the physisorption of a given molecule. GC is well known for the exhibition of a wide range of functional groups, including carboxylic acids, quinones/hydroquinone, phenols, peroxides, aldehydes, ethers, esters, ketones, and alcohols, which could interact differently with DNA molecules stabilizing the adsorbed molecule, but may also improve the electron transfer, acting as mediators. The activation method most commonly used relies on the electrochemical activation to obtain anodized GC ($GC_{(ox)}$). It was found that the dominant process during electrochemical activation of the GC surface is the formation of a near-transparent homogeneous different phase [15]. The layer was shown to be porous, hydrated and nonconductive, containing a significant amount of microcrystallinity and graphite oxide. Once the film is grown, the surface becomes richer in oxygenated groups that make it more hydrophilic. It is observed that the anodization of the GC induces adsorption: despite the nonconductive nature of graphite oxide, it intercalates aromatic molecules quite well. Only the portion immediately adjacent to the GC substrate seems to be electronically connected to the substrate. The outer

nonelectroactive portion of the layer concentrates the redox species near to the electroactive surface.

PG is made by the pyrolysis of light hydrocarbons onto a hot (800 °C) stage, often followed by heat treatment to higher temperatures. Highly-oriented PG (HOPG) is made from PG by pressure annealing in a hot press at 3000 °C and several kilobars. HOPG has a smooth, shiny basal surface, while PG is mottled and dull [13]. The dominant structural property of PG and HOPG is the long-range order of the graphitic layers (Fig. 1) and the remarkable anisotropy and hydrophobic behavior. HOPG is single-crystal graphite with edge planes and cleavage surfaces (basal plane) that serve as the oriented surface for electrochemical studies. An important advantage of HOPG with respect to other carbonaceous materials is the possibility of performing studies by means of high resolution techniques—even down to the atomic level—by scanning probe microscopy, such as atomic force microscopy (AFM). The rough and complex surface of GC is not suitable for AFM surface characterization. For AFM studies, an atomically flat substrate is required to clearly resolve the molecular adsorbed layer. GC presents a root-mean-square (rms) roughness of 2.10 nm while HOPG surface presents a rms roughness of less than 0.06 nm (both calculated from AFM images in air) [16]. This fact has stimulated the use of HOPG instead of other carbonaceous materials such as GC or CP [17].

Carbon composites result from the combination of carbon with one or more dissimilar materials. Each individual component maintains its original characteristics while giving the composite distinctive chemical, mechanical and physical properties. The capability of integrating various materials is one of their main advantages. Some components incorporated within the composite result in enhanced sensitivity and selectivity. The best composite compounds will give the resulting material improved chemical, physical and mechanical properties. As such, it is possible to choose between different binders and polymeric matrices in order to obtain a better signal-to-noise ratio, a lower nonspecific adsorption, and improved electrochemical properties (electron transfer rate and electrocatalytic behavior).

Powdered carbon is frequently used as the conductive phase in composite electrodes due to its high chemical inertness, wide range of working potentials, low electrical resistance and a crystal structure responsible for low residual currents. A key property of polycrystalline graphite is porosity. Most polycrystalline graphite—such as powdered carbon—is made by heat treatment of high molecular weight petroleum fractions at high temperatures to perform graphitization. The term "graphite" is used to designate materials that have been subjected to high temperatures, and thus have aligned the sp^2 planes parallel to each other.

Regarding their mechanical properties carbon composites can thus be classified as rigid composites [18, 19] or soft composites—the carbon pastes – [20]. The composites are also classified by the arrangement of their

particles, which can be either dispersed or grouped randomly in clearly defined conducting zones within the insulating zones.

The inherent electrical properties of the composite depend on the nature of each of the components, their relative quantities and their distribution. The electrical resistance is determined by the connectivity of the conducting particles inside the nonconducting matrix, and therefore the relative amount of each composite component has to be assessed to achieve optimal composition. Carbon composites show improved electrochemical performances, similar to an array of carbon fibers separated by an insulating matrix and connected in parallel. The signal produced by this macroelectrode formed by a carbon fiber ensemble is the sum of the signals of the individual microelectrodes. Composite electrodes thus showed a higher signal-to-noise (S/N) ratio than the corresponding pure conductors, accompanied by an improved (lower) detection limit.

Rigid composites are obtained by mixing graphite powder with a nonconducting polymeric matrix, obtaining a soft paste that becomes rigid after a curing step [18, 19]. They could be classified according to the nature of the binder or the polymeric matrix, in epoxy composites, methacrylate composites, or silicone composites. Graphite–epoxy composite (GEC) has been extensively used in our laboratories showing to be suitable for electrochemical sensing due to its unique physical, and electrochemical properties.

Soft composites or CPs are the result of mixing an inert conductor (e.g., graphite powder) with an insulating compound (e.g., paraffin oil, silicone, Nujol, mineral oil) [20]. The insulating liquid has a specific viscosity and the paste has a certain consistency. The resulting material is easy to prepare and inexpensive. Compared with other solid materials, CP electrodes have shown some advantages, including wide potential window and low background current. However, these pastes have limited mechanical and physical stabilities, especially in flow systems. Additionally, the pastes are dissolved by some nonpolar solvents.

Fullerenes (C_{60}) (Fig. 3) have a structure similar to that of truncated icosahedron, made out of five- and six-member rings of sp^2 carbons. Higher fullerenes are also made of five- and six-member carbon rings.

In late 1991, the first synthesis and characterization of carbon nanotubes (CNTs) was reported [21]. CNTs are attractive carbonaceous materials with well defined nanoscale geometry. They have a closed topology and tubular structure that are typically several nanometers in diameter and many micrometers in length. CNTs are produced as single-wall Carbon Nanotubes (SWCNTs) and multi-wall carbon nanotubes (MWCNTs). SWCNTs are made out of a single graphite sheet rolled seamlessly with 1–2 nm in tube diameter (Fig. 3). MWCNTs are composed of coaxial tubules, each formed with a rolled graphite sheet, with diameters ranging from 2 to 50 nm. The concentric single-walled cylinders are held together by relatively weak Van der Waals forces with an interlayer spacing of 0.34 nm (Fig. 3). CNTs aggregate

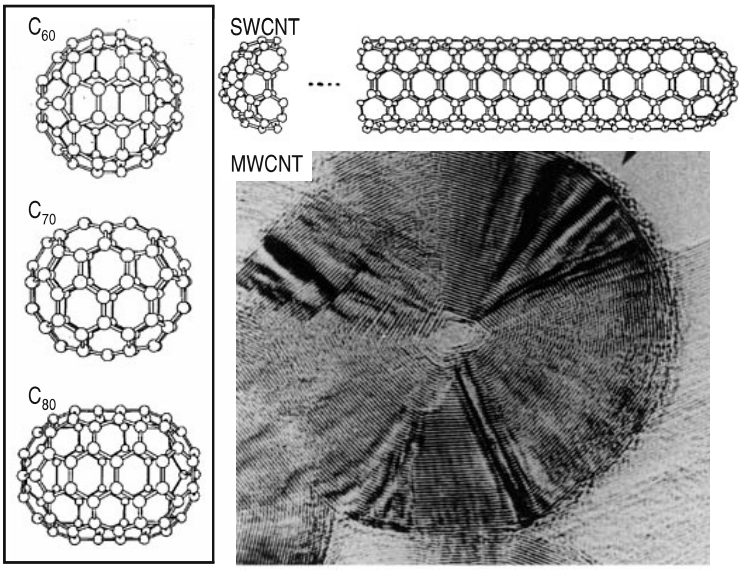

Fig. 3 Structure of fullerenes C_{60}, C_{70}, C_{80} and single-wall carbon nanotube. The figures were taken with permission of Prof. C. Dekker from the image gallery found at http://online.itp.ucsb.edu/online/qhall_c98/dekker/. Transmission electron microscopy image of multi-wall carbon nanotube (*MWCNT*) treated with iodinated and platinate DNA. The figure was taken from [24] with kind permission from Prof. P. Sadler

easily, forming bundles of tens to hundreds of nanotubes in parallel and in contact with each other [22]. CNTs can be grown by the arc discharge method or laser ablation of a graphite rod, as well as by chemical vapor deposition (CVD) [23].

Changes in the winding angle of the hexagonal carbon lattice along the tube (i.e., the chirality) would have a strong effect on the conductive property, resulting in either semiconducting or metallic behavior [23] of CNTs. Mechanically, the CNT is stronger than steel, but lighter. Thermally, it is more conductive than most crystals. Chemically, it is inert everywhere along its length except at the ends or at the site of a bend or kink [24, 25]. It has been shown that while amorphous carbon can be attacked from any direction, CNTs can be oxidized only from the ends. When treated with concentrated oxidizing acid, the ends and surfaces of carbon nanotubes become covered with oxygen-containing groups such as carboxyl groups and ether groups [26]. As graphite is considered to be hydrophobic, CNTs—which correspond to hollow cylinders of rolled-up graphene—and fullerenes are found to have a low solubility in water. The presence of hydrophilic groups (e.g., – OH and – COOH) in the interior of the CNT could play an important role in its properties [26, 27]. Isolated SWCNTs are insoluble in most solvents unless a surfactant is used or chemical modifications to the tubes are carried out.

Such insolubility and the strong Van der Waals attraction between tubes cause them to bundle together as ropes.

Compared with SWCNTs, the much cheaper MWCNTs produced by the CVD method are known to have more defects and can provide more sites for the immobilization of DNA.

CNTs present a larger surface area and outstanding charge-transport characteristics and might therefore greatly promote electron transfer reactions which can dramatically improve electrochemical performance compared to that of other carbonaceous materials [26]. The open end of a MWCNT is expected to show a fast electron transfer rate similar to the graphite edge-plane electrode while the sidewall is inert like the graphite basal-plane (Figs. 1 and 3). Fast electron transfer rate is demonstrated along the tube axis [28]. CNTs are expected to present a wide electrochemical window, flexible surface chemistry, and biocompatibility, similar to other widely used carbon materials [28].

The next section will be focused on the description of the most important features related to DNA adsorption strategies that have found applications in DNA electrochemical analysis.

3
DNA Adsorption Strategies

3.1
Nucleic Acid Structure and Adsorption Properties

Adsorption is an easy way to attach nucleic acids to surfaces, since no reagents or modified DNA are required. Adsorption is a complex interplay between the chemical properties, structure and porosity of the substrate surface with the molecule being adsorbed. Regarding the solid support, the roughness, the size of pores, the uniformity and the permeability, the chemical nature, surface polarity and the presence of chemically reactive functional groups should all be considered. In the case of carbon-based materials, these parameters vary dramatically depending on the nature and the source of carbon: graphite powder composites, graphite leads, PG, GC, CNTs.

The main parameters affecting the adsorption process of a given molecule in solution involve its size, shape, polarity, and chemical structure.

DNA is a structurally polymorphic macromolecule which, depending on nucleotide sequence and environmental conditions, can adopt a variety of conformations. The double helical structure of DNA (dsDNA) consists of two strands, each of them on the outside of the double helix and formed by alternating phosphate and pentose groups in which phosphodiester bridges provide the covalent continuity. The two chains of the double helix are held

together by hydrogen bonds between purine and pyrimidine bases. The sugar–phosphate backbone is responsible for the polyanionic characteristic of DNA. In the double helix structure, the bases exist in a highly hydrophobic environment inside the helix, while the outer, negatively charged backbone allows the dsDNA molecule to interact freely with the hydrophilic environment. The dsDNA is considered a highly hydrophilic molecule. As a negatively charged molecule, it can be easily stabilized on positively charged substrates. While dsDNA only partially shows its hydrophobic domain through its major and minor grooves or through those sites where dsDNA is open and exposing DNA bases, ssDNA has the hydrophobic bases freely available for interactions with hydrophobic surfaces. As such, ssDNA is dual in nature, the highly hydrophilic backbone and the hydrophobic DNA moieties coexisting in the same molecule. These structural and chemical differences between ss and dsDNA are reflected in different adsorption patterns for both molecules. The greater size and the more rigid shape of dsDNA with respect to ssDNA are other parameters affecting the adsorption. Another important compound that should be considered for the adsorption of DNA is its oxidation product 8-oxoguanine that can arise from DNA through the direct attack of reactive oxygen species on chromatin [29]. It is directly associated with promutagenic events and other cellular disorders both in vivo and in vitro. The formation of 8-oxoguanine in the DNA moiety, considered the most commonly measured product of DNA oxidation, causes important mutagenic lesions. In the DNA double helix this adduct pairs more easily with adenine (A) than with cytosine (C). This could lead to the substitution of C in the complementary chain by A, which in turn leads to the substitution of the original guanine (G) by thymine (T) initiating a cellular dysfunction. PNA is an analogue of DNA in which the entire negatively charged sugar–phosphate backbone is replaced with a neutral "peptide-like" backbone consisting of repeated N-(2-aminoethyl)glycine units linked by amide bonds [30]. The four natural nucleobases (i.e., A, C, G, and T) come off the backbone at equal spacing to the DNA bases. Such a structure is not prone to degradation by nucleases or proteases, thus offering high biological stability. The unique chemical properties of the neutral PNA molecule have been extensively studied and compared with the negatively charged DNA counterpart.

Beside the DNA molecule and the carbon substrate, the solvent, normally water, and in particular the ionic strength, pH and the nature of the solutes, play an important role in the adsorption process, mainly in the stabilization of the adsorbed molecule on the substrate.

DNA adsorption properties were first studied using a variety of solid supports for classical analysis methods including Southern and Northern transfers, dot-blotting, colony hybridization and plaque-lifts [31, 32]. Studies of the interactions between nucleic acids and nitrocellulose revealed that molecular weight, finite macromolecular conformation, ionic forces and weaker forces of attraction all play a role. DNA is retained on nitrocellulose only in

buffers of high ionic strength. This may be because increasing salt concentration correlates with decreasing electrostatic repulsion between the phosphate groups of the DNA backbone, yielding more aggregated DNA molecules that are more easily retained on the filter. Nylon membranes are able to bind both native and denatured nucleic acids in buffers of low ionic strength [33]. Positively charged nylon membranes provide an ionic interaction between the negatively charged phosphate groups of the nucleic acid and the positively charged groups of the membrane. Although nylon and nitrocellulose are the most commonly used solid supports in DNA classical analysis, studies of the interaction between DNA and other surfaces such as polystyrenes (microwells, beads), glass, dextran, latex and magnetic beads have also been reported.

Although DNA has been widely attached onto carbonaceous materials, the underlying mechanism of adsorption has not been fully clarified. The next section focuses on the different strategies for the adsorption of nucleic acid (ssDNA, dsDNA, ODN and DNA bases) on carbon-based material.

3.2 DNA Adsorption Methods

The unique practical properties of adsorption have promoted its extensive use in genetic analysis. The disadvantages of adsorption with respect to covalent immobilization are mainly that (1) nucleic acids may be readily desorbed from the substrate, and (2) base moieties may be unavailable for hybridization if they are bonded to the substrate in multiple sites [34]. However, the electrochemical detection strategy based on the intrinsic oxidation of DNA requires the DNA to be adsorbed in close contact with the electrochemical substrate by multi-point attachment. This multi-site attachment of DNA can be thus detrimental for its hybridization but is crucial for the detection based on its oxidation signals.

The common methods for the multi-site adsorption of DNA on carbonaceous-based material can be classified into physical (dry and wet) adsorption and electrostatic adsorption.

Dry adsorption relies on leaving DNA to dry on the carbonaceous surface. Dry adsorption can be assisted by light treatment (except UV, which is able to induce changes in the DNA molecule) or heated until 100 °C. DNA can adopt a variety of conformations depending on the degree of hydration. The most familiar double helix DNA—called "B-DNA"—can turn into the "A-DNA" form if it is strongly dehydrated. A structural alteration occurs due to a greater electrostatic interaction between the phosphate groups, leading to A-DNA. The different structural forms of the double helix promote different dynamic interactions, and the width of the grooves between the strands is important in allowing or preventing access to bases. Both ss- and dsDNA can be adsorbed firmly if it is dried on the carbonaceous surface. When the DNA solution is evaporated to dryness, the bases of DNA which have been dehy-

drated are exposed, and thus the hydrophobic bases are strongly adsorbed flat on the electrode surfaces. Once it is adsorbed, DNA is difficult to re-hydrate. Hence, DNA is not desorbed, no matter how long the adsorbed DNA is soaked in water, characteristic of irreversible adsorption. The "irreversible" behavior of the dry-adsorbed DNA layer has been previously reported [35].

Wet adsorption relies on leaving DNA to interact with the carbonaceous surface through physical forces in the presence of water. During wet adsorption, the stabilization of B-DNA is expected to occur on the carbonaceous surface, by keeping the hydration water of the DNA molecule. As the water is kept on the DNA adsorbed molecule, it can be more easily desorbed from the substrate if soaked in aqueous solutions. The stringency of wet adsorption is related to the use of static or convection conditions. In order to perform DNA adsorption, the convection conditions—which can be achieved by the use of stirring as well as the use of "heated" substrates—prove to be more effective than static conditions. Although a thick or a thin layer of DNA can be attached on the surface during dry adsorption by controlling the concentration of the DNA solution being dried, the wet adsorption normally yields a thin DNA monolayer. During wet adsorption, the substrate is progressively modified with negative charges coming from the DNA being adsorbed, thus repealing the successive DNA molecules that are approaching the substrate. Wet adsorption thus leads to a "self-control" surface coverage and is less stringent than dry adsorption. Depending on the application of the DNA-modified substrate, a thick or thin DNA layer would be necessary. If a stringency control of nonspecific DNA adsorption issues is required, a thick DNA layer is more convenient. However, the yield in hybridization is better on a thin DNA layer.

The electrostatic adsorption can be performed—given the polyanionic nature of DNA molecule—by modifying the ion charge of the carbon substrate by both (1) chemical modification, with polycationic molecules, and (2) by applying a positive potential taking advantages of the conducting properties of the carbon substrate. Both of them are based on the same principle that keeps DNA attached on the widely used, positively modified nylon membranes. The electrostatic adsorption by chemical modification of the substrate is based on the formation of a stable compound between the polycationic molecule that modified the substrate and the polyanionic phosphodiester backbone of DNA, either native or denatured. The potential-driven electrostatic adsorption has been widely used for immobilizing DNA on carbon materials. Taking into account that the DNA bases—A and G—can be oxidized, the applied potentials used to provide the positive charge to the substrate are lower than those producing DNA oxidation. It appears that the adsorption occurs through the negatively charged phosphate backbone, leaving the bases accessible for hybridization reactions in the case of ssDNA and ODNs. There is evidence that the positive potential considerably enhances the robustness and stability of the DNA layers to mechanical stress, through multiple electrostatic interactions between the negatively charged hydrophilic

sugar–phosphate backbone and the positively charged carbon surface. The electrostatic adsorption performed by applying a positive potential is usually driven under stirring conditions in solution (wet adsorption) until full DNA coverage of the substrate is achieved.

The next section will focus on carbonaceous materials that have found applications as transducers for DNA biosensing based on the adsorption of DNA.

4
Adsorption of DNA on Carbon-Based Materials

4.1
Glassy Carbon

Adsorption of dsDNA can be performed on GC surfaces by either dry or electrostatic adsorption procedures yielding a thick or a thin layer of DNA, respectively [36]. The thin layer dsDNA-modified GC electrode was prepared by immersion in a dsDNA solution by applying a potential of + 0.40 V. The resulting DNA layer was non-uniform leaving many bare GC-uncovered regions. The thick layer dsDNA-modified GC electrode was prepared by covering a GC electrode with dsDNA and then transferring it into a solution containing ssDNA for electrochemical conditioning [37]. Briefly, the dsDNA was dry-adsorbed overnight on the GC surface. This led to an almost uniform layer of DNA, 0.1 mm thick when dried, which in aqueous solution swelled to about 1 mm thickness with a gel-like appearance [38]. After drying, the electrode was immersed in ABS and a constant potential of + 1.4 V (vs SCE) was applied for 5 min. It was then transferred to a solution containing ssDNA and differential pulse voltammograms were recorded in the range of 0 to + 1.4 V until stabilization of the peak currents corresponding to A and G electro-oxidation. This procedure produces a thick multilayer of DNA covering the GC surface completely and uniformly with no pinholes or bare GC regions. H-DNA triple helical structure is supposed to occur at the surface of the GC electrode. This thick-layer dsDNA-modified GC electrode allowed the study of DNA interactions and damage by health-hazardous compounds such as metronidazole, mitoxantrone [39], and niclosamide [40] based on their binding properties to nucleic acids. According to the ohmic resistance, there was also evidence that the thick DNA layer on the GC surface is a reasonably good conductor [38]. Additionally, the thick dsDNA layer obtained by dry-adsorption has been demonstrated to be unstable to alkali and to heat, but stable to acid solutions [35, 41]. When the solution containing ds- or ssDNA is evaporated to dryness, dehydrated DNA molecules can be irreversibly adsorbed on the surfaces of GC, which has proved to be very stable for long storage in a dry state [35, 41].

It was also demonstrated that ssDNA is better adsorbed onto the GC electrode than dsDNA. The dsDNA molecule has some difficulty reaching the surface contours of the rough GC electrode surface, while ssDNA can approach closer to the electrode surface because of its greater flexibility.

Although dsDNA can be adsorbed at the GC surface, it is not easily oxidized while ssDNA can be easily adsorbed and oxidized, giving higher oxidation signals, which is attributed to the oxidation of G ($\sim$ 0.8 V) and A ($\sim$ 1.1, vs SCE) respectively [38]. The dsDNA structure had greater difficulty transferring the electrons from the inside of the double-stranded structure to the electrode surface than the flexible ssDNA structure where the bases are in closer proximity to the GC surface.

The electrochemical processes of adsorption and oxidation of ds- and ssDNA on the GC electrode were discussed and studied by in situ FTIR [42]. It was also demonstrated that the well-known oxidation product 8-oxoguanine adsorbs strongly on the GC surface [29]. Adsorbed ssDNA can form a DNA layer which impedes the oxidation product diffusing away, blocking the GC surface [43, 44].

In contrast to the potential dependence observed for the accumulation of ODN at other carbonaceous materials such as CP, both ss- and dsDNA were adsorbed on GC in a broad range of applied potentials (from – 0.60 to + 0.40 V), even when using solutions of different ionic strengths [43, 44]. A slight influence of the GC surface charge was thus observed, indicating that there is a small contribution of the negatively charged phosphate backbone in the adsorption of nucleic acids on the GC surface (especially at high ionic strengths) [44]. Other factors influencing the rate of adsorption of DNA on GC are the size of the ODN, which would produce an easier adsorption of smaller molecules, and the conformation of the nucleic acid in solution prior to the immobilization at the electrode surface [44].

4.1.1 Pretreated Glassy Carbon

The influence of different pretreatment strategies on the adsorption of DNA on the GC surface has been extensively discussed. The sensitivity for ssDNA detection at the GC surface was improved greatly (tenfold) by modifying the electrode surface with an electrochemical oxidation treatment at + 1.75 V (vs SCE) for 300 s in PBS, pH 5.0. The same results were reported when $GC_{(ox)}$ was obtained at (1) 1.60 V (vs SCE) for 15 s in 10% HNO_3 solution with 2.5% $K_2Cr_20_7$, [35] and, (2) 1.20 V (vs Ag/AgCl) in 0.5 M NaOH for 10 min [45].

This improvement was due to an easy adsorption of ss- and dsDNA on the $GC_{(ox)}$ surface [46, 47]. Regarding the nonconductive nature of graphite oxide film formed on the surface during anodization [15], the activation of GC would affect primarily the adsorption process but not the charge transfer of the G and A residues. The ssDNA was preconcentrated on $GC_{(ox)}$ surface

under stirring by means of either its wet-adsorption for 5 min, or its electrostatic adsorption at + 0.3 V (vs SCE) for 90 s. In both cases, the adsorption of DNA on $GC_{(ox)}$ surface are close to the theoretical value of a monolayer. The stirring during the DNA adsorption was critical for enhancing the adsorption while the positive potential was found to accelerate the adsorption process.

Not only was an improvement in the detection for ssDNA at $GC_{(ox)}$ observed, but also for G and A bases [47]. These results suggest that the increased adsorption of DNA on the $GC_{(ox)}$ depends more on the DNA bases than on the phosphate–sugar DNA backbone.

This conclusion is also supported by the fact that, in contrast to ssDNA, the oxidation signal coming from dsDNA is poorly developed at both GC and $GC_{(ox)}$. This is probably attributable to the electroactive A and G residues in dsDNA being inaccessible to the surface, while most bases in denatured DNA can freely interact with the $GC_{(ox)}$ surface. On the other hand, the hydrogen-bonded bases in native DNA are hidden within the double helix, a serious steric barrier to electron transfer between the purine and the $GC_{(ox)}$.

However, when the potential of the pretreatment of the GC exceeded + 1.75 V (vs SCE) or it was driven longer than 300 s in PBS (pH 5.0), the adsorption of ssDNA at the electrode was found to decrease [46], showing that different conditions for obtained $GC_{(ox)}$ were detrimental for the DNA adsorption and oxidation. A similar negative effect was observed when the adsorption of the DNA was performed on polished GC previously exposed to air for a given time [44].

The beneficial effects of the graphite oxide film on the adsorption and oxidation of DNA on $GC_{(ox)}$ seem to be strongly dependent on the thickness of this film, obtained under different conditions (supporting electrolyte, applied voltage, duration of the anodization treatment and pH).

Once the film is grown, the surface becomes richer in oxygenated groups, making it more hydrophilic. It is clear that this increased hydrophilic environment does not favor the adsorption of nucleic acids on GC. The increased adsorption of DNA on the $GC_{(ox)}$ may depend more on the DNA bases than on the phosphate–sugar DNA backbone.

A mixed activation procedure, based on both preanodization and precathodization treatments, respectively, was shown to produce a further 100-fold improvement of the DNA oxidation signal on GC. The electrochemical oxidation was performed at + 1.75 V (vs SCE) for 10 min and cyclic sweep between + 0.3 V and – 1.3 V for 20 cycles in pH 5.0 PBS [48]. The ssDNA was accumulated at the GC surface at an open circuit by wet-adsorption. As previously explained, a dielectric layer is formed on GC during anodic oxidation. Such a graphitic oxide layer possesses insulating properties, is electrochemically inactive and does not contribute to the double-layer capacitance. After the electrode is reduced, the whole layer becomes electrochemically active again, resulting in a significant increase in double-layer capacitance. However, no increase in surface roughness was observed with AFM after being oxidized

and reduced. The oxidation followed by reduction of GC for a very short time produces the C = O functional group on the carbon electrode surface. The adsorptive capacity was thus found to be related to the amount of these surface functional groups and double-layer capacity. The increase in current was not produced by an increased surface area due to porous structure, but by some chemical interaction between the C = O groups and ssDNA. One possible reason for the preferential adsorption of ssDNA on the modified GC could be the positive chemical interaction between the ssDNA and the surface-produced C = O groups. As explained, in ssDNA, all bases can be freely accessible to the electrode surface. Hydrogen bonds can be formed between the more acidic H of nucleic bases in ssDNA and the C = O groups present on the electrode surface [48]. As for dsDNA, the sites that can form hydrogen bonds, have already formed a part of the Watson-Crick hydrogen bonding system, and cannot form hydrogen bonds with the C = O groups on the electrode surface. Therefore, dsDNA cannot accumulate on the modified electrodes as much as ssDNA [48].

4.1.2
Adsorption of DNA Bases on Glassy Carbon

Differential pulse voltammetry and electrochemical impedance have demonstrated that G, A, guanosine, and their oxidation products are electrostatically adsorbed on GC and $GC_{(ox)}$ surfaces [47, 49]. The strength of adsorption of the DNA bases on the GC surface were found to be similar [49]. Strongly adsorbed G dimers were formed on GC between G and the adsorbed G oxidation products, which slowly cover and block the surface. The application of ultrasound led to removal of the adsorbed species. The effect of this was mainly to enhance transport of electroactive species and to clean the electrode in situ, avoiding electrode fouling.

4.1.3
Nature of the Interactions Between Nucleic Acids and Glassy Carbon

To summarize, the adsorption of nucleic acid may involve electrostatic interactions with the negatively charged DNA backbone. However, strong evidence indicates that the adsorption depends mostly on the hydrophobic interactions between the free bases and the surface of GC. The slight influence of the charge of the GC surface during adsorption (especially produced at high ionic strengths) indicates that there is a small contribution of the negatively charged phosphate backbone in the adsorption of nucleic acids on the GC surface. Moreover, the DNA but also DNA bases (without the negatively charged phosphate backbone) are adsorbed on GC in similar conditions. The dsDNA is poorly adsorbed, because its bases are hidden in the interior of the double-helical molecule forming a part of the Watson-Crick hydrogen bond-

ing system. In contrast, ssDNA is highly adsorbed on GC, because its bases are freely accessible for interaction with the surface.

An increased adsorption of ssDNA on GC, (and oxidized/reduced GC) was observed. Taking into account the nature of the film formed on the $GC_{(ox)}$ surface, the higher affinity of ssDNA could be explained by the formation of hydrogen bonds.

4.2
Modified Glassy Carbon

4.2.1
Chemically-Modified Glassy Carbon

An improved adsorption of DNA bases has been observed at a chemically modified electrode based on a Nafion/ruthenium oxide pyrochlore ($Pb_2Ru_{2-x}Pb_xO_{7-y}$ modified GC (CME). Nafion is a polyanionic perfluorosulfonated ionomer with selective permeability due to accumulation of large hydrophobic cations rather than small hydrophilic ones. The Nafion coating was demonstrated to improve the accumulation of DNA bases, while the ruthenium oxide pyrochlore proved to have electrocatalytic effects towards the oxidation of G and A. The inherent catalytic activity of the CME results from the Nafion-bound oxide surface being hydrated. The catalytically active centers are the hydrated surface-bound oxy-metal groups which act as binding centers for substrates [50].

4.2.2
Polymer Surface-Modified Glassy Carbon

GC material was widely modified with conducting (or nonconducting) polymers in order to obtain an improved surface for DNA adsorption and detection. The initial approaches were performed by the physical attachment of nylon or nitrocellulose membranes on GC electrodes [51]. As explained, these membranes were extensively used in classical DNA analysis due to their well-known adsorption properties [33]. Other approaches were performed by the direct adsorption of the polymeric film on the GC surface. Finally, polymeric films were electrochemically grown on the GC substrate. These conducting polymers are particularly promising for the adsorption, but also for inducing electrical signals obtained from DNA interactions.

4.2.2.1
Chitosan-Modified Glassy Carbon

A chitosan oligomer film was used as an active coating for the immobilization of ssDNA at a GC electrode. Chitosan oligomer is a kind of β-1,4-linked

glucosamine oligomer. It is a natural biocompatible, biodegradable and non-toxic cationic polymer that can form a stable complex through its amino groups with the polyanionic phosphodiester backbone of DNA, either native or denatured. Thus, chitosan and its derivatives may represent potentially safe and efficient cationic carriers for gene delivery. Chitosan was dry-adsorbed on the GC surface. The ssDNA was immobilized on the chitosan-modified GC by wet-adsorption [52]. The main advantage of using chitosan as a modifier of GC was that it could form a tight electrostatic complex with DNA which made the immobilization very stable [53, 54].

4.2.2.2
Layer-by-Layer Deposited Film Modified Glassy Carbon

Fabrication of organic thin films based on spontaneous molecular assembly has been considered as one of the powerful approaches to create novel supramolecular systems. In this context, multilayer films were fabricated by layer-by-layer electrostatic deposition techniques based on the electrostatic interaction between dsDNA and the positively charged polymer poly(diallyldimethylammonium chloride) (PDDA) on GC surfaces. A uniform assembly of PDDA/DNA multilayer films was achieved, based on the adsorption of the negatively charged DNA molecules on the positively charged substrate [55].

4.2.2.3
Polypyrrole-Modified Glassy Carbon

Conducting polymers based on polypyrrole (PPy) display many interesting properties such as redox activity, excellent conductivity, and strong adsorptive capabilities towards negatively charged macromolecules such as DNA and ODNs. These interesting adsorptive properties achieved with the positively charged PPy-modified GC have been extensively studied [56]. The PPy film was grown on GC using nitrate [57] or chloride [58] as dopant counter anions. The PPy-coated GC was demonstrated to be sensitive for detecting adsorbed ODN, DNA, and RNA onto the film. Such adsorption behavior was facilitated by electrostatic interactions between the negatively charged nucleic acids and the positive charge density of the PPy backbone. The different response patterns observed in the presence of different dopants hold great promise for the development of multielectrode nucleic acid arrays. The thickness of the PPy film affected the DNA immobilization effectiveness and its own conductivity property. Thicker PPy layers did not improve the hybridization capability or detection sensitivity. It was also possible to dope nucleic acid probes within electropolymerized PPy films. The ODN served as the sole counter anion during the growth of conducting PPy films, and maintained their hybridization activity within the host polymer network [59]. The

anionic ODN was incorporated within the growing film for maintaining its electrical neutrality.

4.2.3
Liposome-Modified Glassy Carbon

Since lipids are known to associate with DNA with high affinity, the adsorption of ssDNA at lipid membranes as a medium for DNA incorporation on a GC surface was extensively studied [60]. Exploiting DNA–lipid interactions, various approaches were designed for the incorporation of ssDNA [61] and dsDNA [62] at a modified bilayer lipid membrane (BLM) GC surface, such as (1) the formation of self-assembled BLMs over ssDNA previously adsorbed on GC, (2) the direct adsorption of ss- and dsDNA [62] into a previously BLM-modified GC and, (3) formation of a BLM with incorporated ssDNA at the GC surface using the monolayer folding technique [61].

The ssDNA was immobilized stronger and faster on the GC surface in the presence of the lipid membrane than on a bare GC surface and using milder conditions [61]. The lipid membrane enhanced the stability of ssDNA towards desorption from the GC surface [61, 62]. Moreover, the adsorption of ssDNA on BLM induced a conductance enhancement due to (1) structural changes (i.e., defect sites) within the membrane and (2) the increase in negative surface charge density of the membrane. The charge of the phosphate groups of ssDNA induced an increase of cation concentration in the electrical double layer [63].

4.3
Pyrolytic Graphite

One of the first attempts to adsorb DNA onto carbonaceous materials was performed on PG [64].

The use of HOPG as a substrate for the adsorption of DNA made a notable contribution to a better understanding of the adsorption process on carbonaceous material due to the use of high resolution image techniques such as AFM.

In preliminary studies, it was found that dsDNA was adsorbed on HOPG more easily by applying a potential of + 0.4 V (vs Ag/AgCl) for 15 min while ssDNA was adsorbed almost equally whether or not this potential was applied. The adsorption of ssDNA was thus only slightly influenced by the potential, suggesting a different adsorption pattern for ssDNA than for dsDNA on HOPG. The dsDNA could be adsorbed on HOPG mainly by phosphate–sugars whereas ssDNA could be attached not only by phosphate–sugars but also by DNA bases. In contrast to other carbonaceous materials such as GC, dsDNA was easily immobilized on HOPG from the solution (by applying a positive potential). Since the HOPG is a smooth single-crystal plane, the less flexible dsDNA molecule would have more contact with the smooth electrode

surface than with a rough surface such as GC [38, 39]. The oxidation products of dsDNA were not easily removed from the HOPG surface, suggesting that these products are strongly adsorbed. In preliminary studies, electrochemical AFM images of dsDNA adsorbed on a HOPG substrate showed that some segments of dsDNA were adsorbed to form a layer on the surface and other parts of the strands form a DNA island above the layer on the surface. The adsorption of dsDNA did not occur with the molecule lying flat against the HOPG surface but rather through some segments [17], perhaps those where dsDNA is open, thereby exposing DNA bases. These preliminary observations have been confirmed using magnetic AC mode AFM [16, 65, 66].

Since the HOPG surface presents hydrophobic characteristics and DNA is a highly charged hydrophilic molecule, the capacity for spontaneous interaction of DNA with the HOPG surface should be reduced. However, both ss- and dsDNA showed a tendency to spontaneously self-assemble from solution onto the HOPG surface and the process was found to be very fast. Magnetic AC mode AFM images in air revealed good coverage of the surface in a film with the aspect of a two-dimensional network, which has been extensively described [16]. For these studies, DNA was first wet-adsorbed in an open circuit on HOPG and then the layer was dried. The immobilization procedure produced A-DNA molecules over the HOPG due to the strong dehydration after adsorption. The continuous dissociation–association of the bases of the dsDNA extremities exposed the hydrophobic core of the DNA helix sporadically. The dsDNA at the surface was thus stabilized through the interaction between the hydrophobic bases and the hydrophobic surface of the HOPG. The interaction of DNA with the hydrophobic HOPG surface induced DNA superposition, overlapping, and intra- and intermolecular interactions. The topography of the ssDNA-modified HOPG suggested that ssDNA interacted and adsorbed more strongly to the HOPG surface than dsDNA. This can be explained because the ssDNA had bases exposed to the solution, which facilitated the interactions with the hydrophobic carbon surface [16].

The application of a positive potential of + 0.300 V (vs Ag wire) to the HOPG surface during adsorption was also studied [16]. The applied potential considerably enhanced the robustness and stability with respect to mechanical stress of the DNA layers through multiple electrostatic interactions between the negatively charged hydrophilic sugar–phosphate backbone and the positively charged carbon surface. The applied potential increased the attractive lateral interaction between adjacent dsDNA helices and caused spontaneous condensation of the dsDNA layer in a complex network on the HOPG surface. The stability of the dsDNA layer was much increased by electrostatic interaction with the positively charged HOPG surface by structural rearrangement of the molecule. During reorientation and equilibration of the DNA on the surface, the helix was destabilized and some phosphate groups detached from the charged electrode, facilitating electrostatic binding on the HOPG surface of the phosphate groups from the same strand and leading

to no formation of helical DNA parts. As a consequence, parts of the phosphate backbone of one strand lay down flat on the surface. The destabilization and local stretching of the DNA duplex may involve a significant loss of base-stacking and hydrogen-bonding. The DNA bases initially protected inside the helix appeared more exposed to the solution and free to undergo intermolecular interactions by hydrogen bonding and base-stacking with bases from other chains that bind nearly on the surface.

As in the case of dsDNA, the application of a potential of + 0.300 V (vs Ag wire), enhanced the strength, robustness, and resistance to mechanical stress of the ssDNA layer. Electrostatic interactions between the negative charges along the dsDNA and ssDNA phosphate backbone and the positively charged HOPG surface were very strong, which increased stability of the molecules on the substrate. Consequently the adsorbed molecules were less compressible by the AFM tip. Many molecules interacted together by hydrogen bonding during equilibration on the substrate, and hydrophobic interactions and van der Waals forces also contributed to adsorption of DNA on the HOPG electrode [16].

The thin layers formed in ABS (pH 5.3) always presented a better coverage of the HOPG surface with DNA molecules than layers formed in pH 7.0 PBS [65]. Comparing the thickness and the electrode coverage of the layers obtained with both ss and ds DNA at different pHs on applying a potential of + 0.300 V it was concluded that the layer obtained at pH 5.3 presented a self-assembled lattice that was more relaxed and extended on the surface. The results that were obtained by AFM corroborate previous observations that the best binding efficiency of dsDNA on hydrophobic surfaces occurs at approximately pH 5.5 [65].

Owing to these characteristics, PG has been extensively used for the adsorption of DNA and its derivatives. DNA was successfully adsorbed on PG by dry-adsorption at 100 °C [67]. The electrodes were stored in TriS buffer at 4 °C without loss of DNA, showing that DNA was firmly adsorbed on PG. It was demonstrated that the adsorbed ODN was also able to be hybridized with its complementary strand, suggesting that although DNA bases are compromised in the adsorption, they are still available for hybridization [67]. A composite film of DNA and the polyanionic perfluorosulfonated ionomer Nafion was cast on PG by the layer-by-layer procedure performed by dry-adsorption [68]. In another approach, the PG surface was electrochemically pretreated at – 1.7 V for 60 s. DNA was then wet-adsorbed at the pretreated electrode surface from solutions containing 0.2 M NaCl, 10 mM Tris– HCl, pH 7.4 , for 1 min followed by rinsing the electrode with distilled water [69, 70].

4.4 Highly Boron-Doped Diamond

The boron-doped diamond (BDD) thin films are particularly attractive for electroanalytical applications due to their unique characteristics, including

chemical inertness, wide potential window, excellent electrical conductivity and extraordinarily low catalytic activity and very low background current within the working potential range [71]. These properties provide superior sensitivity, , reproducibility, and stability of BDD compared to other conventional materials for electroanalysis.

The BDD film was grown on Si(100) substrates [72]. The adsorption and oxidation of ss- and dsDNA has been investigated in ABS (pH 5.0) at a BDD film. Although BDD films are commonly H-terminated, they usually acquire oxygen on the surface during polishing or anodic oxidation processes. The surface termination has been shown to have significant effects on the adsorption and redox processes of ss- and dsDNA. Owing to the difference in the electronegativities of C (2.5), H (2.1) and O (3.4), the surface acquires C – H and C – O dipoles depending on the termination, thus making the surface partially charged [71]. In the case of hydrogen termination, the surface acquires a very small positive polar charge, while the O-terminated surface acquires a relatively high negative polar charge due to the higher dipole moment, causing electrostatic interactions with charged molecules such as DNA. O-terminated diamond was found to repel the DNA molecule, while H-terminated diamond attracted the DNA due to its weak positive charge, enhancing its adsorption on the surface [71]. In contrast, the surface termination did not show much influence on free A and G adsorption. The influence of the negatively charged phosphate-containing sugar backbone in the electrostatic interaction was thus quite obvious. The adsorption of DNA at H-terminated diamond was almost independent of ionic strength, due to the small electrostatic interaction between the H-terminated surface and negative charge of DNA, where the ionic strength did not influence the adsorption much. However, on the O-terminated diamond, a drastic increase in the adsorption would be expected with increased ionic strength, which indicates the masking of surface charge by an increasing number of the positive counter ions in the solution, resulting in a relatively neutral surface. The ssDNA molecule was more firmly adsorbed on the surface of BDD than dsDNA. This difference could be assumed a consequence of the difference in the flexibilities of the DNA. The more rigid dsDNA covered less efficiently the roughness of BDD surface than ssDNA [71].

4.5
Carbon Composites

4.5.1
Soft Carbon Composites. Carbon Pastes

The adsorption of DNA and its derivatives on CP materials has been widely reported. CP for DNA adsorption could be successfully prepared by the

mixing of 70/30 (w/w) graphite powder/mineral oil [73, 74], a composition which yielded the most favorable signal-to-background characteristics.

Of the several ways that nucleic acid could be immobilized on CP surface, electrostatic adsorption proved to be an effective and simple route, and thus was widely used [75]. It was found that the anodic pre-treatment of CP [at + 1.7, 60 s in ABS (pH 5)] greatly enhances the electrostatic adsorption (+ 0.5 V vs Ag/AgCl) of dsDNA, ssDNA, RNA and its derivatives [75]. However, the treated surface did not show electrocatalytic activity. The anodization produced—as in other carbonaceous materials—a substantially larger background current contribution. The electrochemical pre-treatment led to an increase in the density of surface oxygenated groups, a more hydrophilic surface state, and a concomitant removal of organic and pasting-liquid layers from the surface [76]. Such a change in the surface state appeared to facilitate the interfacial adsorption of RNA [73] and DNA [76, 77] on CPs, but not the charge-transfer. Similar behavior was observed at GC, as previously described.

However, after the study of inosine-substituted ODN, there was evidence that the pretreatment improved the electrochemistry of purine bases, with a smaller effect on the interfacial accumulation [78]. The G oxidation signal was strongly affected by the surface pre-treatment of CP. However, the inosine-modified probe response was less affected by this treatment [78], suggesting a lesser effect on adsorption over the electrochemistry of purine base. However, if inosine (a non-purine base) substituted G in the ODN sequence, the stability of the adsorbed probe on CP was similar to that observed with G-containing ODN, i.e., being stable in a stirred PBS for up to 15 min. Such behavior indicated that the inosine substitution has little effect upon the stability of the adsorbed probe [78].

As in other carbonaceous materials, higher electrostatic adsorption efficiencies for short nucleotide sequences (ssDNA) were observed [76]. Shorter ODNs penetrated more readily into the grooves and pores of the rough CP surface. Such behavior increased the accessibility of the base moieties to the graphite particle electron-transfer sites. In contrast, the access of longer oligomers (10 basepairs or more) into the porous surface was restricted. They were unable to follow the contours of the surface and, accordingly, their oxidation currents were smaller [79]. Such interaction with the surface was found to also depend on the flexibility of the DNA molecule, with more rigid molecules following the rough surface less efficiently. Those length-dependent differences on the surface penetration and accessibility of synthetic ODN have shown a profound effect on the adsorption properties. Additionally, it was found that the adsorption and oxidation were influenced not only by the length and rigidity of the ODN, but also by its base content and sequence [79]. However, the less flexible and longer dsDNA molecule was also electrostatically adsorbed at + 0.5 V yielding a high stable layer for the biosensing of pollutants [80].

The coupling of the CP pre-treatment and the electrostatic adsorption results in a stable immobilization layer of ODN. The adsorbed ODN layer on CP remained stable throughout 60 min in stirred solutions of PBS [74]. Moreover, the electrostatic adsorption procedures at + 0.5 V led to a reactive and accessible probe. A comparison study between CP and Hg electrodes showed that no significant hybridization of the DNA adsorbed on Hg was taking place, probably due to a strong interaction of hydrophobic bases with the hydrophobic surface of the mercury electrode. The bases of the probe, interacting strongly with the surface, cannot be accessible to form specific base pairs with the target DNA. Compared with the negatively charged mercury electrode, a different orientation of the adsorbed DNA molecule can be expected at the positively charged CP electrode. The DNA could be attached to the CP surface via the negatively charged hydrophilic sugar–phosphate backbone with bases oriented toward the solution and available for the hybridization with the target DNA. The results of the hybridization experiments matched up to this expectation [81].

This strong adsorption of DNA and its derivatives on carbon materials has made possible the adsorption (and preconcentration) of DNA on CP and its further separation from interferences. It has been shown that low molecular mass substances did not interfere with the analysis of DNA and RNA if the nucleic acid was previously adsorbed at the CP electrode, which was then washed and transferred to a blank electrolyte. This procedure was called adsorptive transfer stripping voltammetry (AdTSV) [75, 82, 83]. Although the electrostatic adsorption results in a strong and irreversible accumulation, the ability to remove DNA layers from CP microelectrodes under potential control was demonstrated. The electrostatic release of surface-confined DNA layer was performed in PBS (pH 7.4) at a potential of – 1.2 V for 2 min. The application of the negative potential at the DNA-modified CP has been shown to electrostatically repel the negatively charged nucleic acid molecules from the CP negatively charged surface [75].

It was also demonstrated that the application of increased temperatures during the electrostatic adsorption results in dramatic enhancement of the oxidation signal, ascribable to an improved electrostatic adsorption at the heated electrode. Forced thermal convection near the electrode surface facilitated the electrostatic adsorption and the use of quiescent solutions [84–86]. The main role of the high temperature in CP was found to be the enhancement of the adsorption efficiency (e.g., through faster localized convection and faster kinetics) but not the preactivation of the surface. The temperature effect strongly depended on the chain length and structure of the nucleic acid molecule [84]. The reason could be a change of structure in the molecule which is suspected to be temperature-dependent. Faster molecular movement and changes in structure could facilitate the adsorption. More electrochemically active sites of the nucleic acid molecules could come into close contact with the electrode surface, thus increasing the signal. In highly complex

molecules such as dsDNA, this effect has proved to be relatively strong compared to that in less complex ones such as tRNA [84].

Another CP pre-treatment that was found to greatly enhance the electrostatic adsorption at + 0.5 V (vs Ag/AgCl) of ODN [87], dsDNA and ssDNA [88, 89] was performed at almost the same conditions (+ 1.7 V, 60 s) but in neutral solutions (PBS pH 7.5). A combination of + 1.5 V, 1 min, PBS pH 7.0 as a pre-treatment step with a further electrostatic adsorption at + 0.3 V was also demonstrated to be successful for immobilizing dsDNA on CP [90].

4.5.1.1 Surface-Modified Carbon Pastes

CP was surface-modified with cetyltrimethyl ammonium bromide (CTAB) by dry adsorption (CTAB/CP) [91]. CTAB could change the surface properties of CP, forming a compact monolayer on the electrode surface with a high density of positive charges. The stabilization of the monolayer was achieved by hydrophobic adsorption of CTAB on the hydrophobic surface of CP. The paraffin oil layer covering the carbon particles had hydrophobic properties similar to those of the CTAB layer. Thus, CTAB could form a stable monolayer on the surface of CP. The CTAB/CP material was applied to the immobilization of dsDNA [91]. The procedure for immobilizing DNA was electrostatic adsorption. With the modification of dsDNA, the CP surface turned from poor to high hydrophilicity and the hydrophilic surface could survive the thorough washing with water, which indicated the tight combination of DNA on the electrode surface [91].

A chitosan-modified CP (ChiCP) material was prepared for the electrostatic adsorption of dsDNA, ssDNA and ODNs [92]. The immobilized ODN could selectively hybridize with the target DNA to form a hybrid on the ChiCP surface.

4.5.1.2 DNA Modifying Carbon Pastes as an Additive

Additives such as polyethylene glycol, cationic antibiotics, polymers, small uncharged molecules, and negatively charged proteins have been used extensively in order to avoid the denaturing of enzymes or to improve the sensitivity and operational stability of biosensors. DNA has been proposed as an additive to improve the response and stability of biosensors based on CP. The biomolecules studied, such as tyrosinase [93], peroxidase [94], cytochrome C [95], have been shown to improve its performance by using adsorbed DNA within CP as an additive.

The presence of DNA in the biosensor improved the durability and greatly increased the sensitivity of the sensor. When the CP-DNA-Tyr was first exposed to the electrolyte, some swelling was observed as a result of hydration

of the DNA. The DNA thus provided a more hydrophilic environment for the enzyme. The direct interaction of DNA with the functional groups of amino acids occurred through hydrogen bonding, with partial displacement of the well-ordered water shell of DNA or with individual water molecules acting as bridges of the hydrogen bonding. Through such interactions, DNA could improve the stabilization of the tertiary structure of the enzyme in comparison with other additives [93]. The DNA molecules have been proved to be an efficient promoter for a direct electron transfer reaction [95], increasing the sensitivity of the biosensors [94]. This behavior was also shown during the evaluation of the Doyle catalyst performance when adsorbed on CP in the presence and the absence of DNA, suggesting a good hydrophilic and conductor character of DNA [96].

4.5.2 Rigid Carbon Composites

Rigid carbon composites have been widely used in our laboratories for the adsorption of ssDNA, dsDNA, ODN and DNA derivatives. In particular, we have used graphite-epoxy composite (GEC) made by mixing the nonconducting epoxy resin (Epo-Tek, Epoxy Technology, Billerica, MA, USA) with graphite powder (particle size below 50 μm). An ideal material for electrochemical genosensing should allow an effective immobilization of the probe on its surface, a robust hybridization of the target with the probe, a negligible nonspecific adsorption of the label and a sensitive detection of the hybridization event. GECs fulfill all these requirements.

Owing to its improved electrochemical characteristics, ss- and dsDNA and ODN have been immobilized by dry adsorption on GEC [97, 98], yielding a thick DNA layer. Beside its improved electrochemical properties, GEC has shown unique and selective adsorption behavior. While DNA is firmly adsorbed under dry conditions, the wet-adsorption of nonspecific DNA, proteins, enzymes or other biomolecules has proved to be negligible under stirring or convection conditions in solution. The DNA-modified GEC surface does not require blocking steps to minimize the nonspecific adsorption on the free sites of the surface. The dual nature of GEC composed of islands of conducting material within the nonconducting and hydrophobic epoxy resin could play an important role in stabilizing the dehydrated A-form of DNA adsorbed on GEC.

Besides thick-layer DNA/GEC surface, a thin-layer DNA/GEC could be achieved by wet-adsorption of ss- and dsDNA and ODN onto a GEC transducer under static conditions [99, 100]. In this case, the hydrated B-DNA form was stabilized over the GEC surface by weaker forces. Unlike the GEC surface modified by the thick DNA layer —produced in dry conditions—the thin-layer DNA/GEC surface required blocking treatment to avoid nonspecific

adsorption. The wet-adsorption procedure produced a less compact DNA layer with wider gaps exposing free GEC surface.

Although DNA can be firmly adsorbed on GEC, it retains its unique hybridization properties, which can be monitored using various strategies [99, 100], suggesting that the DNA bases are not fully committed in the adsorption mechanism.

Moreover, the unique adsorption properties of GEC allowed the very sensitive electrochemical detection of DNA based on its intrinsic oxidation signal that was shown to be strongly dependent of the multi-site attachment of DNA and the proximity of G residues to GEC [100]. The thick layer of DNA adsorbed on GEC was more accessible for hybridization than those in nylon membranes obtained with genosensors based on nylon/GEC with a changeable membrane [99, 101, 102]. Although GEC has a rough surface, it is impermeable, while nylon is more porous and permeable. DNA assays made on an impermeable support are less complex from a theoretical standpoint [7]: the kinetics of the interactions are not complicated by the diffusion of solvent and solutes into and out of pores or by multiple interactions that can occur once the DNA has entered a pore. This explained the lower hybridization time, the low nonspecific adsorption and the low quantity of DNA adsorbed onto GEC compared to nylon membranes.

Compared to GC (a transducer widely used in electrochemical genosensors), the higher sensitivity of GEC can be explained by its higher active surface and rugosity, as is evident from scanning electron microphotographs of both surfaces and also a behavior mimicking that of a random assembly of microelectrodes [97] (Fig. 4). Unlike CP, the rigidity of GEC permits the

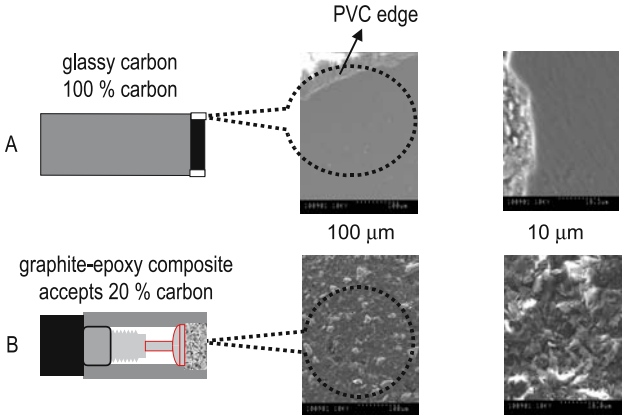

Fig. 4 Scanning electron microphotographs of the surfaces of glassy carbon (GC) (**a**) and graphite epoxy composite (GEC) (**b**). The same acceleration voltage (10 kV) and the same resolution (100 and 10 μm) were used in both cases. Taken from [97]. Reprinted with permission

design of different configurations, and these materials are compatible with non-aqueous solvents.

A new class of sol-gel-based carbon composite material can be formed by homogeneous dispersion of graphite powder in a suitable sol-gel precursor/monomer (mainly based on methanol and methyltrimethoxysilane) [103, 104]. The resulting homogeneous sol-gel CP was allowed to polymerize and left to dry, obtaining the silica sol-gel-derived carbon composite material. Electrodes prepared on the basis of this material have been reported to have various desirable properties for electroanalysis: low background current, good chemical and mechanical stability, easy preparation and wide potential window. CPs proved to have inferior mechanical stability compared with this composite material. At certain and non-stringent conditions, A (but also G) was demonstrated to be electrostatically adsorbed onto this porous material.

4.6 Carbon Inks

DNA has been widely adsorbed on carbon inks. These carbon inks were previously printed onto alumina ceramic plates or other substrates such as polyester for fabricating thick film sensors. Carbon inks are commercially available but normally their composition is not precisely known. As a consequence, it is difficult to predict interactions between DNA and carbon inks, which contain various components such as binders besides graphite. They usually require a curing step at high temperatures. Unlike the CP materials, some carbon inks require a short (10 s) precathodization [at – 2.0 V) prior to the 1 min oxidative activation (1 min at + 1.8 V in ABS (pH 5.0)] [76]. DNA adsorption was performed as in the case of CP by electrostatic adsorption at a potential of + 0.5 V in pH 5.0 ABS (vs Ag/AgCl) [105, 106]. The short anodic pre-treatment was found to enhance the electrostatic adsorption of DNA. The enhanced adsorption was attributed to the increased surface roughness and hydrophilic properties following such treatment [106]. It was also demonstrated that the pre-treated graphite inks at + 1.6 V for 1 min in PBS (pH 7.0) [107] or ABS (pH 5.0) [108, 109] showed lower background currents. The anodization probably removed undesirable compounds from the electrode surface and graphite impurities. Higher oxidation times (up to 60 min) for pre-treatment increased the noise and the background current [107]. The adsorbed nucleic acid layer (ssDNA, dsDNA and ODN) on the carbon inks was demonstrated to be stable for at least 30 min under stirring in ABS (pH 5.0) at + 0.5 V [105].

Besides DNA adsorption driven by a positive potential (electrostatic adsorption) DNA was also wet-adsorbed at an open circuit on a home-made polystyrene-based carbon ink [110]. This ink was prepared by a 2 : 3 mixture of polystyrene and graphite particles in mesitylene, and then printed on a polyester film. DNA was wet-adsorbed over the ink at 37 °C overnight. The nature of the electrode surface (graphite particles embedded in a polystyrene

binder) was found to be a suitable solid phase for the reproducible adsorption of DNA. Moreover, this solid phase led to a negligible nonspecific adsorption of the non complementory ODN probe [110].

DNA modification of a commercial carbon ink without any electrochemical preconditioning by dry-adsorption was also reported. The surface was modified by covering with dsDNA solution and leaving the electrode to dry overnight. A stable, thin (about 100 μm) DNA layer was obtained [111, 112]. The dsDNA was also demonstrated to be stably adsorbed when entrapped in a cellulose-acetate-based film on the surface of a carbon-based ink [113].

4.7
Graphite Pencil Leads

Renewable graphite pencil leads have been demonstrated to be excellent materials for the adsorption of DNA. Various pencil lead materials have been studied [114]. As in the case of GC and CP, the graphite leads were electrochemically oxidized at + 1.4 V for 30 s prior to the DNA electrostatic adsorption, performed at + 0.5 V (vs Ag/AgCl) for 60 s in stirred ABS (pH 5.0) [114, 115]. The adsorption of DNA was shown to be similar to that at a CP electrode. However, substantial differences in adsorption and electrochemical performance were observed at the various types of graphite leads. Such different responses are to be expected considering the different composition and roughness of the various graphite leads containing various insulating polymeric binders and clays besides graphite [116]. However, these non-graphite constituents do not yield a background peak. In the view of the composite nature of the leads, these differences could reflect the differences in the adsorption properties of the nucleic acid, in the kinetics of DNA oxidation processes, or in the effective surface area (roughness) [114].

4.8
Carbon nanotubes

Since it was initially reported [21], several methods have been presented in order to attach DNA onto CNTs, including adsorption. First, transmission electron microscopy showed that the DNA molecules tended to cover the surface of the nanotubes evenly, suggesting a strong interaction with the carbon surface [24].

DNA/SWCNTs interactions were studied by IR and UV spectroscopy and it was found that CNTs could self-organize with DNA molecules during adsorption processes [117, 118]. Moreover, some evidence indicated that SWCNTs influenced the DNA structure more strongly than graphite [119]. The interaction between DNA and CNTs would cause changes in the hydrogen bonds [119] and the partial unwrapping of the dsDNA when dry-adsorbed on CNTs [118]. The SWCNTs could cause A–B transition in some fragments of DNA sugar–

phosphate backbone. This could be in agreement with the model of DNA interaction with SWCNTs based on wrapping the nucleic acid molecule around the CNT [120]. A similar type of DNA behavior occurs in vivo in chromosomes during the process of DNA-assembling by histones.

The regular system of hydrogen bonds in DNA is destroyed in DNA/NaOH solution and the DNA molecule is partly transformed from a double spiral to a chaotic ball [118]. This transformation may promote the interaction of DNA molecules with CNTs. The ssDNA adsorption on CNTs was greater than for dsDNA molecules [117, 118], suggesting that the adsorption of DNA on CNT is presumably via hydrophobic interactions between the nanotubes and the hydrophobic bases on DNA.

4.8.1 Surface-Modified Carbon Nanotubes Approaches

To take advantages of the unique properties of CNTs, a general approach is the immobilization of DNA on CNTs and the further immobilization of the DNA-modified CNTs on an easier-to-handle pure conductor, e.g., GC [26], Pt [121], Au [122]. Another approach consists of the prior modification of the pure conductor (GC) with the CNTs through dry-adsorption and the further DNA or DNA derivatives adsorption on the CNT-modified surface [123–125].

Compared with the bare substrate material (GC, Pt, Au), it was demonstrated generally that the background current of the MWCNTs surface-modified conductor was apparently larger [123, 124]. The surface modification of the conducting material with MWCNTs could thus significantly enhance the effective electrochemical surface area as well as provide a larger surface for DNA immobilization [26]. Unlike the commonly used CP, GC or graphite leads, the CNTs/GC material does not require a surface pre-treatment for enhancing electrochemical signals [123], reflecting a substantial interfacial accumulation onto the CNT-modifier rather than an accelerated electron transfer. Such interfacial adsorption reflects the nature of the MWCNT surface, and its large surface area/volume ratio [123].

As an example, dsDNA was wet-adsorbed on MWCNTs over 24 h. The DNA-modified MWCNT was deposited on Pt and allowed to dry overnight [121]. The thickness of the DNA/MWCNT layer was 160 nm. The modified electrode was stored at 4 °C for 2 months. The good reproducibility and long-term performance can be attributed to the stability of the DNA/MWCNT layer [121]. The DNA molecule was also wet-adsorbed on previously modified SWCNT/GC [124] for 5 min in an open circuit from a PBS (pH 7.2) solution. Under these conditions, the same electrochemical response was obtained for ds- and ssDNA, again suggesting a strong interaction between dsDNA and SWCNTs. As a result of this interaction, the primary redox sites of A and G residues were exposed because of the unwrapping of the DNA double helix and changes in the hydrogen bonds between the bases of the dsDNA

molecule [124]. Moreover, not only dsDNA, but also its oxidation product was strongly adsorbed on the SWCNT–GC surface [124].

Additionaly, the electrostatic assembly of calf thymus DNA on MWCNTs via a cationic polyelectrolyte [poly(diallyldimethylammonium chloride), (PDDA)] was reported [122]. The positively charged PDDA molecule played a key role in the attachment of DNA to MWCNTs, acting as a bridge to connect the negatively charged DNA molecule with MWCNTs, although the direct adsorption of DNA on MWCNTs was observed [122]. By repeating the PDDA/DNA adsorption cycle several times, a PDDA/DNA multi-layer could be formed on MWCNTs.

4.8.2
Bulk-Modified Carbon Nanotubes Approaches

Among the surface-modified CNTs materials, a bulk-modified CNT paste (CNTP) has also been reported [126]. The new composite electrode combined the ability of CNTs to promote adsorption and electron-transfer reactions with the attractive properties of the composite materials. The CNTP was prepared by mixing MWCNTs powder (diameter 20–50 nm, length 1–5 μm) and mineral oil in a 60 : 30 ratio. The oxidation pretreatment [performed in ABS (pH 5.0) for 20 s at 1.30 V, vs Ag/AgCl] proved to be critical in the state of the CNTP surface. Pretreatments improved the adsorption and electrooxidation of both DNA and DNA bases, probably due to the increase in the density of oxygenated groups.

Although the adsorption of DNA at CP was shown to be favored at positive potentials, almost no dependence with the potential was observed at CNTP. No changes in adsorption were observed for dsDNA in the potential range of 0.50 to – 0.20 V, indicating that there is a poor contribution of the negatively charged phosphate backbone in the adsorption of nucleic acids at CNTP, as in the case of GC [44]. Considering the structure of CNTs, it is reasonable to expect that the character of the interaction between the DNA bases and CNTP is mainly hydrophobic [117, 118, 124, 126]. It was also observed that the size of the molecules has a significant effect, producing better adsorption of smaller ODNs on CNTs.

5
Concluding Remarks

A wide range of carbonaceous materials can be modified with a stable DNA adsorbed layer. The multi-site attachment of DNA on carbon surfaces seems to be strongly dependent on hydrophobic interactions between DNA bases and carbon substrates such as GC and $GC_{(ox)}$, HOPG, CNTs and GECs. Al-

though multi-site adsorption was previously claimed to be a disadvantage for hybridization, DNA can be perfectly hybridized with its complementary strand when adsorbed on most of the carbon-based materials. Moreover, adsorbed dsDNA can be easily detected without the need for external markers because multi-site adsorption is known to produce an improved oxidation signal coming from DNA bases moieties.

With regard to its unique properties, a carbon substrate can be considered an excellent alternative material to continuous metal conductors and semiconductors for the construction of DNA sensors and chips.

Acknowledgements Universidad Nacional del Litoral (Argentina) (M.I.P) is gratefully acknowledged. Financial support from Ministry for Education and Science, Madrid (program "Juan de la Cierva" and project BIO2004-02776), is also acknowledged.

References

1. Baltimore D (2001) Nature 409:814
2. Bowtell DDL (1999) Nature Genet [suppl] 21:25
3. Collins FS (1999) Nature Genet [suppl] 21:2
4. Lander ES (1999) Nature Genet [suppl] 21:3
5. Sanders GHW, Manz A (2000) Trends Anal Chem 19:364
6. Pividori MI, Merkoçi A, Alegret S (2000) Biosensor Bioelectron 15:291
7. Southern E, Mir K, Shchepinov M (1999) Nature Genet [suppl] 21:5
8. Paleček E (1958) Naturwiss 45:186
9. Paleček E (1960) Nature 188:656
10. Streat M, Malik DJ, Saha B (2004) Adsorption and ion-exchange properties of engineered activated carbons and carbonaceous materials. In: SenGupta AK, Marcus Y, Marinsky JA (eds) Ion exchange and solvent extraction, chap 1. Dekker, New York
11. Chu X, Kinoshita K (1997) Mater Sci Eng B 49:53
12. Regisser F, Lavoie MA, Champagne GY, Belanger D (1996) J Electroanal Chem 415:47
13. McCreery RL, Cline KK (1996) Carbon electrodes. In: Kissinger PT, Heineman WR (eds) Laboratory techniques in electroanalytical chemistry, chap 10. Dekker, New York
14. Hu IF, Karweik DH, Kuwana T (1985) J Electroanal Chem 188:59
15. Kepley LJ, Bard AJ (1988) Anal Chem 60:1459
16. Oliveira Brett AM, Chiorcea AM (2003) Langmuir 19:3830
17. Wu L, Zhou J, Luo J, Lin Z (2000) Electrochim Acta 45:2923
18. Alegret S (1996) Analyst 121:1751
19. Céspedes F, Martínez-Fàbregas E, Alegret S (1996) Trends Anal Chem 15:296
20. Adams RN (1958) Anal Chem 30:1576
21. Iijima S (1991) Nature 354:56
22. Sherigara BS, Kutner W, D'Souza F (2003) Electroanalysis 15:753
23. Tsui R, Siragusa L, Goronkin H (2000) C R Acad Sci Paris 1:875
24. Guo ZJ, Sadler PJ, Tsang SC (1998) Adv Mater 10:701
25. Xu J (2003) Proc IEEE 91:1819
26. Cai H, Cao XN, Jiang Y, He PG, Fang YZ (2003) Anal Bioanal Chem 375:287

27. Walther JH, Jaffe RL, Kotsalis EM, Werder T, Halicioglu T, Koumoutsakos P (2004) Carbon 42:1185
28. Li J, Ng HT, Cassell A, Fan W, Chen H, Ye Q, Koehne J, Han J, Meyyappan M (2003) Nano Lett 3:597
29. Oliveira Brett AM, Piedade JAP, Serrano SHP (2000) Electroanalysis 12:969
30. Wang J (1998) Biosensor Bioelectron 13:757
31. Sambrook J, Fritsch EF, Maniatis T (1989) Molecular cloning: a laboratory manual, 2nd edn. Cold Spring Harbor Laboratory Press, New York
32. Meinkoth J, Wahl G (1984) Anal Biochem 138:267
33. Reed KC, Mann DA (1985) Nucleic Acids Res 13:7207
34. Rasmussen SR, Larsen MR, Rasmussen SE (1991) Anal Biochem 198:138
35. Pang DW, Zhang M, Wang ZL, Qi YP, Cheng JK, Liu ZY (1996) J Electroanal Chem 403:183
36. Oliveira Brett AM, Vivan M, Fernandes IR, Piedade JAP (2002) Talanta 56:959
37. Oliveira Brett AM, Serrano SHP, Gutz I, La-Scalea MA, Cruz ML (1997) Electroanalysis 9:1132
38. Brett CMA, Oliveira Brett AM, Serrano SHP (1999) Electrochim Acta 44:4233
39. Oliveira Brett AM, Macedo TRA, Raimundo D, Marques MH, Serrano SHP (1998) Biosensor Bioelectron 13:861
40. Abreu FC, Goulart MOF, Oliveira Brett AM (2002) Biosensor Bioelectron 17:913
41. Lu X, Zhu K, Zhang M, Liu H, Kang J (2002) J Biochem Biophys Methods 52:189
42. Wang ZX, Liu DJ, Dong SJ (2001) Bioelectrochemistry 53:175
43. Wang ZX, Liu DJ, Dong SJ (2001) Biophys Chem 89:87
44. Pedano ML, Rivas GA (2003) Biosensor Bioelectron 18:269
45. Tang TC, Huang HJ (1999) Electroanalysis 11:1185
46. Wang HS, Ju HX, Chen HY (2001) Electroanalysis 13:1105
47. Wang HS, Ju HX, Chen HY (2002) Anal Chim Acta 461:243
48. Wang HS, Ju HX, Chen HY (2002) Electroanalysis 14:1615
49. Oliveira Brett AM, da Silva LA, Brett CMA (2002) Langmuir 18:2326
50. Zen JM, Chang MR, Ilangovan G (1999) Analyst 124:679
51. Napier ME, Thorp HH (1999) J Fluorescence 9:181
52. Xu C, Cai H, He P, Fang Y (2001) Analyst 126:62
53. Cai H, Wang Y, He P, Fang Y (2003) Anal Chim Acta 469:165
54. Zhu N, Cai H, He P, Fang Y (2003) Anal Chim Acta 481:181
55. Luo L, Liu J, Wang Z, Yang X, Dong S, Wang E (2001) Biophys Chem 94:11
56. Li Z, Wang H, Dong S, Wang E (1997) Anal Sci 13:305
57. Wang J, Jiang M, Mukherjee B (1999) Anal Chem 71:4095
58. Cai H, Zhu N, Jiang Y, He P, Fang Y (2003) Biosensor Bioelectron 18:1311
59. Wang J, Jiang M, Fortes A, Mukherjee B (1999) Anal Chim Acta 402:7
60. Nikolelis DP, Hianik T, Krull UJ (1999) Electroanalysis 11:7
61. Siontorou CG, Oliveira Brett AM, Nikolelis DP (1996) Talanta 43:1137
62. Tong Y, Han X, Song Y, Jiang J, Wang E (2003) Biophys Chem 105:1
63. Siontorou CG, Nikolelis DP, Tarus B, Dumbrava J, Krull UJ (1998) Electroanalysis 10:691
64. Brabec V, Dryhurst G (1978) J Electroanal Chem 89:161
65. Oliveira Brett AM, Chiorcea AM (2003) Electrochem Comm 5:178
66. Chiorcea AM, Oliveira Brett AM (2002) Bioelectrochemistry 55:63
67. Hashimoto K, Ito K, Ishimori Y (1994) Anal Chim Acta 286:219
68. Rusling JF, Zhou L, Munge B, Yang J, Estavillo C, Schenkman JB (2000) Faraday Discuss 116:77

69. Palecek E, Fojta M, Jelen F (2002) Bioelectrochemistry 56:85
70. Fojta M, Havran L, Kizek R, Billová S (2002) Talanta 56:867
71. Ivandini TA, Sarada BV, Rao TN, Fujishima A (2003) Analyst 128:924
72. Rao TN, Yagi I, Miwa T, Tryk DA, Fujishima A (1999) Anal Chem 71:2506
73. Wang J, Cai X, Wang J, Jonsson C, Palecek E (1995) Anal Chem 67:4065
74. Wang J, Cai X, Rivas G, Shiraishi H (1996) Anal Chim Acta 326:141
75. Wang J, Zhang XJ, Parrado C, Rivas G (1999) Electrochem Comm 1:197
76. Wang J, Cai X, Jonsson C, Balakrishnan M (1996) Electroanalysis 8:20
77. Wang J, Rivas G, Cai X, Dontha N, Shiraishi H, Luo D, Valera FS (1997) Anal Chim Acta 337:41
78. Wang J, Rivas G, Fernández JR, Lopez Paz JL, Jiang M, Waymire R (1998) Anal Chim Acta 375:197
79. Wang J, Kawde AN, Sahlin E, Parrado C, Rivas G (2000) Electroanalysis 12:917
80. Wang J, Chicharro M, Rivas G, Cai X, Dontha N, Farias PAM, Shiraishi H (1996) Anal Chem 68:2251
81. Palecek E, Fojta M, Tomschik M, Wang, J (1998) Biosensor Bioelectron 13:621
82. Cai X, Rivas G, Farias PAM, Shiraishi H, Wang J, Palecek E (1996) Anal Chim Acta 332:49
83. Wang J, Bollo S, Lopez Paz JL, Sahlin E, Mukherjee B (1999) Anal Chem 71:1910
84. Wang J, Gründler P, Flechsing GU, Jasinski M, Rivas G, Sahlin E, Lopez Paz JL (2000) Anal Chem 72:3752
85. Korbut O, Bucková M, Tarapcík P, Labuda J, Gründler P (2001) J Electroanal Chem 506:143
86. Korbut O, Bucková M, Labuda J, Gründler P (2003) Sensors 3:1
87. Erdem A, Kerman K, Meric B, Akarca US, Ozsoz M (1999) Electroanalysis 11:586
88. Erdem A, Meric B, Kerman K, Dalbasti T, Ozsoz M (1999) Electroanalysis 11:1372
89. Meric B, Kerman K, Ozkan D, Kara P, Erensoy S, Akarca US, Mascini M, Ozsoz M (2002) Talanta 56:837
90. Radi A (1999) Anal Chim Acta 386:63
91. Hu C, Hu S (2004) Electrochim Acta 49:405
92. Kara P, Kerman K, Ozkan D, Meric B, Erdem A, Nielsen PE, Ozsoz M (2002) Electroanalysis 14:1685
93. Dantoni P, Serrano SHP, Oliveira Brett AM, Gutz IGR (1998) Anal Chim Acta 366:137
94. Rosatto SS, De Oliveira Neto G, Kubota LT (2001) Electroanalysis 13:445
95. Lee TY, Kim HJ, Moon JO, Shim YB (2004) Electroanalysis 16:821
96. Gil ES, Kubota LT (2000) Bioelectrochemistry 51:145
97. Pividori M I, Merkoçi A, Alegret S (2003) Biosensor Bioelectron 19:473
98. Pividori M I, Merkoçi A, Barbé J, Alegret S (2003) Electroanalysis 15:1815
99. Pividori M I, Alegret S (2003) Anal Lett 36:1669
100. Erdem A, Pividori M I, del Valle M, Alegret S (2004) J Electroanal Chem 567:29
101. Pividori M I, Merkoçi A, Alegret S (2001) Biosensor Bioelectron 16:1133
102. Pividori M I, Merkoçi A, Alegret S (2001) Analyst 126:1551
103. Teh HF, Yang X, Gong H, Tan SN (2004) Electroanalysis 16:769
104. Li J, Chia LS, Goh NK, Tan SN (1999) J Electroanal Chem 460:234
105. Wang J, Cai X, Rivas G, Shiraishi H, Dontha N (1997) Biosensor Bioelectron 12:587
106. Wang J, Rivas G, Cai X (1997) Electroanalysis 9:395
107. Marrazza G, Chianella I, Mascini M (1999) Biosensor Bioelectron 14:43
108. Chiti G, Marrazza G, Mascini M (2001) Anal Chim Acta 427:155
109. Marrazza G, Chianella I, Mascini M (1999) Anal Chim Acta 387:297
110. Azek F, Grossiord C, Joannes M, Limoges B, Brossier P (2000) Anal Biochem 284:107

111. Bucková M, Labuda J, Sandula J, Krizková L, Stepánek I, Duracková Z (2002) Talanta 56:939
112. Labuda J, Bucková M, Heilerová L, Caniová-Ziaková A, Brandsteterová E, Mattusch J, Wennrich R (2002) Sensors 2:1
113. Labuda J, Bucková M, Jantová S, Stepánek I, Surugiu I, Danielsson B, Mascini M (2000) Fresenius J Anal Chem 367:364
114. Wang J, Kawde AN, Sahlin E (2000) Analyst 125:5
115. Wang J, Kawde AN, Erdem A, Salazar M (2001) Analyst 126:2020
116. Wang J, Kawde AN (2001) Anal Chim Acta 431:219
117. Matyshevska OP, Karlash AY, Shtogun YV, Benilov A, Kirgizov Y, Gorchinskyy KO, Buzaneva EV, Prylutskyy YI, Scharff P (2001) Mater Sci Eng C 15:249
118. Buzaneva E, Karlash A, Yakovkin K, Shtogun Y, Putselyk S, Zherebetskiy D, Gorchinskiy A, Popova G, Prilutska S, Matyshevska O, Prilutskyy Y, Lytvyn P, Scharff P, Eklund P (2002) Mater Sci Eng C 19:41
119. Dovbeshko GI, Repnytska OP, Obraztsova ED, Shtogun YV (2003) Chem Phys Lett 372:432
120. O'Connell MJ, Boul P, Ericson LM, Huffman C, Wang Y, Haroz E, Kuper C, Tour J, Ausman KD, Smalley RE (2001) Chem Phys Lett 342:265
121. Wang G, Xu JJ, Chen HY (2002) Electrochem Commun 4:506
122. Guo M, Chen J, Nie L, Yao S (2004) Electrochim Acta 49:2637
123. Wang J, Kawde AN, Musameh M (2003) Analyst 128:912
124. Wang J, Li M, Shi Z, Li N, Gu Z (2004) Electroanalysis 161:140
125. Xu Y, Jiang Y, Cai H, He PG, Fang YZ (2004) Anal Chim Acta 516:19
126. Pedano ML, Rivas GS (2004) Electrochem Commun 6:10

Top Curr Chem (2005) 260: 37–56
DOI 10.1007/128_003

Published online: 16 September 2005

Immobilization of Oligonucleotides for Biochemical Sensing by Self-Assembled Monolayers: Thiol-Organic Bonding on Gold and Silanization on Silica Surfaces

F. Luderer (✉) · U. Walschus

Neubrandenburg University of Applied Sciences, Department of Technology, Fachhochschule Neubrandenburg, Brodaer Strasse 2, D-17033 Neubrandenburg, Germany
luderer@fh-nb.de

Abstract The covalent immobilization of biomolecules on surfaces is of great interest for many medical and bioanalytical applications. Currently, there is a wide range of procedures available for the modification of surfaces to achieve covalent immobilization. Self-assembled monolayers (SAMs) are easy to generate, offer a high level of flexibility and can be precisely modified on a molecular level. Therefore, the use of SAMs for various fields in research and commercial applications is increasing fast. One of the most interesting applications is the utilization of such layers for the attachment of biomolecules. The emphasis of this review is the discussion of different aspects of uniform, mixed, and functionalized monolayers regarding their use for the immobilization of biological recognition molecules such as oligonucleotides (DNA, RNA) in comparison to proteins (especially antibodies and receptor molecules) for bioanalytical applications. In doing so, we focus on the generation of self-organizing monolayers either on smooth gold surfaces by attachment of thiol compounds or on silica surfaces by silanization.

Keywords Antibodies · DNA · Self-assembled monolayers (SAMs) · Silanization · Thiol-organic compounds

Abbreviations

Å	angstrom (metric unit)—Ten billion angstroms equal 1 meter
APTMS	3-aminopropyltrimethoxysilane
APTES	3-aminopropyltriethoxysilane
AFM	atomic force microscopy
ELISA	enzyme-linked immunosorbent assay
FMOC	9-fluorenylmethoxycarbonyl
FT-IR	Fourier transform infrared spectroscopy
GMBS	*N*-(γ-maleimidobutyryloxy)succinimide ester
HSAB	*N*-hydroxysuccinimidyl-4-azidobenzoic acid
NHS	*N*-hydroxysuccinimide ester
PEG	poly(ethylene glycol)
QCM	quartz crystal microbalance
SAM	self-assembled monolayer
SCE	saturated calomel electrode
SNOM	scanning near field optical microscopy
SPM	scanning probe microscopy
SPR	surface plasmon resonance
STM	scanning tunneling microscopy
Sulfo-SMCC	sulfosuccinimidyl 4-*N*-maleimidomethyl cyclohexane-1-carboxylate
THF	tetrahydrofuran
TMOS	tetramethylorthosilicate
XPS	X-ray photoelectron spectroscopy

1 Introduction

Many applications, especially the use of biochemical sensing for bioanalytical methods, require the attachment of biomolecules on a suitable surface. A large number of procedures have been developed for this purpose, ranging from simple physiosorption to Langmuir–Blodget films to direct and covalent immobilization of biomolecules on surfaces using self-assembled monolayers or coupling on polymers. Each of these methods has its advantages and disadvantages. For example, adsorptive coupling (physiosorption) is still widely used today in bioanalysis for microtiter plate-based immunoassays (Enzyme-linked Immunosorbent Assays, ELISA) and for test strips. In both test formats, a regeneration of the immobilized component (antibody molecules) is not necessary. On the other hand, if a higher functional availability of the biomolecules is needed together with the possibility of regeneration and a low susceptibility for nonspecific binding, as in the case of biosensors and biochips, it is very likely that covalent attachment will yield superior results over physiosorption. The main disadvantages of simple adsorption, like limited accessibility of the recognition sites of the biomolecules (for example due to interactions between the DNA bases or the Fab-region of antibodies with the surface) and desorption processes, can largely be avoided

with covalent coupling methods. Therefore, the emphasis of this review is the immobilization of recognition biomolecules on uniform or mixed functionalized monolayers, with a focus on the presentation of applications for bioanalytical purposes.

These monolayers form themselves spontaneously by adsorption of suitable components from a diluted solution directly onto a surface. The formation of ordered and orientated monomolecular layers by spontaneous adsorption from a diluted solution is called self-assembling, the respective layers are called self-assembled monolayers (SAM) or self-organized monolayers. In the first part of this review, the coating of surfaces with functionalized SAMs will be examined. After that, some aspects of the attachment of the biomolecules onto these SAM-modified surfaces will be discussed.

The selection of the substrate for immobilization depends on the intended application. For example, SAMs are often used for the development of biosensors with electrochemical, piezoelectric, or optical detection. Glass and silica are typical materials for optical sensors, whereas gold is preferred for electrochemical sensors because of its outstanding inert properties. On the other hand, only certain chemicals can be used to form self-organizing layers on these substrates. The combination of thiol compounds and gold is one of the best established combinations. In addition to that, in recent years carboxyl acid- and silicon-organic derivatives as well as diphosphonates have been examined on different metal oxide surfaces with the aim to establish procedures suitable for the formation of adhesive self-organizing layers. Therefore, an overview of self-assembled monolayers based on gold surfaces and thiol compounds on the one hand and silanization on silica surfaces on the other hand will be given in the following sections.

2
Formation of SAMs from Thiol Compounds on Gold Surfaces

A well researched and popular class of monolayers is based on the strong adsorption of thiols (R – SH), disulfides (R – S – S – R) and sulfides (R – S – R) onto metal surfaces. Although thiols, disulfides, and sulfides strongly align with a number of different metals like gold, silver, platinum, or copper, gold is usually the substrate of choice because of its inert properties and the formation of a well-defined crystal structure.

The generation of SAMs on such surfaces strongly depends on the crystalline morphology of the underlying metal. The crystallographic orientation of gold which yields the monolayer with the highest density and degree of regularity is that of Au(1,1,1) which is, therefore, the most used metal for the application of SAMs onto a gold substrate. The (1,1,1)-lattice orientation of gold is easy to obtain by applying gold films onto polished glass, silicon, or freshly cleaved mica. The thermal deposition of gold onto silicon wafers

is the most feasible method for the preparation of gold substrates. Using an intermediate layer of chromium (5–150 Å) [1] or titanium (~ 40 Å) [2] promotes the adhesion of gold on the silicon wafers. The preparation of an ultra-thin gold surface is described in detail elsewhere [3]. Briefly, gold is vapor deposited onto freshly split mica (the best known form being muscovite, $KAl_2(OH)_2AlSi_3O_{10}$). The mica is then bonded with the noncoated site onto a glass surface and later removed by exposure to tetrahydrofurane (THF). These "template-stripped" gold surfaces exhibit the same atomic flatness as the removed mica template.

Absence of impurities and contaminations from the gold substrate is preferable but not absolutely essential, because thiols are able to detach contaminating compounds from the gold due to the high affinity of the sulfur groups to gold [4]. A common procedure for the cleaning of gold surfaces is treatment with hot Piranha solution, a mixture of seven-parts concentrated sulfuric acid with three-parts 30% (v/v) hydrogen peroxide. The result of this treatment is a clean and hydrophilized gold surface. A less known and used cleaning method is the application of a shifting electric potential ranging from – 0.5 V to + 1.4 V with a saturated calomel electrode (SCE)-counter electrode in 0.5 M sulfuric acid. Outside this range, the monolayers tend to desorb, leaving a clean gold surface. Due to this reason, thiol-SAMs are only stable in a potential range of – 400 mV to + 1400 mV against a SCE-electrode. Pure gold has a characteristic anodic current peak at + 1.1 V and a single cathodic peak at + 0.9 V [5].

The characteristic of alkane thiols of exhibiting stability on gold electrodes only in a particular potential range is being examined by the group of Mirsky et al. [6] to achieve an electrically controllable immobilization of thiol-modified DNA probes. An array of sensors can be assembled by applying an adsorption potential to some of the electrodes while applying a desorption potential to the remaining electrodes. In that way, a stepwise construction of an array is possible by using variations of the adsorption and desorption potentials.

2.1 Nature of Thiol-SAM Formation

Thiols, sulfides, and disulfides are dissolved in a sufficiently pure solvent (in general, ethanol for nonpolar compounds and water for polar ω-substituted alkane thiols) and then applied onto the cleaned gold surface.

As a first step, the sulfur donor atoms align strongly with the gold (typical bond energy 126 kJ mol^{-1} [7]) and initiate the self-assembling process of the alkyl thiols on the gold surface. The respective bond between the sulfur and the gold is noncovalent. A novel structure is formed in which each sulfur atom is bonded coordinatively with three gold atoms, resulting in a lattice spacing of 0.4995 nm (as compared to an unmodified gold lattice with a spacing

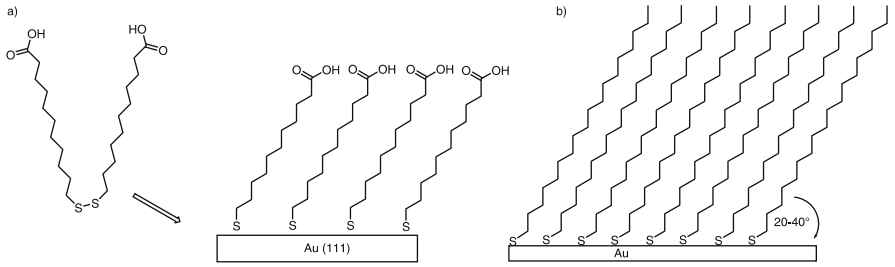

Fig. 1 S – S-bond cleavage of disulfides on gold (**a**) and tilting of thiol chains on gold (**b**)

of 0.2885 nm). Thiol groups are deprotonized ($RSH + Au \rightarrow RS - Au + e^- + H^+$) [8], and for disulfides the S – S-bond is cleaved during the process of adsorption (see Fig. 1a). The sulfur is in a sp^3-hybridized configuration, which is also the explanation for the tilting of the thiol chains from the surface level by 20–40° [9] (see Fig. 1b). Furthermore, the axis of the alkyl chains are twisted by approximately 55° against the surface level [2].

In a second step, the tail-tail interactions (nonbinding interactions such as van der Waals, repellent, steric, and electrostatic forces) between the molecules are responsible for the parallel alignment of the molecules on the gold surface. In doing so, the tail groups form a crystalline film. Above all, van der Waals forces between the methylene groups of the hydrocarbon chains are responsible for the orientation and stabilization of the monolayer. Porter et al. [10] demonstrated that long-chain alkane thiols (number of methylene groups $n > 10$) align themselves in a crystalline configuration. Chains with a length of fewer than ten methylene groups result in a monolayer structure which is less ordered and more labile. The two-step mechanism for the formation of SAMs which is described above is reflected by the two-phase formation kinetics of monolayers: the diffusion-controlled adsorption is followed by the slower crystallization process. Densely packed monolayers form themselves in less than one hour from a diluted solution of alkane thiols, but it can take several days until this monolayer reaches a well-ordered state.

It is difficult to compose a general protocol for the formation of thiol-based SAMs as the route of synthesis depends to a large degree on the desired features of the layers. Reaction factors to keep in mind for the achievement of a good monolayer are the selection of a suitable solvent, the duration of the formation process, and the concentration of the thiol compound. For example, it was found that the use of weaker solvents results in better thiol-based monolayers [11].

The terminal groups of the heterobifunctional thiol compounds are important for the interaction of the monolayers with biomolecules. For this purpose, several functionalized thiols are used to couple biomolecules with the monolayer, for example amino-, carboxyl- and hydroxyl-terminated thiols. As

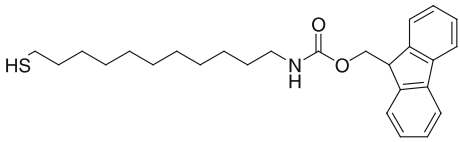

Fig. 2 *N*-FMOC-aminoundecanethiol ($C_{26}H_{35}NO_2S$ = 425.63)

long as the terminal groups (e.g. NH_2, OH) are relatively small (< 5 Å) [12], they have no or little influence on the orientation of the monolayers. In contrast, groups which are more sophisticated from a steric point of view (e.g. COOH, ferrocene) reduce the packing density and order of the monolayer. In a similar way, adsorption studies with asymmetric dialkane sulfides have demonstrated that the resulting monolayers show a lower density and degree of orientation compared to alkane thiol monolayers. In addition to this it is known for some functionalized thiol SAMs that their conformation depends on their chemical environment. A good example is a SAM with a terminal alkoxy-group which shows well-ordered structures when exposed to air. In contrast, the same monolayer is largely unordered in water and tetrachloromethane because the layer is penetrated by the respective solvent liquid [13].

It can prove to be useful to shield the nonthiolic functional group of heterobifunctional thiols prior to the SAM formation by using a protective group. For example, Brockmann et al. [14] used 11-amino-1-undecanthiols protected by a 9-fluorenylmethoxycarbonyl (FMOC) group for the formation of 11-amino-1-undecanethiol SAMs to prevent interaction between the amino groups and the gold surface during the formation of the SAM. The FMOC group can be removed under relatively mild conditions, for example by treatment with 20% piperidine/acetonitrile (v/v) for 30 min, resulting in the release of the original amino group (see Fig. 2).

A problem of prime importance for bioanalytical applications is the nonspecific binding of biomolecules on the substrate surface. SAMs with a negatively charged terminal group (like COOH groups) demonstrate good results regarding the suppression of such nonspecific binding effects. Effective reduction of nonspecific adsorption has been achieved for a wide range of peptides by the use of hydrophilic hexa(ethyleneglycol)-terminated SAMs [15].

2.2 Mixed SAMs

In addition to uniform monolayers formed by using a single thiol compound, mixed SAMs are increasingly used for the immobilization of biomolecules. The aim of combining different thiols is to avoid known disadvantages of uniform monolayers.

In principle, the molar ratio of different thiols in a mixed SAM is the same as their original molar ratio in the solution which was used for the formation. In other words, for a mixture of two thiol compounds which does not show demixing tendencies (phase segregation), a random attachment of both compounds onto the surface can be assumed [16]. This observation offers the potential to mix a ω-substituted alkane thiol with short-chain nonsubstituted thiols. As the result, anchor molecules are available for which steric hindrance is minimized (cf. Fig. 3).

Other possible applications of this behavior are the use of a component in a mixture of thiols which serves as a dilution reagent to control the density of reactive groups on the gold surface, or the use of a blocking component to suppress nonspecific binding of analytes on the surface. Herne et al. [17] created mixed SAMs from thiol-modified single-strand DNA (HS-ssDNA) and 6-hydroxyl-1-hexanethiol on a gold surface to reduce nonspecific binding of HS-ss-DNA (see Fig. 4).

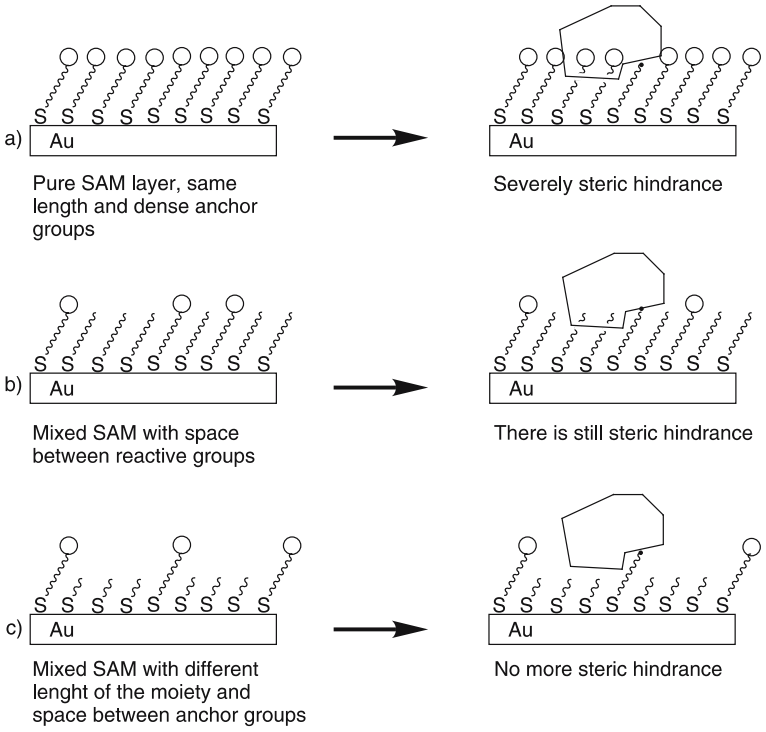

Fig. 3 Schematic illustration of different SAM layers: **a** A SAM layer with the same chain lengths and dense anchor groups leads to severe steric hindrance; **b** a mixed SAM with the same chain lengths but with space between reactive groups, there is still steric hindrance; **c** a mixed SAM with a different length of the moiety and space between anchor groups—no steric hindrance

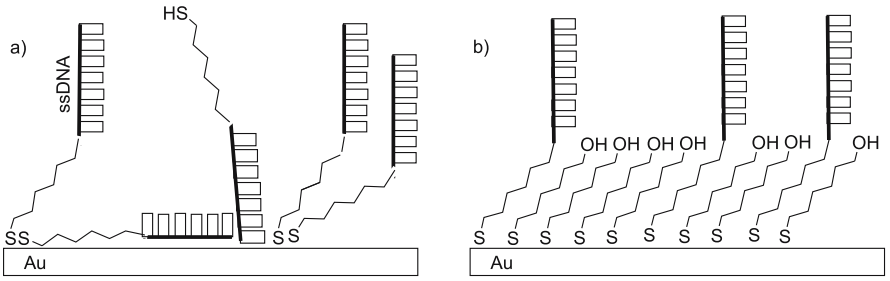

Fig. 4 A schematic illustration of pure and mixed SAMs: **a** thiol-derivatized single-stranded DNA only and **b** mixed SAM layer of thiol-derivatized single-stranded DNA and 6-hydroxy-1-hexanethiol

Instead of single-stranded DNA, double-stranded DNA with only one of the strands being coupled to a thiol-linker is immobilized in some applications. After a denaturating treatment, immobilized single-stranded probes are available for subsequent hybridization which are arranged in a better density and layout than probes after a simple ss-DNA immobilization protocol. For example, faster hybridization kinetics and a higher efficiency of double-strand coupling was demonstrated for DNA slides which were manufactured according to the ds-DNA immobilization procedure [18].

3 Silanization

In general, the silanization of hydroxyl-terminated substrates such as silica or glass is an effective method which is used quite often for chemical modification of the substrate surface for immobilization of biomolecules. The main focus for silanization procedures is once again the examination of the self-organizing silane-monolayers. The properties of the monolayer depend on the chemical structure of the silanization reagent, the density of silanol-groups which are available on the surface and the physical surface structure on a nano-scale level.

Principally, the main differentiation for uniform monolayers made by silanization is whether they are formed from long-chain or short-chain organosilanes. For long-chain silanes, a number of alkyltrichlorosilanes is described in the literature (for example 1-thioacetato-16-(trichlorosilyl)-hexadekane [19]), and for silanization with short-chain compounds several different alkyltrialkoxysilanes are used (for example 3-aminopropyltriethoxy-silane, APTES).

3.1 Formation of Silane-SAMs

The exact mechanism of silanization depends on the reaction conditions. It is generally accepted that silanization in a liquid solution is a three-step process [20]. In a first step, the silanes mentioned before form silanetriols by hydrolyzation in the presence of water on the surface or in the solvent. These silanetriols attach themselves by physiosorption via hydrogen bonds onto the substrate surface. Subsequently, the silanol groups react with the free hydroxyl groups on the surface according to a S_N2 reaction mechanism (see Fig. 5).

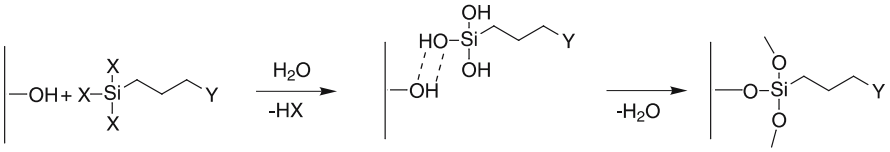

Fig. 5 Depictions of the silanization mechanism

As the quantity of free hydroxyl groups is often too low (for example, no more than 4 hydroxyl groups per nm^2 for glass [21]) to form more than one siloxane group on the surface, crosslinking of the molecules occurs because of the reactivity of unreacted silanol groups, resulting in an even stronger attachment of the layer on the substrate surface. Crosslinking is not possible for monoalkoxy- and monochlorosilanes. For this reason, these compounds cannot close the gaps between the hydroxyl groups on the surface. As a result, layers formed from monoalkoxy- and monochlorosilanes are more labile and less stable.

In general, the formation of monolayers with silanization reagents requires a precise reaction scheme regarding humidity, the selection of solvents, temperature, and reaction time. Often, not enough consideration is given to these factors. As a result a number of authors concluded that the reproducibility of homogeneous silane-monolayers is insufficient, that their stability in aqueous solution is limited, or that they are prone to the formation of multilayers.

3.2 Trialkoxysilanes

Among functionalized silanes, trialkoxysilanes are used most often for immobilization purposes (see Fig. 6).

Because of their short carbon chain (propylene spacer) they have a lower tendency for self-organization than alkyltrichlorosilanes with longer chains. In addition to that, the introduction of a terminal amino group (as for example with APTES) also reduces the uniformity of the monolayer because of

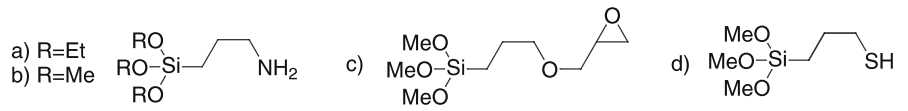

Fig. 6 Common silanizing trialkoxysilanes that promote covalent DNA immobilization: **a** 3-aminopropyltriethoxysilane (APTES) **b** 3-aminopropyltrimethoxysilane (APTMS) **c** 3-glycidoxypropyltrimethoxysilane (GOPS) **d** 3-mercaptopropyltrimethoxysilane (MPTS)

hydrogen bonds between the amino group and the silanol groups (SiOH) on the surface [22, 23]. Another possible source of interference is polymerization of the silane molecules with each other prior to attachment on the substrate surface, initiated by too much water in the reaction medium [24].

Despite all of these problems and possible challenges, short-chain alkylalkoxysilanes have a wide range of use for various tasks in research and commercial applications, mainly because they are readily available, cost-effective and easy to use. Nonetheless, the formation of well-defined monolayers from short-chain functionalized silanes can be achieved by precise control of the concentration of the silanization reagent, the reaction time and the water concentration in the reaction medium [24]. Of equal importance for the creation of dense monomolecular silane films is the cleaning and pre-activation of the substrate [25]. The physical and chemical properties of the untreated silica surface depend heavily on its previous treatment. Depending on the production process and storage conditions, siloxane bonds can be found instead of silanol groups. It is, therefore, important to pre-treat the surface of the carrier material with acids and bases to remove contaminants and impurities and to ensure that only free silanol groups are found on the surface [26]. A number of very different protocols for silanization can be found in the literature. An example for silanization with APTES is given here. The cleaned and preactivated silica substrate is dipped into a solution of 1% (v/v) of APTES in a mixture of 95% acetone with water for 15 min. Subsequently, the substrate is washed with acetone in five cycles with five minutes per cycle. After that the substrate is dried for 45 min at 110 °C [27]. During the drying step, crosslinking of the APTES molecules occurs via the free silanol groups. This reduces hydrolysis of the silane film in subsequent applications [28].

Similar to thiol SAMs, nonspecific interactions can be reduced by mixing PEG-terminated silanes into the monolayer. Another simple method is rinsing of the silanized surface with Tween 80 after the preparation [29].

A new class of trialkoxy-, respectively dialkoxysilanes, developed and sold by Wacker-Chemie GmbH [30], offers a number of functional groups which are of interest for coupling biomolecules, for example amino-, glycidoxy-, sulfur- and methacryloxy-groups. These new compounds offer an interesting alternative to the classic and conventional trialkoxysilanes which are currently widely used. For these so-called α-silanes, the propylene group be-

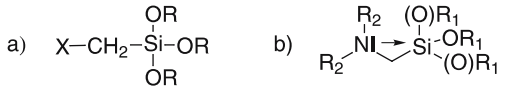

Fig. 7 A new class of trialkoxysilanes: **a** α-silanes. **b** Backbonding by α-silanes

tween the silicon atom and the functional group is replaced by a methylene group (see Fig. 7a).

This small change has a significant influence on the chemical properties of the silanes, with a substantial increase of the reactivity of the Si-alkoxy groups being the most important change. This increase in reactivity is the result of interactions between the functional group and the silicon atom. An electronegative donor like nitrogen or oxygen in the α-position to the silicon atom, only separated by the methylene group, activates the alkoxy groups which are bound to the silicon atom (see Fig. 7b). An explanation for this effect is the backbonding of the free electron pair of the nitrogen atom, resulting in a weakening of the Si – O-bond. The backbonding increases with increasing basicity of the nitrogen atom, and the basicity of the nitrogen atom can be selectively controlled by its organic substituents. The increased reactivity can be observed with nucleophilic reagents, for example by a faster hydrolysis in the presence of water. This results in a faster and more simplified immobilization procedure. Another possibility is that dialkoxysilanes, which have limited significance until now due to their low reactivity compared to trialkoxysilanes, are now of increased interest for immobilization purposes. On the other hand it remains to be seen whether the short carbon backbone, which is even shorter than for the conventional short-chain trialkoxysilanes, has negative effects for the self-organization abilities of these compounds.

3.3
Mixed Silane Monolayers

As described earlier for thiol-based SAMs on gold surfaces, the use of mixed or hybrid monolayers consisting of two or more silanes is possible to improve the properties of the transducer layer regarding the immobilization of biomolecules. For example, a hybrid layer of APTMS [$(CH_3O)_3Si(CH_2)_3NH_2$] and TMOS [$Si(OCH_3)_4$] yields a higher DNA binding density than pure APTMS monolayers [31]. In contrast to mixed thiol-SAMs, the usable range for the mixture ratio of both components is known to be restricted. An excessive quantity for one of the mixture components often leads to the quick formation of nanocrystalline siloxane particles which interfere with the formation of a monolayer. The probable reason for this observation is the different crosslinking behavior of different silanes.

4
Immobilization of Cognitive Biomolecules on SAMs

For the immobilization of biomolecules onto the functionalized surfaces, a wide range of different coupling reagents and methods is available [32]. Defining some general conditions and requirements prior to immobilization is helpful to find and optimize the best suited and most feasible way for the specific application in mind.

4.1
Immobilization Using Covalent Binding

In general, biomolecules offer many functional groups which are suitable for coupling purposes (for example NH_2, COOH), or it is often easy to add such groups by chemical modifications (for example NH_2-functionalization using a spacer at the 5′- or 3′-end of oligonucleotides). Using these moieties, a biomolecule can be coupled covalently by its functional groups to SAMs by a large number of suitable coupling compounds and reactions. A selection of such procedures is given in Table 1. When choosing such a method, it has to be kept in mind that the reaction should not interfere with the functionality of the biomolecules.

It is also possible to modify the functional groups of the monolayer prior to coupling of the biomolecules. For example, a SAM with terminal amino groups can be modified to exhibit carboxyl groups by exposure to succinic acid anhydride. However, in most situations heterobifunctional, respectively homobifunctionalized molecules are introduced between the modified surface and the biomolecules. This results in a larger distance and more flexibility between the biomolecule and the surface, which often increases the availability of the biological recognition function of the biomolecule [34].

The following examples are taken from the literature for homobifunctional crosslinkers. Homobifunctional crosslinkers carry two functional groups of

Table 1 Some methods for covalent coupling of biomolecules onto functionalized surfaces

Anchor group	Binding partner	Reaction
– COOH	– NH_2	via carbodiimide
epoxide	– NH_2, – SH, – OH	direct [33]
– NH_2	– NH_2	glutaraldehyde
acid hydrazide	– CHO	direct
– COR	– NH_2	reductive amination
– OH	– NH_2	with bromcyane
chloromethyl group	– NH_2	direct

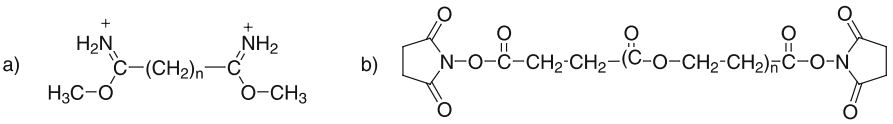

Fig. 8 Examples of homobifunctional crosslinkers: **a** bisimidate; and **b** *N*-hydroxysuccinimide ester

the same type within their molecular structure. One such substance with a rather simple structure is glutaraldehyde which has two aldehyde groups and a spacer length of five carbon atoms between those groups. A reagent with a similar spacer length is 1,4-phenylendiisothiocyanate which also reacts with primary amino groups. Additional examples for homobifunctional crosslinkers include bisimidates with varying chain lengths (ranging from dimethylsuccinimidate with $n = 2$ to dimethylsecacimidate with $n = 8$) and succinimide esters, also with different sizes and structures (for example, the spacer length for $n = 2$ is 16.1 Å) (see Fig. 8).

A special form of homofunctional linking utilizes so called dendrimers. Dendrimers are nanospherical structures for which the exact size depends on the number of branching points and which carry reactive functional units in their periphery (for example aldehyde-, thiol-, epoxy groups etc). The structure of dendrimers is similar to a tree, and their ramifications consist of repetitive units. It should be noted that their size is limited due to the fact that the packing density of their terminal groups increases. With increasing size, their macroscopic structure approximates the form of a sphere.

For example, if the initiatory core has three reactive groups and a branching is generated during a synthesis sequence with two new reactive groups then the total number of reactive groups is six after this first step (generation 0). In the next generation the number already increases to 12, and so forth. In other words, an exponential increase in the number of terminal groups can be observed. Only a few steps are required to generate large and complex molecules. Jean Francois et al. [35] demonstrated that DNA microarrays could be generated by using dendrimer-based linking of modified DNA probes on a functionalized glass slide, resulting in microarrays with a higher reliability and sensitivity compared to microarrays prepared by conventional linking via spacer molecules with a linear structure. Starting from hexachlorocyclo-triphosphazene ($N_3P_3Cl_6$) as a central core, they used 4th generation dendrimers with 96 active aldehyde groups and a size of 75 Å (see Fig. 9).

These dendrimers were then used to achieve a stable coating of aminosilanized glass surfaces with NH_2-modified DNA-probes (see Fig. 10). DNA chips which were prepared according to this procedure exhibited several advantages regarding the signal-to-noise ratio and their reliability over commercial chips prepared by conventional linking.

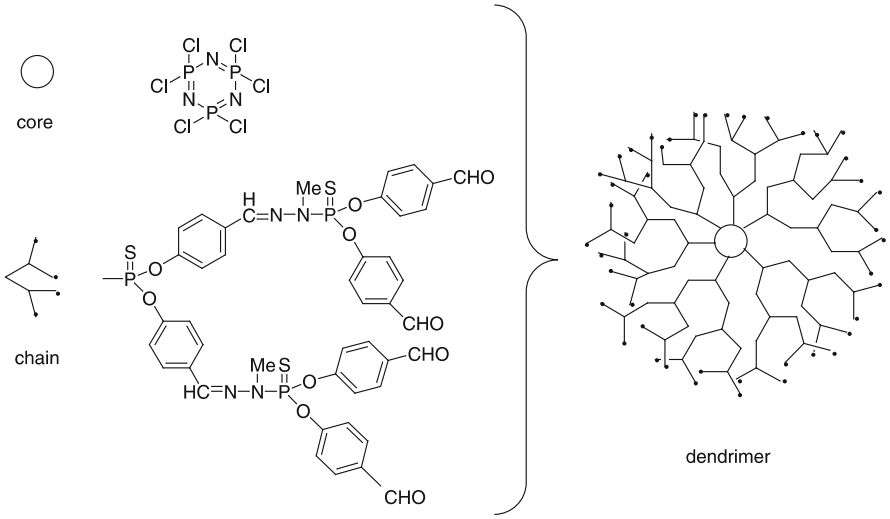

Fig. 9 Special homofunctional crosslinker-dendrimer: an initiatory core is extended through a number of branding reactions to form a dendrimer

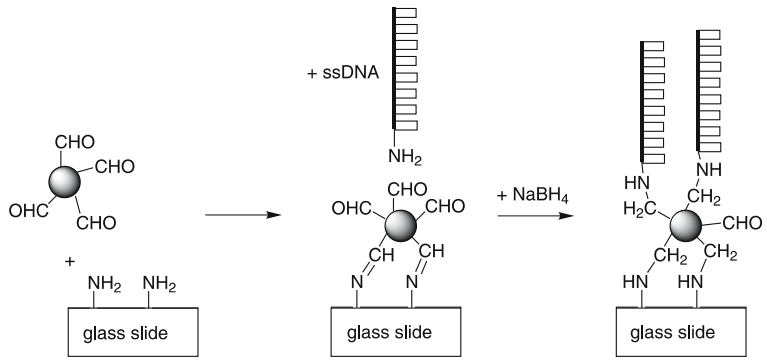

Fig. 10 Dendrimer-based linking of modified DNA probes on a functionalized glass slide

In the following, a small selection of heterobifunctional crosslinking reagents is indicated. Sulfosuccinimidyl 4-(*N*-maleimidomethyl)cyclohexane-1-carboxylate (Sulfo-SMCC) is a water-soluble heterobifunctional crosslinking reagent with one *N*-hydroxysuccinimide ester (NHS) and one maleimide group each within the same molecule. NHS-esters react with primary amino groups at a pH of 7–9, and the maleimide group reacts with sulfohydryl groups at pH 6.5–7.5 [36]. Another heterobifunctional cross-linking agent is *N*-(γ-maleimidobutyryloxy)succinimide ester (GMBS) which has a spacer length of seven atoms and which also exhibits a reactivity for amino- and sulfohydryl groups [37]. Usually, the coupling of this cross-linking reagent starts with a free amino group, resulting in the formation of an amide bond at

a pH of 6.5–8.5. In a second step, a molecule with a free sulfohydryl group is coupled via a thio-ether bond at pH 6.5–7.0. Another group of heterobifunctional covalent cross-linking reagents contains an NHS ester group as mentioned before and in addition to that an aryl azide functionality which can be photoactivated. The NHS ester group reacts with primary amino groups as described previously, and the photosensitive aryl group is activated by UV radiation in the range of 260–305 nm, resulting in the formation of short-lived nitrene compounds. These nitrenes are very aggressive and able to react with a C – H-bond. Examples of such substances include *N*-hydroxysuccinimidyl-4-azidobenzoic acid (HSAB), Lomant's reagent and sulfosuccinimidyl 2-(*m*-azido-*o*-nitrobenzamido)ethyl 1,3′-dithiopropionate (SASD) (see Fig. 11).

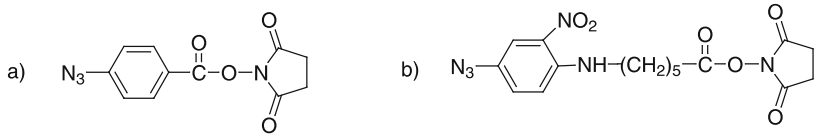

Fig. 11 Examples of heterobifunctional crosslinkers: **a** *N*-hydroxysuccinimidyl-4-azidobenzoic acid (HSAB) and **b** Lomant's reagent

Another possible strategy is the uniform immobilization for which the biomolecules are first coupled to bifunctional crosslinking chemicals or groups (for example by thiolation) and then applied directly onto the untreated surface [38]. However, this approach is not examined further within this article.

4.2 Immobilization Using Affinity Reactions

A coupling method which is used quite often is the binding between avidin (respectively streptavidin) and biotin. Streptavidin and avidin have a very high affinity for biotin ($K_d = 10^{-15}$ M). Therefore, this combination is a suitable method for the firm attachment of biomolecules onto surfaces. Usually, the biological component is coupled to the small biotin molecule, often via a flexible spacer. Such a biotinylated DNA oligonucleotide [39] or biotinylated antibody [40] then forms a strong bond with avidin or streptavidin on the SAM surface. The availability of the surface-bound avidin or streptavidin can be improved by the preparation of a biotinylated mixed monolayer for which long-chain coupling molecules are diluted with short-chain molecules [41] (see Fig. 12).

Avidin is a glycoprotein which was initially extracted from chicken egg white and which exhibits four deep binding pockets for biotin. Streptavidin is an analogous protein with a molecular weight of about 70 kD which is prepared from the recombinant bacteria strain *Streptomyces avidinii* and which

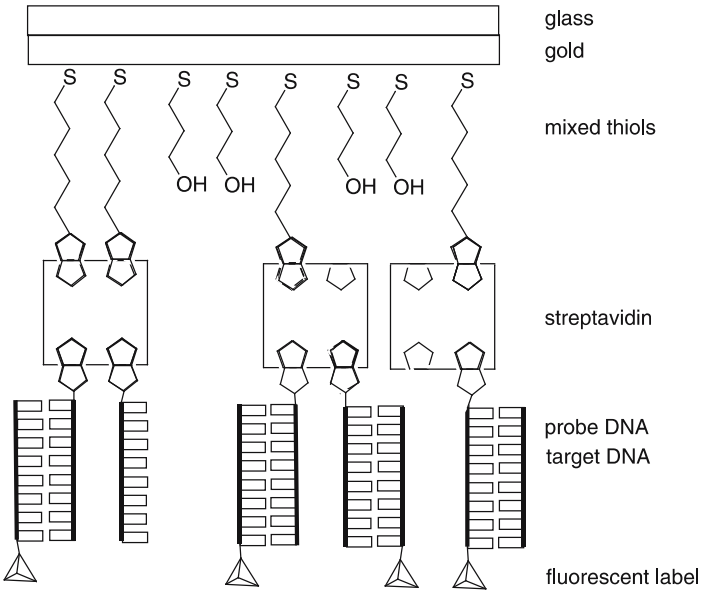

Fig. 12 Schematic illustration of immobilization strategy using affinity reactions via avidin-biotin coupling. Biotinylated mixed monolayers improve the availability of the surface-bound avidin or streptavidin to biotin coupled probe biomolecules

no longer possesses carbohydrate moieties. Although avidin and streptavidin are very similar in a number of ways, they also differ in some properties which are to be considered prior to using them for a specific application. For example, due to some physical characteristics of streptavidin a higher signal-to-noise ratio can be expected than for the combination of biotin with avidin. The solubility in water is significantly lower for streptavidin than for avidin, which in turn reduces nonspecific binding for a number of biomolecules.

The strong bond between biotin and avidin/streptavidin can only be released by extreme and often denaturating conditions. For a reversible binding based on this complex, D-desthiobiotin can be used instead of biotin (see Fig. 13). This conjugate can be separated at room temperature by exposure to an excess amount of biotin, respectively desthiobiotin [42].

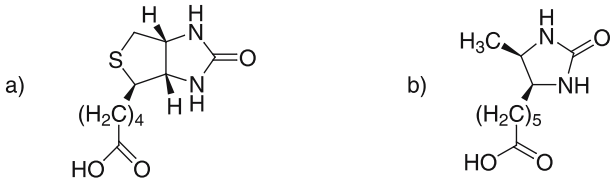

Fig. 13 Structural comparison of biotin (**a**) and desthiobiotin (**b**)

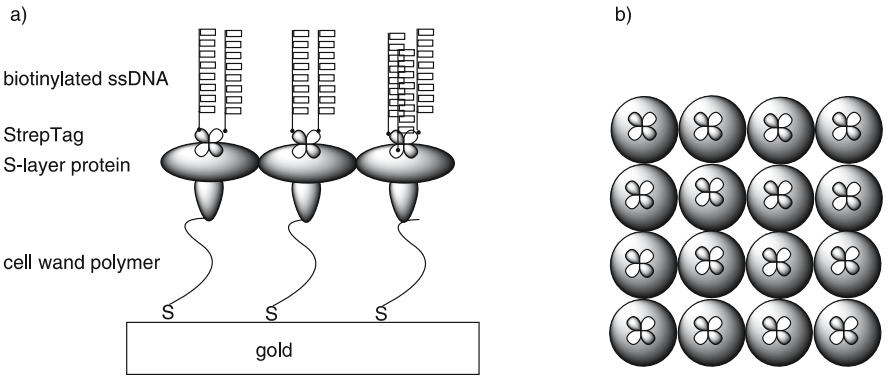

Fig. 14 A schematic illustration of an orientated immobilization strategy via crystallized S-layer proteins: **a** side view of the crystalline ordered S-layer proteins fused with the recognition center streptavidin for biotinylated biomolecules probes; **b** front view of the orientated and crystalline ordered S-layer proteins

A complex but interesting way for immobilization of cognitive biomolecules onto surfaces in a regular and dense layout is the use of so-called S-protein layers. S-layer proteins are originally found in the outermost cell boundary layer of many procaryotes and form crystalline monomolecular protein lattices. They can be functionalized by chemical or biotechnological methods. One such example is a S-layer protein which was fused with streptavidin and therefore recognizes biotinylated molecules. An orientated crystallization of the S-layer proteins is achieved by attaching the natural anchor molecule (the so-called cell wall polymer, a heteropolysaccharide) covalently to different functionalized surfaces. According to the principle of the lectin-carbohydrate-interaction, the S-layer proteins recognize the suitable cell wall polymer and crystallize in a predefined orientation, exposing the added functional sequence to the outside of the S-layer (see Fig. 14) [43, 44].

4.3 Immobilization via Ionic Binding

Immobilization of biomolecules onto SAM functionalized surfaces is also possible by electrostatic interactions. Most suitable for doing so are surfaces which are modified to exhibit amino- or carboxyl groups. For example, nucleic acids which carry negatively charged phosphate groups can be coupled to SAMs with protonized amino groups. Glenn et al. [45] used carboxyl-terminated monolayers to couple an enzyme via poly-L-lysine using electrostatic interactions (see Fig. 15).

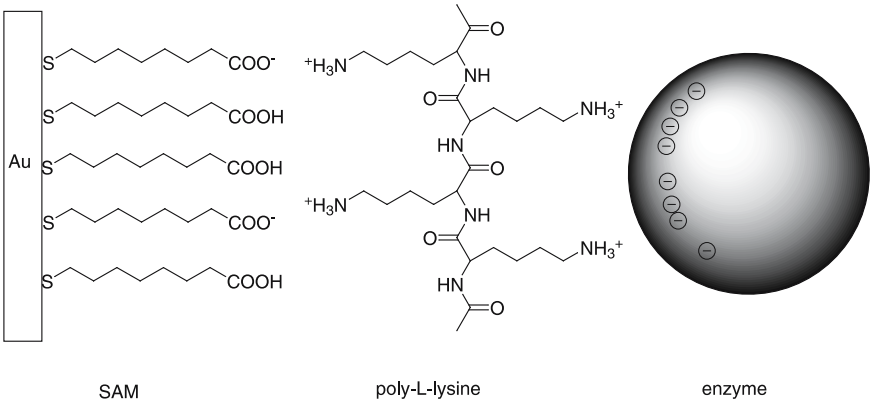

Fig. 15 Carboxyl-terminated monolayer couples an enzyme via poly-L-lysine

5 Characterization, Imaging, and Measurement

A number of methods are available for the characterization and examination of SAMs as well as for the observation of the reactions with the immobilized biomolecules. Only some of these methods are mentioned briefly here. These include surface plasmon resonance (SPR) [46], quartz crystal microbalance (QCM) [47, 48], ellipsometry [12, 49], contact angle measurement [50], infrared spectroscopy (FT-IR) [51, 52], Raman spectroscopy [53], scanning tunneling microscopy (STM) [54], atomic force microscopy (AFM) [55, 56], sum frequency spectroscopy, X-ray photoelectron spectroscopy (XPS) [57, 58], surface acoustic wave and acoustic plate mode devices, confocal imaging and optical microscopy, low-angle X-ray reflectometry, electrochemical methods [59] and Raster electron microscopy [60].

A deeper understanding about the kinetics of the adsorption of alkane thiols was possible due to the application of SPR and QCM because these methods allow for real-time monitoring of the attachment processes [61]. For the examination of the chemical structure of monolayers (e.g. concentration of their elements, their chemical environment) XPS [62] and FT-IR [63] methods have been used. Contact angle measurements [64] provided insight into the properties of the outermost side of the monolayers. For example, methyl-terminated SAMs exhibit large contact angles with water while small contact angles are observed for carboxyl- and hydroxyl-terminated monolayers with water. This behavior can be used to detect the successful coating of surfaces with compounds carrying such groups. With electrochemical methods [5] it is easily possible to detect so-called pinholes in monolayers on gold surfaces. For a precise surface analysis on a single molecule level for a better understanding of the interactions between the immobi-

lized biomolecules and the surface as well as other biological components, scanning probe microscopy has proven to be useful. SPM methods include technologies like AFM, STM as well as scanning near field optical microscopy (SNOM) and are reviewed elsewhere in more detail regarding their application for the analysis of biological interfaces [65].

References

1. Aqua T, Naaman R, Daube SS (1993) Langmuir 19:10573
2. Nuzzo RG, Dubois LH, Allara DL (1990) J Am Chem Soc 112:558
3. Wagner P, Hegner M, Kernen P, Zaugg F, Semenza G (1996) Biophys J 70:2052
4. Keller H, Schrepp W, Fuchs H (1992) Thin Solid Films 210/211:799
5. Finklea HO, Avery S, Lynch M, Furtsch T (1987) Langmuir 3:409
6. Riepl M, Wolfbei OS, Mirsky M (1999) Mikrochim Acta 131:29
7. Schreiber F (2000) Prog Surf Sci 65:151
8. Widrich CA, Chung C, Porter MD (1991) J Electroanal Chem 310:335
9. Doblhofer K (1992) Langmuir 8:1811
10. Porter MD, Bright TB, Allara DL (1987) J Am Chem Soc 109:3559
11. Kepley LJ, Crooks RM, Ricco AJ (1992) Anal Chem 64:3191
12. Chidsay CED, Loiacono DN (1990) Langmuir 6:682
13. Zolk M, Eisert F, Pipper J, Herrwerth S, Eck W, Buck M, Grunze M (2000) Langmuir 16:5849
14. Brockmann JM, Frutos AG, Corn RM (1999) J Am Chem Soc 121:8044
15. Mrksich M, Sigal GB, Whitesides GM (1995) Langmuir 11:4383
16. Bain CD, Whitesides GM (1989) J Am Chem Soc 111:7164
17. Herne TH, Tarlov MJ (1997) J Am Chem Soc 119:8916
18. Peterson AW, Heaton RJ, Georgiadis RM (2001) Nucl Acid Res 29:5163
19. Balachander N et al (1990) Langmuir 6:1621
20. Sagiv J (1980) J Am Chem Soc 102:92
21. PCT patent WO 99/20640 (1999)
22. Bierbaum K, Kinzler M, Wöll C, Grunze M, Hähner G, Heid S, Effenberger F (1995) Langmuir 11:512
23. Horr TJ, Arora Ps (1997) Colloids Surf A 126:113
24. Hu M, Noda S, Okubo T, Yamaguchi Y, Komiyama H (2001) Appl Surf Sci 18:307
25. Cras JJ, Rowe-Taitt CA, Nivens DA, Ligler FS (1999) Biosens Bioelectron 14:683
26. Halliwell CM, Cass AEG (2001) Anal Chem 73:2476
27. Möller R, Csáki A, Köhler M, Fritsche W (2000) Nucl Acids Res 28:1
28. Naviroj S, Culler R, Koenig JL, Ishida H (1984) J Colloid Interface Sci 97(2):308
29. Vandenberg E, Elwing H, Askendal A, Lundström I (1991) J Colloid Interface Sci 143:327
30. www.wacker.com: Geniosile®
31. Saal K, Tätte T, Kink I, Kurg A, Lõhmus R, Mäeorg U, Rinken A, Lõhmus A (2003) Surf Sci 532–535:1085
32. Hermanson GT (1996) Bioconjugate Techniques. Academic Press, San Diego
33. Hang CT, Guiseppi-Elie A (2004) Bios Bioelectron 19:1537
34. Rusin KM, Fare TL, Stemple JZ (1992) Biosens Bioelectron 7:367
35. Berre LV, Trevisiol E, Dagkessamanskaia A, Sokol S, Caminade AM, Francois J (2003) Nuc Acid Res 31:16

36. Mattson G et al (1993) Mol Bio Rep 17:167–183
37. Radtke SM, Alocilja EC (2005) Biosens Bioelectron 20:1662
38. Berggren B, Stalhandske P, Brundell J, Johansson G (1999) Electronanalysis 11:156
39. Schumaker-Parry JS, Zaraie MH, Aebersold R, Campbell CT (2004) Anal Chem 76:918
40. Schmitt FJ, Häussling L, Ringsdorf H, Knoll W (1992) Thin Solid Films 210/211:815
41. Spinke J, Liley M, Schmitt FJ, Guder HJ, Angermaier L, Knoll W (1993) J Chem Phys 99:7012
42. US Patent 4,656,252; Anal Biochem (2002) 308:343
43. Mader C, Huber C, Moll D, Sleytr UB, Sára M (2004) J Bacteriol 186:1758
44. Pleschberger M, Saerens D, Weigert S, Sleytr UB, Muyldermans S, Sára M, Egelseer EM (2004) Bioconj Chem 15(3):664
45. Glenn JHD, Bowden EF (1996) Chem Lett 339
46. Mrksich M, Grunwell JR, Whitesides GM (1995) J Am Chem Soc 117:12009
47. Shimizu K et al (1992) Langmuir 8:1385
48. Schneider TW, Buttry DA (1993) J Am Chem Soc 115:12391
49. Ohtsuka T, Sato Y, Uosaki K (1994) Langmuir 10:3658
50. Bain C, Evall J, Whitesides GM (1989) J Am Chem Soc 111:7155
51. Sato Y, Ye S, Haba T, Uosaki K (1996) Langmuir 12:2726
52. Sato Y, Shimizu K, Yagi I, Uosaki K (1994) Bull Chem Soc Jpn 67:21
53. Bryan MA et al (1991) J Am Chem Soc 113:8284
54. Schonenberger C et al (1995) J Phys Chem 99:3259
55. Wibur JL (1995) Langmuir 11:825
56. Kienberger F, Mueller H, Pastushenko V, Hinterdorfer P (2004) EMBO reports 5:579
57. Bain CD et al (1988) J Am Chem Soc 110:3665
58. Laibinis PE et al (1991) J Phy Chem 95:7017
59. Finklea HO (1996) In: Electroanalytical Chemistry: A Series of Advances, Vol 19. Marcel Dekker, New York p 110
60. Strong L, Whitesides GM (1988) Langmuir 4:546
61. Karpovich DS, Blanchard GJ (1994) Langmuir 10:3315
62. Nuzzo RG, Zegarski BR, Dubois LH (1987) J Am Chem Soc 109:733
63. Truong KD, Rowntree PA (1995) Prog Surf Sci 50:207
64. Bain CD, Troughton EB, Tao YT, Evall J, Whitesides GM, Nuzzo RG (1989) J Am Chem Soc 111:321
65. Tiefenauer L, Ros R (2002) Colloid Surf B 23(2):95

Top Curr Chem (2005) 260: 57–75
DOI 10.1007/128_002

Published online: 16 September 2005

Preparation and Electron Conductivity of DNA-Aligned Cast and LB Films from DNA-Lipid Complexes

Yoshio Okahata (✉) · Takayoshi Kawasaki

Department of Biomolecular Engineering, Tokyo Institute of Technology, Nagatsuda, Midori-ku, 226 Yokohama, Japan
yokahata@bio.titech.ac.jp

Abstract We describe here a simple preparation of a DNA-lipid complex that is soluble in organic media, and preparations of DNA-aligned thin films from the cast-stretching method and the Langmuir–Blodgett (LB) method. The DNA-lipid complex in which counter cations of phosphate anions are changed to cationic lipophilic amphiphiles was prepared by simply mixing aqueous solutions of DNA and cationic amphiphiles. The DNA-lipid complex is soluble and forms a double-strand structure in organic solutions. A self-standing, water-insoluble DNA-lipid film could be prepared by casting from the organic solution or a hot-press method, and DNA strands were easily aligned in the film by stretching it in one direction. Another method of preparing DNA-aligned thin film is the LB method: anionic DNA strands are transferred with cationic lipid monolayers at the air-water interface by the vertical dipping method and DNA strands are aligned along the dipping direction. The film structure was confirmed by X-ray diffraction, CD spectra of DNA strands, and polarized absorption spectra of intercalated dye molecules. The aligned-DNA film showed a large anisotropic and ohmic electric current (10^{-3} S cm^{-1}, $A\perp/A// = 10^5$) along stacked base-pairs of DNA strands aligned in the film. The large anisotropic photo current could also be observed through DNA strands with acridine orange intercalators depending on visible photo irradiation.

Keywords Anisotropic electron conductivity · Cast film · DNA-lipid complex · Orientation · LB film

1 Introduction

DNA is a biopolymer having the primary structure of an alternating copolymer of phosphate and deoxyribose. The secondary structure of DNA is a rod-like, stereo-chemical double helical structure with π-electron-rich base-pair stacking: the base distance is 3.4 Å while the diameter of the helix is about 20 Å [1] (Fig. 1). These stereo regular structures are interesting as naturally-occurring molecular materials. DNA shows structural polymorphism in aqueous solution. In the usual aqueous solution, DNA forms a B-form due to the hydration of water molecules to the minor grooves of dsDNA. When ethanol or NaCl is added to the solution, the hydration is lost and DNA reversibly turns to the A- or C-form (Fig. 1b). Flat molecules having both two or three conjugated aromatic rings and positive charges, such as ethidium bromide, proflavine, and safranine T, are known to intercalate between base pairs of dsDNA (Fig. 1c).

DNAs are soluble only in aqueous solutions and their fibrous crystals can be prepared by slow evaporation from the aqueous solution. Duplex structures in the fibers have been studied by X-ray diffraction [2, 3] and solid state NMR [4–6]. Orientation of DNA strands by using hydrodynamic flow gradients in the dilute aqueous solution [7, 8] and lyotropic liquid crystal

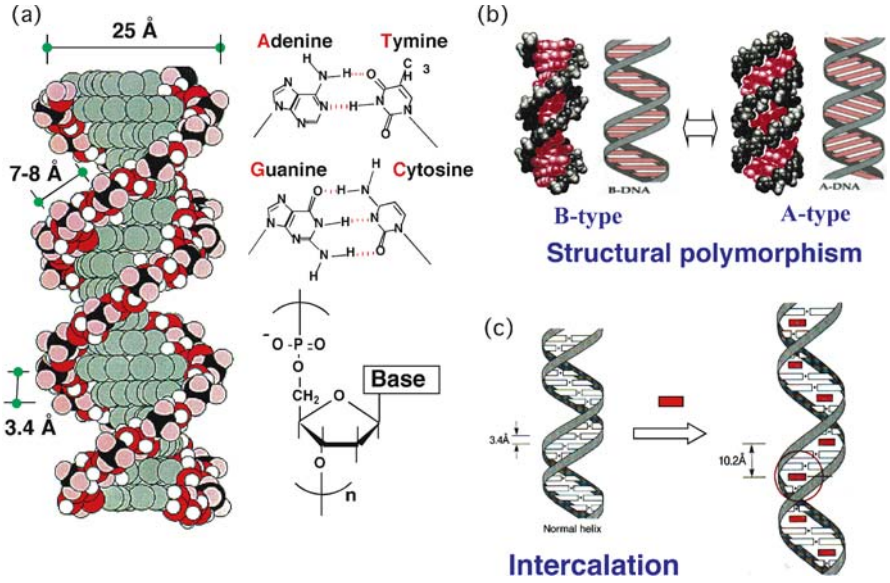

Fig. 1 **a** DNA structures, **b** polymorphism of DNA, and **c** intercalation of dye molecules into DNA

properties of rod-like DNA in the concentrated aqueous solution [9] have been investigated. Water molecules have been shown to play an important role in the internal conformation of DNA strands by interacting with minor grooves of DNA strands [10]. However, it is difficult to discuss effects of water molecules in aqueous media and fibers. If DNA strands can be solubilized in non-aqueous organic media, it is useful to study the effects of water molecules on the conformation of the DNA strands. If a self-standing film in which rod-like DNA strands are aligned in one direction could be prepared by a simple method, it would be of interest as a molecular material with an electron transfer field.

However, we have to solve two problems to use DNA as functional materials; the amount of purified DNA available and the solubility of DNA. In the molecular biology field, DNA is treated usually on the mug scale and we need DNA at the 100 g or 1 kg scale for use as materials. As a second problem, DNA is soluble only in an aqueous solution and DNA should be modified to be soluble in organic solvents or to melt under moderate heating in order to form a film or fiber for use as materials.

We describe here a simple preparation of a DNA-lipid complex that is soluble in organic media, and preparations of DNA-aligned thin films from the cast-stretching method and the LB method. The DNA-lipid complex in which counter cations of phosphate anions are changed to cationic lipophilic amphiphiles was prepared by simply mixing aqueous solutions of DNA and cationic amphiphiles (see Fig. 1). The DNA-lipid complex is soluble and forms a double-strand structure in organic solutions. A self-standing, water-insoluble DNA-lipid film could be prepared by casting from the organic solution, and DNA strands were easily aligned in the film by stretching it in one direction. Another method of preparing DNA-aligned thin films is the LB method: anionic DNA strands are transferred with cationic lipid monolayers at the air-water interface by the vertical dipping method and DNA strands are aligned along the dipping direction. The film structure was confirmed by X-ray diffraction, CD spectra of DNA strands, and the polarized absorption spectra of intercalated dye molecules. The aligned-DNA film showed a large anisotropic and ohmic electric current (10^{-3} S cm^{-1}, $A\perp/A// = 10^5$) along stacked base-pairs of DNA strands aligned in the film. The large anisotropic photo current could also be observed through DNA strands with acridine orange intercalators depending on visible photo irradiation.

2
Separation and Purification of Double-Strand DNA

We have purified natural double-strand DNA from salmon testes, in which anionic DNA complexes with cationic proteins of protamine. After mincing salmon testes, the homogenized solution was treated with protease in order

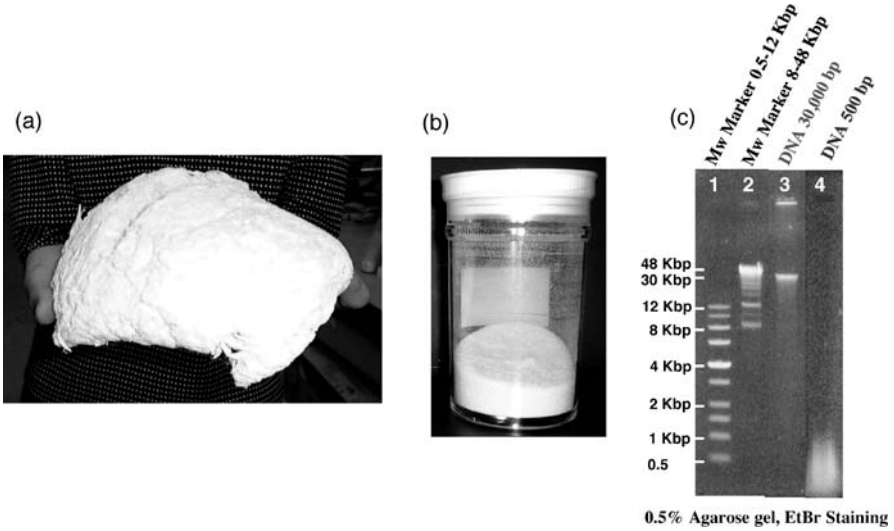

Fig. 2 **a** Purified cotton-like high-molecular-weight DNA (ca. 30 000 bps, 20 000 kDa, and 10 μm length per molecule), **b** purified powder-like low-molecular-weight DNA (ca. 500 bps, 300 kDa, and 0.2 μm length per molecule), and **c** their gel-shift assay (0.5% agarose gel, ethidium bromide staining)

to hydrolyze protamines, and SDS was added to precipitate the hydrolyzed cationic protamines. After centrifugation, the transparent aqueous solution of DNA was obtained. DNA was separated by the addition of excess ethanol. The obtained DNA occurred as cotton-like fibers; the protein content: less than 1%; the content of double strands: more than 90%; the average molecular weight: ca. 30 000 bps, $Mw = 2 \times 10^7$ Da: the average stretched length per molecule: 10 μm.

When proteases containing a small amount of DNase were employed, a low-molecular weight powder-like DNA could be obtained, in which the protein content was less than 1% and the content of double strands in DNA was more than 90%. The average molecular weight of the DNA was ca. 500 bps ($Mw = 3 \times 10^5$ Da) and the average stretched length per molecule was 0.2 μm. Photographs of two different DNAs and their gel-shift assay are shown in Fig. 2.

3
DNA-Lipid Complexes in Organic Solution

A DNA-lipid complex was prepared by simply mixing two aqueous solutions of DNA and cationic lipids as follows. An aqueous solution of DNA^-Na^+ from salmon testes (ca. 30 000 bps or 500 bps) and an aqueous solution of 1.1 eq. mol of cationic amphiphiles were mixed at room temperature and

polyion-complex precipitates were gathered by centrifugation and freeze-dried (Fig. 3). The white powder was solubilized in chloroform and reprecipitated to diethyl ether twice. The obtained DNA-lipid complex was confirmed by elemental analysis to form 1 : 1 complexes of a phosphate anion and the cationic amphiphile. The DNA-lipid complex was soluble only in organic solvents such as chloroform, benzene, and ethanol, but not in an aqueous buffer solution.

Figure 4 shows CD spectra of (a) the DNA-lipid complex in organic solution containing a small amount of water ($CHCl_3/EtOH/H_2O = 4 : 1 : 0.07$, 790 mM of H_2O), and (b) native DNA in an aqueous buffer solution (20 mM NaCl, 10 mM Tris, pH 7.8). The DNA-lipid complex shows a positive Cotton effect at 270 nm and a negative Cotton effect at 245 nm similar to native DNA in aqueous solution, which indicates the B-form structure for the DNA strands [11]. Thus, the DNA-lipid complex forms a double helical B-form

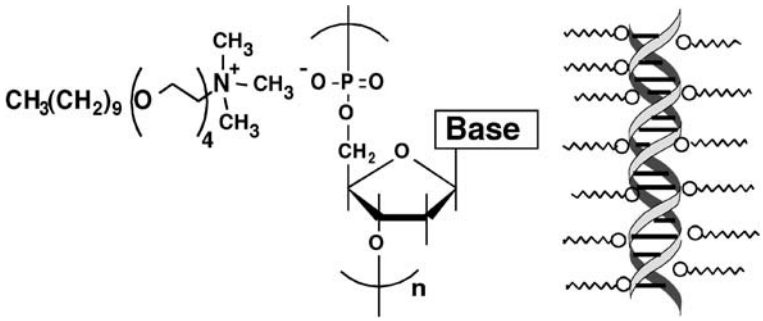

Fig. 3 A schematic illustration of a DNA-lipid complex

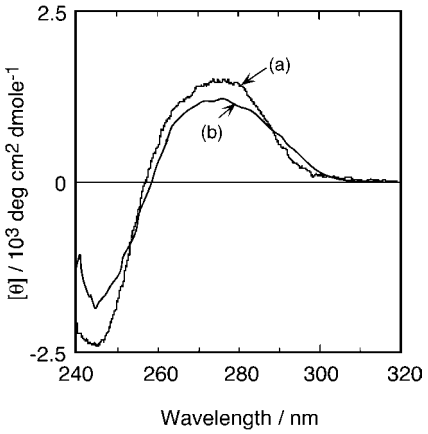

Fig. 4 CD spectra of **a** DNA-lipid complex in $CHCl_3/EtOH/H_2O = 4 : 1 : 0.07$, and **b** native DNA in aqueous buffer solution (20 mM NaCl, pH 7.8, 10 mM Tris, [DNA] = 50 $\mu M\,bp^{-1}$, 23 °C)

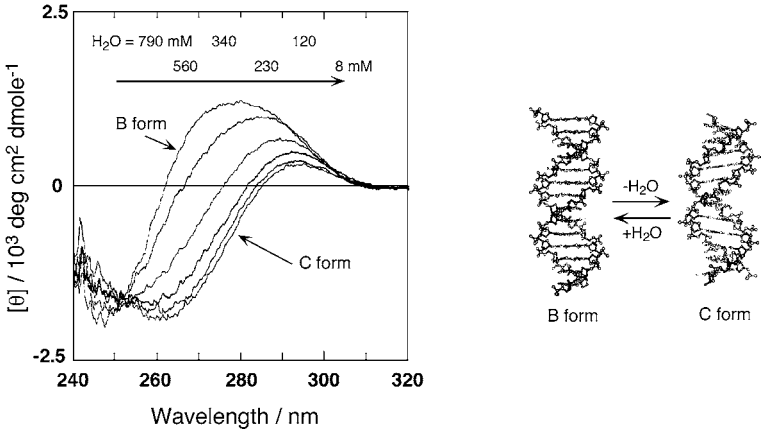

Fig. 5 Effect of water contents on CD spectra of the DNA-lipid complex in $CHCl_3$/EtOH (4 : 1) solution ([DNA] = 50 μM bp^{-1}, 23 °C)

structure even in an organic solvent similar to the native DNA in an aqueous solution.

Figure 5 shows the effect of water content in an organic solvent ($CHCl_3$/EtOH = 4 : 1, water content: 8–790 mM) on CD spectra. The positive Cotton effect at 270 nm was shifted to a longer wavelength and the θ value was decreased gradually with decreasing water content from 790 to 8 mM in the $CHCl_3$/EtOH solution. The CD spectrum of the DNA-lipid complex in the dry solution (8 mM of water) was similar to that of the C-form of native DNA strands in aqueous solution in the presence of a high salt content [12] or a high ethanol concentration [13]. Dickerson and coworkers reported that water molecules are important for the formation of the B-structures of DNA, in which water molecules interact with oxygen molecules of ribose and phosphate and a minor or major groove of the DNA strands [10]. Thus, the conformation of the DNA-lipid complex can be reversibly changed (B-form and C-form) by controlling the water content in an organic solution as for the native DNA depending on the salt and ethanol concentrations.

4
DNA-Aligned Cast Films from DNA-Lipid Complexes

The $CHCl_3$/EtOH/H_2O (4 : 1 : 0.07) solution of the DNA-lipid complex (0.25 g) was cast on a Teflon plate and the solvent was evaporated slowly under the saturated vapor at room temperature. The obtained self-standing film was (ca. 60 μm thick) water-insoluble, and physically stable (Fig. 6a). The DNA film can be obtained also from the hot-press method. Here, the powder of the DNA-lipid complex was hot-pressed at 120 °C for 1 min under

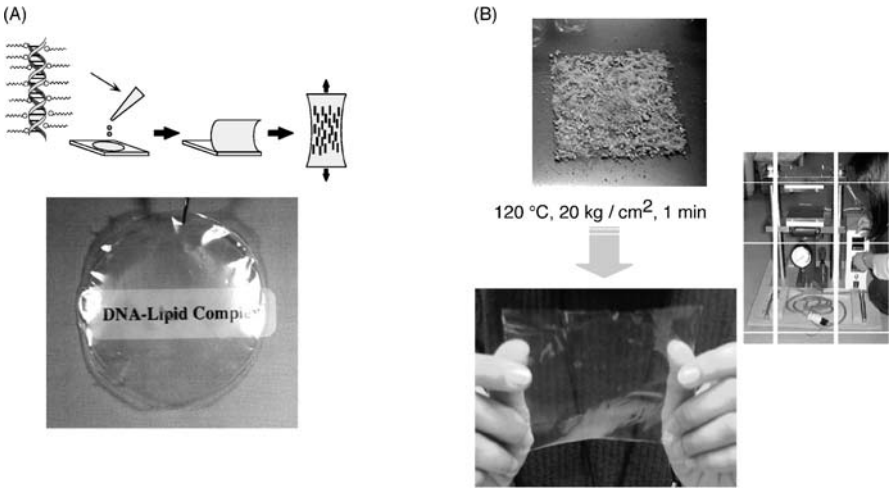

Fig. 6 A DNA-lipid cast film prepared from a solution of DNA-lipid complexes

20 kg cm^{-2} pressure by setting between two hot plates (Fig. 6b). The hot-press method is better suited for preparing a large, uniform, and thick film than the cast method.

4.1 X-ray Diffractions

Figure 7 shows X-ray diffraction patterns of an as-cast film of the DNA-lipid complex. When the incident beam was irradiated perpendicular to the film plane, a circular reflection of 41 Å was observed that corresponds to a DNA-lipid complex, in which the diameters of dsDNA are 25 or 20 Å for the B-form and A-form, respectively. When the beam was exposed parallel to the film plane (side-edge view), hexagonal spots with 41 Å spacing were observed. They indicate the DNA-lipid strands whose diameter is 41 Å and which aggregate into hexagonal close-packed structures in the film plane. Thus, aggregates of hexagonal-packed DNA-lipid strands are aligned on the film plane in random directions, as schematically shown in Fig. 7a.

The DNA-lipid cast film was stretched ca. three times in length (ca. 20 μm thick) in the wet state, and X-ray diffraction patterns are shown in Fig. 7b. When the incident beam was irradiated parallel to the top edge of the stretched film, the circular reflection of 41 Å was observed. When the beam was exposed parallel to the side edge and perpendicular to the film plane, the diffraction on the equator appeared as two spots of 41 Å indicating a distance between the DNA-lipid strands and the diffraction on the meridian of 3.4 Å. The distance between parallel stacked base-pairs was clearly observed [2–4]. These findings clearly show that DNA strands are aligned

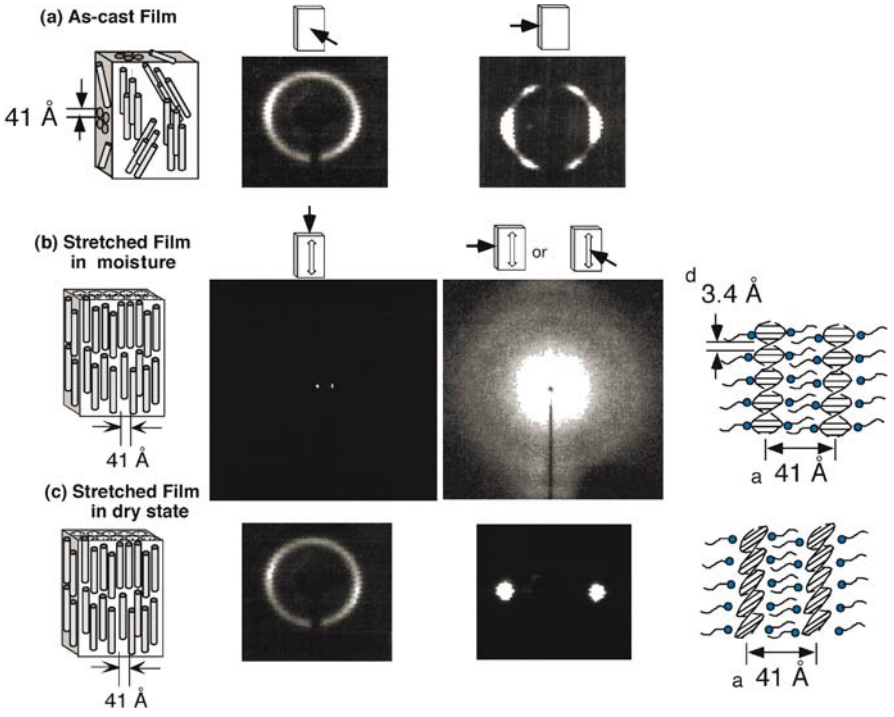

Fig. 7 X-ray diffraction patterns of **a** the as-cast film, **b** the stretched film of the DNA-lipid complex in water moisture, and **c** the stretched DNA-lipid film in the dry state. *Open, two-headed arrows* show the stretching direction of the film. *Closed arrows* show the incident beam of the X-rays. X-ray photographs of **a** and **c** were enlarged to show diffraction more clearly

parallel to the stretched direction in the film, and that base-pairs are stacked perpendicular to the direction of the DNA strands as shown in the illustration. Neither the diameter nor the distance between strands (41 Å) was affected by stretching.

When the stretched film was dried in air (simply applying a hair-dryer for 2 min), only diffraction on the equator as two spots of 41 Å was observed but not diffraction on the meridian for base-pairs (Fig. 7c). This suggests that the orientation of the base pairs is not perpendicular to the stretched direction, although the DNA strands are aligned parallel to the stretched direction. Figure 8 shows CD spectra of the cast film of the DNA-lipid complex in wet (a) and dry states (b). The CD spectrum of the wet film was consistent with a B-form structure of native DNA in fibers obtained from aqueous solution [1–3]. On the contrary, the CD spectrum in the dry state resembles the A-form of DNA in which the base pairs slant to the axis of the strands [2, 3]. These results are consistent with CD spectra of the DNA-lipid complex in an organic solution: DNA exists in the B-form in the presence of water and the C-form in the ab-

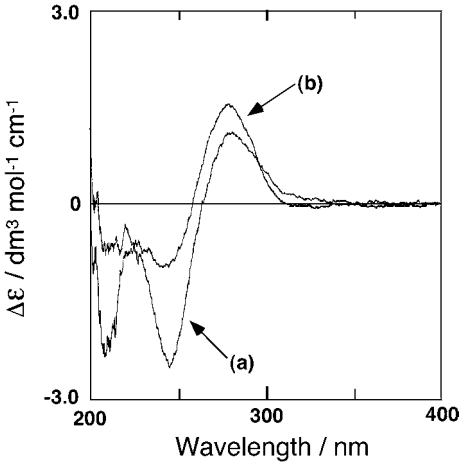

Fig. 8 CD spectra of the cast film of the DNA-lipid complex **a** in water and **b** in the dry state (23 °C, film thickness: 3 μM)

sence of water. The conformational changes between the B-form and A-form of DNA strands in the film dependent on water moisture were reversible.

4.2 Polarized Spectra of Intercalated Cast Film

When the stretched DNA-lipid film was soaked in an aqueous solution of ethidium bromide (λ_{max} = 480 nm) for a day at room temperature, the transparent film turned red (λ_{max} = 520 nm) and the aqueous solution became clear (Fig. 9a). Thus, the ethidium intercalated completely between base pairs of the DNA film. When the film was moved into the new aqueous buffer solution, the intercalated dye molecules were hardly removed from the film at least for a day. Similar intercalation behavior into the film was observed for other dyes such as proflavine, acridine orange, and safranine T [14–17].

Figure 9b shows polarized absorption spectra of ethidium intercalated in the stretched DNA-lipid film in water. The absorption at 520 nm of the light polarized perpendicularly to the stretched direction of the film was 3.3 times larger than that of the light polarized parallel to the stretched direction. In the case of the as-cast DNA-lipid film, there were no differences in absorption of the parallel and perpendicular light. The large dichroic ratio of $A\perp/A// = 3.3$ indicates that the intercalated dyes are aligned perpendicular to the stretched direction of the film: the DNA strands are aligned parallel to the stretched direction. The secondary order parameter (orientation moment) [18] of the DNA strands in the film was calculated to be ca. 0.7 from the $A\perp/A// = 3.3$. This value is close to the orientation of synthetic rod-like polymers such as poly(arylenes) prepared by a uniaxial stretching method [19, 20].

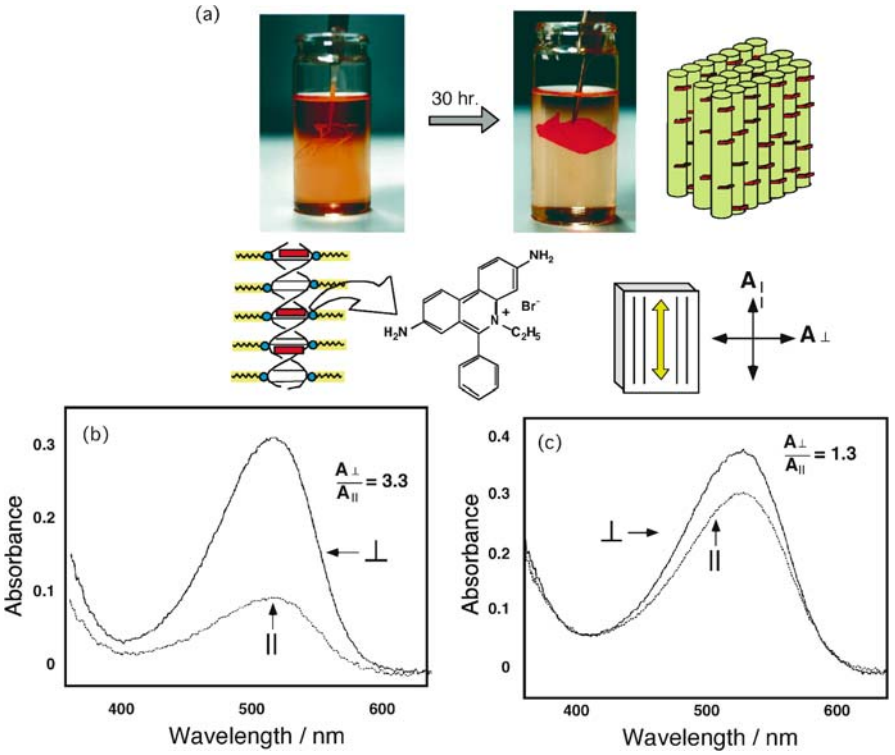

Fig. 9 **a** Observation of intercalation of ethidium bromide into the DNA-lipid film in an aqueous solution, and polarized absorption spectra of the ethidium-intercalated stretched DNA-lipid film **b** in the wet state and **c** in the dry state. Ethidium bromide was intercalated one molecule per 10 base-pairs at 25 °C. *Open, two-headed arrows* show the stretching direction of the film

When a polarized spectrum of the film was taken in the dry state, a small dichroic ratio was observed (A⊥/A// = 1.3, see Fig. 9c). This is due to the slant structures of base pairs and intercalated dyes to the axis of the strands, since the DNA strands were confirmed to be aligned along the stretching direction even in the dry film (see Fig. 7c). These changes of polarized absorption spectra dependent on water moisture were reversible at least 10 times.

5
DNA-Aligned LB Films

Rod-like polymers such as polyglutamate [21], polysiloxane [22], alkylated cellulose [23], and discotic crystals [24], have been reported to form LB films in which rod-like molecules aligned in one direction during the compres-

sion process on the subphase [25, 26] or the deposition process of monolayers [27]. DNA forms a rod-like strand and is a good candidate to form an oriented LB film in the same manner [28]. However, DNA is soluble only in the water phase due to the anionic phosphate backbone. We could transfer water-soluble DNA strands by complexing with cationic lipid monolayers using vertical dipping LB methods (see Fig. 10).

Cationic amphiphiles $2C_{18}$-glu-N^+ spread on pure water, in the solution of 10 μM DNA containing 10 μM intercalating dyes (proflavine). The dye-intercalated DNA anions were expected to adsorb to the cationic lipid monolayer due to electrostatic interactions and was transferred to a hydrophobized glass plate at a surface pressure of 35 mN m^{-1} at 20 °C. From a moving area of a barrier, two layers of the monolayer were confirmed to be transferred in each one cycle (Y-type deposition). When the QCM plate was employed as a transfer plate, the transferred mass could be calculated from frequency decreases (mass increase on the QCM) [29–31]. It was confirmed that 203 ± 10 ng of two lipid monolayers and 74 ± 5 ng of DNA strands were transferred on to the substrate per dipping cycle, which means ca. 95% of the monolayer area was covered by DNA molecules.

The LB film of the DNA-/proflavine/2C18-glu-N^+ complex was transferred with 44 layers (22 cycles) on one side of a glass plate (total 88 layers on both sides) and measured by polarized absorption spectra in aqueous solution (see Fig. 11a). The LB film did not swell and did not remove from the substrate

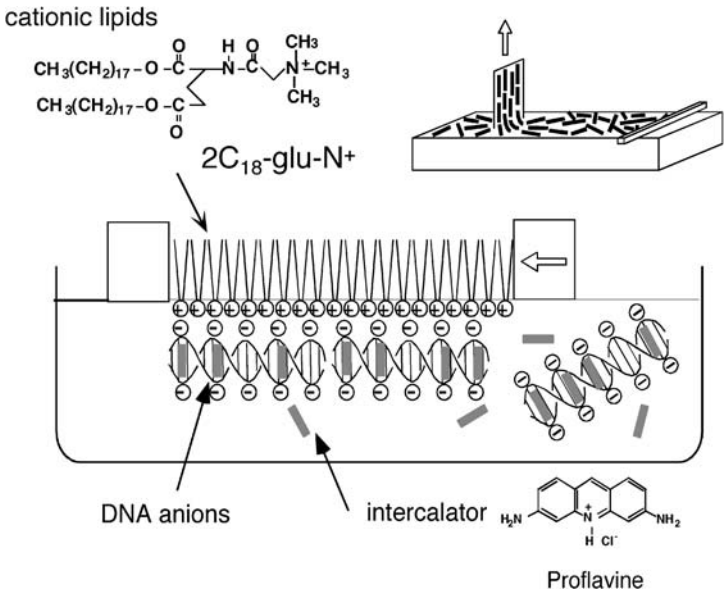

Fig. 10 Schematic illustrations of the formation of a DNA-oriented LB film by using a polyion complex of DNA/intercalator and cationic lipid monolayers

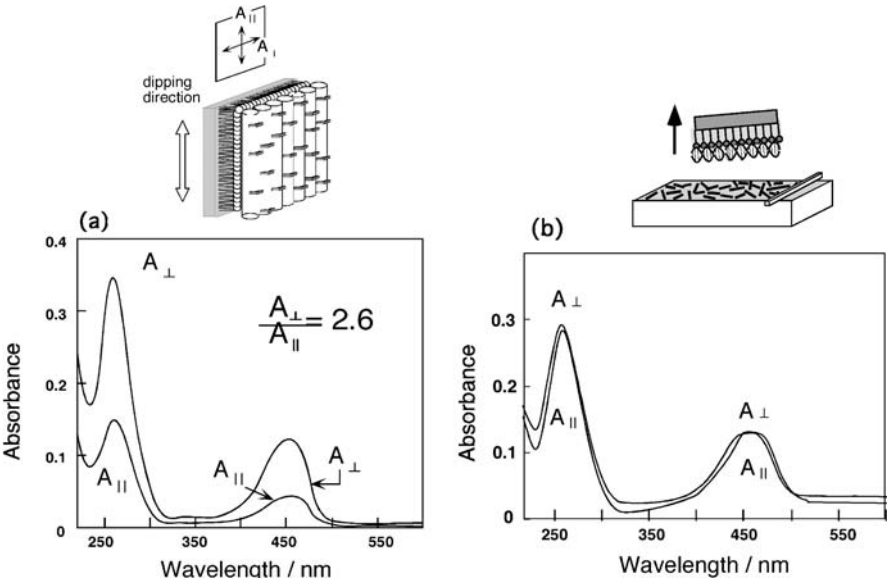

Fig. 11 Polarized absorption spectra of DNA^-/proflavine/$2C_{18}$-glu-N^+ LB films (88 layers) deposited by **a** vertical dipping method and **b** horizontal lifting method

in the aqueous water. The absorption of the intercalated proflavine at 450 nm for the light polarized perpendicular to the dipping direction was 2.6 times larger than that for the parallel polarized light ($A\perp/A// = 2.6$). This indicates that the absorption moment of the intercalated dyes between base-pairs is aligned perpendicular to the dipping direction. Thus, DNA strands in the LB film are aligned parallel to the dipping direction. The absorption spectra hardly changed after soaking in the aqueous solution at least for 2 days: reorientation of DNA strands and/or removal of intercalated dyes hardly occurred.

The monolayer of the DNA^-/proflavine/2C18-glu-N^+ complex could be transferred using a horizontal lifting method on the hydrophobized glass plate. Two lipid monolayers (Y-type) with 95% coverage of DNA were confirmed to be transferred in one cycle of the horizontal lifting process by using a QCM method [29–31]. As shown in Fig. 11b, the absorption spectra were independent of the polarized direction of the light. This indicates that the DNA strands are not aligned in the LB film deposited with the horizontal lifting method. The advantage of the horizontal lifting method is that it is known to deposit the real monolayer structure on the subphase, in contrast to the vertical dipping method. Thus, it is concluded that the DNA strands are not oriented on the subphase after and/or during the compression process of the monolayer, but the DNA stands are aligned parallel to the dipping direction during the vertical dipping process.

6
Anisotropic Conductivity of DNA-Aligned Cast Films

We could obtain the DNA-aligned cast film by stretching the film in one direction. This is a good candidate for use as molecular material for one-dimensional energy transfer and conduction along the π-electron clouds of stacked bases.

There have been many approaches to the study of electric conductivity along a DNA strand [32–48]. Barton and co-workers reported in their pioneering work that photo-induced charge transfer between donors and acceptors immobilized at both ends of DNA strands could be observed in homogeneous aqueous solution [32–34]. Photo-induced or long-range charge transfer along DNA molecules has also been studied in aqueous solution [35–37]. The conductivities of a DNA monolayer on a Au electrode have been studied by cyclic voltammetry [38] and AFM [39] in aqueous solution. Fink and Schonenberger directly measured electrical conductivity of dry DNA fibers across two electrodes whose distance was very short 8 nm [40]. Recently, superconductivities of DNA fibers across a submicronic slit on a mica plate have been reported [41]. The conductivity values obtained in these studies are roughly in the wide range of $1-10^{-5}$ S cm^{-1} and are still a matter of controversy. This is due to differing sample preparation, and the different measurement methods and media used.

We studied molecular level evidence of *electron* conductivity through DNA strands in the DNA-aligned cast film prepared from two different lengths of DNA (ca. 0.2 and 10 μm per molecule), by measuring direct or alternating currents on comb-type electrodes (5 μm distance between the two electrodes) at different temperatures. The stretched DNA film (5×5 mm, 20 ± 5 μm) was put on a comb-type electrode plate, in which the distance between the two electrodes was 5 μm. The dc conductivity was measured with an ampmeter (R8340A, Advantest Co., Tokyo) at 20 °C in a dry box. Typical results are shown in Fig. 12. When the stretched DNA film prepared from long DNA strands (10 μm length, 30 000 bps) was put on the comb-type electrodes (5 μm distance) with the DNA strand axis aligned perpendicular to the electrodes, large ohmic currents (0–0.7 mA) were observed that increased linearly with increasing applied voltage in the range of – 0.5 to + 0.5 V (Fig. 12a). The conductivity was calculated from the slope to be 5×10^{-3} S cm^{-1}. The currents were constant during measurements and did not reduce for at least 10 min.

On the contrary, when the same film prepared from the long DNA strands was placed with DNA strands aligned *parallel* to the two electrodes, electric current was hardly observed even at a voltage up to 100 mV (less than 0.001 mA or 10^{-6} S cm^{-1}, data not shown) [46–48]. When the DNA-aligned film prepared from the short DNA molecules (0.2 μm length, 500 bps) was aligned perpendicular to the electrodes, very small ohmic currents (0–1 μA,

10^{-6} S cm^{-1}) were observed depending on the applied voltage, and the current diminished immediately (within 5 s; Fig. 12b). The constant, large, and ohmic currents along the long DNA strands indicate the electron conduction along the DNA strands aligned in the film, since one 10 μm DNA molecule can be expected to bridge the distance of 5 μm between the two electrodes in the film. On the contrary, the short 0.2 μm DNA could not bridge the two electrodes (5 μm distance) and very small and immediately-diminished currents were observed due to the rate-limiting diffusion of impurity ions between intermolecular short DNA strands in the film.

Figure 13 shows temperature dependencies of Cole-Cole plots of DNA-aligned cast film, in which DNA strands are placed perpendicular to the two comb-type electrodes. Alternating currents were measured by using a universal impedance analyzer (Model 53131A, Hewlett Packard Co., Tokyo), changing frequencies from 10 Hz to 10 MHz at 20–100 °C in the dry box. When the film was prepared from the long DNA (10 μm molecular length), the apparent resistances at the zero imaginary of impedance were constant (400 Ω) independent of temperatures in the range 25 to 60 °C (Fig. 13a). When the film prepared from the short DNA (0.2 μm length) was employed, in which DNA molecules can not bridge the two electrodes (5 μm distance), the resistance increased to 100–650 kΩ depending on the temperature applied (Fig. 13b).

The conductance (s) obtained from the resistance was plotted against temperature in Fig. 14. The conductance obtained from the long DNA film was 10^{-3} S cm^{-1} which is consistent with the result obtained by direct current measurements in Fig. 12a, and was independent of temperatures in the range 20 to 60 °C. On the contrary, the conductance of the short DNA film

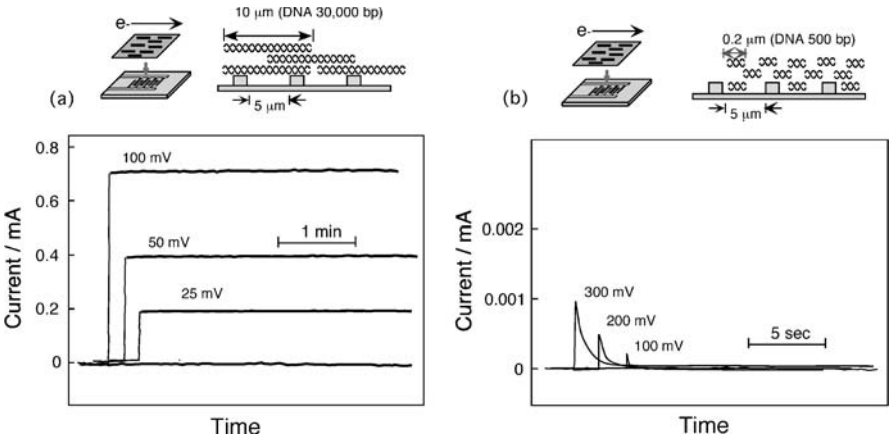

Fig. 12 Direct currents of DNA-aligned films (5 × 5 mm, thickness 20 ± 5 μm) on a comb-type electrode (distance between the two electrodes: 5 μm) at 25 °C in a dry box. **a** The film prepared from the long DNA strands (10 μm, 30 000 bps) and **b** the film prepared from the short DNA strands (0.2 μm, 500 bps) placed perpendicular to the two electrodes

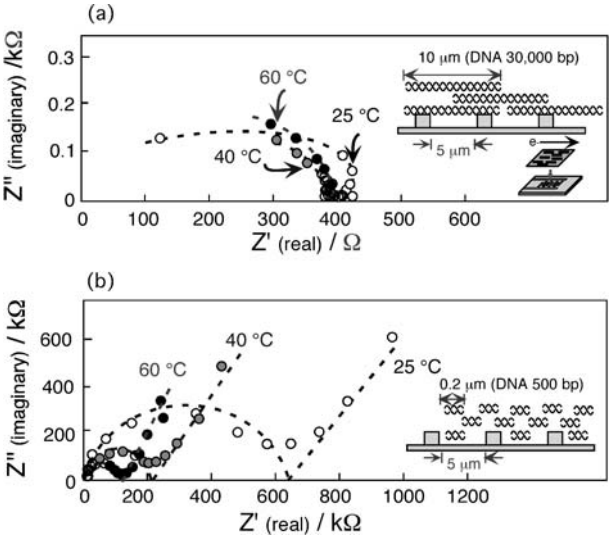

Fig. 13 Cole-Cole plots (10 Hz to 10 MHz frequencies) of alternating currents of the DNA aligned film placed perpendicular to the comb-type electrodes (5 μm distance). **a** The film prepared from the long DNA molecules (10 μm, 30 000 bps) and **b** the film prepared from the short DNA molecules (0.2 μm, 500 bps)

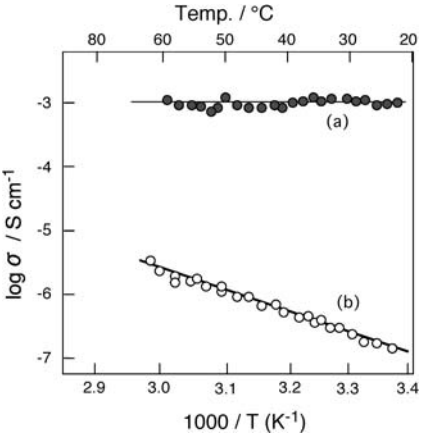

Fig. 14 Temperature dependence of alternating conductivities of **a** the film prepared from the long DNA molecules (10 μm, 30 000 bps) and **b** the film prepared from the short DNA molecules (0.2 μm, 500 bps)

was very small and increased linearly with increasing temperature (10^{-7} to 10^{-5} S cm^{-1}). Thus, the temperature-independent conductance of the long DNA film indicates again electron conductance along intramolecular DNA strands. The temperature-dependent conductance of the short DNA film shows the small ionic transportation between short DNA molecules.

Barton and other workers reported that photo-induced electron transfer between donors and acceptors intercalated into DNA strands could be observed in homogeneous aqueous solution [32–34, 49, 50]. We could also observe anisotropic photo-induced electron transfer mediated by intercalated dye molecules through aligned DNA strands in the film. When the aligned DNA film (20×10 mm, 30 ± 5 μm thickness) was soaked in an aqueous solution (10^{-3} M) of acridine orange (AO, $\lambda_{max} = 440$ nm) for a day at room temperature, the transparent DNA film turned orange (470 nm), and the aqueous solution became colorless. Adsorbed dye molecules have been confirmed from polarized absorption spectra to be intercalated between base-pairs and to be aligned perpendicular to DNA strands in the film. Intercalated dyes could not be readily removed from the film after soaking and washing with water for a day. One AO molecule was calculated from absorption measurements of these films to intercalate per ca. 10 base pairs.

After drying the film completely in a vacuum for several days, a photocurrent was observed using the same electrode setup shown in Fig. 15, with pulsed irradiation of light above 380 nm using a 150 W xenon lamp (Hamamatsu Photonics). As shown in Fig. 15, a large ohmic photocurrent was observed when DNA strands were aligned perpendicular, but not paral-

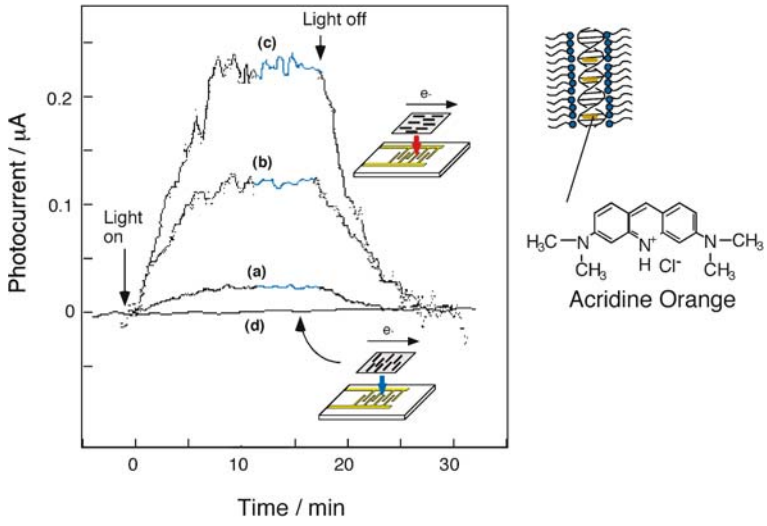

Fig. 15 Photo-induced current of aligned-DNA films (20×10 mm, thickness: 30 ± 5 μm) in which one acridine orange intercalates per ca. 10 base-pairs. **a** At 0.01 V, **b** 0.05 V, and **c** 0.1 V of applied voltage to the comb electrodes, in which the DNA strands are aligned perpendicular to the two electrodes. **d** DNA strands in the film placed parallel to the two electrodes at 0.1 V applied voltage. The pulse light above 380 nm was irradiated from a 150 W xenon lamp at 25 °C

lel, to the two electrodes. Photocurrents increased linearly (0–0.22 μA) with increasing applied voltage up to 0.1 V. This photocurrent was reproducible through at least ten continuous experiments. Dark currents along the AO-intercalated DNA strands (20 μA at 0.1 V) were five times larger than that of the DNA film without intercalators (4 μA at 0.1 V). Thus, the total current (20 + 0.2 μA at 0.1 V) increased by about 1% using photo irradiation. When the unstretched film was employed, both dark- and photocurrents were hardly affected by the AO intercalation. When the DNA-lipid film was prepared from a single strand poly(dA) and soaked in the aqueous solution of AO, dyes did not intercalate (adsorb) into the film and the resulting photocurrent was hardly detectable. These results indicate that photocurrents pass through stacked base-pairs of the aligned DNA strands in the film [42–45]. Photo-induced current along the DNA strand was calculated to be 7 μA cm^{-2}, which is fairly large compared to 0.5–1 μA for fullerene-containing conventional polymer films [51].

7 Summary

The DNA-lipid complex was soluble in an organic solution and formed double helical structures whose conformation could be changed reversibly depending on the water content. In the self-standing cast film of the DNA-lipid complex, DNA strands could be aligned in one direction simply by stretching the cast film. The conformation of the DNA strands could be changed reversibly even in the film state dependent on the moisture content. Water molecules are shown to be important for the formation of the B-structure of DNA even in organic solvents and in film.

The DNA-aligned thin film could also be obtained with the LB method, in which anionic DNA strands were transferred with cationic monolayers at the interface using vertical dipping method. DNA was aligned along the dipping directions.

We have observed both dark and photo-induced one-dimensional currents along DNA strands aligned in the flexible film. The DNA-lipid film, in which aligned rod-like strands with hairy alkyl side chains occur, shows thermotropic liquid crystal properties.

The aligned-DNA, transparent, self-standing, and flexible film is of interest as a new naturally-occurring functional material, as well as an anisotropic conductive film. For example, the DNA-lipid film is effective as an adsorption filter of carcinogens such as acridine orange and ethidium bromide. The aligned-DNA film also shows polarization of light.

References

1. Saenger W (1987) Principles of Nucleic Acid Structure. Springer, Berlin Heidelberg New York
2. Leslie AGW, Arnott S, Chandrasekaran R, Ratliff RL (1980) J Mol Biol 143:49
3. Fuller W (1967) J Mol Biol 27:507
4. Alam TM, Orban J, Drobny G (1990) Biochemistry 29:9610
5. Alam TM, Drobny GP (1993) Chem Rev 91:1545
6. Brandes R, Vold RR, Kearns DR (1988) Biopolymers 27:1159
7. Wada A (1964) Biopolymers 2:361
8. Norden B, Kubista M, Kurucsev T (1992) Q Rev Biophys 25:51
9. Strzelecka TE, Rill RL (1987) J Am Chem Soc 109:4513
10. Prive GG, Heinmann U, Chandrasegaren S, Kan LS, Kopra ML, Dickerson RE (1987) Science 238:498
11. Moore DS, Wagner MF (1974) Biopolymers 13:977
12. Hanlon S, Brudno S, Wu TT, Wolf B (1975) Biochemistry 14:1648
13. Girod JC, Johnson WC Jr, Huntington SK, Maestre MF (1973) Biochemistry 12:5092
14. Warning MJ (1965) J Mol Biol 13:269
15. Nelson JW, Tinoco I (1984) J Biopolymers 23:213
16. Chandrasekaran S, Jones RL, Wilson WD (1985) Biopolymers 24:1963
17. Okahata Y, Ijiro K, Matsuzaki Y (1993) Langmuir 9:19
18. Stein RS (1958) J Polym Sci 31:327; 34:709
19. Skotheim TA (ed) (1986) Handbook of Conducting Polymers, vol I and II. Marcel Dekker, New York
20. Yamamoto T, Maruyama T, Zhou Z, Ito T, Fukuda T, Yoneda Y, Begum F, Ikeda T, Sasaki S, Takezoe H, Fukuda A, Kubota K (1994) J Am Chem Soc 116:4832
21. Duda G, Wegner G (1988) Macromol Chem Rapid Commun 9:495
22. Erbach R, Hoffmann B, Schaub M, Wegner G (1992) Sensors and Actuators B 6:211
23. Gaines G Jr (1991) Langmuir 7:834
24. Karthaus O, Ringsdorf H, Tsukruk VV, Wendorff JH (1992) Langmuir 8:2279
25. Malcom BR (1975) Adv Chem 145:338
26. Jones R, Tredgold RH (1988) J Phys D Appl Phys 21:449
27. Schwiegk S, Vahlenkamp T, Xu Y, Wegner G (1992) Macromolecules 25:2513
28. Sukhorukhov GB, Yerokhin VV, Tronin A (1992) Biophysics 38:243
29. Ariga K, Okahata Y (1994) Langmuir 10:3255
30. Okahata Y, Ariga K (1987) J Chem Soc Chem Commun, p 1535
31. Okahata Y, Ariga K, Tanaka K (1992) Thin Solid Films 210/211:702
32. Murphy CJ, Arkin MR, Jenkins Y, Ghatlia ND, Bossmass SH, Turro NJ, Barton JK (1993) Science 262:1025–1028
33. Homlin RE, Dandliker PE, Barton JK (1997) Angew Chem Int Ed 36:2714–2730
34. Kelly SO, Jackson NM, Hill MG, Barton JK (1999) Angew Chem Int Ed 38:941–945
35. Lewis FD, Letsinger RL, Wasielewski MR (2001) Acc Chem Res 34:159–170
36. Shuster GB (2000) Acc Chem Res 33:253–260
37. Giese B (2000) Acc Chem Res 33:631–636
38. Hartwith G, Caruana DJ, de L Woodyear T, Wu Y, Campbell CN, Heller A (1999) J Am Chem Soc 121:10803–10812
39. Wold DJ, Frisbie CD (2000) J Am Chem Soc 122:2970–2971
40. Fink HW, Schonenberger C (1999) Nature 398:407–410
41. Kasumov AY, Kociak M, Gueron S, Roeulet B, Volkov VT, Klinov DV, Bouchiat H (2001) Science 291:280–282

42. Ijiro K, Okahata Y (1992) J Chem Soc Chem Commun 1339–1341
43. Tanaka K, Okahata Y (1996) J Am Chem Soc 118:10679–10683
44. Okahata Y, Kobayashi T, Tanaka K (1996) Langmuir 12:1326–1330
45. Okahata Y, Tanaka K (1996) Thin Solid Films 284/285:6–8
46. Okahata Y, Kobayashi T, Tanaka K, Shimomura M (1998) J Am Chem Soc 120:6165–6166
47. Okahata Y, Kobayashi T, Nakayama H, Tanaka K (1998) Supramol Sci 5:317–320
48. Okahata Y, Nakayama H (2000) Proc Japan Acad B 76:145–150
49. Kumar CV, Barton JK, Turro NJ (1985) J Am Chem Soc 107:5518
50. Fromherz P, Rieger B (1986) J Am Chem Soc 108:5361
51. Bensasson RV, Garaud JL, Leach SL, Miquel G, Seta P (1993) Chem Phys Lett 210:141

Top Curr Chem (2005) 260: 77–111
DOI 10.1007/b137073

Published online: 16 September 2005

Substrate Patterning and Activation Strategies for DNA Chip Fabrication

Aránzazu del Campo[1] · Ian J. Bruce[2] (✉)

[1]Max-Planck Institut für Metallforschung, Heisenbergstraße 3, 70569 Stuttgart, Germany
delcampo@mf.mpg.de

[2]Department of Biosciences
University of Kent, Canterbury, Kent CT2 7NJ, UK
i.j.bruce@kent.ac.uk

Abstract The immobilization of nucleic acids onto substrates in array fabrication is a complex process involving three major steps: (i) the chemical modification of the arrayed material in such a fashion that it can interact with complementary functionalities present on the substrate to form a stable bond; (ii) the coating of the support surface with adequate functional groups to allow specific binding and prevent nonspecific adsorption of the material to be arrayed; and (iii) the use of a delivery system that brings small quantities of the arrayed material to specific positions on the surface.

Different types of nucleic acids or their analogues (cDNA, oligonucleotides or peptide nucleic acids), supports (silica, gold, polymeric membranes and gels), surface activation chemistries (organosilanes, thiols) and patterning tools can be used for these purposes and will be described in this review.

Keywords DNA immobilization · Surface chemistry · Surface activation · Patterning · DNA arrays

1 An Introduction to DNA Arrays

DNA arrays are addressable assemblies of nucleotide sequences tethered to a solid surface, each of which represents a single gene, splice variant, or other DNA element. These tools permit scientists and clinicians the possibility of studying the expression of many genes in parallel and, as a consequence, genes which are over- or under-expressed can be identified in diseased cells, or in response to drug treatments. In this context, cancers can be graded with unprecedented precision, meaning that one day patients could see individually tailored drug regimens. Finally, DNA arrays can be used to rapidly sequence genomes, or to genotype single nucleotide polymorphisms [1].

A typical DNA array fabrication and application process involves three major steps. First, nucleic acids (the capture sequences or probes) are immobilized at discrete positions on surface activated substrates. Secondly, the resulting array is hybridized with a complex mixture of fluorescently labelled nucleic acids (the target), and thirdly subsequent to hybridization, the fluorescent markers are detected using a high-resolution scanning laser that quantifies the interaction. This chapter focuses on the first of these processes and provides the reader with an overview of substrates, surface activation methods and delivery systems available for nucleic acid immobilization.

2 Processes and Materials Involved in the Immobilization of Nucleic Acids onto Surfaces

The immobilization of nucleic acids (NA) onto substrates in array fabrication involves three major steps (Fig. 1): (i) the chemical modification of the arrayed material in such a fashion that it can interact with complementary functionalities present on the substrate to form a stable bond; (ii) the coating of the support surface with adequate functional groups to allow specific binding and prevent nonspecific adsorption of the arrayed material; and (iii) the use of a delivery system that brings small quantities of the arrayed material to specific positions on the surface [2, 3].

In principle, one could take advantage of any kind of molecular interaction (electrostatic, H-bonding, covalent, etc.) to immobilize NAs onto surfaces, provided that the substrate and arrayed material carry the appropriate functionalities. However, in reality the surface chemistries and mechanisms employed in substrate modification are limited. In some cases coupling molecules (cross-linkers) are necessary to increase the affinity (or reactivity) of the interacting groups.

The final performance of the immobilized NA probes in the hybrid capture of target molecules (sensitivity and discrimination) is strongly dependent upon a number of parameters related to the immobilization process. These include: (i) the chemical and physical properties of the surface, since they can influence nonspecific binding of target and nontarget (in mixtures) molecules; (ii) the distance between the immobilized NA probes and the solid surface and the orientation of the immobilized probe; (iii) the density of the

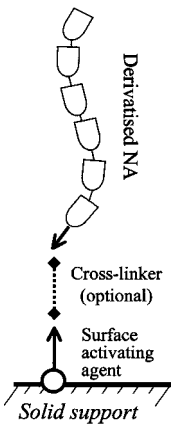

Fig. 1 Representation of the different components participating in the immobilization of NA onto a substrate: the solid support, a surface activating molecule, a cross-linker and the NA probe

probes arrayed on the surface which can limit its sensitivity; and (iv) the sequence and length of the immobilized NAs.

All these issues will be addressed in the following sections.

3 The Arrayed Material

Different types of NA probes can be used in the fabrication of DNA arrays: complementary DNA (cDNA), oligonucleotides (OND) and peptide nucleic acids (PNA).

The principal physical characteristic of cDNA and ONDs to be taken into account when immobilizing them onto a surface for array applications, is their polyionic nature, which is a consequence of the acid-base behavior of their constituent nucleotides (Fig. 2). In nucleotides, the phosphate unit looses one proton at pH = 1, and a second proton at pH = 7, whereas the bases and pentoses remain uncharged within the range $5 < pH < 9$. This gives a net negative charge of the DNA or OND molecule under physiological conditions. This can be advantageous if NAs are to be immobilized onto positively charged surfaces. Alternatively, NAs can be immobilized onto negatively charged surfaces in concentrated salt solutions (chaotropic conditions), where there is a shielding effect provided by the positively charged ions present in solution [4].

Immobilization by electrostatic interaction results in a tight association of the NA backbone with the surface that may leave part of the molecule in an unfavorable conformation for its subsequent hybridization with complementary sequences. This could result in a loss of hybridization efficiency and is the primary reason why this method is recommended principally if the arrayed material is available in large quantities and its price is not an issue for consideration. Alternatively, this method can also be used if the NA does not possess specific chemical functionalities which can be used in other more directed immobilization strategies (e.g. covalent bonding).

Electrostatic immobilization is often employed when **cDNA** is used for array production, as this material, usually a product of the polymerase chain reaction (PCR), is available in relatively large amounts at low cost.

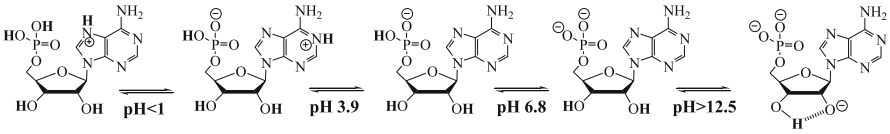

Fig. 2 States of protonation of the nucleotide adenosine 5′-phosphate depending on the pH of the solution

ONDs are synthetic molecules produced in the laboratory and their immobilization to surfaces usually makes use of covalent bonds. They are considerably more expensive than their cDNA counterparts and their cost increases the expense of array fabrication. Specific groups involved in their covalent immobilization to surfaces are introduced into the OND structure during conventional automated synthesis via phosphoramidite derivatives. Moieties that can be used in linking can be added at the 3′ or 5′ terminus or at internal positions of the OND depending on the point within the synthetic pathway at which they are introduced. Carboxylic and amine functionalities are the modifications most frequently used, although aldehyde [5, 6], thiol [7, 8], oxyamino [9, 10] or biotin [11] modifications are alternatives. ONDs have also been modified with octyl alkyl chains for immobilization via Van der Waals interactions with hydrophobic surfaces [12] and with metal-complexing groups like benzotriazol for attachment to Cu or Ag surfaces [13]. Post-synthesis modification of the OND is also possible, like silanization [14, 15], bioconjugation to carbohydrates that bind to surfaces via molecular recognition mechanisms [16] or bioconjugation to cationic

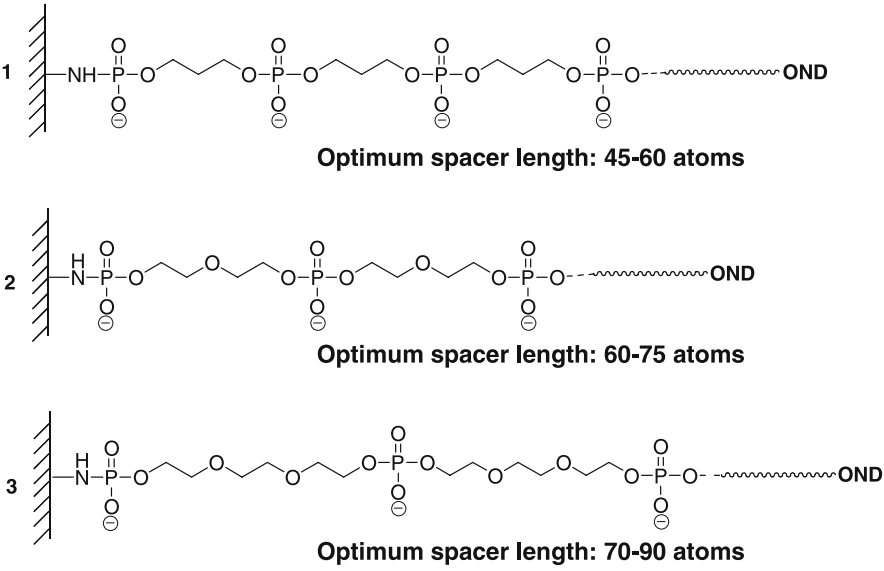

Fig. 3 Immobilization of ONDs to a surface through spacers derived from glycol synthons with different lengths [ethylenglycol (1), diethyleneglycol (2), and triethyleneglycol (3)] [18]. The optimum spacer length for a maximum hybridization efficiency varies with the chemical composition of the spacer. In the example given the main difference between the spacers is their charge density, which decreases in the order **1** > **2** > **3** and suggests that the introduction of negatively charged groups in the spacer diminishes the yield of hybridization. This may be as a consequence of repulsive forces between the spacer and the target sequence when the latter approaches the support surface

lipids via electrostatic interactions that may bind to surfaces through their hydrophobic tails [17].

Attachment of one of the ends of the OND to a solid phase introduces a steric constraint to hybridization which is not encountered when considering molecules free in a solution. This effect can be minimized if a spacer is introduced between the linking group and the 3′ or 5′ terminus of the OND. The spacer can be of virtually any desired length and possess a variety of chemical characteristics, i.e. it can be rigid or flexible, hydrophilic or hydrophobic, charged or neutral. In this context, studies have been conducted of the influence of the type and length of the spacer on the final performance of the immobilized OND. It has been observed that by increasing the spacer length a 150-fold increase in the efficiency of hybridization may be achieved [18]. Interestingly, there is an optimum spacer length beyond which hybridization efficiency declines, possibly because the ONDs "dissolve" in the spacer itself and become less accessible to the target. The optimum spacer length depends on the particular chemical structure of the spacer (see Fig. 3 for optimum spacer lengths which have been reported for various spacer architectures).

Other authors have also observed an enhancement in hybridization efficiencies when using dT spacers of increasing lengths [19, 20] in NA capture experiments. The magnitude of this enhancement is also dependent on the length of the probe. Figure 4 shows that efficiency increases for 50 to 70mer probes, but no significant improvement is observed for long OND probes (100 to 150mer). For 25mers much longer spacers are required to show a significant effect.

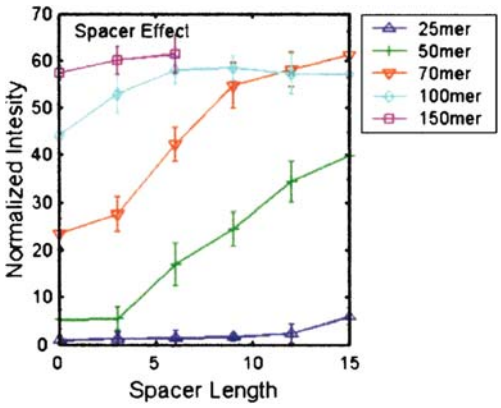

Fig. 4 Effect of spacer length on the mean hybridization intensity at five probe lengths. The basic single spacer unit had a length equivalent to a dT_3 OND, so the scale is based on the equivalent number of nucleotides. Intensities were normalized to the intensity obtained using the 25mer probe with no added spacer [20]

Recent studies have indicated that the base composition of the OND can affect the efficiency of its ability to bind to a surface. This is most probably a consequence of the different affinity that each base shows for any particular surface [21–24]. This has been clearly demonstrated in adsorption studies using homo-ONDs (unmodified and thiol modified) onto gold surfaces [23, 24]. It was observed that unmodified homo-ONDs adsorb on gold with relative affinities A > C ≥ G > T (Figs. 5 and 6). When performing competitive adsorption experiments with unmodified and thiol modified ONDs,

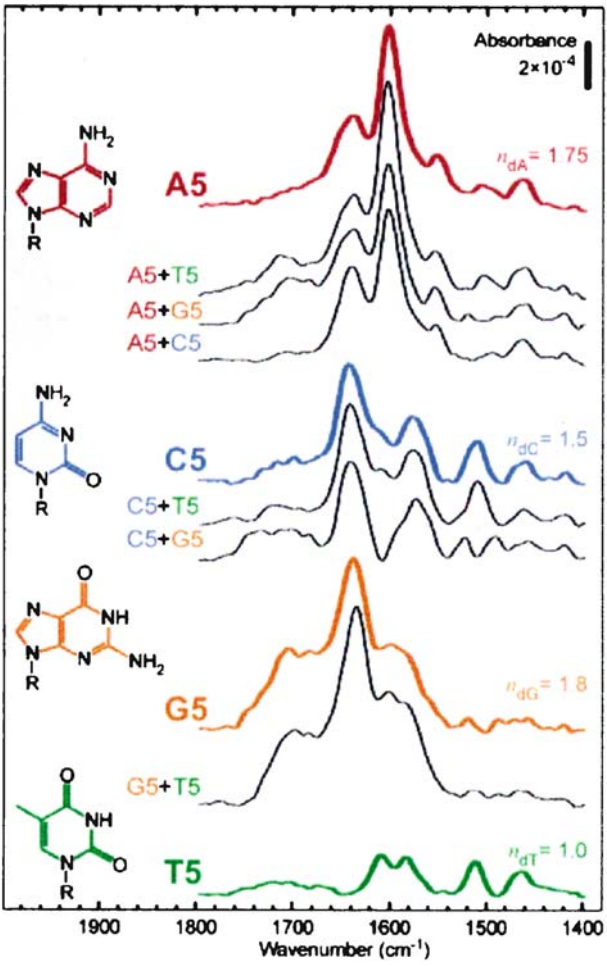

Fig. 5 FTIR spectra of ssDNA films adsorbed onto gold surfaces from aqueous solutions. Reference spectra for films of individual 5-mer homo-ONDs are shown along with spectra following competitive adsorption from their equimolar mixtures. The corresponding surface density, n, is indicated for each of the homo-ONDs (10^{14} OND cm^{-2}) [23]

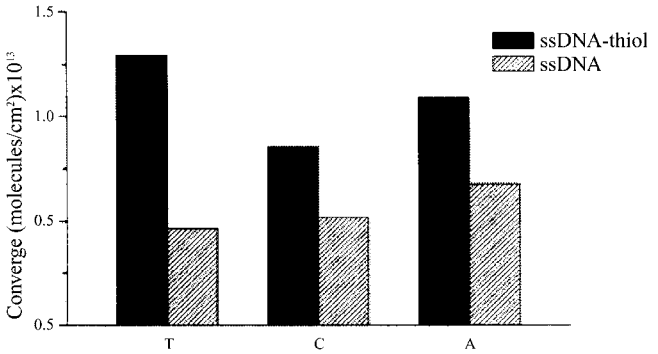

Fig. 6 Average coverage of unmodified (*hatched bars*) and thiol-modified (*solid bars*) homo-OND films after one hour adsorption onto gold surfaces in 1 M KH_2PO_4. The ratio between both bars indicates the ability of nonspecific binding to interfere with specific thiol binding for each sequence, i.e. the relative strength of nonspecific adsorption for each OND [24]

it was observed that the high adsorption affinity of oligo-d*A* allows it to compete effectively against chemisorption of thiolated oligo-d*T* and even caused the dissociation of oligo(d*A*)/oligo(d*T*) duplexes.

PNA oligomers are synthetic DNA mimics possessing an amide backbone which are able to base pair with DNA and RNA in an anti-parallel fashion (Fig. 7) [25]. The most interesting difference between DNA and PNA is the neutral backbone possessed by PNA at physiological pH. Consequently this leads to an increased stability of the duplexes they form with DNA and PNA oligomers can therefore be shorter than corresponding ONDs when used

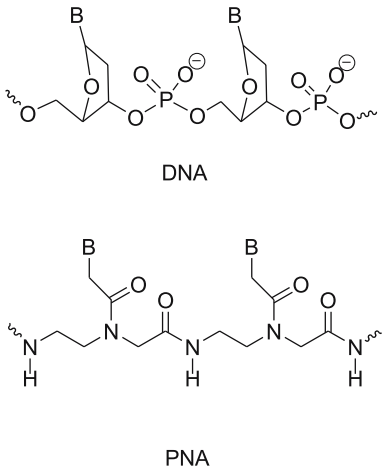

Fig. 7 Comparative structures of DNA and PNA

as hybridization probes. In turn, mismatches have a more destabilizing effect, thus improving their discriminatory power. PNAs are also capable of hybridizing to DNA samples under low or zero salt conditions, since no interstrand repulsion occurs as in the case between two negatively charged DNA strands. In addition, PNAs are stable under acidic conditions and resistant to both nucleases and proteases.

A number of chemical modifications and spacers for the covalent immobilization of PNAs onto surfaces are already available [26]. The spacer at the terminus of PNA strands has an additional function. Due to their uncharged backbone, solubility of PNAs in water is sometimes a problem and therefore hydrophylic spacers (like polyethyleneglycol derivatives) are introduced into the PNA structure not only for steric reasons, but also to avoid solubility problems.

However, PNA chemistry is still rather expensive and for this reason its use in arraying is still limited.

4
Substrates and Surface Modification Chemistries Involved

Classic solid phase substrates used in biotesting, such as microtiter plates, membrane filters or microscope slides, have been the first supports used for NA immobilization in array fabrication [27]. Desired attributes of any DNA array substrate include: (i) chemical homogeneity; (ii) thermal and chemical stability; (iii) ability to control surface chemical properties such as polarity or hydrophobicity; (iv) ability to be activated with a wide range of chemical functionalities; (v) reproducibility of the surface modification processes involved; (vi) inert with respect to enzymatic activity especially ones involved in DNA manipulation; and (vii) ultra-low intrinsic fluorescence.

4.1
Inorganic Flat Surfaces

4.1.1
The Silica Surface

Glass slides are the favored substrate for immobilizing probes for a number of reasons: (i) availability; (ii) flatness, rigidity and transparency; (iii) resistance to high temperature; (iv) the variety of surface chemical modifications possible; and (v) the nonporous nature of the glass surface [2, 28, 29]. Glass slides as substrates for DNA arrays have undergone considerable commercial development, and have been produced with highly uniform surface properties and chemistries.

Activation of the Si-OH Surface with Organosilanes

In the early stages of array development, glass slides were coated with poly-L-lysine (PL) to promote the adsorption of cDNA. The positively charged PL chain (pKa ~ 9) adsorbs onto the negatively charged silica surface (pKa ~ 2) via electrostatic interactions. In a similar way, cDNA adheres to the PL surface through electrostatic interactions between the PL ammonium groups and the cDNAs negatively charged phosphate groups at physiological pH. Hybridization with analyte DNA does not appear to disrupt this adhesion.

Alternatively, cDNA can be "cross-linked" onto PL surfaces by exposure to UV light. This increases the stability of the cDNA-surface. Although the underlying mechanism of this process is poorly understood, it is believed to involve the creation of radicals that induce interchain cross-linking between the thymidine residues of the DNA and the amino groups of the PL [30].

Covalent immobilization methods of NAs to a silica surface require its chemical modification. Functionally inert surface silanols (Si – OH) need to be transformed into reactive species to which the NAs can be attached irreversibly. To date, the main method for the attachment of biological moieties to silica surfaces has involved substrate reaction with organofunctional silanes of the general structure $(RO)_3Si(CH_2)X$, followed by the covalent attachment of the biological molecule to the newly introduced functional group on the surface [31, 32]. Examples of organofunctional silanes used this way include: (3-glycidoxypropyl)trimethoxysilane, (3-aminopropyl)triethoxysilane,

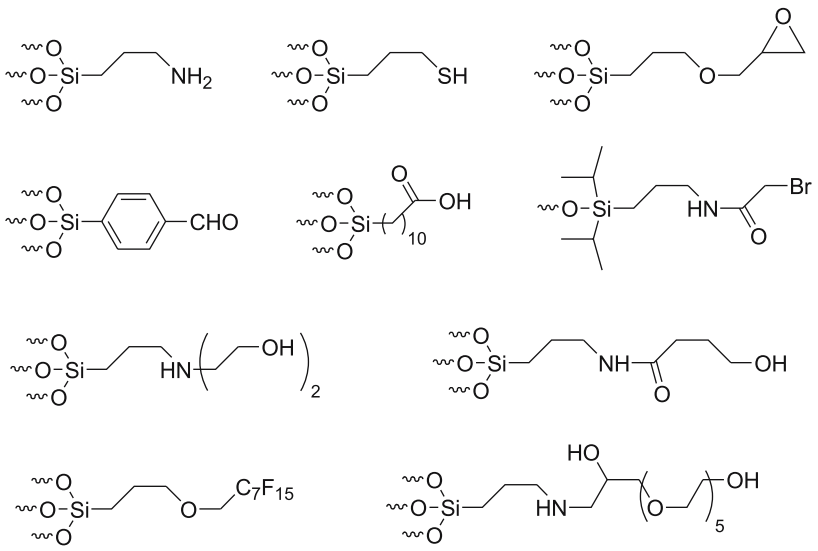

Fig. 8 Reagents for the derivatization of surfaces [35]

aminophenyltrimethoxysilane, (3-mercaptopropyl)trimethoxysilane, and haloacetamidosilanes (see Fig. 8).

It is possible to use mixtures of organosilanes carrying different headgroups for tailoring of surface properties. By doing so, issues like nonspecific adsorption or crowding of the active surface functionalities can be addressed. In order to find the best surface composition for the immobilization of the ONDs it is necessary to perform systematic studies varying the silane concentrations and other reaction parameters. Examples of this kind of study with mixtures of epoxy- and amine-silanes has been reported recently [33, 34].

In theory, the mechanism of silanization of surfaces with mono-, di-, or trialkoxysilanes (either as one or multicomponent mixtures) is relatively simple: hydrolysis of the silane alkoxy groups yields hydroxyl groups that can covalently interact with the silanol surface. However, in reality the situation is much more complicated and the exact process of modification is still not fully understood. It is thought that an initial step involves the rapid hydrolysis of the silane alkoxy groups to liberate silanols and release alcohols (Fig. 9). The silanol groups then condense with the surface residues to form siloxane linkages. In the case of di- and trifunctional silanes, the presence of two or three silanol residues in the hydrolysis product can lead to the possibility of multiple surface attachments, or to the possibility of polymerization in solution prior to condensation with the solid substrate [36]. If this process is not carefully optimized, this may lead to heterogeneous surface modification. Post-silanization curing of the substrate has been shown to improve the stability of silane films by cross-linking of free silanols.

A range of procedures have been described for the silanization of glass, including approaches employing both elevated and room-temperature organic phase, aqueous phase, vapor phase, and chemical vapor deposition of the silane. However, little has been published with regard to the reliability and

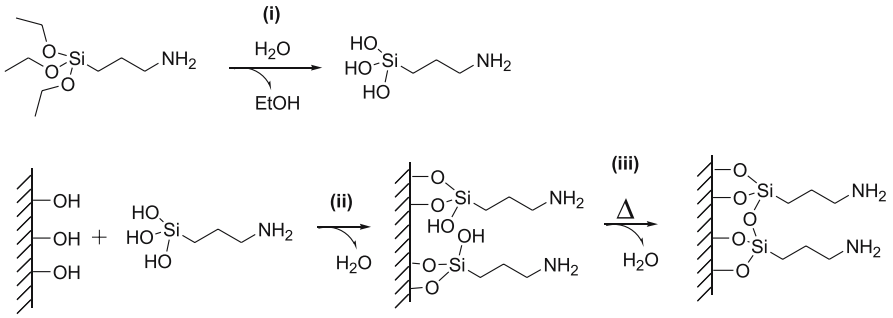

Fig. 9 Silanization of silica surfaces with aminopropyl(triethoxysilane). In (i) the reactive groups of the triethoxysilane are hydrolyzed by water, followed by condensation (ii) with the surface and (iii) thermal curing of the film, which further cross-links the free silanol groups

reproducibility of silanization conditions, or how this might also affect NA probe immobilization and hybridization efficiency. A significant contribution to this subject has been described by Halliwell [37], who reported on the influence of parameters like surface pretreatment, silane concentration, reaction temperature, post-reaction treatment, reaction time and reaction solvent in the modification of glass slides with mercaptopropyltriethoxysilane and their use for DNA attachment and hybridization.

Two Methods for Increasing the Binding Capacity of Si-OH Surfaces

The density of active surface groups is one key factor that can influence the number of NA probes which can be immobilized onto a specific surface area and consequently the sensitivity of the array. On flat surfaces (eg. glass slides) the surface density of active groups can be maximized by building ordered monolayers (SAMs) where the surface activating molecules are separated by the minimum possible distance from their closest neighbors (eg. self-assembled monolayers of functionalized thiols onto gold substrates, see ahead). Other alternatives are the generation of a 3D structure onto the planar substrate by deposition of a colloidal silica film, or the use of dendritic molecules as modification agents.

Dendrislides

Dendrimers are branched chemical structures which can possess a range of terminal functionalities. Covalent attachment of dendrimers to a support builds a 3D structure along its surface which can subsequently be grafted with ligands which, as a consequence of the larger surface area, can yield higher probe densities.

The dendritic structure can either be synthesized in-situ, by derivatization of the surface with multifunctional linkers [38] or generated by direct surface modification with the presynthesized branched structure [39–42]. In general, the second strategy is preferred, since reactions performed directly on the surface suffer from lower yields when compared with those performed in solution, and therefore the density of activated groups at the surface using the second method is higher. Results have indicated that dendrimer-modified surfaces can generate a surface coverage with capture oligomers about two- to sevenfold greater than that observed for the corresponding nonmodified surface. In addition, experiments have suggested that hybridization of these supports with complementary sequences occurs with greater efficiency probably as a consequence of decreased steric hindrance. However, it is worth noting that a twofold increase in surface density may not balance the synthetic effort involved in generating these dendrimer structures and therefore the utility of this approach may be limited. The low increase in performance efficiency suggests that many of the dendritically located capture sequences

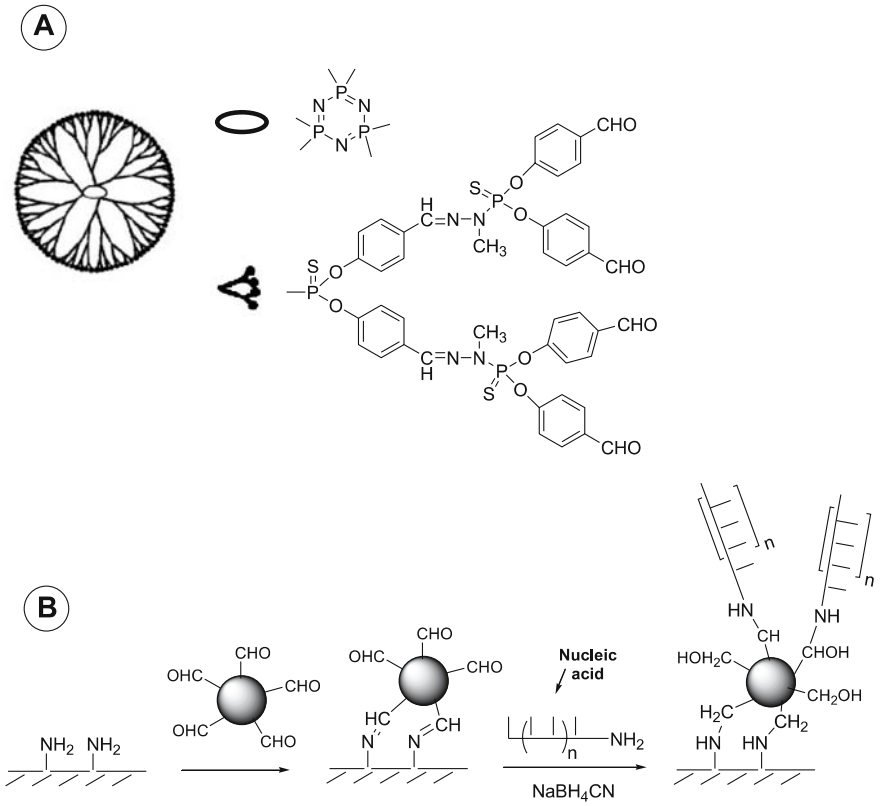

Fig. 10 **a** Scheme of dendrimer "generation 4" and **b** description of surface activation to fix the dendrimers and immobilization method for covalent binding of NAs on the activated glass surface [42]

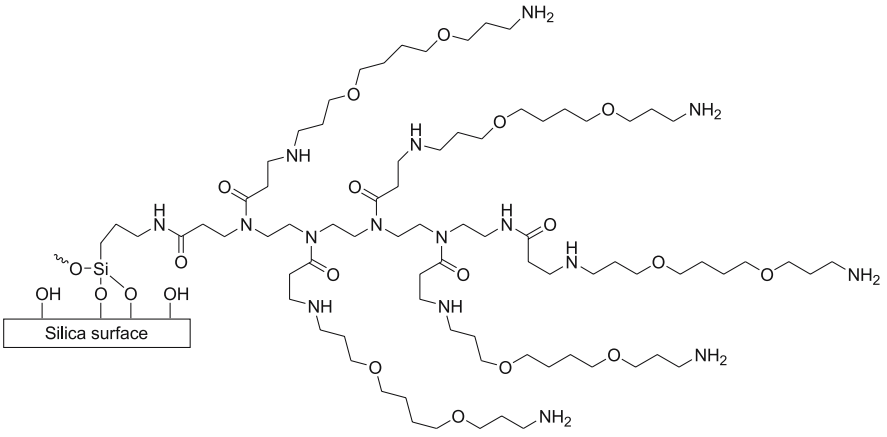

Fig. 11 In-situ synthesized dendrimeric structure prepared from an aminosilanized surface and multifunctional linkers [38]

may be inaccessible due to steric crowding. See Figs. 10 and 11 for a representation of these structures.

Colloidal Silica Films

Colloidal silica films spin-coated onto a glass substrate constitute another method to increase the surface area and therefore number of capture sequences which can be available for hybridization [43]. In this context, 0.3 μm layers have been deposited from 20 wt % colloidal silica suspensions (particle size 16 to 65 nm). Heating to 350 °C for four hours is required to render the films stable (through partial sintering of the film with the underlying substrate). The particles pack randomly with no noticeable short- or long-range order.

DNA arrays have been synthesized on the resulting surfaces by photolithographic patterning, and the products performance in hybridization assays compared to that of standard flat glass surfaces. The colloidal silica film coated surfaces demonstrated equivalent performance to flat glass substrates in terms of the efficiency of chemical synthesis and resolution of photolithographic patterning, and it appears that complementary DNA target sequences are able to penetrate the porous layers. The result is an enhanced hybridization signal that is 20 times higher than flat glass for a colloidal particle layer that is 0.5 μm thick.

4.1.2
The Silicon Surface and its Activation with ω-functionalized Alkenes

Silicon wafers can act as substrates in the fabrication of DNA arrays. Chemical functionalization of silicon surfaces is complicated by the fact that silicon spontaneously oxidizes in air to produce an amorphous silica layer.

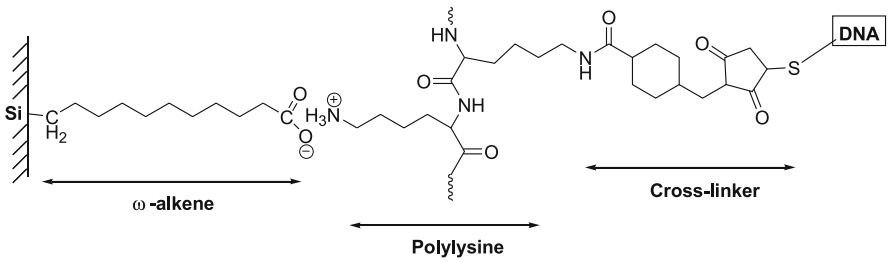

Fig. 12 Illustration of the chemistry employed for preparation of a modified Si(111) surface. Firstly, a layer of alkenyl acid is bound to the surface by covalent attachment. Secondly, a layer of polylysine is electrostatically bound to the carboxylic activated surface and finally the DNA is bound to the surface in a reaction mediated by sulfosuccinimidyl 4-(*N*-maleimidomethyl)-cyclohexane-1-carboxylate [27]

Therefore, surface modification strategies for the formation of direct silicon-carbon bonds require, first, a special pre-treatment of the silicon surface to prevent oxidation and, second, an activation of the silicon surface for subsequent reaction with organic moieties. This has been achieved by treatment of the silicon surface with hydrofluoric acid to generate a hydrogen-terminated Si(111) surface, which can further react with unsaturated ω-functionalized alkenes in the presence of UV irradiation or by thermal activation [27, 44, 45]. Using this method, carboxylic acid modified silicon substrates have been successfully generated and coupled to thiol modified ONDs via a polylysine/sulfosuccinimidyl 4-(*N*-maleimidomethyl)-cyclohexane-1-carboxylate coupling (Fig. 12).

4.1.3
Gold-Coated Surfaces: Self-Assembled Monolayers of Thiols

Gold surfaces have been extensively used in biosensing applications and offer the advantage of being easily activated with SAMs of ω-functionalized thiols. The chemistry of the gold-thiol interface is well-known and is much easier to control than organosilane chemistry. For this reason and for particular applications, gold-coated glass slides are used in the generation of DNA patterned surfaces. However, a significant additional cost is involved in the gold-coating, which must be considered when thinking of using this method in routine applications.

By choosing the appropriate head-group functionality of the thiol, SAMs of different chemical nature can be generated (carboxylic and amine are the most frequently used examples). Modified ONDs can be attached to these SAMs using common coupling methods [46], or thiolated ONDs can be directly attached to the gold surface.

SAMs of thiols (and thiol-modified ONDs) can be highly ordered and densely packed, improving the availability of active surface groups (and capture probes) for binding and hybridization. However, dense packing may not always be advantageous in DNA hybrid capture. Steric hindrance effects can occur if the immobilized capture probes are too close together.

Two methods have been used to control and optimize surface group density and distribution for maximum hybridization efficiency. If a passive molecule is co-adsorbed during the surface modification process, e.g. in the competitive co-adsorption of mercaptohexanol and thiol-modified ONDs onto gold substrates to form mixed SAMs, the resulting probe density can be controlled by varying the amount of time that the solid support is exposed to the mixture, or by varying the relative concentrations of the mixture's components. Another approach is to immobilize dsONDs instead of ssONDs. If these are then denatured, after surface attachment, a surface patterning is obtained which permits sufficient spacing of the capture ONDs for entry of complementary target sequences [47].

Mixed SAMs also possess utility in minimizing nonspecific DNA binding to surfaces [48, 49]. In this context "repelling molecules" (mainly thiols modified with noncharged hydrophilic polymers like polyethylene glycol, polyvinylpyrrolidone, polyvinyl alcohol, dextrans or hyaluronic acid) can be co-adsorbed with the capture sequences which lowers the affinity of NA for the surface, therefore increasing the efficiency of the specific hybrid capture of the target sequence. Mixed SAMs of DNA-functionalized thiols and triethyleneglycol-terminated thiols have already been fabricated and used [49].

4.2 Polymeric Flat Surfaces

4.2.1 Polydimethylsiloxane (PDMS)

The recent implementation of microfluidic platforms in the fabrication of DNA chips has focused attention onto the polymeric materials that can be used in the construction of such devices. In this regard, PDMS is probably the most important mainly because its use in the fabrication of such chips is exceedingly easy, it seals well to a wide range of materials, and is optically transparent. Polymethylmetacrylate (PMMA) can also be used in a similar fashion [50].

PDMS in its native form does not possess reactive groups that can be used for the covalent attachment of NAs [51]. However, the PDMS surface can be plasma induced oxidized and then functionalized with organosilanes carrying the desired head group. For example, a PDMS surface has been modified with 3-mercaptotrimethoxysilane to yield a thiol-terminated surface, to which a 5′-acrylamide modified DNA has been covalently attached [52]. See Fig. 13 for a representation of the PDMS surface-modification process.

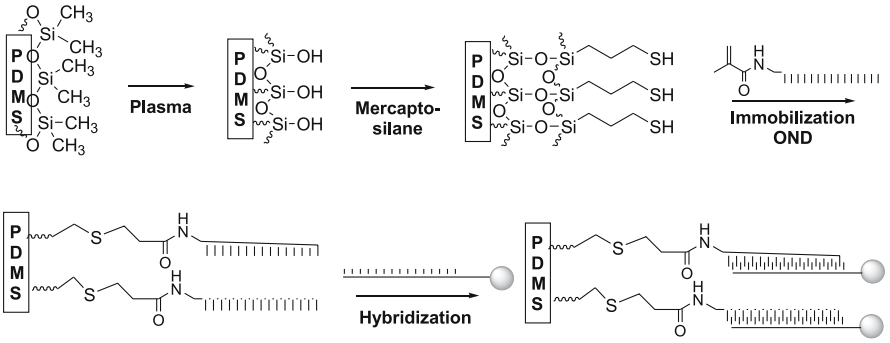

Fig. 13 PDMS surface modification [52]

4.2.2
Polypyrrole

Polypyrrol is a polymeric support that can be used in immobilization of ONDs to surfaces. The generation of polypyrrol films can be by electrochemical co-polymerization of pyrrole and pyrrole-modified ONDs onto platinum electrodes. The polymer forms a black and insoluble film that is electrically conducting and whose thickness depends on the current used during the polymerization process (Fig. 14). The final surface density of the OND can be controlled by the ratio of pyrrole/OND being polymerized [53–55].

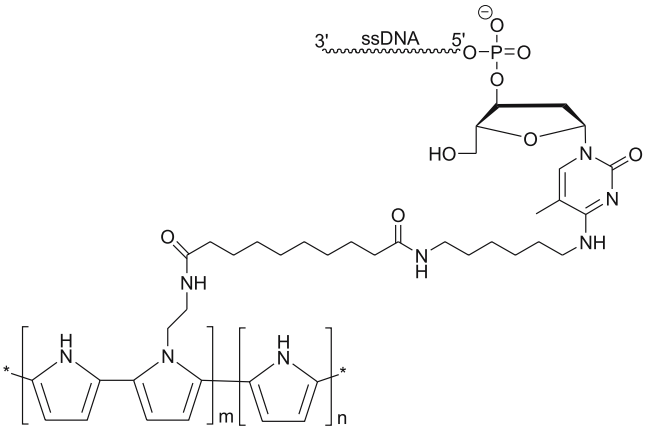

Fig. 14 Structure of OND-modified polypyrrol film

4.3
Membranes

The term membrane encompasses a wide range of potential substrates that can be used for the immobilization of NAs. It includes traditional polymeric "cast membranes", such as nitrocellulose, nylon or polypropylene, and also innovations such as ceramic or track-etched materials (alumina membranes). Membranes as substrates in DNA array fabrication can possess advantages over other surfaces: their surface area can be much greater (200% more in cast membranes and 500% more in aluminium membranes) than certain other alternatives. This is primarily a consequence of their possession of pores.

4.3.1
Nitrocellulose and Nylon

The first membrane used for NA immobilization was nitrocellulose. Its principal advantages were its availability and familiarity with its chemical and

physical characteristics. However, it is friable (unless cast on a polyester backing) and possesses a lower binding capacity than other membranes. NAs are believed to bind to nitrocellulose membranes by means of hydrophobic interactions [28].

Latterly, nylon has been promoted as a substrate for NA immobilization as a consequence of its greater physical strength and binding capacity, and the wider range of available surface chemistries it can offer (neutral, positively, and negatively charged nylon membranes are available) which can improve NA attachment. Immobilization of NAs on nylon membranes can be mediated in various ways (electrostatic interaction, UV cross-linking or chemical reaction) and the attachment is generally more stable than that to nitrocellulose. However, charged nylon membranes usually display a much higher nonspecific background in detection systems than nitrocellulose.

Membranes can also be made of charge-modified polyvinylidenedifluoride binding NAs through electrostatic interaction of the positively charged groups of the membrane polymer with the phosphate backbone of the NA.

Nitrocellulose and nylon membranes have been widely used in the production of macroarrays (arrays with probe sites of diameter 0.5 to 1 mm), but not so much in the production of microarrays (feature size of 25 to 200 μm) because of a lack of spot resolution (see Sect. 5.2, Spotting of Capture Probes). These membranes exhibit lateral wicking characteristics and the probe therefore tends to spread out from the point of application. Casting of these membranes onto the surface of glass slides is a solution to this problem [28].

4.3.2 Polypropylene

Polypropylene (PP) is a hydrophobic and chemically inert polymer which needs to be activated in order to be functional as a support for NA immobilization. Typically, PP membranes are aminated by exposure to an ammonia plasma generated by radiofrequency plasma discharge. Once aminated, the PP membranes can be reacted with derivatized ONDs using common coupling methods [56–58].

4.3.3 Anodic Alumina

Membranes have been developed that possess improved characteristics with respect to their lateral wicking and spot resolution. The best example of this type of material is anodically oxidized alumina whose structure consists of pores, with very little material forming the walls, possessing a surface area ratio of approximately 500 : 1. The benefits of this material are its higher sensitivity (more immobilized capture probe) and higher probe densities.

However, these membranes tend to be very friable and their fragility may limit their potential for use as substrates for microarray fabrication.

The immobilization of NAs onto these membranes is usually achieved through electrostatic interactions of the NA and surface under chaotropic conditions. However, chemical activation of the membrane by silanization is also possible and would allow covalent linkage of NAs to the support surface.

4.4 Polymeric Gels

Polymeric gels (mainly polyacrylamide and polysaccharides) have been also used as substrates for the attachment of NAs. These materials represent three-dimensional hydrophilic matrices through which the biomolecules can diffuse and interact. Polymeric gels cannot be used as substrates for DNA array production without their previous immobilization to a solid support (usually a glass slide) in the form of pads. This fixation can be stabilized covalently or electrostatically, depending on the type of gel and the support involved.

In theory, this kind of substrate permits the immobilization of large amounts of NA probe due to the greatly enhanced surface area of their 3D structure, providing the potential for enhanced sensitivity compared to planar substrates. However, the kinetics and the physical processes involved in the immobilization of NAs to this kind of substrate are different to those involved in their attachment to planar surfaces and therefore, whether a gel structure is a real advantage for a particular application may be questionable.

The kinetics of the immobilization of a NA onto a polymeric gel depends in part upon the diffusion of the probe through the gel structure. The rate of this process is determined by the viscosity of the gel and the possible non-specific interactions that occur between the NA and the polymeric matrix. On the contrary, considering planar substrates, NAs have direct access to the surface active groups for their attachment and the immobilization process proceeds more rapidly. The same principles are relevant when considering the hybridization and washing processes involved in using these materials in applications. These are generally slower when diffusion of the reactants comes into play in gel systems.

4.4.1 Polyacrylamide Gels

Conventionally, solutions of acrylamide or other acrylic monomers, or mixtures of them, can be photopolymerized onto flat glass surfaces which have previously been derivatized with acrylic groups to promote covalent and robust binding of the gel (e.g. by reaction with 3-(triethoxysilylpropyl)acrylamide) [59]. Irradiation of the substrate occurs through a mask, so that poly-

merization occurs only in the irradiated regions, leading to the formation of arrays of polyacrylamide "gel pads".

In a second step, the gel is functionalized for NA attachment. Common methods for polyacrylamide gel functionalization are based on the treatment of the polymerized support with reagents such as hydrazine or ethylenediamine. These treatments generate amine groups in the gel that can react with amine-modified ONDs via glutaraldehyde coupling, or directly with oxidized DNA probes (Fig. 15). Alternatively, the functional groups may be introduced by copolymerization reactions (e.g. co-polymerization with *N*-hydroxysuccinimide acrylic or oxirane acrylic derivatives) [59].

The capacity for 3D immobilization of acrylamide gels with ONDs has been reported to be at least 100 times superior to that of planar substrates [60].

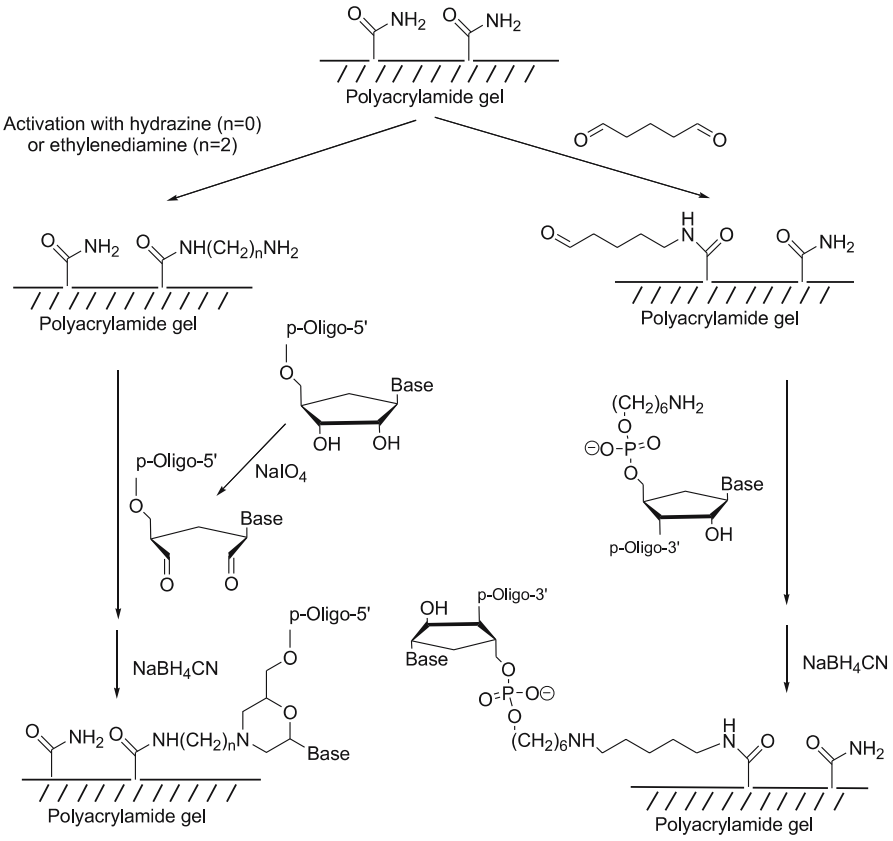

Fig. 15 Chemistry of immobilization of OND probes into polyacrylamide gel pads

4.4.2 Chitosan

Chitosan (Fig. 16) is an amino-modified natural polysaccharide that can be also used as a polymeric gel for the covalent binding of OND probes [61]. Chitosan offers several advantages for NA immobilization. Its pH responsive properties allow it to be easily immobilized onto glass slides for the construction of arrays. Specifically, chitosan is soluble at low pH, when its amine groups are protonated, but becomes insoluble when the pH is raised above its pKa ($\approx$ 6.3). Chitosan films are also transparent in the UV and visible regions of the light spectrum and thus have little effect on most optical detection methods. Also, chitosan's amine groups are more reactive in aqueous environments compared to other polyamines because of the low pKa value possessed by the primary amine (6.3 for chitosan vs. 10.5 for polylysine). Finally, other advantages of chitosan are that it is safe, abundant and inexpensive.

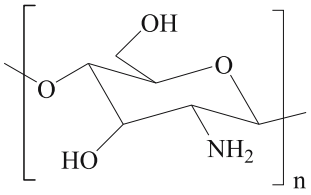

Fig. 16 Structure of chitosan

Amino-modified ONDs have been covalently immobilized to chitosan and their ability to hybridize with complementary fluorescent sequences has recently been demonstrated [61]. An appreciable nonspecific binding of OND to the chitosan matrix was observed as a consequence of electrostatic interaction between the polyphosphate backbone and the amine groups of the chitosan. This effect is reduced when glutaraldehyde is used as the coupling system, as in this case the amines are replaced by noncharged aldehyde groups. Alternatively, nonspecific adsorption can be reduced by washing with $MgCl_2$ and urea. Divalent cations (Mg^{2+}) stabilize the negatively charged OND backbone, removing electrostatic nonspecific interactions between chitosan and NAs. Urea on the other hand, interrupts hydrogen bonds between the OND and the chitosan [61].

4.4.3 Activated Dextrans

Dextrans are another class of carbohydrates that can be used as polymeric gels for the immobilization of NAs [62]. In their native form, dextrans cannot interact electrostatically or covalently with NAs and therefore must be acti-

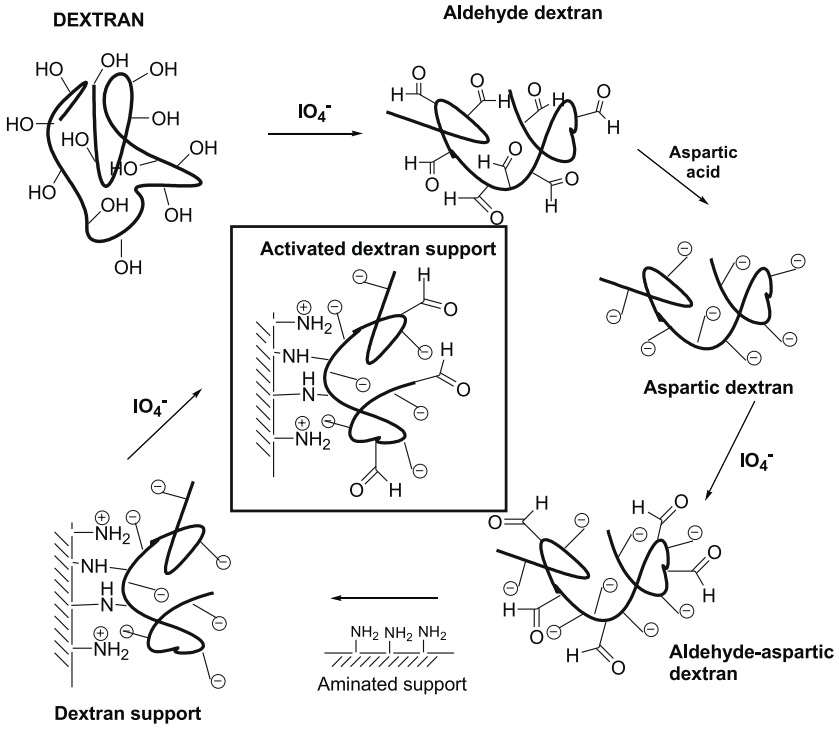

Fig. 17 Activation of dextran substrates with aspartic acid to reduce nonspecific adsorption [62]

vated so as to possess chemical functional groups before being used for such purposes. However, dextran hydroxyl groups can interact through H-bonding with NA backbones and consequently promote nonspecific adsorption of NAs, a less desirable property.

One way to reduce this nonspecific binding involves the modification of the dextran matrix to possess negatively charged species that will repel the negatively charged NA backbone. This has been achieved by oxidation of the chitosan hydroxyl groups to aldehydes and reaction of these groups with aspartic acid (Fig. 17). The aldehyde groups can be also used to fix the dextran to aminated glass supports to build a stable substrate. The same functionalization can be also used for the covalent attachment of amino-modified ONDs.

4.5 Other Substrates: Optical Fibers and Encoded Microspheres

All of the supports discussed previously can be used in the fabrication of flat ("positional") DNA arrays. New approaches to fabricating and applying arrays are continuously being developed, some of which do not rely on

the spatial location of the NA probe onto a particular substrate. Among these alternative approaches, optical fibers and microspheres have been used as supports for the fabrication of fiber-optic and suspension arrays, respectively.

Optical fibers (3 to 10 μm diameter) consisting of a glass core surrounded by a cladding material can be selectively etched on one end to form a microwell capable of hosting molecular species if modified with suitable surface chemistries [63]. Like any other glass surface, optical fibers are functionalized by treatment with organosilanes, whose head groups can be used to immobilize NAs [31]. By fusing thousands of individual optical fibers into a densely packed bundle, an "array" of NA-modified optical fibers can be constructed.

Suspension arrays are based on addressable nano- or micrometric beads of various chemical natures (polymeric, silica, gold) and architectures (uniform composition, core-shell particles) to which NAs can be immobilized by means of activating chemistries similar to those described for flat supports [64, 65] depending on the composition of the particles' outmost layer.

5
Patterning Techniques for the Delivery of Materials to the Substrate

The number of probe sites (features) per unit surface area in a DNA array reflects its information density and versatility in terms of parallel analysis of different sequences. In order to maximize these parameters, the features and their spacing in the array should be as small as possible, while retaining full sensitivity and discrimination in terms of detection. Decreasing the size of the features has the additional advantage of reducing the amount of target sample required for analysis in the application.

Different patterning techniques have been used in the fabrication of DNA arrays and are discussed in the following section.

5.1
In-situ Synthesis of Capture Probes

Arrays with short ONDs (15 to 25mers) can be manufactured by in situ OND synthesis onto the substrate. In order to get arrays with a high number of different OND sequences onto the same support, each specific sequence must be synthesized onto a defined area of the surface. Three different strategies have been used to achieve this: (i) photochemical deprotection of nucleotide precursors by site-selective irradiation through a mask (photolithographic); (ii) ink-jet delivery of nucleotide precursors (ink-jetting); and (iii) physical confinement of nucleotide precursors using intersecting channels and chambers in a microfluidics device. These are described below.

5.1.1 Photolithographic

In-situ photofabrication of OND arrays involves light-directed, spatially addressable, parallel (combinatorial) chemical synthesis [35, 43, 66–68]. A surface, usually a silicon wafer or a glass slide, is coated with linker molecules

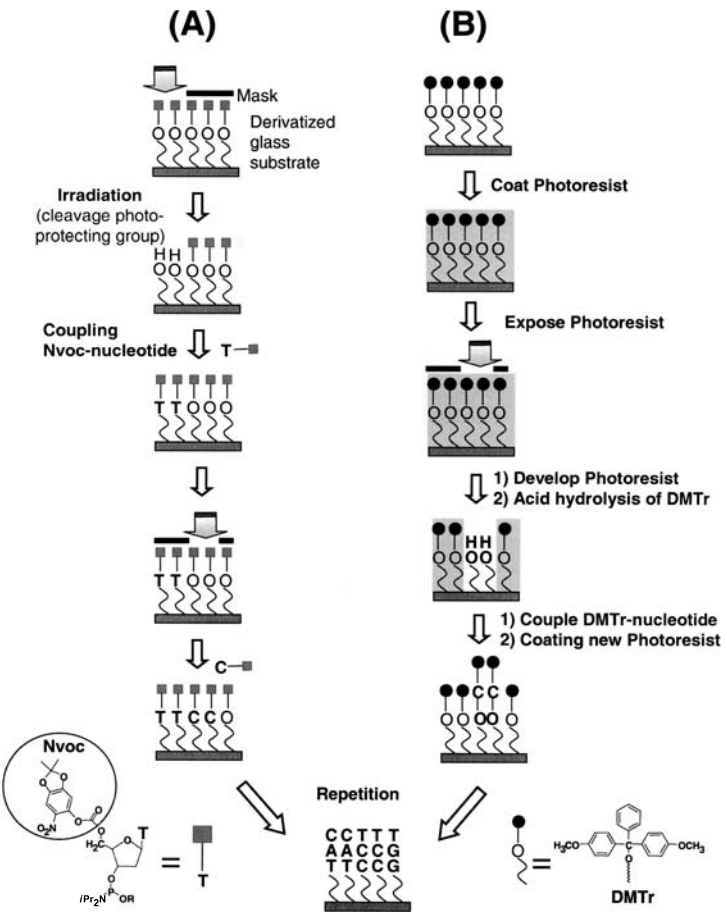

Fig. 18 Light directed OND synthesis onto substrates. **a** The patterning is mediated by photolabile groups (eg. Nitroveratryl, Nvoc) which protect the surface active groups. Light is directed through a mask to deprotect and activate selected sites, and protected nucleotides couple to the activated sites. The process is repeated, activating different sets of sites and coupling different bases allowing arbitrary DNA probes to be constructed at each site. In **b** the patterning is mediated by irradiation of a photoresist layer spin-coated onto the functionalized substrate. Irradiation through a mask removes the photoresist layer from selected places and allows coupling of nucleotides on those sites with surface functional groups

that bear photoremovable protecting groups or that are covered by a photoresist layer (Fig. 18). The pattern of irradiation (dictated by masks) deprotects (or removes photoresist from) certain regions, which are coupled to nucleotide monomer units that are exposed. The process is repeated to build up different sequences at different sites. This method enables 4^n different sequences of length n to be prepared in $4 \times n$ chemical steps. Using this method OND arrays of 1.6 cm^2 bearing up to 400 000 distinct probe sites have been prepared. In principle, the minimum feature size in these arrays is dictated by the wavelength of the irradiation source ("diffraction limit"). However, in practice current technologies have only produced features down to 25 μm.

The in-situ photolithography strategy has the advantage of generating arrays possessing the highest feature density and accuracy and reproducibility in application. However, the strategy also has some drawbacks. The effective maximum length of the immobilized ONDs is restricted to 25mers as a consequence of the efficiency of their synthesis, and the fact that "failed" sequences cannot be removed from the support's surface. In addition, light-sensitive deprotection reactions involve expensive chemistry and special, costly clean rooms are required for the fabrication of such arrays [69]. For these reasons, in-situ photolithographic synthesized OND arrays are not easily customizable and their price restricts their use in research labs.

These drawbacks may be overcome in the near future, if the promise of bench-top synthesizers that allow the in situ synthesis of OND arrays is realized [70]. These devices make use of a more flexible technology that replaces the chrome masks with virtual masks generated on a computer, which are relayed to a digital micromirror array. In this way OND arrays containing more than 76 000 features measuring 16 μm^2 have been constructed [70].

PNAs can be also synthesized in situ in a parallel manner by using the so-called SPOT method [71, 72]. Decamer PNA strands have already demonstrated sufficient selectivity and stability in screening assays compared to ONDs [26]. The number of steps in SPOT array fabrication is therefore substantially less than that for OND arrays.

5.1.2 Ink-jetting

This method for in-situ synthesis of ONDs involves the delivery of small amounts of the synthesis reagents to the appropriate sites on the substrate using technology similar to that involved in ink-jet printing. Droplets of between 30 to 100 μL of nucleotide phosphoramidite reagents are projected through a nozzle as a consequence of a piezoelectric impulse to create synthesis sites about 50 μm in diameter on the support surface. A complete synthesis cycle starts by delivering the first phosphoramidite monomer to each probe site on a support modified with hydroxyl groups. The entire support is then

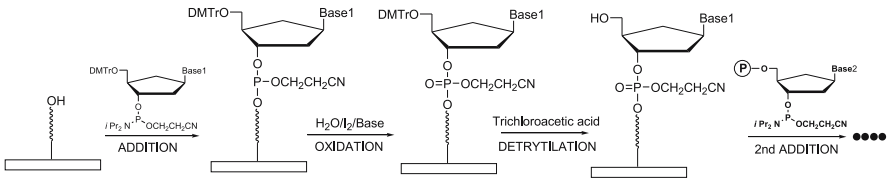

Fig. 19 Basic steps in a cycle of nucleotide addition by the phosphoramidite method in-situ synthesis using ink-jetting. DMTr = dimethoxytrityl group

rinsed to remove excess reagent and then treated with acid to deprotect the 5′ terminus (detritylation) of the growing OND in preparation for the next round of synthesis. Figure 19 shows the basic chemistry involved in these steps. Up to 100 000 different ONDs of up to 60 bases in length have been immobilized onto a 75 mm diameter silicon wafer and used in hybridization to target sequences [73].

The surface tension between the support surface and the solvent used are crucial factors influencing this method, since they determine (together with the volume of the droplet delivered) the dimensions of the feature ultimately produced. In principle, polar solvents and hydrophobic surfaces should be employed to minimize the drop diameter in contact with the surface. However, the hydrophobicity of the surface is limited by the fact that it must also have reactive groups to which the phosphoramidite nucleotide can become conjugated. Hydrophobic surface coatings containing exposed hydroxyl groups and propylene carbonate solvent have been already used for such purposes [73]. Alternatively, the surface may be patterned with "reactive" wells surrounded by hydrophobic regions (perfluorinated or alkyl chains) in order to "localize" the droplets by virtue of surface tension effects [74].

5.1.3
Reagent Confinement in Microchannels

Flooding nucleotide precursors through orthogonally intersecting channels has been used to make arrays of ONDs of any desired length [28]. This procedure does not require the use of expensive photoremovable groups. However, the fact that the microfluidics capillary system requires a very accurate control of the volumes of reagents delivered, and that the patterning technology required for its fabrication is not particularly economic, makes this approach not particularly attractive currently [75–77].

5.2
Spotting of Capture Probes

As an alternative to in-situ synthesis of DNA arrays, presynthesized OND material can be delivered onto specific positions of flat surfaces by means of

different delivery systems. Spotting cDNA or OND (50 to 120mers) solutions onto a surface can involve either bringing a "pin" or needle into contact with the surface (printing technology) or projecting a liquid droplet from a jet nozzle under pressure (ink-jetting technology). Usually multiple pins or jets integrated in a printhead are used to speed up array production. Using these techniques, arrays consisting of more than 30 000 spots can be fitted onto the surface of a conventional microscope slide with typical spot sizes being between 75 to 500 μm in diameter.

A quality issue in spotting is the inhomogeneous immobilization of the cDNA or ONDs within each spot that can arise as a consequence of solvent evaporation; the so-called "doughnut effect". Means to avoid this problem involve controlling environmental conditions during deposition (relative humidity) and changing the wettability properties of the drop by using a different solvent mixture for the solution. Another issue is the spread out of the spot once it is delivered on the surface. This can be avoided by modification of the surface with hydrophobic coating agents, which can lead to an increase in surface tension and contact angle of the drop.

Spotted arrays have the advantage over in-situ synthesized arrays of being easily customizable, since they can be produced directly in the laboratory by individual investigators. Practically speaking, however, managing large clone libraries can be a daunting task for most laboratories, and making high-quality spotted arrays can be difficult.

5.2.1 Printing

In this approach, NAs are directly deposited onto a glass support using a robot able to deliver with high precision a sample to a specific x:y programmed location. The NA sample is loaded into a spotting pin (highly miniaturized stainless-steel fountain-pen nibs with a gap) by capillary action, and small volumes are transferred to a solid surface, such as a microscope slide, by direct physical contact between the pin and the solid substrate. Spot size depends on the acceleration of the pen towards and away from the slide, and the surface tension of the slide. After the first spotting cycle, the pin is washed and a second sample is then transferred to an adjacent address. A robotic control system and multiplexed print heads allow the automated immobilization of many different probes simultaneously onto the slide [29].

Crucial factors affecting array fabrication using the printing method are the reproducibility of the immobilization process, the durability of the spotting pins and the wastage of printing material, since the pin needs to be washed after every spotting process. The development of noncontact spotting methods (ink-jet) may potentially reduce the wastage of print material while offering increased precision and speed.

5.2.2
Ink-jetting

Spotting NA solutions by ink-jetting uses the same technology described for in-situ synthesis. The "ink" (NA solution) is ejected in the form of droplets from a reservoir through a nozzle as a consequence of an acoustic pulse that is generated either thermally or piezo-electrically. In a thermal inkjet printer, ink is heated locally to form a rapidly expanding vapor bubble that ejects an ink droplet. Piezo-electric inkjet printing relies on the deformation of a piezo-electric membrane to generate the acoustic pulse [78].

The most crucial part of inkjet printing technology is the "ink" and its physical properties: its surface tension needs to be high enough to prevent dripping of the "ink" from the nozzle, but its viscosity needs to be low enough for it to be ejected without the need of large forces. High surface tension (hydrophobicity) of the support surface is essential as well for maintaining drop shape and size on the surface after printing.

5.3
Microcontact Printing of Capture Probes

Microcontact printing (μCP) is another technique that can be used to place NAs onto different target surfaces. This technique makes use of an elastomeric stamp of polydimethylsiloxane (PDMS) and produces features with lateral resolution in the submicrometer range. The PDMS stamp is topographically structured by casting a PDMS prepolymer against a 3D master. The stamp is then "inked" with the molecules of interest, rinsed with buffer, blown dry under a stream of nitrogen, and then used to print the material onto the substrate surface (see Fig. 20).

The transfer of the printing material from the PDMS stamp to the support is a process driven by a careful balance based upon the affinity of the two surfaces (that of the stamp and that of the substrate) for the NA molecules. The surface of the PDMS stamp has to be attractive enough to DNA molecules to

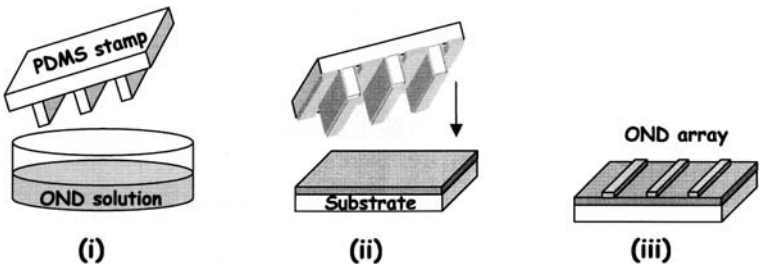

Fig. 20 Patterning DNA arrays by the micro-contact printing method

bind them reversibly from the "inking solution" so that the release of the DNA is not hindered when the stamp is contacted and removed from the target surface. Since NAs are negatively charged polyelectrolytes, electrostatic interactions play a major role in determining adsorption and transfer properties of the NAs.

One possibility for increasing the affinity of the surface of the PDMS stamp and the support for NA molecules is their modification with amino functionalities. Tight binding of the NA to the aminated surface is promoted at a pH below the pKa of the amine due to the electrostatic attraction forces between the negatively charged NA and the positively charged surface. Such an approach has been used for printing DNA layers on glass slides [79]. The DNA pattern obtained lacked the typical inhomogeneities mentioned previously for spotted arrays (mainly due to the absence of a drying process), and possesses feature sizes down to 1 μm. Figure 21 shows the fluorescence image of such a pattern.

An advantage of μCP could be its demonstrated capability of printing multiple arrays from one loaded stamp without loosing homogeneity of the surface or edge definitions of features [79]. The parallel transfer of 16 different NAs in a single printing step for array production using this method has been described [79]. This has been performed by means of microfluidic networks. If different regions of a topographically structured PDMS stamp are

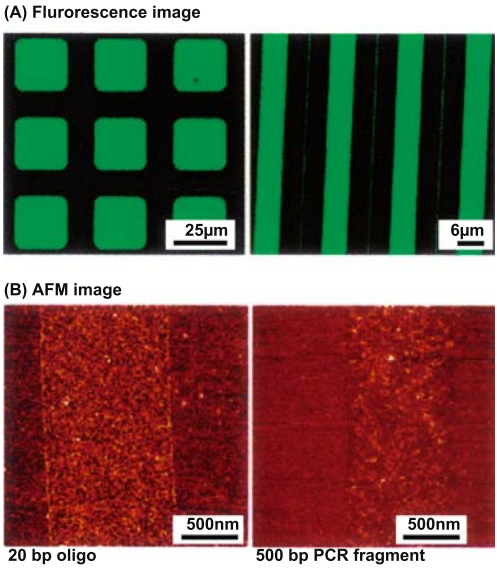

Fig. 21 **a** Fluorescence images of μCP-immobilized fluorescein labeled ONDs on a glass surface. The pattern size is limited only by the use of manufactured molds with the desired feature size. **b** AFM images of stamped 1 μm lines of 20-bp ONDs (*left*) and 500bp PCR fragments (*right*) on mica substrates [79]. Reprinted with permission

brought in contact with parallel microchannels, each loaded with a different sample, arrays with 16 different probe sites may be printed.

5.4 Scanning Probe Lithography of Capture Probes

5.4.1 Dip-Pen Nanolithography

DNA arrays have been also generated by "Dip-Pen Nanolithography" (DPN) [80]. DPN involves the transfer of NAs directly from a coated Atomic Force Microscope (AFM) tip to the substrate of interest by virtue of direct molecular diffusion. Using this technique, thiol-modified ONDs have been patterned onto gold substrates and acrylamide-modified ONDs onto glass slides that were previously modified with mercaptopropyltrimethoxysilane. Feature sizes ranging from many micrometers to less than 100 nanometers could be obtained. The deposition of two different OND sequences onto the same substrate has also been reported [80], but the application of this principle to the fabrication of high-density arrays remains to be addressed.

5.4.2 Nanografting

Nanografting is another lithography technique involved in NA immobilization. In this case, the substrate surface is first modified with a resist (such as a monolayer of alkanethiol) and placed in an AFM fluid cell containing the NA in solution needing to be patterned [81, 82]. At high contact force (10 to 20 nN), the resist molecules are removed by the AFM tip, exposing the bare surface to the NA solution. The arrayed material can then adsorb to the substrate at the patterned (bare) regions. Using this technique, features as small as 10 nm have been produced. Alternatively, nanografting can be performed without a fluid cell by delivering the patterning molecules from a coated AFM tip through a resist with high contact force, in what could be called "dip-pen nanografting" [83, 84]. See Fig. 22 for a representation of these methods.

Another related technique is meniscus force nanografting (MFN), whereby the patterning material is applied as a small drop on a resist-covered substrate, and an AFM tip selectively penetrates the resist, delivering the patterning material to the gold surface [85]. The surface tension of the liquid drop itself supplies the constant force necessary to displace the resist molecules. This fact constitutes the main difference between MFN and the previously described DPN and AFM-based nanografting. In these techniques, the normal force between the AFM tip and the substrate necessary to displace the resist layer is supplied by the flexing of the AFM cantilever and is kept constant by AFM feedback. MFN eliminates the need for AFM feedback control allowing

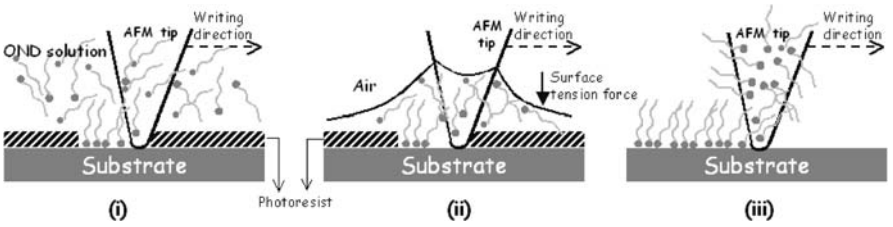

Fig. 22 Patterning of OND or DNA solutions by means of an AFM tip. (i) Nanografting, (ii) Meniscus-Force Nanografting, (iii) Dip-pen lithography

more rapid fabrication of the array. In particular, pattern lines of less than 100 μm have been produced by MFN at a speed as fast as 320 μm/s (more than 3 orders of magnitude faster than traditional AFM-based nanografting and 2 orders of magnitude faster than DPN).

5.5 Site-Selective Attachment of Capture Probes onto Chemical Templates

An alternative to the delivery techniques described previously involves using surface chemistry alone to assist in site-selective attachment of NAs at predetermined locations. This approach relies on the generation of a surface chemical pattern possessing adsorbing and nonadsorbing regions, in such

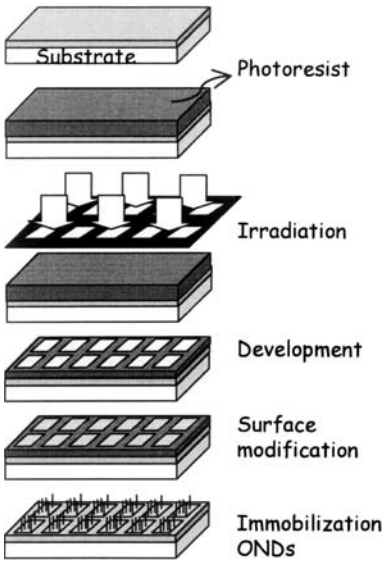

Fig. 23 Site-selective attachment of NAs onto chemically patterned surfaces

a way that DNA attachment is directed towards the former without the use of additional positioning tools.

Various fabrication schemes have emerged using this approach. A common one is the site-selective photochemical etching of an organosilane-modified surface by irradiation through a mask [86]. This results in a chemically patterned surface with active sites, where modified ONDs can be attached, surrounded by bare (irradiated) regions.

Alternatively, chemical patterns can be generated by photolithography of a photoresist layer that has been spin-coated over a silane film. Upon irradiation through a mask and subsequent development of the photoresist pattern, the underlying modified layer is revealed and is able to react with the ONDs. By sequentially irradiating the surface, it is possible to immobilize different ONDs.

Other examples include the generation (via photolithography and surface chemical modification techniques) of substrates bearing alkyl or perfluorinated hydrophobic backgrounds and carboxylic-terminated areas to which ONDs can be immobilized (Fig. 23) [46, 87, 88].

6 Conclusions

With the increasing use of DNA chips, different systems and strategies for the patterned immobilization of NAs have arisen and some in particular have become well established. Each different method is championed by different groups as the best procedure [89–92]. Often the comparisons of methods reported in the literature include different substrates (which may have different densities of functional groups, different hydrophobicity, or different roughness) and different coupling chemistries or delivery systems without systematic characterization of which parameters are affecting each step of the immobilization process. Together with the intrinsic difficulties associated with handling materials as complex as biomolecules it is therefore almost impossible to make valid comparisons between the methods.

In reality there is probably neither a "best" method nor substrate for NA immobilization in array fabrication and certainly array fabrication is neither a simple nor straightforward process [93]. For these reasons, at least for the time being it seems likely that array fabrication will remain in the hands of "experts" and that it will become ever more common for dedicated organizations to act as service providers in array screening for researchers, clinicians etc.

A truly systematic and integrated study is required to compare and contrast, as well as optimize the approaches described in this chapter for DNA immobilization to provide an "industry standard" for the future.

Acknowledgements The authors wish to acknowledge the European Union for support from Framework Program 5 and specially the CHEMAG RTD project (G5RTD-CT-2001-00534).

References

1. Hitt E (2004) Scientist 18:38
2. Holloway AJ, van Laar RK, Tothill RW, Bowtell DDL (2002) Nat Gen 32:481
3. Stears RL, Martinsky T, Schena M (2003) Nature Medicine 9:140
4. Wheatley JB, Lyttle MH, Hocker MD, Schmidt DE (1996) J Chromatography A 726:77
5. Skrzypczynski Z, Wayland S (2004) Biocon Chem 15:583
6. Skrzypczynski Z, Wayland S (2003) Biocon Chem 14:642
7. Rogers YH, Jiang-Baucom P, Huang ZJ, Bogdanov V, Anderson S, Boyce-Jacino MT (1999) Anal Biochem 266:23
8. Charles PT, Vora GJ, Andreadis JD, Fortney AJ, Meador CE, Dulcey CS, Stenger DA (2003) Langmuir 19:1586
9. Defrancq E, Hoang A, Vinet F, Dumy P (2003) Bioorg Med Chem Lett 13:2683
10. Boncheva M, Scheibler L, Lincoln P, Vogel H, Akerman B (1999) Langmuir 15:4317
11. Fang SY, Bergstrom DE (2003) Biocon Chem 14:80
12. Guzaev A, Lonnberg H (1999) Tetrahedron 55:9101
13. Brown R, Smith WE, Graham D (2001) Tetrahedron Lett 42:2197
14. Kumar A, Larsson O, Parodi D, Liang Z (2000) Nucleic Acid Res 28:e71
15. Kumar A, Liang Z (2001) Nucleic Acid Res 29:e2
16. Maier MA, Yannopoulos CG, Mohamed N, Roland A, Fritz H, Mohan V, Just G, Manoharan M (2003) Biocon Chem 14:18
17. Safinya CR (2001) Curr Opin Struc Biol 11:440
18. Shchepinov MS, CaseGreen SC, Southern EM (1997) Nucleic Acid Res 25:1155
19. Guo Z, Guilfoyle RA, Thiel AJ, Wang R, Smith LM (1994) Nucleic Acid Res 22:5456
20. Chou CC, Chen CH, Lee TT, Konan P (2004) Nucleic Acid Res 32:e99
21. Bruce IJ, Taylor J, Todd M, Davies MJ, Borioni E, Sangregorio C, Sen T (2004) J Magn Magn Mat 284:145–160
22. Petrovykh DY, Kimura-Suda H, Tarlov MJ, Whitman LJ (2004) Langmuir 20:429
23. Kimura-Suda H, Petrovykh DY, Tarlov MJ, Whitman LJ (2003) J Am Chem Soc 125:9014
24. Wolf LK, Gao Y, Georgiadis RM (2004) Langmuir 20:3357
25. Brandt O, Feldner J, Stephan A, Schroder M, Schnolzer M, Arlinghaus HF, Hoheisel JD, Jacob A (2003) Nucleic Acid Res 31
26. Matysiak S, Hauser NC, Wurtz S, Hoheisel JD (1999) Nucleosid Nucleotid 18:1289
27. Strother T, Cai W, Zhao XS, Hamers RJ, Smith LM (2000) J Am Chem Soc 122:1205
28. Southern E, Mir K, Shchepinov M (1999) Nat Gen 21:5
29. Cheung VG, Morley M, Aguilar F, Massimi A, Kucherlapati R, Childs G (1999) Nat Gen 21:15
30. Frey BL, Corn RM (1996) Anal Chem 68:3187
31. Beaucage SL (2001) Curr Med Chem 8:1213
32. Consolandi C, Castiglioni B, Bordoni R, Busti E, Battaglia C, Bernardi LR, De Bellis G (2002) Nucleosid Nucleotid Nucleic Acids 21:561
33. Chu SK, Hsu M, Ku WC, Tu CY, Tseng YT, Lau WK, Yan RY, Ma JT, Tzeng CM (2003) Biochem J 374:625

34. Sen T, Bruce IJ (2005) Langmuir 21:7029–7035
35. Pirrung MC (2002) Angew Chem-Int Edn 41:1277
36. Oh SJ, Cho SJ, Kim CO, Park JW (2002) Langmuir 18:1764
37. Halliwell CM, Cass AEG (2001) Anal Chem 73:2476
38. Beier M, Hoheisel JD (1999) Nucleic Acid Res 27:1970
39. Dolan PL, Wu Y, Ista LK, Metzenberg RL, Nelson MA, Lopez GA (2001) Nucleic Acid Res 29:e107
40. Benters R, Niemeyer CM, Wohrle D (2001) Chembiochem 2:686
41. Trevisiol E, Le Berre-Anton V, Leclaire J, Pratviel G, Caminade AM, Majoral JP, Francois JM, Meunier B (2003) New J Chem 27:1713
42. Le Berre V, Trevisiol E, Dagkessamanskaia A, Sokol S, Caminade AM, Majoral JP, Meunier B, Francois J (2003) Nucleic Acid Res 31:e88
43. Glazer M, Fidanza J, McGall G, Frank C (2001) Chem Mater 13:4773
44. Lin Z, Strother T, Cai W, Cao XP, Smith LM, Hamers RJ (2002) Langmuir 18:788
45. Strother T, Hamers RJ, Smith LM (2000) Nucleic Acid Res 28:3535
46. Schouten S, Stroeve P, Longo ML (1999) Langmuir 15:8133
47. Peterson AW, Heaton RJ, Georgiadis RM (2001) Nucleic Acid Res 29:5163
48. Aqua T, Naaman R, Daube SS (2003) Langmuir 19:10 573
49. Bamdad C (1998) Biophys J 75:1997
50. Wang Y, Vaidya B, Farquar HD, Stryjewski W, Hammer RP, McCarley RL, Soper SA, Cheng YW, Barany F (2003) Anal Chem 75:1130
51. Shamansky LM, Davis CB, Stuart JK, Kuhr WG (2001) Talanta 55:909
52. Liu DJ, Perdue RK, Sun L, Crooks RM (2004) Langmuir 20:5905
53. Livache T, Bazin H, Mathis G (1998) Clin Chim Act 278:171
54. Livache T, Guedon P, Brakha C, Roget A, Levy Y, Bidan G (2001) Synt Met 121:1443
55. Livache T, Maillart E, Lassalle N, Mailley P, Corso B, Guedon P, Roget A, Levy Y (2003) J Pharm Biomed Anal 32:687
56. Matson RS, Rampal J, Pentoney SL, Anderson PD, Coassin P (1995) Anal Biochem 224:110
57. Matson RS, Rampal JB, Coassin PJ (1994) Anal Biochem 217:306
58. Matson RS, Rampal JB, Coassin PJ (1994) Anal Biochem 220:225
59. Timofeev EN, Kochetkova SV, Mirzabekov AD, Florentiev VL (1996) Nucleic Acid Res 24:3142
60. Proudnikov D, Timofeev E, Mirzabekov A (1998) Anal Biochem 259:34
61. Yi HM, Wu LQ, Sumner JJ, Gillespie JB, Payne GF, Bentley WE (2003) Biotech Bioeng 83:646
62. Fuentes M, Mateo C, Garcia L, Tercero JC, Guisan JM, Fernandez-Lafuente R (2004) Biomacromol 5:883
63. Epstein JR, Leung APK, Lee KH, Walt DR (2003) Biosens Bioelectr 18:541
64. Battersby BJ, Trau M (2002) Trends Biotech 20:167
65. Lam KS, Renil M (2002) Curr Opin Chem Biol 6:353
66. McGall G, Labadie J, Brock P, Wallraff G, Nguyen T, Hinsberg W (1996) Proc Nat Acad Sci USA 93:13 555
67. Pirrung MC, Fallon L, McGall G (1998) J Org Chem 63:241
68. Lipshutz RJ, Fodor SPA, Gingeras TR, Lockhart DJ (1999) Nat Gen 21:20
69. Saluz HP, Iqbal J, Limmon GV, Ruryk A, Wu ZH (2002) Curr Sci 83:829
70. Singh-Gasson S, Green RD, Yue Y, Nelson C, Blattner F, Sussman MR, Cerrina F (1999) Nat Biotech 17:974
71. Matysiak S, Reuthner F, Hoheisel JD (2001) Biotechniques 31:896
72. Frank R (1992) Tetrahedron 48:9217

73. Hughes TR, Mao M, Jones AR, Burchard J, Marton MJ, Shannon KW, Lefkowitz SM, Ziman M, Schelter JM, Meyer MR, Kobayashi S, Davis C, Dai HY, He YDD, Stephaniants SB, Cavet G, Walker WL, West A, Coffey E, Shoemaker DD, Stoughton R, Blanchard AP, Friend SH, Linsley PS (2001) Nat Biotech 19:342
74. Blanchard AP, Kaiser RJ, Hood LE (1996) Biosens Bioelectr 11:687
75. Maskos U, Southern EM (1993) Nucleic Acid Res 21:2267
76. Maskos U, Southern EM (1993) Nucleic Acid Res 21:4663
77. Southern EM, Maskos U, Elder JK (1992) Genomics 13:1008
78. de Gans BJ, Schubert US (2003) Macromol Rapid Commun 24:659
79. Lange SA, Benes V, Kern DP, Horber JKH, Bernard A (2004) Anal Chem 76:1641
80. Demers LM, Ginger DS, Park SJ, Li Z, Chung SW, Mirkin CA (2002) Science 296:1836
81. Xu S, Liu GY (1997) Langmuir 13:127
82. Wadu-Mesthrige K, Xu S, Amro NA, Liu GY (1999) Langmuir 15:8580
83. Amro NA, Xu S, Liu GY (2000) Langmuir 16:3006
84. Delamarche E, Hoole ACF, Michel B, Wilkes S, Despont M, Welland ME, Biebuyck H (1997) J Phys Chem B 101:9263
85. Schwartz PV (2001) Langmuir 17:5971
86. Chrisey LA, Oferrall CE, Spargo BJ, Dulcey CS, Calvert JM (1996) Nucleic Acid Res 24:3040
87. Blanchard AP, Kaiser RJ, Hood LE (1996) Biosens Bioelectr 11:687
88. Gillmor SD, Thiel AJ, Strother TC, Smith LM, Lagally MG (2000) Langmuir 16:7223
89. Zammatteo N, Jeanmart L, Hamels S, Courtois S, Louette P, Hevesi L, Remacle J (2000) Anal Biochem 280:143
90. Lindroos K, Liljedahl U, Raitio M, Syvanen AC (2001) Nucleic Acid Res 29:e69
91. Walsh MK, Wang XW, Weimer BC (2001) J Biochem Biophys Met 47:221
92. Taylor S, Smith S, Windle B, Guiseppi-Elie A (2003) Nucleic Acid Res 31
93. Manning M, Harvey S, Galvin P, Redmond G (2003) Mater Sci Eng C-Bio S 23:347

Top Curr Chem (2005) 260: 113–160
DOI 10.1007/b136672

Published online: 15 September 2005

Scanning Probe Microscopy Studies of Surface-Immobilised DNA/Oligonucleotide Molecules

Dan V. Nicolau (✉) · Prashant D. Sawant

Swinburne University of Technology, BioNanoEngineering Labs, PO Box 218, VIC 3122 Hawthorn, Australia
dnicolau@swin.edu.au

Abstract Although most in vivo biomolecular recognition occurs in solution, in many practical situations (e.g., diagnostics, drug discovery and biosensing) biomolecular recognition occurs between "target" biomolecules immobilised on surfaces and "probe" complementary biomolecules approaching the surface from solution. DNA-based devices

are by far the most common biomolecular and cellular planar biodevices with a still-commanding growth rate. A second, but chronologically older, interest derives from the need to understand the fundamentals of biomolecular interactions at single molecule level and in large supramolecular assemblies. Again, DNA molecules are not only essential objects of study, but also more attractive candidates as the building blocks of artificial biomolecular devices than, e.g., proteins, because of their relative simplicity and robustness.

Among the many microscopy-based techniques for the study of biomolecular interactions on surfaces, scanning probe microscopies, and especially the atomic force microscopies (AFM), are the most used because of their molecular and sub-molecular level resolution and in situ imaging capability. Apart from the high resolution mapping of surface nanotopographies, AFM can be used for the quantification and visualisation of the distribution of chemistry, hydrophobicity and local mechanical properties on surfaces, and for the fabrication of nanostructures on surfaces.

The present article, which reviews from classical and latest developments regarding AFM studies of DNA molecules immobilised on surfaces, is organised along the nature of DNA aggregates on surfaces, i.e., single molecules, self-assembled layers and amorphous layers, with the last two emerging areas receiving a relatively higher emphasis. Within these three areas of application, the material is organised along the main functions of the AFM, namely imaging, probing biomolecular interactions and fabrication of nanodevices.

1 Introduction

Most, if not all, in vivo biomolecular recognition events happen in solution with complementary biomolecules interacting freely and individually with each other due to the unhindered molecular orientation and low concentration. However, in many practical situations, the biomolecular recognition events in vitro, e.g., for diagnostic, drug discovery and biosensing, occur between "target" biomolecules immobilised on surfaces and "probe" complementary biomolecules approaching the surface from solution. The immobilised biomolecules are aggregated on surfaces at high concentrations, hence in molecularly hindered positions, and possibly in constrained conformations, which all conspire to result in decreased and/or non-specific biomolecular recognition. Moreover, the importance of understanding the differences between biomolecular recognition in vivo and in vitro (the latter being used to mimic the former) is greatly amplified by the increased use of the immobilisation of biomolecules on surfaces for advanced biodevices (e.g., biochips and microarrays), which are fabricated using planar technologies derived from semiconductor manufacturing. Among the several types of biomolecular and cellular planar biodevices, the DNA-based devices are by far the most common and with a still-commanding growth rate. For instance, the market for DNA chips and microarrays, which have been the powerhorses of the genomics revolution, expanded from less than US$50 mil in 1997 to more than $500 mil in 2000, i.e., an annual growth of approximately 150%,

reaching an expected US$1.2 bil by 2006. It follows that an important motivation for the study of the behaviour of biomolecules on surfaces is the design, fabrication and operation of cost-effective, sensitive and efficient biodevices, which comprise high density, amorphous biomolecular layers on engineered surfaces.

Another motivation for the study of surface-immobilised biomolecules is the opposite of the above. If the study of high concentrations of surface-immobilised biomolecules is application-driven, in many instances fundamental studies regarding the processes involving individual biomolecules can be observed and quantified only if the biomolecules are immobilised on surfaces. The immobilisation on flat or profiled surfaces allows very precise imaging and manipulation of biomolecules and, when required, the measurement of forces involved in biomolecular recognition. While the surface-immobilised single molecule studies address one of the potential problems mentioned above, i.e., the individual molecular interaction, inherently associated with the extrapolation of biomolecular recognition from in vitro to in vivo, the surface-induced conformational change is still an open problem. Luckily, the fact that the DNA molecules are relatively robust compared with other biomolecules, especially proteins, reduces the magnitude of the problem. On the other hand, this very robustness (and relative structural simplicity) allowed the development of advanced manipulation techniques of single DNA molecules on surfaces. These molecular manipulation techniques, together with the information storage capabilities and electrical properties of DNA molecules, open the possibility of DNA-based molecular devices.

A third motivation for the study of biomolecules immobilised on surfaces is given by the opportunities, rather than the drawbacks, offered by surface-induced effects. At molecular concentrations, or rather molecular densities, slightly higher than those used for single molecule studies, and especially if the surfaces are structured at nano- and sub-nanolevel, the biomolecules interact between themselves and the surface to produce self-assembled structures that have a molecular organisation expanding more laterally than vertically (as it is the case for self-assembled monolayers and Langmuir–Blodgett films) well beyond the individual component molecules. Whilst several proteins, e.g., actin, are also capable of surface-induced self-assembly, the DNA molecules seem to be the ideal building blocks for laterally organised self-assembled layers because of their properties mentioned above, i.e., relative robustness and simplicity. These DNA self-assembled layers are promising candidates for biomolecular computation nanodevices, given the information-driven self-assembly of DNA molecules.

The motivations for the study of biomolecules immobilised on surfaces, briefly outlined above, also provide an explanation for the increased popularity of microscopy-based techniques. Indeed, while for single molecule and self-assembled layers the use of microscopy techniques is obvious, the commercial biodevices are increasingly micro- and even nanoscale devices.

Moreover, for many of these, the microscopy techniques are not only used for research and development but also for the readout (e.g., confocal microscopes for microarrays) and even for the fabrication (e.g., AFM) of nanoarrays. Also, the continuous miniaturisation of biodevices will eventually reach the desired single molecule detection level—another strong incentive for the general use of advanced microscopy techniques.

Among the many microscopy-based techniques for the study of biomolecules immobilised on surfaces, scanning probe microscopies (SPM) and especially atomic force microscopies (AFM) are arguably the most used techniques because of their molecular and sub-molecular level resolution and in situ imaging capability. Moreover, the invasiveness of AFM, which is less of a problem for the DNA molecules, is essential for another two functions, apart from the mapping of surface nanotopographies, namely the quantification and visualisation of the distribution of chemistry, hydrophobicity and local mechanical properties on surfaces; and the fabrication of nanostructures.

An expression of this increased interest is the increase of the publications [1] dealing with DNA or oligonucleotides and SPM or AFM (Fig. 1), along with several very good reviews [2–8]. Comparing with these reviews, and apart from updating the reader with the most recent information regarding AFM studies of DNA molecules immobilised on surfaces, the present work is different in its organisation along the nature of DNA aggregates on surfaces, i.e., single molecules, self-assembled layers and amorphous layers. The last two areas received a relatively higher emphasis than the actual number of references would suggest, because they are more application-oriented, emerging areas and because they received less attention in the literature. Within these three application areas, i.e., single molecules, self-assembled layers and amorphous layers, the material is organised along the main functions of

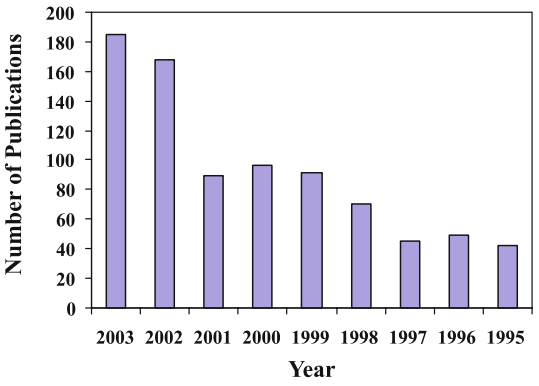

Fig. 1 Evolution of the number of papers with "atomic force microscopy" and "DNA" as keywords (analysis using ISI database [8])

AFM, namely imaging, probing biomolecular interactions and fabrication techniques.

2 Atomic Force Microscopy

The invention of the scanning tunnelling microscope by Rohrer and Binning in 1981 [9] triggered the emergence of many related SPMs [10] (Fig. 2), including the AFM [11]. Although all these techniques are useful for the study of different properties of different materials, AFM is arguably the most popular due to several limitations of the SPMs. For instance, the resolution of the scanning near field optical microscopy (SNOM) is limited to around 100 nm, the photon scanning tunnelling microscope (PSTM) requires operation in vacuum, while other scanning microscopes are limited to a very specific functionality. A common drawback of the SPM instruments, including AFM, is the imaging and analysis of very small area—an acceptable price to pay for their very high resolution.

The essential constitutive elements of an AFM instrument (Fig. 3) are:

- An extremely sharp tip which is dragged on the probed sample, which is mounted on a precision xy table
- A vibrating cantilever on which the tip is mounted
- An optical system used to determine the position of the cantilever and integrated tip

The optical system comprises a laser, which is reflected by a mirror mounted on the back of the cantilever to another mirror that sends the reflected beam to an array detector. The position of the beam translates in the position of the cantilever in the vertical direction, whereas the lateral position in xy coordinates is inferred from the movement of the xy table. Essentially, AFM uses a feedback system to measure and regulate the force applied on the scanned sample, which allows the acquisition of images using very low forces.

The cantilevers can be modelled as elastic springs (Fig. 4), generally characterised by spring constants calculated from the resonant frequency of the spring as follows:

$$resonant\ frequency = \frac{1}{2\pi}\sqrt{\frac{spring\ const}{mass}} \tag{1}$$

The above relationship shows that, for a cantilever of small mass, a combination of a low spring constant and high resonant frequency is needed. The spring constants of the commercially available cantilevers vary over four orders of magnitude, from 0.005 to 40 N/m. Thicker and shorter tips tend to be stiffer and have higher resonant frequencies.

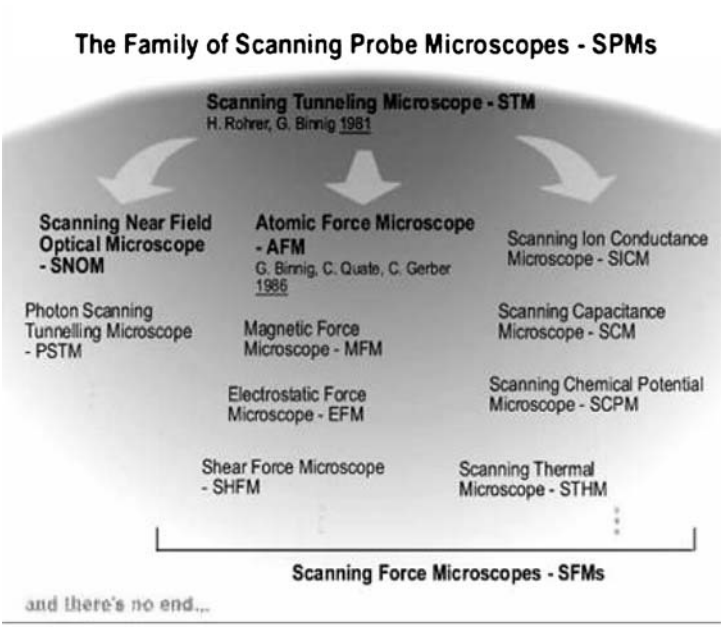

Fig. 2 Family of scanning probe microscopy [10]. Reprinted with permission

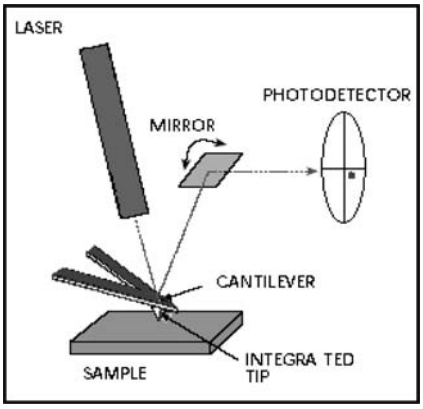

Fig. 3 Principle of operation of AFM

This inherent nanomechanical versatility of AFM translates in the capacity to analyse not only hard, incompressible samples but also soft, compressible ones, such as biomolecules and cells. Moreover, the AFM has the capability to operate in air (i.e., no vacuum needed) and in liquid environments. This is very advantageous when compared with other high resolution techniques such as electron microscopy or optical techniques which operate in vacuum and need special sample preparation. Finally, the atomic scale reso-

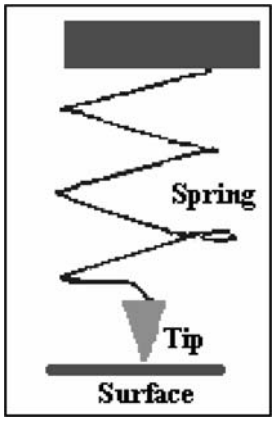

Fig. 4 Spring model of the AFM cantilever. Reprinted with permission from http://stm2.nrl.navy.mil/how-afm/how-afm.html

lution offered by AFM is difficult to achieve even using electron microscopy. For instance, and in the context of this review, only AFM has been capable of detecting the formation of a triplet 20 nucleotide DNA, while TEM could only locate the triple helical complex [3]. Furthermore, the DNA stretching and rupturing, used to understand the enthalpic and entropic changes correlated with the base pairing, can be done only by AFM. Laser tweezers, for example, are not as accurate as AFM due to the larger objects (beads and tips, respectively) that DNA molecules have to be immobilised upon. Finally, the AFM system comprises flexible cantilevers, atomically sharp tips, high-resolution tip-sample positioning and force feedback, which makes AFM the tool of choice for DNA imaging, molecular measurements, as well as for the manipulation of, and fabrication with, DNA molecules.

2.1
Forces Exerted in an AFM Experiment

The interplay between the attractive (e.g., Van der Waals or capillary forces) and repulsive forces involved during the approach of the tip to different surfaces under different environments are presented in Fig. 5 and discussed here. When the cantilever approaches a hard and non-compressible surface (Fig. 5a), at first the forces are too small to produce any measurable deflection of the cantilever, and therefore the position of the cantilever remains unchanged. At a certain distance the attractive forces overcome the cantilever spring constant and the tip leaps into contact with the specimen surface (Fig. 5b). As the cantilever continues to press down while the tip rests on the surface, the separation between the base of the tip and the sample decreases further, which results in the deflection of the tip with a subsequent increase

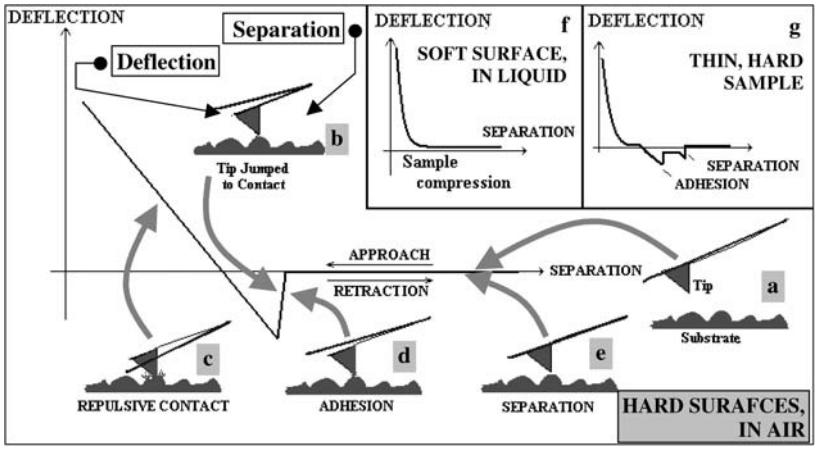

Fig. 5 Evolution of the forces during an AFM experiment. Note that the original position of the cantilever is shown in *blue*

in the repulsive contact force (Fig. 5c). Conversely, when the cantilever is retracted from the specimen surface, the tip still remains in contact with the surface due to adhesion forces (Fig. 5d) and the cantilever is deflected downwards. After a certain separation distance, the build up of the forces applied on the cantilever is enough to prevail over adhesion, and the tip breaks free (Fig. 5e).

The above description is idealistic. Firstly, soft samples, such as biomolecules (especially amorphous layers) and cells, will be compressed by the tip to exhibit a gradual increase in the force without a sharp onset of interactions (Fig. 5f). Therefore it is difficult to define a single contact point between the tip and sample, as the initial surface compression causes very little deflection of the cantilever. As the sample is indented by the tip, the gradient of the repulsive contact region will change. Also the apparent stiffness may change because of the compression of the structure. Secondly, in most cases involving biological samples, the approaching and the retracing curves are not identical, resulting in a hysteresis curve. Thirdly, and especially for experiments performed in liquids, the snap-on to and snap-off from the surface may not be obvious in the approach and retracing curves, respectively, even over a hard surface such as mica. Fourthly, for thin samples on a hard surface, a large deflection can be expected in the linear repulsive contact regime, as the tip may indent the sample enough and reach the supporting surface below. Due to this change in the contact area when the tip indents a soft surface, the actual interactions involved in compression are hard to quantify, and different levels of compression will be experienced at different points within the region (Fig. 5g). When the tip is retracted from the surface, which is not perfectly elastic, then a hysteresis and many different adhesion responses can be experienced.

If long molecules are present on the sample or on the tip, the cantilever can pull the tip free in stages due to extendable contacts formed between the tip and the surface. As the base of the cantilever retracts, the tip is deflected down towards the sample until the force is strong enough to break the molecular contacts. Different molecules or parts of the sample may adhere to the tip and each part may be broken separately or together. These complex molecular processes translate in a variety of adhesion and rupture events leading to different responses in successive force curves. By controlling the interplay of attractive and repulsive forces between the tip, the substrate and the molecules in between, the reversible voltage on the tip and the surface chemistry of the surface, one can use AFM not only for imaging or probing purposes but also as a nanotool for the manipulation and the fabrication of various DNA architectures.

2.2 Operation Modes of the AFM

The versatility of AFM is exemplified by the number of different operation modes, which have been employed with various degrees of success for the analysis of DNA molecules on surfaces. As mentioned before, AFM operates by measuring the attractive or repulsive forces between a tip and the specimen using a feedback system, with the cantilever deflection yielding the actual topography of the specimen. Different setups of the feedback and cantilever deflection result in different AFM operation modes, as summarised in Table 1.

In the classical contact mode (Fig. 6a) AFM measures the hard-sphere repulsion forces between the tip and the sample. As a raster-scan drags the tip over the sample surface, the detector measures the vertical deflection of the cantilever, which indicates the local sample height. A feedback loop adjusts the position of the cantilever above the surface as it is scanned and monitors the changes in the surface height, generating a 3D image—a decisive advantage of AFM over TEM [3].

Table 1 Operation modes of AFM

Mode of operation	Force of interaction
Contact	Strong (repulsive) – constant force or constant distance
Non-contact	Weak (attractive) – vibrating probe
Intermittent contact	Strong (repulsive) – vibrating probe
Lateral force	Frictional forces exert a torque on the scanning cantilever
Magnetic force	Imaging magnetic field of the surface
Thermal scanning	Imaging distribution of thermal conductivity

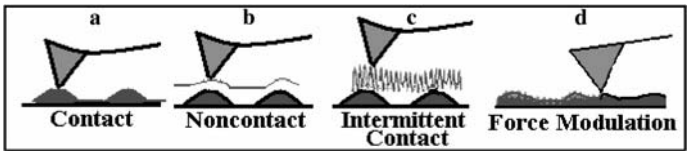

Fig. 6 AFM operation modes

In the non-contact mode (Fig. 6b), AFM acquires the topographic images from measurements of attractive forces in close proximity of the surface, as the tip does not touch the sample and the cantilever oscillates close to the sample surface [12]. This mode is difficult to work with in ambient conditions due to the interference of the capillary forces. Very stiff cantilevers are needed so that the attraction does not overcome the spring constant of the cantilever. However, the lack of contact with the sample means that this mode should be the least invasive and hence cause the least disruption. The disadvantage of this method is that the tip may jump into contact with the surface due to attractive forces.

There are several other operation modes, such as the intermittent contact mode, (Fig. 6c) where the cantilever oscillates and the tip records the repulsive contact with the surface at the lowest point of the oscillation, and the force modulation mode (Fig. 6d) where the tip does not leave the surface at all during the oscillation cycle.

Lateral force microscopy (LFM) [13, 14], which has the potential to close the gap between the classical macroscopic tribology and molecular, nanoscale understanding of surface tribology and chemistry, maps the relative differences in the surface frictional characteristics as recorded by the cantilever-tip system while probing a surface. LFM records the lateral deflections caused by the twisting of the cantilever due to the frictional forces exerted on it parallel to the plane of the surface. As the lateral deflections of the cantilever arise from changes in surface friction and changes in slope, to separate one effect from the other the post-processing of LFM and topographic images, which are collected simultaneously, is needed. The coefficient of friction is then the ratio between the lateral and normal forces exerted on the tip. An improvement on the LFM method, i.e., the simultaneous measurement of normal and lateral forces, resulted in a new microscopic technique called the friction force microscopy [15, 16].

Apart from improving the image contrast [17, 18] and helping to differentiate the real image from experimental artefacts, LFM is useful for imaging the chemo-physical heterogeneity of surfaces as inferred from the respective surface friction. The scanning of hydrophobic surfaces, especially with hydrophobic tips, will experience a lesser friction than the scanning of hydrophilic surfaces [19], especially with hydrophilic tips due to the condensation of water molecules, on the surface-tip system [20]. When the same

tip is used for the scanning of a chemically and/or physically heterogeneous area, as it is mostly the case, the frictional force can be used to shed light on the surface biomolecules (e.g., DNA) interactions. The post-processed image, which is obtained by subtracting the LF image obtained in the forward direction from the one obtained in the reversed direction, respectively, provides more information on the hydrophilic or hydrophobic nature of the sample [17, 18, 21–24]. Although the friction is in general attributed to the different surface chemistry and subsequent hydrophobicity, the correlation between chemistry and hydrophobicity is unequivocal only if the surfaces contain few chemical species. Also, it has been argued and demonstrated [25] that it is natural to expect that a higher LF is needed to move the tip across the soft layer, due to the larger penetration of the tip into the sample and therefore the local stiffness of the material can also have a role in the apparent LF. Unfortunately, the information from LFA is to a large extent sample-specific, as calibration of friction forces from sample to sample is difficult and error-prone, and because minute changes in experimental conditions (e.g., humidity, tip shape) can result in important changes in friction forces. Moreover, the best LF contrast is obtained when the imaging software benchmarks the highest and the lowest friction force, which are again sample-specific. With all these qualifications, and in the absence of chemical analysis methods with submicrometer resolution, the LF spatial distribution can be used to infer the spatial distribution of the surface chemistry and if applicable, the local stiffness of the material.

Chemical force microscopy (CFM) [26] is a progression from the physicochemical based detection of LFM to specific chemical detection. CFM performs the nanoscale chemical analysis of the sample, through the measurement of forces related to specific chemical interaction between a chemically functionalised tip (e.g., with carbon nanotubes or oligonucleotides) and a surface that is chemically functionalised with complementary (or non-complementary) chemical species, e.g., complementary oligonucleotides.

2.3 Substrates for AFM Experiments

The analysis of biomolecules by AFM is sometimes [3] referred to as surface biology, as opposed to the so-called test-tube biology, because the immobilisation of oligonucleotides on solid surfaces is central to the design, fabrication and operation of DNA-based microdevices, such as biosensors, DNA micro- and nanoarrays, microPCR and lab-on-a-chip devices. As the analysed biomolecules are in close contact and very often in intimate interaction with the surface, sample preparation for the AFM analysis of surface-immobilised biomolecules is both critical and delicate. The biomolecules need to be firmly anchored on the substrate, which has to have a sufficiently minimal or easily discriminated topography [1]. The Kleinschmidt method [6] for the DNA

immobilisation on surfaces, which comprises the spreading of DNA solution on the surface of a water subphase, is the oldest of many surface preparation methods (many reviewed in [27]). The immobilisation of biomolecules, including DNA/oligonucleotides, by covalent and non-covalent binding has been recently comprehensively reviewed [28, 29].

The substrates used for DNA immobilisation can be, at the level of the AFM analysis, either rigid (e.g., glass) or flexible (e.g., polymers). An atomically flat surface is preferable, but sometimes this is difficult to achieve. The DNA immobilisation mechanisms can be (i) physio-sorption, (ii) charge complementarity and (iii) covalent binding. Depending on the actual objective of the AFM study, each combination of the surface-immobilisation mechanism has both benefits and drawbacks.

The physio-sorption of DNA for the AFM analysis was achieved using many hard/flat substrates, the most common being glass [3], silica [30], and modified mica [31]. While glass is flat enough for the AFM imaging of cells, chromosomes or cell organelles, it is generally too rough for reliable visualisation of DNA molecules, especially under fluid conditions [2]. Some of the surfaces used for DNA immobilisation by covalent bonding are hydrophobic surfaces such as carbon-coated mica, which is a hydrated aluminium or potassium silicate that cleaves perfectly along the crystallographic surface but needs coating to make it hydrophobic [32], silatrane-surfaces [33] and modified mica, especially by amino-propyl-triethoxysilane (APTES) [34] and colloidal gold [35]. APTES- (sometimes denominated APS or AP) modified surfaces induce a robust DNA immobilisation because of the charge complementarity between the functionalised surface (positive charges) and DNA molecules (negative charges). It has been also noted [32] that the hydrophobic surfaces, such as carbon-coated mica, are good substrates for imaging DNA in air with a very good lateral resolution and specimen stability, possibly because of the strong hydrophobic surface–hydrophobic DNA base interaction.

The rapid development of, and the increasing demand for, DNA-based microdevices pushed for lower cost, easily processable materials, and towards disposable devices. In this context, polymers seem to be the logical choice from the manufacturing point of view. Consequently, the last few years have witnessed a new impetus in the development of new techniques for the covalent binding of DNA/oligonucleotide on polymer surfaces [36]. Some examples are (i) photochemical immobilisation [37], use of (ii) carboxylic groups [38–40], (iii) hydroxyl groups [41, 42] and (iv) amino groups [43–45]. Despite this application-driven interest, the immobilisation of DNA molecules on polymers is less studied by AFM methods than by fundamental studies. This is especially true for single biomolecule studies because of the complexity of the polymer surface, which can interfere with the analysis of biomolecules. However, it is precisely the analytical power of AFM that recommends this tool for studies regarding the complex interaction of DNA biomolecules with the complex polymeric surface.

3
Atomic Force Microscopy Studies of Single DNA Molecules

3.1
DNA Molecule and Small Molecular Assemblies

The DNA molecular assembly contains two chains of repeating nucleotides, each consisting of a phosphate group, a 2-deoxyribose sugar and a nitrogen-containing base, i.e., cytosine, adenine, guanine and thymine. The chains spiral in antiparallel direction, with purine opposite to pyrimidine, and H-bonding holding together complementary guanine–cytosine and adenine–thymine pairs. The DNA assembly can exist in several forms of chiral organisation, i.e., A, B, C and Z (Fig. 7), and local organisation, i.e., single- (ssDNA), double- (dsDNA), and triple-stranded (tsDNA) DNA, depending on the per-

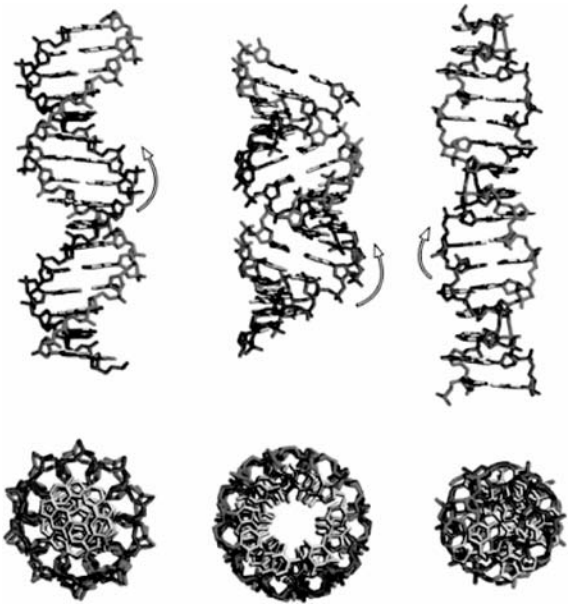

Form	Turn direction	Bases/360°	Helix diameter (nm)
A (top middle)	Right	11	2.3
B (top left)	Right	10	1.9
C	Right	11	1.9
Z (top right)	Right	11	1.8

Fig. 7 Supramolecular assemblies of DNA strands. Structures adapted from http://www2.muw.edu/~rwhitwam/ABZDNA.html; data adapted from http://www.ndsu.nodak.edu/instruct/mcclean/plsc731/dna/dna4.htm. Reprinted with permission

sistence lengths (i.e., the length within which the DNA axis remains constant) for ssDNA and dsDNA, and the difference in strand lengths for dsDNA and tsDNA [46, 47].

The analysis of single DNA molecules or small self-assemblies is equally important for medical research, e.g., for the understanding of the DNA sequence-dependent and structure-dependent diseases (recently reviewed [48]), as well as for nanoengineering-oriented research, e.g., understanding of the mechanical properties of DNA [49] that are useful for the construction of future nanodevices. In the following section we will refer to the AFM studies concerning DNA molecules and small self-assemblies as "single molecule studies".

3.2 Experimental Techniques for Single Molecule Studies

Apart from the AFM-based experiments, the study of single DNA molecules can be performed by other techniques, e.g., using microneedles [50] for imaging and nanofabrication [3] and optical [51] or magnetic tweezers [52] for probing. As discussed in the previous section, AFM has certain advantages over alternative experimental techniques, in particular regarding resolution—an important issue in single molecule studies. Apart from resolution, the advantages of studying single DNA molecule with AFM comprise the minute amounts required, the possibility of probing molecular properties or configurations, which are averaged out when using alternative techniques or which are normally not occupied in the thermodynamic equilibrium. Due to these advantages, the AFM-based DNA single molecule studies have potential applications in drug identification and sequence analysis [53–56], biomolecular and medical nanotechnology [57–59], nanowire fabrication [60, 61] and biosensors [62], to name just a few. Still, the benefits offered by the AFM techniques should be judged against experimental challenges.

The immobilisation of DNA molecules for single molecule studies has to be achieved at low concentrations [63, 64] on suitable surfaces, because at high concentrations the DNA molecules tend to condense in quasi-amorphous aggregates. Strong hydrophobic polymeric surfaces, e.g., poly(vinyl butaryl), poly(vinyl carbazole) and poly(phenazasiline), have been used [63] for fixing and straightening DNA molecules using π–π stacking between the polymer aromatic species and the DNA aromatic bases. A very different approach is to use positively charged surfaces, e.g., poly-L-lysine-coated mica surfaces [64], which will fix the phosphate groups of single- and double-stranded DNA.

For imaging applications, minimisation of the damage to DNA molecules by the AFM tip is essential. One method of less-invasive imaging is based on phase (rather than height) imaging, which employs for instance 100 mm long silicon nitride cantilevers with narrow arms inserted into a fluid cell [65]. Alternatively, or better complementary, the operation in liquids [66], and

especially the tapping mode in fluid [67–70], can be used to achieve a less-invasive imaging. In the tapping mode, the scanning AFM tip mounted on an oscillating cantilever, with oscillation frequency of approximately 13 kHz (close to the thermal resonance of the cantilever) being reported [65] for DNA imaging, briefly touches the surface during each oscillation. Unfortunately, AFM imaging under liquids is much noisier than AFM imaging in air or vacuum, resulting in images with less contrast but, fortunately and unlike the proteins, the conformation of DNA molecules is far less affected by dry conditions. The extreme resolution of AFM in dry conditions has been demonstrated [71] by using the tapping mode in an atmosphere of dry helium and standard silicon cantilevers to image short to very long DNA molecules.

The probing, manipulation and nanofabrication with AFM using DNA molecules on surfaces will require rather opposite experimental parameters, i.e., higher invasiveness but still maintaining good imaging capability. Consequently, the experiments have to use a wide range of tips and cantilevers, tight loop control and very accurate measurement of forces. For instance, a dynamic force microscopy study [72] that measured the binding forces of complementary DNA strands under physiological conditions (25 °C in PBS buffer, pH 7.3), by pulling at the opposite 5 "ends" as a function of the loading rate, had to use eight different cantilevers with spring constants ranging from 12 to 17 pN/nm.

3.3 Imaging of Single DNA Molecules

A well-stretched DNA molecule immobilised on a flat surface is essential for an accurate image because, apart from linear DNA molecules and assemblies, three-way [48, 73] or four-way junctions [74–76] can also be related to several genetic diseases [77, 78]. Atomically flat surfaces, such as mica and modified mica, are the preferred substrates in most studies [71, 79–81]. Positively charged modified mica (e.g., APTES-modified) provides a substrate on which DNA molecules can be immobilised through a simple, one-step, very efficient binding [80, 81]. The strong binding of DNA molecules on positively charged mica results in the shortening of its persistence length up to half of the value obtained for DNA immobilised on aminosilylated and on bare mica [78, 82].

3.3.1 Chiral Organisation of DNA

In dry conditions, the very high resolution imaging of various lenghts of DNA molecules has been achieved [71], as follows:

- Short DNA molecules (25–100 bp) on mica
- Entire, 16 μm long molecule of λ-DNA on mica

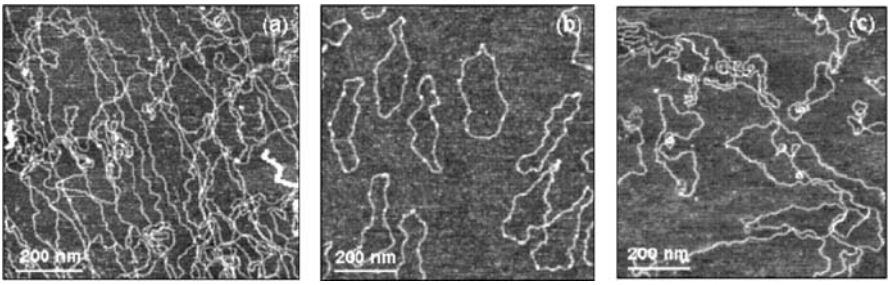

Fig. 8 Topview of AFM images of different dsDNA topologies on amino-terminated mica: **a** linear λ-DNA (48.5 kbp), **b** non-twisted circular DNA plasmids (3.2 kbp), **c** circular supercoiled DNA with twists and writhes due to internal supercoiling (supercoiled DNA ladder 2–16 kbp) [48]. Reprinted with permission

- Plasmid DNA and DNA from phage lambda (48 000 bp) on silicon
- Triple-stranded DNA
- A well-extended single-stranded polynucleotide, poly(A)

The study demonstrated that single-stranded polynucleotide, such as poly(A), is more flexible than a generic dsDNA. On mica, the long B-DNA binds to mica at many sites and remains intact during drying, while the short DNA binds at fewer sites and settles to an A-DNA structure during dehydration.

Different topologies of dsDNA on amino-terminated mica have been imaged using the tapping mode and ambient conditions [48]. Fig. 8 presents linear λ-DNA, non-twisted circular DNA and circular supercoiled DNA. The measured width and height of dsDNA are 3–7 nm and around 1 nm, respectively.

3.3.2 Abasic Sites on DNA

The sugar-phosphate backbone of DNA can be mutagenically or enzymetically altered by exposing the so-called abasic or apurinic/apyrimidinic (AP) sites where a base was removed. Although these sites are non-functional, their presence is a potential cause of severe DNA alterations and cellular death, as well as carcinogenesis [39, 83, 85]. Although several methods are available to quantify the AP sites from a population of chromosome or cells [39, 83], until AFM had been used for single molecule studies no method was available to point to the physical position or a distribution of AP sites along an individual DNA molecule. The AP sites on individual 250 bp DNA molecules have been detected [84] by marking them with biotinylated aldehyde reactive probes and avidin. The tapping mode AFM imaging (at 290 kHz to minimise the molecular damage) of the altered DNA molecules immobilised on mica revealed the location of the avidin-tagged AP sites without directional ambiguity.

3.3.3 DNA Junctions

Due to its very long aspect ratio and base pairing, and under heat or salt-induced denaturation and annihilation, the DNA molecule is capable of exhibiting twists and turns resulting in branched junctions that translate in different structures such as hairpin, crucified, and slipped strand, depending on the bonding between bases (Fig. 9, [48]). The repeat lengths of three-way DNA junctions that cause 14 genetic neurodegenerative diseases and three fragile sites have been already identified [48].

The three-way DNA junction (also called Holliday junction) has been studied by single molecule AFM analysis [48]. DNA molecules have been dispersed in saline buffer injected in a fluid cell mounted on the top of the APTES mica. Fig. 10 presents two consecutive AFM scans (separated by approximately 3 min) of 301 bp DNA molecules containing a 7 bp hairpin. Also Fig. 11 presents the AFM images of representative slipped strand DNA structures. The 3D projections of the $(CGG)_{50} \cdot (CCG)_{50}$ slipped strand structures

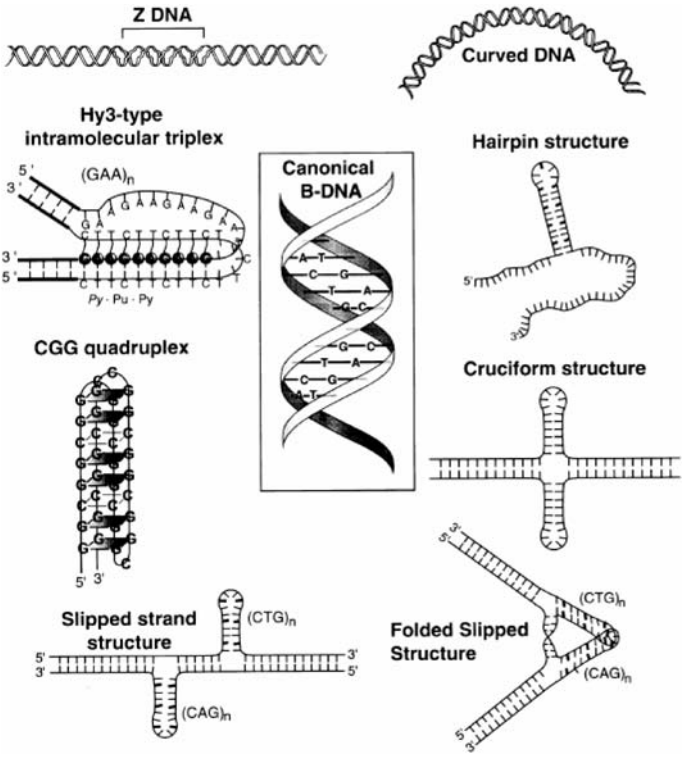

Fig. 9 Alternative DNA structures formed in repeated DNAs [48]. Reprinted with permission

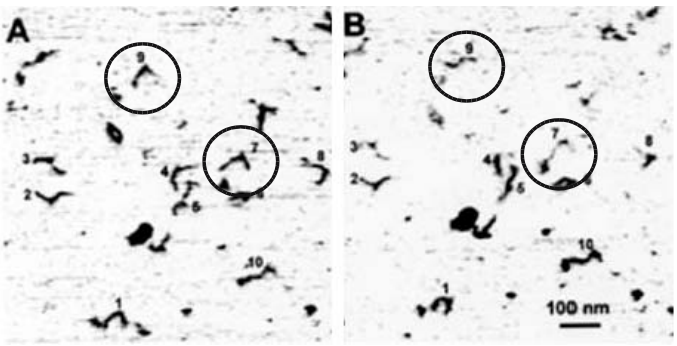

Fig. 10 AFM analysis of three-way junction dynamics in liquid [48]. Reprinted with permission. Ten DNA molecules in the field are numbered. Molecules 7 and 9 (*circled*), in particular, change shape dramatically

of (Fig. 11a–c) present a pyramidal structure at the apex of a bent molecule, which may represent two looped out strands interacting above the plane of the DNA molecule. The 2D projections of the AFM images (Fig. 11d–e and f–g) present the loops of the two major slipped strand isomers from

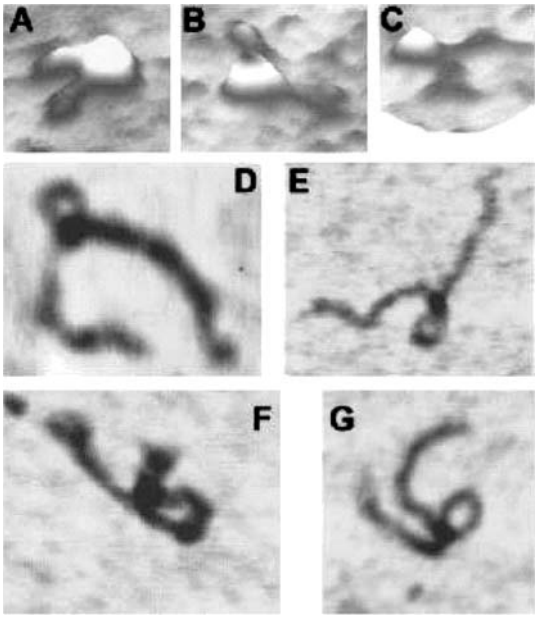

Fig. 11 AFM images of slipped-strand DNA structures [48]: **a**, **b** and **c** present 3D projections of three slipped-strand DNA molecules of $(CTG)_{50} \cdot (CAG)_{50}$. **d**, **e** and **f**, **g** present the two major slipped strand isomers from $(CGG)_{54} \cdot (CCG)_{54}$ with a clear loop from both isomers. Reprinted with permission

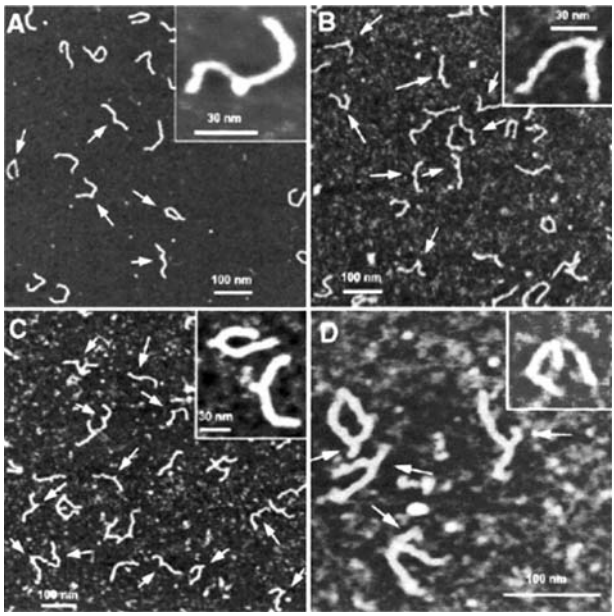

Fig. 12 AFM images of three-way junctions with different hairpin (indicated by *arrows*) lengths, i.e. **a** 7 bp, **b** 18 bp, **c** 27 bp, **d** 50 bp [73]. Reprinted with permission

$(CGG)_{54} \cdot (CCG)_{54}$, which may attributed to the interaction of two long loop out structures or the looping of the very flexible $(CGG) \cdot (CCG)$ linear helix held together by interactions between short loops.

The conformation of three-way DNA junctions with one hairpin arm (50, 27, 18 and 7 bp long) and two relative long linear arms has been also visualised by AFM [73] (tapping mode, APTES-modified mica, argon-dried samples, imaging under ambient conditions and in fluid). The structure has been obtained by annealing one strand of a DNA fragment from a parental plasmid with one strand of an inverted repeat-containing fragment. The DNA hairpins are formed after the denaturation of the fragments containing inverted repeats of specific length. The AFM imaging (Fig. 12) revealed the dynamic nature of the three-way junction, e.g., the high variability of the inter-arm angles in the dried sample and the mobility of junctions in liquid, and the presence of the pyramid-like structure, suggested by the angle between arms.

3.4 Probing Molecular Characteristics and Interactions

An increase of the invasiveness of AFM experiments allows the probing of the molecular parameters of, and molecular interactions associated with, the DNA molecule rather than merely its imaging. As mentioned before, other

techniques, e.g., optical traps and microneedles, are also available but AFM still has the advantage of versatility and the possibility of visualisation prior and after the molecular probing experiment.

3.4.1 Persistence Length of DNA Chains

A measure of the flexibility of the DNA molecule, which is conformationally labile with a variety of structural forms [85] (discussed above), is its persistence length. Studies estimating the persistence length are intermediary between the imaging studies, on which they rely from the experimental point of view, and mechanical probing, as they provide a nanomechanical parameter of the DNA molecule by imaging rather than by physical measurement. The persistence length, which is proportional to the rigidity of a polymeric chain, is the distance along which the chain will preserve its quasi-linear structure before bending. The persistence length of a DNA chain has been calculated [71] assuming that each DNA molecule is a chain of 10 nm segments. If θ is the angle between the DNA segments separated by the contour length (L), then the relationship between the contour length and the apparent persistence length (a) is:

$$\langle \cos \theta(L) \rangle = \exp(-L/2\mathrm{a}) \tag{2}$$

The apparent persistence length of dsDNA deposited on mica from aqueous solutions is 40 nm [71]. This is about half the value of the calculated persistence length for poly(A), a single stranded polynucleotide, implying a higher rigidity. Using the persistence lengths calculated from AFM images, it was demonstrated [78, 82, 86] that the persistence lengths are:

- Solvent-independent (circular 3000 bp B-DNA lengths lasted in propanol too)
- Sequence-dependent (ssDNA, e.g., poly(A), is more flexible than dsDNA)
- Substrate-dependent (the persistence length of DNA on amino-terminated mica is approximately half compared to bare mica)
- DNA length-dependent (long DNA molecules bind to surfaces at more sites than shorter DNA)
- Temperature-dependent (at 25 °C 907 bp DNA fragments condensate as B-DNA with a contour length of approximately 320 nm, while at 25 °C they condensate as A-DNA with a contour length of approximately 250 nm)

3.4.2 Nanomechanical Probing of Single DNA Molecules

The mechanical properties of DNA have attracted the interest of both physicists and biologists because of their relation to many biological events such as DNA transcription, gene expression and regulation, and DNA replication.

In general terms, the experimental procedure consists [87] in picking a single DNA molecule, which is immobilised with one end to the surface and adheres with its other end to the AFM cantilever tip, and mechanically stretching it with the cantilever. Upon retracting the cantilever tip from the surface, the molecule gets more and more stretched and its mechanical properties under this growing external force can be probed with very high force sensitivity, in the pN range. Fig. 13 [90] illustrates the above principles. The force–extension relations acquired by measuring the force as a function of the position of the transducer [88, 89] has been described [87] as follows. The first minimum in Fig. 13 (on the left) indicates the folded state, whereas the second shallow minimum indicates the unfolded state. These experiments can also probe extreme conformational states of individual molecules that are not occupied in normal thermodynamic environmental states. It is believed [90] that these "high-force" (5–15 pN) states play a role in specific binding events where molecules or molecular complexes are locally unwound, twisted, or undergo structural conformation changes. The AFM experiments, which mechanically probe the DNA molecule, can be focused on different aspects of the force–DNA structure relationship, as follows.

Firstly, studies concerned with the forces associated with conformational change [91, 92] demonstrated that when large forces (5–15 pN) are applied to the DNA molecule, the natural B-DNA structure is converted into a new overstretched conformation, i.e., S-DNA. Theoretical models and molecular dynamics simulations have been developed to understand the overstretching transition, the role of twist stored within the double helix, and stiffness of DNA [63, 92–99]. For example, it has been found [63] that the oligonu-

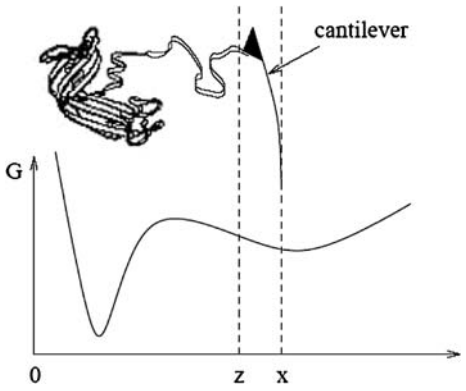

Fig. 13 Schematic view of a typical setup of single molecule pulling experiments and an illustration of the generic free energy potential G(z) [87]. The *x-position* denominates the cantilever and the *z-position* denominates the cantilever tip to which one end of DNA molecule is attached. Reprinted with permission

cleotide extends without a significant energy barrier from a length shorter than of A-DNA to a length 2.4 times the contour length of B-DNA. After this threshold an energy barrier to strand separation was encountered. The calculated forces associated with the barrier were 90 ± 30 pN. These AFM experiments showed that the oligonucleotide strands separate at 2.6 ± 0.8 contour lengths with a force of 130 ± 50 pN. A study [92] of the force–displacement response of a single duplex DNA found that the force saturates at a plateau around 70 pN, which ends when the DNA is stretched about 1.7 times its contour length. Based on these results, many models have been proposed to explain the mechanical properties of DNA molecules [93–98]. These results are produced using the "junction minimisation of nucleic acids" modelling [96]. A "two-state wormlike chain model" was proposed [93] to describe the elasticity of the stress-induced B–S transition and to produce an explicit form of the force–extension relationship. Molecular dynamics simulation [94] and AFM experiments [94, 100] showed that the B-DNA elongation and separation require a force of 83 ± 11pN to separate the $(ACTG)_3$ helix. The conformational "domino effect" that accounts for the stretching-induced phase transition revealed by simulations [95] accounts for approximately 1.6 times the normal extension of B-DNA [91, 93]. However, the conformation of dsDNA beyond 10 pN tension cannot be explained by the inextensible wormlike chain model [97, 98]. The simplest model proposing an extensible wormlike chain with twist rigidity (because stretching DNA is coupled with twisting which perturbs its twist degrees of freedom) offers a better alternative.

Secondly, AFM experiments can study the unzipping or unbinding process of the DNA molecules. The nanomechanical probing of individual λ-DNA molecules [101, 102] has demonstrated that higher unzipping forces are needed when the strands have a higher average content of GC and AT in the zipped segment of the molecule. More sequence-specific experiments [103] with pure CG and AT strands revealed the sequence-specific base unpairing forces in dsDNA. In another study [88] it was found that the pulling forces required for unbinding of DNA duplexes with 10, 20 and 30 bp varied from 20 to 50 pN as a function of the loading rate (in the range 16–4000 pN/s) and sequence length. The unbinding forces vary with the logarithm of the loading rate, which suggests a single energy barrier along the mechanical separation path. Importantly, the distance between the energy barrier and the minimum energy along the separation path and the logarithm of the thermal dissociation rate, were proportional to the number of base pairs of the DNA duplex.

Thirdly, experiments concerned with the whole process of conformational change and the unzipping process (e.g., [49]) studied the mechanical stability of individual double-stranded DNA molecules. It was found that the B–S transition of λ-DNA occurred at 65 pN, followed by a second conformational transition during which the DNA double helix melted into two

single strands. The melting transition exhibited a pronounced force-loading rate dependence and a marked hysteresis, which is characteristic of a non-equilibrium conformational transition—characteristics quite different from the previous B–S transition. It was found that low ionic strength buffers (less than 10 mM NaCl) destabilised the DNA double helix significantly, whereas high ionic strength buffers (1 M NaCl) had the opposite effect. Increasing the temperature decreased the inherent mechanical energy of the DNA double helix before the force-induced melting. The mechanical energy can be correlated with the base-pairing free enthalpy $DG_{bp}(T)$ of the DNA. Experiments with pure poly(dG-dC) and poly(dA-dT) sequences revealed a close correlation between the mechanical energies at which these sequences melt with DG_{bp} (sequence). While depending on the loading rate, the melting transition occurs between 65 and 200 pN in λ-phage DNA, the melting transition occurs at approximately 300 pN and 35 pN, for poly(dG-dC) and poly(dA-dT) DNA, respectively.

3.4.3
Probing Electrical Properties of DNA Molecules

The motivation for studies to measure the electrical properties of individual DNA molecules is generated by the necessity to map these properties and the electrical behaviour of DNA molecules for the design of future molecular electronic devices, for which DNA would be a promising material.

While ssDNA is an insulator, dsDNA bound to gold nanoparticles behaves as a wide band gap semiconductor, which passes significant current outside the 3 eV gap [104]. The electrical behaviour of a single molecule DNA in a three-terminal device has been demonstrated [105] using a triple-probe AFM (T-AFM). The T-AFM connects a single DNA molecule with a carbon nanotube electrode as source, drain, and gate terminals. It has been shown that as the gate bias voltage is increased, the voltage gap region decreased in the current–voltage (I–V) curves. Furthermore, clear steps are observed in the I–V curve at the crossing of the DNA molecule and the carbon nanotube–gate electrode with the gate biased. The I–V characteristics suggest that the carbon nanotube is a good electrode material for a DNA nanoelectronic device.

3.5
Nanofabrication Involving Individual DNA Molecules

Although recombinant DNA technology can "nanofabricate" DNA molecules by cutting and realigning with enzymes at sequence specific sites, the fabrication with individual DNA molecules by mechanical means is in its infancy.

In a sense, the mechanical probing of DNA molecules is a form of nanofabrication, albeit organised vertically and often reversibly. In a more invasive

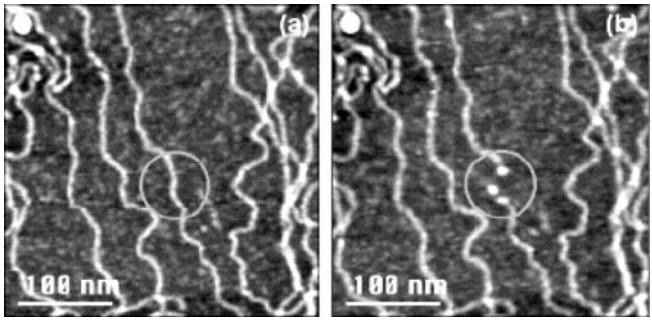

Fig. 14 Two topview AFM images of λ-DNA in AFM tapping mode under ambient conditions **a** before and **b** after mechanically cutting a dsDNA strand in the center of the image (*circles*) with the AFM cantilever tip [106]. Reprinted with permission

approach than described in the previous section, it has been reported [106] that a sharp tip on the silicon cantilever can write features laterally and mechanically cut a dsDNA strand into two pieces (Fig. 14). This controlled molecular manipulation was performed by increasing locally the force interaction between the AFM tip and the DNA molecule and repetitively scanning perpendicularly over the molecule at a defined position. Other studies [107, 108] described the nanomanipulation of a single linear λ-DNA (48.5 kbp) molecule on APTES-mica using tapping mode in air. Crossed and word structures (Fig. 15) were fabricated by first aligning the DNA strands along one direction and subsequently along a second direction by a 2D "molecular combing" process [108, 109]. Also, the DNA strands can be folded up by an AFM tip to form ordered nanostructures such as particles and thick rods [109]. The threshold force to cut DNA was found to vary for different tips between 20 nN and 80 nN.

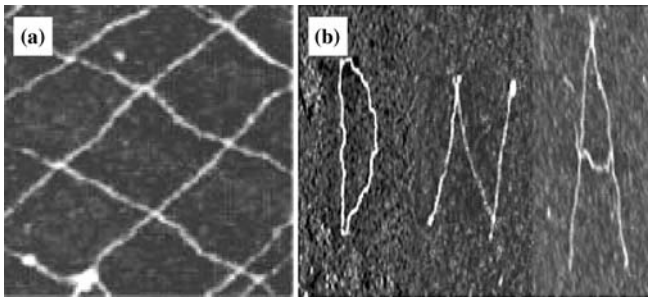

Fig. 15 Nanofabrication with DNA molecules [108, 109]. **a** *Left*: Cross-linking of DNA strands. Image size is 800×800 nm. **b** Combination of three AFM images of characters formed by nanomanipulation of single DNA molecules with the AFM tip (scan size is 500×500 nm). Reprinted with permission

4
Atomic Force Microscopy Studies of Self-Assembled DNA Layers

4.1
Long-Range Self-Assembled DNA Layers

This section reviews the AFM-based advancements regarding the imaging, probing and fabrication of, or involving, long-range DNA self-assemblies. The long-range self-assemblies are defined, in the context of this review, as assemblies of DNA molecules having a molecular organisation that extends laterally on surfaces on distances several orders of magnitude larger than the size of the constitutive modules (DNA molecules).

There are multiple advantages of using DNA as a building block in nanodevices. Firstly, the design of future nanodevices would be eased by the fact that the intermolecular interactions that drive the self assembly of the DNA molecules (i.e., AT and GC pairing) as well as supramolecular structures (i.e., double helix etc.) are well characterised. Secondly, from the logistical point of view, the DNA molecules are readily available in a variety of arbitrary sequences which can be further amplified by PCR. Moreover, more complex molecular modules based on DNA molecules can be easily obtained via decoration with, e.g., biotin, fluorescent labels etc., and the use of enzymes such as DNA ligase, restriction endonucleases, kinases and exonucleases. Thirdly, from the fabrication point of view, DNA molecules are far more robust than other biomolecules that have self-assembly capabilities, such as some proteins (e.g., actin, S-layers) [110–113]. Finally, from the operational point of view, the information encoded in DNA molecules can be read by other biomolecules and by using advanced microscopy techniques, especially AFM (as has been demonstrated in the previous section). For all these strategic reasons, DNA molecules have been widely perceived as good candidates for the building blocks of various nanodevices, including DNA-based computation [63, 114–116], molecular conduction wires [117, 118], and micro- [119, 120] and nanoarrays [121]. All of these applications will greatly benefit from the long-range self-assembled DNA layers, but DNA biocomputation by tiling seems to be the most promising development because it is based on the self-assembly process, rather than being enhanced by it.

The AFM-supported studies of long-range organised DNA nanostructures on surfaces can progress along two experimental approaches. Firstly, AFM can be used as an imaging tool, which helps the studies aiming to understand the effect of external (e.g., buffers, surfaces) and internal factors (e.g., engineered DNA molecules) on the formation of self-assembled DNA structures. Alternatively, AFM can be used for the imaging (sometimes along with TEM) of self-assembled de novo designed DNA nanostructures, especially in the context of DNA computation by tiling. The latter use of imaging is not very different regarding the experimental procedures from the former. How-

ever, its function is—in principle—operational rather than experimental, as the visualisation stands for the readout or validation of the biocomputation. Of the triad of possible usages of AFM for the study of biomolecules on surfaces, i.e., imaging, probing and fabrication, the latter is stricto senso missing as the nanofabrication task is taken over by the self-assembly process itself. However, there are many instances when the nanofabrication involves the nanostructures used as basal layers, especially when DNA molecules have been deposited on pre-self-assembled surfaces.

4.2 AFM Imaging of Long-Range Nanostructured DNA Layers

Several AFM studies examined the effect of buffer conditions on the formation of motifs with DNA molecules. For instance, it has been found that the multivalent cations induce the condensation of DNA molecules into higher ordered structures, including toroids and rods [122]. More specifically, Zn^{2+} and Mg^{2+} ions induce the formation of DNA kinked and perfect circles, respectively [123] (Fig. 16). Also, higher concentrations of spermidine induce the formation of complex "flower-shaped" structures with single crossover points [122] and increased concentrations of ethanol lead to complex and looped structures [124] (Fig. 17).

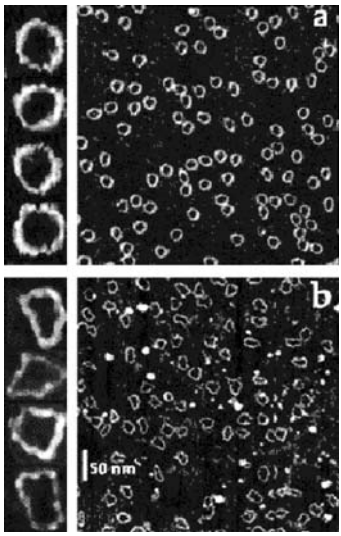

Fig. 16 AFM images of 168 base-pair DNA minicircles in **a** 1 mM $MgCl_2$ and **b** 1 mM $ZnBr_2$, showing a fourfold increase in kink density in Zn^{2+}. Selected molecules are displayed magnified by a factor of four to the left of each image [123]. Reprinted with permission

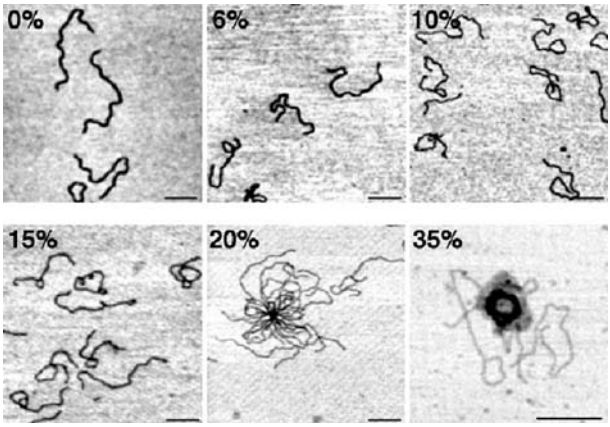

Fig. 17 Typical AFM images of 3000 bp DNA at different ethanol concentrations [124]. Reprinted with permission

Another line of AFM studies examined the effect of the micro- and nanostructuring of surfaces on the formation of long-range DNA nanostructures. At the micro-end of structured surfaces, it has been reported [125] that stretching DNA molecules between two microlithographically patterned DNA-sticky lines or by slowly retracting (molecular combing) a DNA-adsorbing surface results in long DNA wires (Fig. 18). At the nano-end of structured surfaces, it has been found that freshly prepared mica surfaces

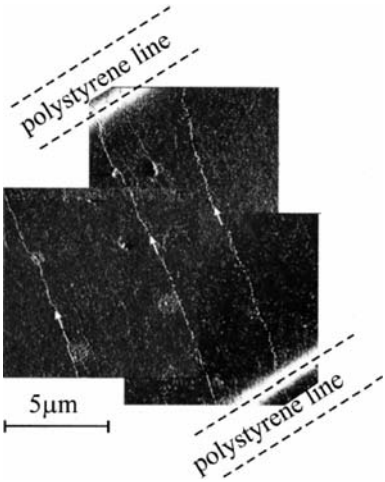

Fig. 18 AFM image showing bacteriophage-λ DNA stretched between patterned polystyrene lines. *White arrows* point to the DNA. The distance between polystyrene lines is 17.5 mm and the height of the lines is 300 nm [125]. Reprinted with permission

transfer their nanoorganisation through electrostatic interactions to the adsorbed G-DNA molecules (a polymorphic family of four-stranded structures containing guanine tetrad motifs) leading to the formation long-range (up to hundreds of microns) G-wires [126, 127] (Fig. 19). Ordered, stretched DNA layers have also been obtained using the Langmuir–Blodgett deposition of DNA molecules on a monolayer of Zn-arachidate [128]. Another study [129] demonstrated that the nanostructure of the dsDNA layer, which was imaged by the AFM, is strong enough to be preserved during enzymatic digestion by DNase I (Fig. 20). Even polymeric surfaces that are not normally expected to induce self-assembly, e.g., chitosan [130] and a PEG-poly(amidoamine) triblock copolymer [131], induced the nanostructuring of plasmid DNA in a variety of motifs, such as toroids and rods (Fig. 21). Finally, the interaction between nanostructured surfaces and DNA molecules can be explored in a more purposefully-oriented manner. For instance, it has been observed [131] that the deposition of polybases on self-assembled monolayers (SAMs) followed by hybridisation with complementary polybases leads to the formation of organised self-assembled molecular rafts.

AFM has been also used to explore the efficiency of several techniques based on DNA molecular engineering for the fabrication of long-range self-assembled nanostructures. One possibility is to use "add-on" modules grafted onto the DNA molecule backbone. For instance, bis-biotinylated ds-DNA molecules self-assemble in linear structures that are bridged by streptavidin (the best results have been obtained for equimolar ratios) [133]. Still, by far the most productive and paradigmatic-shifting approach, which generated the new field of DNA nanotechnology, was triggered by Seeman's seminal work on the purposeful de novo design of DNA molecules specifically tailored to generate new molecular nanostructures [134]. Details of the construction of many branched motifs made of DNA molecules, e.g., truncated octahe-

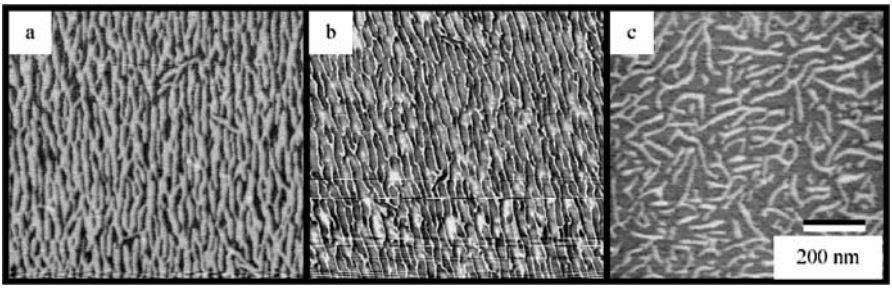

Fig. 19 AFM images of G-wires freshly adsorbed onto mica imaged via tapping mode (**a**). Same sample imaged by the same tip 24 h later after drying in an oven at 37 °C (**b**). Low current scanning tunneling microscopy image of G-wires freshly adsorbed on mica (**c**). Note the preferential orientation is not a sample preparation artefact, e.g., due to rinsing [126]. Reprinted with permission

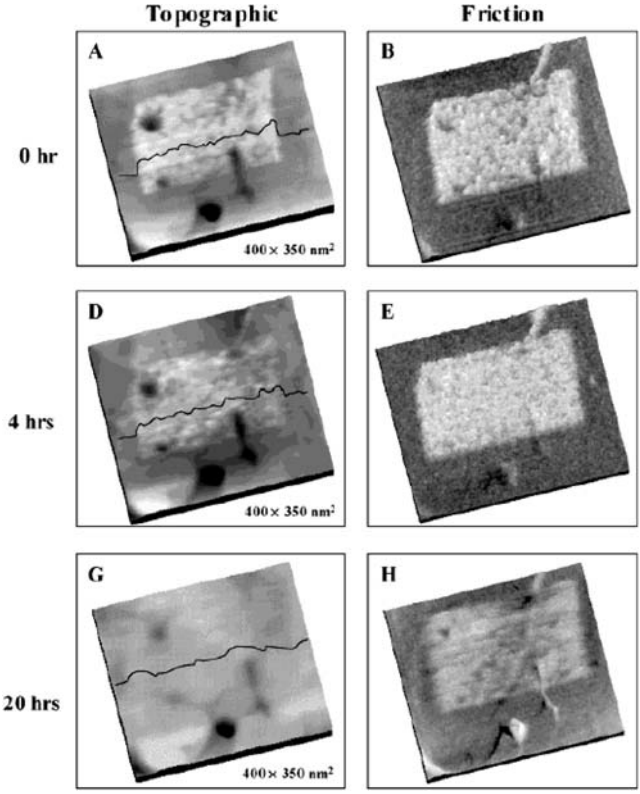

Fig. 20 Time-dependent AFM images of oligonucleotide nanostructure during digestion by DNase I enzyme [129]. Interestingly, the structuring is still visible in the LF image (*right*) even when the DNA layer has been digested according to the topographic image (*left*). Reprinted with permission

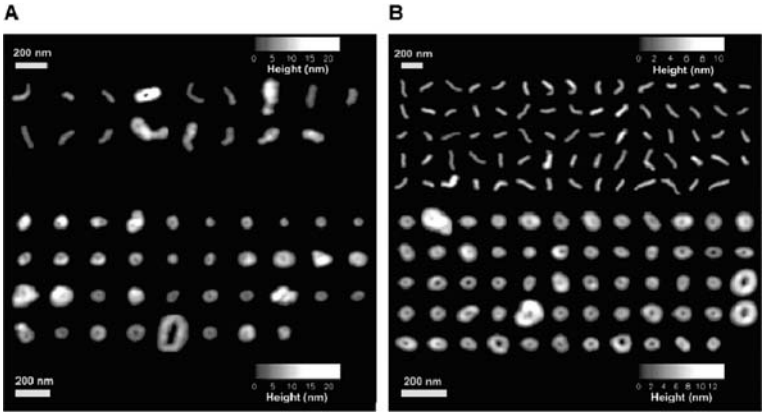

Fig. 21 Image galleries of **a** toroidal and **b** rod-like DNA ensembles on chitosan surface [130]. Reprinted with permission

dron, trefoil, figure-eight shape etc., as well as the topological considerations regarding DNA self-assembly have been reviewed elsewhere [135]. A breakthrough in DNA nanotechnology was achieved in the late 1990s when AFM was used for the first time [136] to validate the presence of the actual motifs of DNA long-range assemblies, (chain of triangles, Fig. 22a). Before, the results could be deduced only from indirect data, e.g., denaturating gel electrophoresis. From that moment on, many studies used AFM (and in many instances TEM as well) to demonstrate the existence of the designed self-assembled long-range (e.g., several microns) DNA nanostructures on surfaces, e.g., regular, parallelogram grids using Holliday junctions [137] (Fig. 22b), large crystal

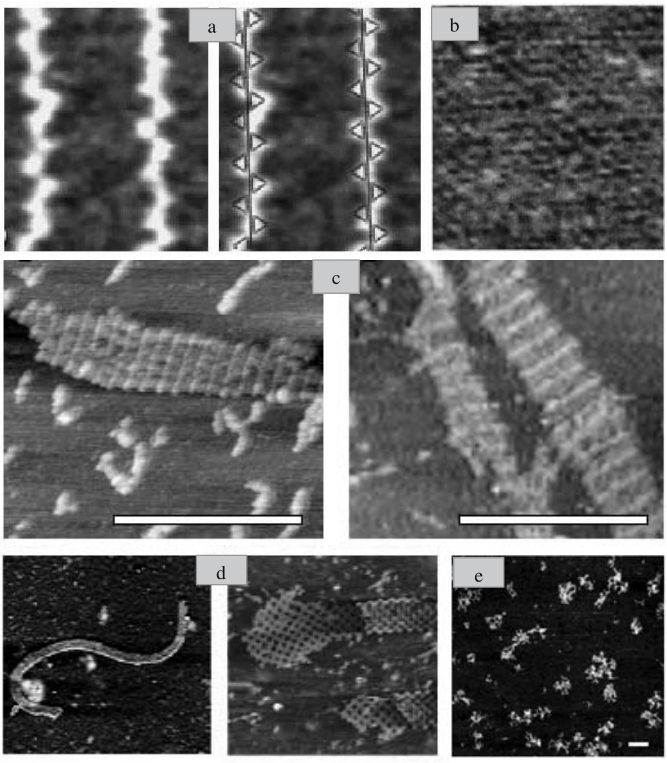

Fig. 22 AFM images of long-range self-assembled DNA nanostructures on surfaces. **a** Triangular DNA ligation products (*left*) and reconstruction of the DNA motif (*right*) (edge of the image approximately 150 nm, adapted from [136], reprinted with permission). **b** Parallelogram DNA grids (edge of the image 273 nm, adapted from [137], reprinted with permission). **c** Large crystal lattices that use DNA double-crossovers (*bars* equal 300 nm, adapted from [138] 1998, reprinted with permission). **d** Self-assembled nanoribbons and nanogrids (edge of the image on the left and right is 1 μm and 500 nm, respectively; adapted from [141], reprinted with permission). **e** Dendritic DNA structures (*scale bars* correspond to 100 nm; adapted from [142]. Reprinted with permission)

lattices that use DNA double-crossovers [138] (Fig. 22c), triple crossover complexes [139], DNA triangles with flexible four-arm DNA junctions [140], 4×4 DNA lattices [141] (Fig. 22d), and dendritic structures [142]. The most recent of the "Foundations of Nanoscience" conferences [143], which present annual updates of the progress of DNA nanotechnology, occasioned a very good and concise ad hoc review [144] on this subject. The long-range ordered DNA nanostructures could be further used as templates for hybrid nanostructures comprising proteins and nanoparticles, usually via the biotin–streptavidin route [138, 141, 145, 146].

4.3 AFM Probing of Nanostructured DNA Layers

A dramatic effect on the impact of AFM imaging was triggered by the bridging between DNA nanotechnology (with developments briefly described above) and DNA computing that followed Adleman's seminal work [147]. The connection between these two fields, which has been named "algorithmic self-assembly of DNA" [148], has been realised by Winfree who observed that the double crossover complexes are the physical (and nano-!) embodiment of Wang's "tiles" problem [149]. Moreover, Winfree proved that this non-trivial mathematical problem is computationally universal. It follows that, in principle, the self-assembly of purposefully designed DNA molecules in nanotiles can solve any conventional problem that a present computer can solve. Moreover, organising the multilayered structures [150] with a bottom, template layer that allows subsequent DNA layers to assemble on top in a certain order, results in a self-assembly computation that is programmed by the bottom template. This multilayered arrangement can speed up computations by computing in parallel, and along multiple dimensions [144].

Indeed solutions to several practical problems have been demonstrated, e.g., computation of Pascal's triangle modulo 2 [151], exclusive or (XOR) calculation using triple crossover [152] or string tiles [151]. Again, the annual conference "Foundations of Nanoscience" [143] provides a good review of the status of development of DNA computation by self assembly. Fig. 23 presents several AFM demonstrations of computation driven by DNA programmed self-assembly.

From the experimental point of view, the AFM imaging or readout of algorithmically assembled DNA nanostructures is next to trivial: the scanning is performed in air, not under fluid conditions (which would downgrade the contrast) or under vacuum (which would require expensive accessories), on hard and very flat surfaces (fresh mica is mostly used) and the scanned structures come from simple mixtures of solutions. The combination of experimental simplicity regarding AFM usage, the elegance, the possibly very large impact of the proposed computation "devices", as well as the vital necessity of AFM (superior to the next competitor, TEM) for readout, conspire

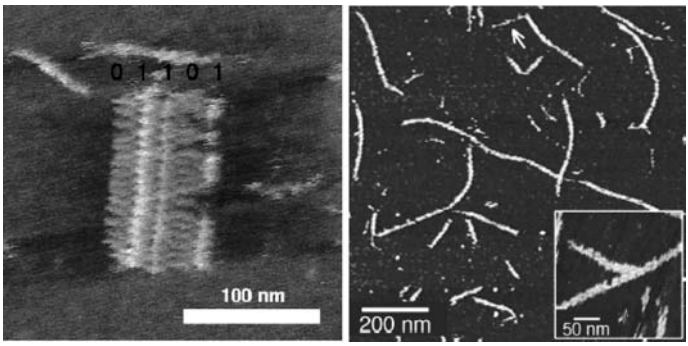

Fig. 23 AFM images of examples of calculations by DNA self-assembly. **a** Section of patterned DNA lattice containing barcode information of 01101; the 1 and 0 bit values are clearly visible as lighter and darker stripes, respectively (from [151] reprinted with permission). **b** Branched tiled DNA nanostructures, mimicking the solution of a Pascal triangle [152]. Reprinted with permission

to create the highest return of investment for AFM usage for the study of DNA molecules immobilised on surfaces.

4.4 AFM Nanofabrication Involving Self-Assembled DNA Layers

The self-assembled monolayers, in particular those containing thiol groups, are commonly used to immobilise DNA molecules. Given the preservation of the nanostructure of the basal layers, the nanofabrication approaches could target the layer beneath the DNA layer. For instance, AFM can be used to plough the SAM molecules, which act as a resist [129, 153], in the presence of DNA molecules in solution. The method, denominated as nanografting, is capable of producing lines as narrow as 10–15 nm (Fig. 24). The stretched conformation of the patterned DNA molecules allow for efficient hybridisation. A different approach would be to apply the nanofabrication procedures after immobilisation and, if needed, after hybridisation. The use of AFM to plough self-assembled DNA layers on ultraflat gold [154] led to the formation of 3.5 nm and 6 nm deep "nanoholes" for ssDNA and dsDNA layers, respectively.

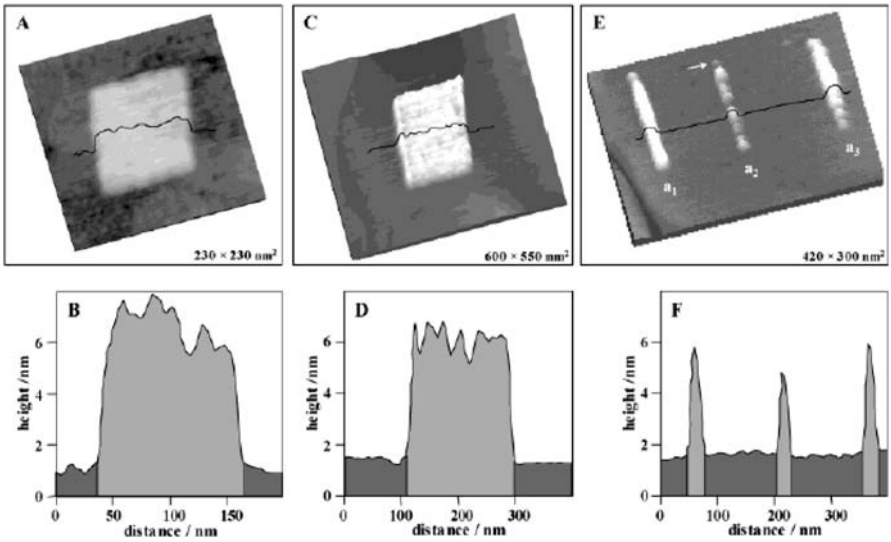

Fig. 24 Nanografting of ssDNA on gold surface. *Top row*: different squares of oligonucleotide nanostructure grafted within a SAM layer. *Bottom row*: corresponding cursor profile as indicated above [129]. Reprinted with permission

5
Atomic Force Microscopy Studies of Amorphous DNA Layers

5.1
Amorphous DNA Layers

The amorphous character of DNA layers emerges when several conditions are met, namely:

- High local molecular density in the film
- Long DNA molecules
- Non-complementarity of the nearby DNA strands
- Lack of organisation of the substrate at the nanolevel [119, 120, 155–161]

These conditions are met in most practical situations, in micro- and even nanobiodevice applications. For instance, the high density of DNA molecules is required to increase the sensitivity of the device; long DNA molecules are commonly (but not exclusively) used as target molecules in e.g., biosensors, microarrays and microPCR devices; single DNA species used as targets translate in lack of complementarity; and most substrates, (e.g., glass, polymers) for micro/nanobiodevices are amorphous. The critical difference between the self-assembled and amorphous DNA layers, which leads to the polymer-like character of the latter, is the lack of complementarity between adjacent strands. Still, as with polymers, the DNA chains have to have a consider-

able length to allow the formation of polymer-like networks. It has been found [161] that DNA strands which are shorter than 24 bases tend to align normal to the surface in rod-like configurations (Model I), whereas strands longer than this approximate threshold behave as flexible chains that aggregate in coiled, polymer-like networks (Model II). The fabrication and operation of biodevices also contribute to the amorphous character of DNA layers. With the possible exception of dip-pen nanolithography, the fabrication of DNA-based devices relies on classical immobilisation techniques, i.e., covalent binding and electrostatic interaction-driven immobilisation [119, 120, 155–159], which dispense the molecules on surfaces in a random manner, and therefore only amplify the random character of the substrates. Finally, and again with very few possible exceptions (e.g., microfluidics devices, where the long probe molecules could be aligned by flow) the operation of DNA-based devices does not increase the order of the DNA layers on surfaces.

An enormous amount of work, part of which has been recently reviewed [28, 29], has been reported regarding the immobilisation of DNA molecules in high concentration layers, mostly referring to hard surfaces (e.g., glass or mica) and mainly for practical devices and AFM experiments. However, the rapid development of, and increasing demand for, DNA-based microdevices both push for lower cost, easily processable materials, and towards disposable devices. As polymers seem to be the logical choice, the resulting DNA layers will almost certainly be amorphous.

Despite the ubiquitousness of amorphous DNA layers in practical applications, AFM has been far less used than for studies dealing with single DNA molecules and even self-assembled DNA layers. This lack of interest can be partially explained by the experimental difficulties related to the amorphous layers, e.g., uneven topography and heterogenous chemistry of surfaces, and the difficulty in interpreting the AFM data. However, polymer science benefitted from in-depth AFM studies as early as the mid-1990s, e.g., the demonstration of superior imaging and more information-rich data provided by AFM than SEM [18], and extensive and conceptually accurate reviews [25]. The similar nature of amorphous DNA layers and polymers, the long history of AFM-based studies of polymer surfaces and the increased interest in cost-effective polymer-based biodevices suggest that AFM will become a major experimental tool for the study of DNA immobilised on surfaces in the form of amorphous layers.

5.2
AFM Imaging of DNA Amorphous Layers

One of the challenges of practical DNA devices is to find the right balance between a high surface density of DNA molecules, which is expected to increase the number of molecular recognition events per unit area of the device, and a loose molecular network, which is expected to increase the

efficiency of molecular recognition per target molecule. Fortunately, the amorphous layers are in principle well positioned regarding the latter desideratum, but complications arise from the mesoscale character of DNA layers, i.e., the presence of aggregates of oligomers on surfaces, instead of continuous "blanket" layers.

AFM imaging helped the quantification, and in some cases the understanding, of the relationship between DNA layer structure and the processing conditions. For instance, the immobilisation of short (16 bases) oligonucleotides on a hard, flat surface (covalent binding of thiol-terminated DNA on self-assembled monolayer-coated silicon wafer, [119]) resulted in a layer with an average thickness of approximately 6 nm (measured by ellipsometry). However, AFM analysis revealed that the ssDNA aggregates in lumps of approximately 90 nm^2 (9.5 nm in height, assuming, for simplicity, a semispherical shape of the aggregates). After hybridisation the dsDNA aggregates (Fig. 25) reached an average size of 360 nm^2 (approximately 19 nm in height). A study [162] focusing on the adsorption of poly(A) (200 bp) on gold and subsequent hybridisation with poly(T) observed that the ssDNA aggregates are approximately 20 nm in diameter and the dsDNA aggregates are approximately 50 nm in diameter, with very little lateral growth occurring.

The immobilisation by electrostatic interactions of longer, 26 bp ssDNA strands on hard, poly(lysine)-coated glass resulted in aggregates of 63 nm (Fig. 26) [163]. Finally, when DNA molecules of the same length (26 bp) were covalently immobilised on the surface of plasma-induced, NHS-

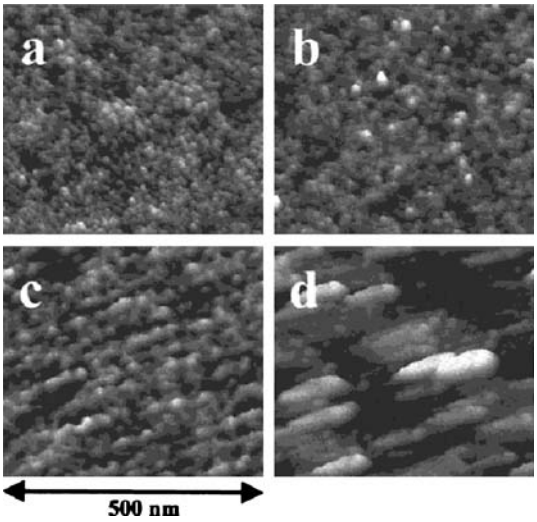

Fig. 25 AFM images of silicon chip surfaces: **a** cleaned, rehydroxylated silicon surface, **b** self-assembled MPTS layer on silicon, **c** immobilised oligonucleotide probe, **d** surface after hybridisation to a complementary target [119]. Reprinted with permission

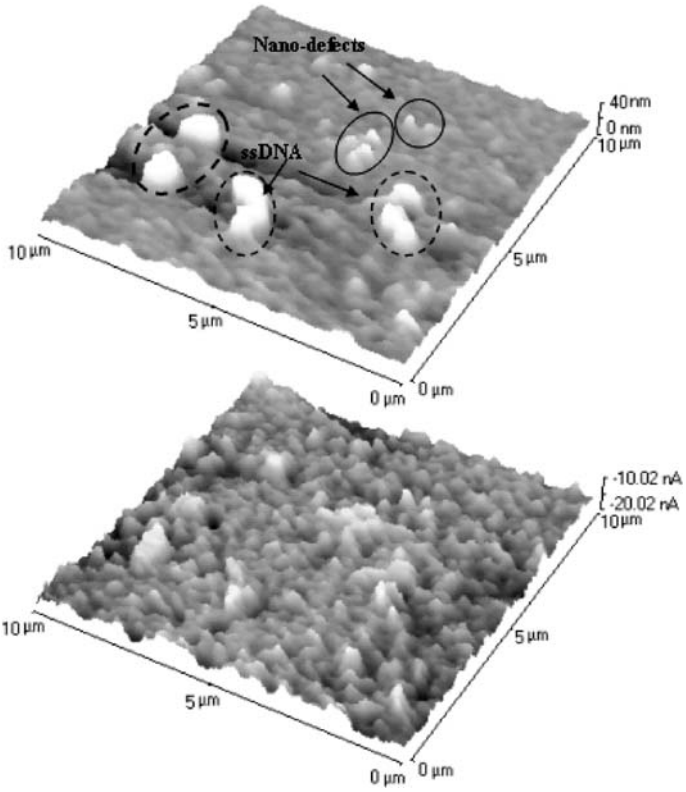

Fig. 26 AFM topography (*top*) and LF (*bottom*) images of a layer of 26 bp oligonucleotide immobilised on poly-L-lysine coated surface. The nanodefects on poly-L-lysine film are indicated with a *solid line* and the immobilised ssDNAs are indicated in *dotted circles* [163]. Reprinted with permission

functionalised model polymers, i.e., polycarbonate and cyclo-olefine copolymer, the dimension of the DNA aggregates was very much dependent on the level of polymer surface crosslinking. The surface coverage with DNA aggregates on the crosslinked harder polycarbonate surface reached approximately 17 % compared with more than 40 % on the non-crosslinked surface of cyclo-olefin copolymer. Also the 26 bp ssDNA aggregates are around 30 nm and 60 nm on polycarbonate and cyclo-olefin copolymer, respectively, compared to the less than 10 nm for 16 bp ssDNA aggregates on silicon surface [119]. The most striking fact, however, is that essentially the hybridisation does not occur within detectable levels on polycarbonate, but it does occur at high levels on cyclo-olefin copolymer, where the dsDNA aggregates reach 190 nm in height (compared with 19 nm for dsDNA on silicon, [119]). This opposite behaviour, which illustrates inter alia both the challenges and opportunities of using polymers for DNA immobilisation, is likely to be caused

by the "sinking in" of ssDNA chains in the crosslinked polycarbonate polymer network and subsequent lack of hybridisation, and the "opening up" of the ssDNA-decorated cyclo-olefin copolymer polymeric chains during hybridisation. Finally, statistical analysis of the topographic data of DNA aggregates before and after hybridisation can reveal the extent of hybridisation [163]. Furthermore, 2D fractal analysis of the DNA aggregates can reveal the effectiveness of rough surfaces with respect to DNA immobilisation [163].

5.3 AFM Probing of DNA Amorphous Layers

AFM can operate in a multitude of modes and can extract physical information beyond topography, in particular through lateral force analysis (LFA). As mentioned in Sect. 12, the apparent LF is modulated by a combination of factors, i.e., (i) topography; (ii) chemistry, which translates in a particular level of surface hydrophobicity; and (iii) stiffness of the scanned material. While the impact of the topography can be factored out by image processing, the interplay between chemistry/hydrophobicity and substrate stiffness, the latter particularly important for soft (e.g., polymer) samples, is more difficult to handle. The separate recording and analysis of the lateral and normal forces resolves most of the problems regarding this overlap of influences.

In principle, there are two methods for the AFM probing of amorphous layers, namely (i) an active probing, which probes the surface chemistry, and (ii) a passive probing, which probes the surface physics. The active AFM probing, which is essentially an extension of the AFM-based single molecule studies, relies on the measurement of LF by an AFM tip that is functionalised with molecular recognition-active molecules (e.g., a potentially complementary DNA).

The active probing of DNA amorphous layers has been used [164] to probe the mechanics of molecular recognition between short segments of ssDNA. First patterned arrays of different DNA strands have been fabricated by upgraded microlithography techniques. A strong friction interaction was measured between the DNA-functionalised latex bead mounted on an AFM tip and patterns functionalised with complementary DNA, as opposed to a low friction for patterns with non-complementary DNA strands (Fig. 27). This result is consistent with the formation of a greater number of hydrogen bonds for the complementary sequence, suggesting that the friction arises from the hybridisation of the DNA-on-the-tip and the surface-bound DNA. More recently, AFM has been used [165] to monitor the molecular interactions between an AFM tip functionalised with molecular beacons, which are fluorescence probes containing an ss-oligonucleotide with a probe sequence embedded in complementary sequences that form a hairpin stem, and DNA molecules covalently bound on surfaces. The interaction force between a lin-

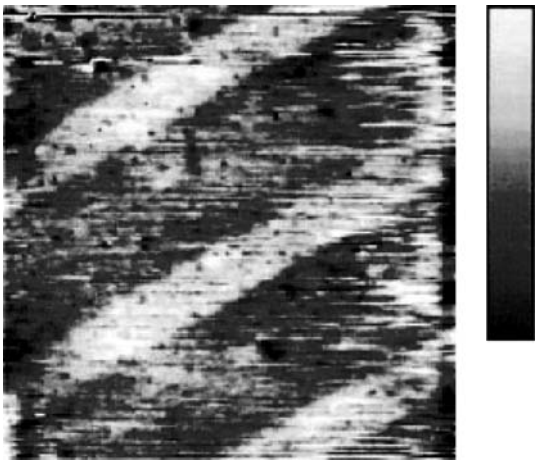

Fig. 27 LF AFM image of a dual-probe array containing stripes of the complement (10 μm) and control (5 μm) oligonucleotides. The length scale is 50 μm and the vertical scale is 250 mV [164]. Reprinted with permission

ear DNA probe and the target DNA was also detected and compared to that between molecular beacons and target DNA molecules.

Passive probing has been demonstrated recently [166] for the surface hydrophobicity modulated by DNA immobilisation and hybridisation. LFA has been performed with normal nitride tips probing the amorphous ssDNA and hybridised DNA layers immobilised on two model polymers (polycarbonate and cyclo-olefin copolymer). The most striking feature is the reversal of the LF image from ssDNA layers (hydrophobic aggregates on both polymers) to dsDNA layers (hydrophilic aggregates, only on cyclo-olefin copolymer) (Fig. 28). The likely explanation is that the orientation of the free side groups on the oligonucleotide (i.e., hydrophobic bases for ssDNA layers) leads to apparent hydrophobic aggregates, whereas hybridisation preferentially blocks the bases and the surface of the dsDNA aggregates preferentially present the hydrophilic phosphate groups. This "image reversal" of hybridised oligonucleotide aggregates compared with ssDNA ones could be used for the readout of DNA micro- and nanoarrays. Also, the surface charging modulated by DNA immobilisation and hybridisation has been investigated by AFM force measurements [167]. The force measurements between a negatively charged silica tip and the substrates comprising immobilised DNA immersed in dilute electrolyte indicate that hybridisation increased the surface charge and surface potential of the substrates through exposure of the phosphate groups.

From the point of view of the operation of DNA-based nanodevices, AFM imaging and probing can be used as a readout method for micro/nanoarrays. The first possibility is to expand on the variation of heights of DNA aggregates

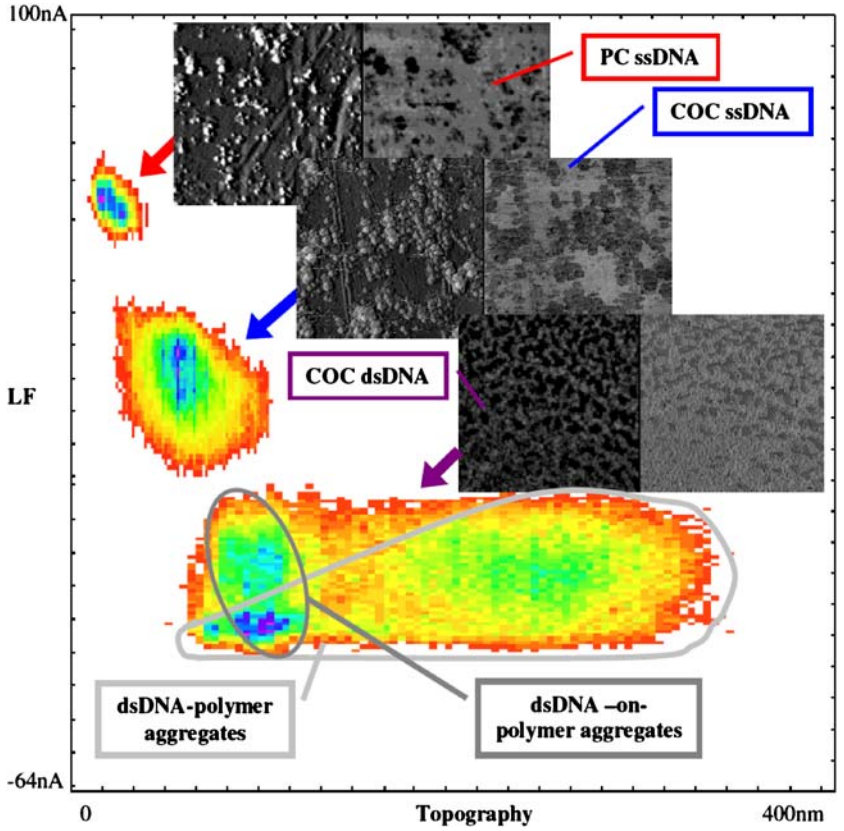

Fig. 28 Bivariate histograms of ssDNA-polymer aggregates on polycarbonate (PC) and cyclo-olefine copolymer (COC) -top left cluster; COC ssDNA-polymer aggregates (middle left cluster); and COC hybridized surfaces (bottom, unhybridised ssDNA aggregates on the subcluster on left and dsDNA aggregates on the subcluster on right). The clusters represent the colour-coded frequency of LF-topography pairs (highest frequency = purple; lowest = red; no data = white). The insets represent AFM images for topography (left) and LF (right). The tone reversal in LF images is evident when comparing the far left images of the middle and bottom insets, respectively. Reprinted with permission.

as a function of their lengths, an approach which has been demonstrated recently [121] (Fig. 29). A somewhat similar approach has been taken for the detection of protein: dsDNA interactions in a microarray format [168, 169]. Essentially, dsDNA strands with asymmetrical disulfide bonds containing a recognition sequence specific to a given restriction enzyme are self-assembled on a gold surface. When site-specific enzymatic cleavage occurs, the change in topography is easily detectable by AFM.

One promising strategy for detecting analyte binding to nanoarrays is the use of labelled nanoparticle probes, using the striking properties of nanopar-

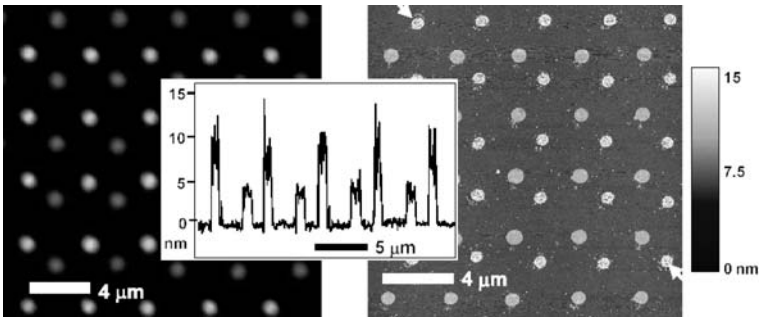

Fig. 29 Epi-fluorescent (*left*) and AFM topography (*right*) images of two different sizes of DNA-modified gold nanoparticles [121]. The image in the middle represents an AFM scan of a line between the two arrows in the right image. Reprinted with permission

ticles [119, 170]. This approach has been recently used in conjunction with topographical AFM to detect the selective binding of different sized DNA-modified nanoparticles to two component nanoarrays [119, 170].

5.4 AFM Fabrication Involving DNA Amorphous Layers

Perhaps the most important recent development in the field of nanofabrication techniques for biodevices is the dip pen nanolithography (DPN) technique reported by Mirkin and coworkers [171–178], which has been recently reviewed [179]. In a typical DPN experiment, an AFM tip is coated with an "ink" by dipping the tip in a solution of the biomolecule (e.g., DNA) to be patterned. The subsequent contact of the tip with the surface releases the molecules via a water meniscus that condenses at the tip–substrate contact (Fig. 30). This diffusion-based process allows modulation of the patterned dimensions, i.e., longer tip–substrate dwell times lead to larger pattern spot areas [171, 175]. The general direct deposition nature of the DPN process allows the patterning of essentially any (bio)molecule and even nanoparticles [119, 171, 176–178] and on any substrate (e.g., metals, insulators and semiconductors). It could be conceived that, in principle, DPN can be used for the alignment of molecules if the tip is dragged on the surface, but at present the method is used largely for the fabrication of dot-pattered surfaces as nanoarrays. The diffusion-controlled deposition process suggests that the DNA molecules are not structured within the DNA aggregate. It has been demonstrated [119] that DNA patterning via DPN is highly controllable in terms of pattern size/shape, and that the immobilised DNA is functional and accessible to specific binding of labelled targets. Initial studies of direct transfer of DNA from an AFM tip to both metal and insulator substrates identified several key components that promote DNA patterning, including precise control of the ambient humidity and careful functionalisation and

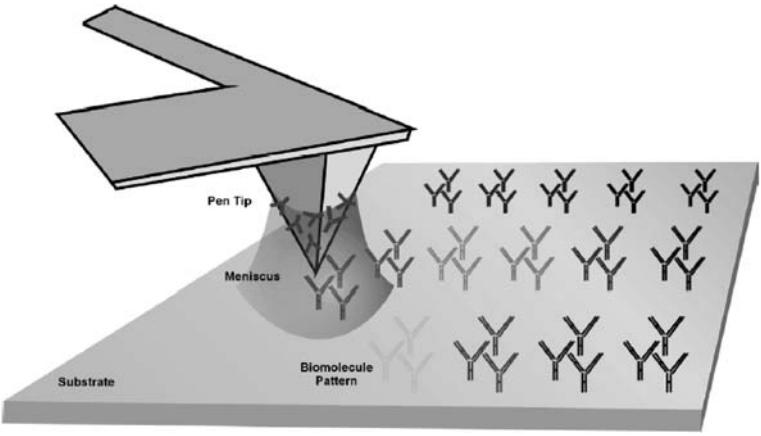

Fig. 30 Principle of operation of dip pen lithography [179]. Reprinted with permission

inking of the AFM tips and a judicious choice of ink–substrate combination. For example, hexanethiol-modified oligonucleotides were directly patterned on gold with features ranging from 50 nm (i.e., 10 000 times denser than those in conventional microarrays) to several micrometers; acrylamide-modified oligonucleotides were deposited onto activated (mercapto-propyl-trimethoxylsilane) oxidised silicon wafers, with the size of DNA spots over a range of several orders of magnitude [171]. The selectivity of the patterned oligonucleotides was verified by hybridisation with fluorescently labelled DNA probes but also through the variations of the AFM-measured topography of DNA spots as a function of the length of the probed DNA molecule (Fig. 29).

The demonstrated resolution of DPN indicates that arrays with 100 000 oligonucleotide spots can be generated in a typical AFM scanning area ($100 \times 100\ \mu m$), making it conceivable that nanoarrays are a viable alternative to microarrays due to the possible use of scanned probe methods for array readout. However, the most significant barrier to using a scanned probe technique is the low overall speed, largely due to the serial or "single pen" nature. Addressing this limitation, parallel scanning has been demonstrated for a passive probe array, i.e., with DPN pens not actuated independently but simultaneously brought into contact with the surface and scanned together, thus allowing the multiplication of spots [172]. While the independent control of pens is much more challenging for both information processing (multiplication of control loops) and also for microfluidic logistics (delivery of different inks on different pens), but it has been also demonstrated [180].

6 Conclusions

The overview of more than a decade of work on the application of AFM to the study of DNA molecules immobilised on surfaces suggests that the field is close to the point of passing the "teenager stage". Many things have been learnt about the fundamentals of biomolecular interactions of DNA molecules, and many more lessons are still to be learnt. Importantly, AFM studies of DNA immobilised on surfaces are increasingly applications-oriented in relative numbers, but there are no signs that the fundamental studies are decreasing in absolute terms—quite the contrary.

The rapid enlargement of the field has translated in an increased diversity of classes of equipment. Firstly, AFM is today, as opposed to just 5 years ago, not "just another microscope". The AFMs that fill this sector are robust, cost-effective and operation-friendly. Fortunately, the DNA molecules are robust enough to allow studies performed by even the most cost-effective AFM. There are areas, such as long-range self-assembly of DNA for biocomputation or more industrially oriented studies of amorphous layers of DNA for lab-on-a-chip devices, where low-end AFMs could fulfil the requirements. Secondly, the initial high-end AFM equipment will also continue to evolve strongly, especially for the probing of single molecules. An important factor would be the development of technical solutions for extremely fast scanning of molecules on surfaces. More advances are expected in the manipulation of, and "fabrication" with, single DNA molecules for applications as diverse as genomics and molecular electronics. AFM will be increasingly integrated in complex imaging and nanomanipulation machines comprising, e.g., a confocal microscope and/or SNOM. Thirdly, in recent years a new breed of AFM equipment has emerged that is specifically focused on industrial nanotechnology applications, with dip pen lithography being the front runner. This trend is expected to continue, especially if robust technical solutions are found for the parallelisation of writing. Another welcome and expected development would be a dual, write–read AFM machine, or even a more complex write–read–erase–write–etc. machine. The development of DNA-oriented industrial nanotechnology infrastructure is strategically important as genomics matures and will possibly enter a stage of "mass production" of gene chips for personalised medicine. In conclusion, all the signs point to a strong and diverse development of the application of AFM to the imaging and probing of, and fabrication with, DNA molecules on surfaces.

Acknowledgements This work was supported by grants from Defense Advanced Research Projects Agency and Australian Research Council.

References

1. Thomson-ISI Web-of-knowledge, http://isi6.isiknowledge.com/portal.cgi
2. Jena BP, Hörber HJK (2002) Biological probe microscopy in aqueous fluids. Atomic force microscopy in cell biology. Academic, San Diego
3. Hansma HG (2001) Annu Rev Phys Chem 52:71–92
4. Hansma HG, Pietrasanta LI, Auerbach ID, Sorenson C, Golan R, Holden PA (2000) J Biomater Sci Polym Ed 11(7):675–683
5. Bowen WR, Lovitt RW, Wright CJ (2000) Biotech Lett 22(11):893–903
6. Lyubchenko YL, Jacobs BL, Lindsay SM, Stasiak A (1995) Scan Microscopy 9(3):705–727
7. Yang J, Tamm LK, Somlyo AP, Shao Z (1993) J Microscopy 171:183–198
8. Blackford BL, Jericho MH, Mulhern PJ (1991) Scan Microscopy 5(4):907–918
9. Binnig G, Rohrer H, Gerber Ch, Weibel E (1982) Phys Rev Lett 49:57–61
10. Binnig G, Quate CF, Gerber Ch (1986) Phys Rev Lett 56:930
11. URL: http://www.jpk.com/tutorial/spm_family.htm
12. Albrecht TR, Grütter P, Horne D, Rugar D (1991) J Appl Phys 69:668
13. Feldman K, Fritz M, Hähner G, Marti A, Spencer ND (1998) Tribol Intern 31(1–3):99–105
14. Gibson CT, Watson GS, Myhra S (1997) Wear 213(1–2):72–79
15. Meyer E, Luthi R, Howald L, Bammerlin M, Guggisberg M, Guntherodt H J, Scandella L, Gobrecht J, Schumacher A, Prins R (1996) Friction force spectroscopy. In: Persson BNJ, Tosatti E (eds) Physics of sliding friction. Kluwer, Dordrecht
16. Singer IL (1994) Dissipative process in tribology. In: Dowson D, Meyer E, Overney R, Frommer J (eds) Proceedings 20th Leed-Lyon Symposium on Tribology. Villeurbanne 7–10 September 1993
17. Beake BD, Leggett JG (2000) Langmuir 16:735
18. Ling JSG, Leggett GJ (1997) Polymer 38:2617
19. Noy A, Frisbie CD, Rozsnyai LF, Wrighton MS, Lieber CM (1995) J Am Chem Soc 117:7943
20. Wilbur JL, Biebuyck HA, MacDonald JC, Whitesides GM (1995) Langmuir 11:825
21. Brewer NJ, Beake BD Leggett JG (2001) Langmuir 17:1970
22. Beake BD, Ling JSG, Leggett GJ (2000) Polymer 41:2241
23. Grafström S, Neitezt M, Hagen T, Ackermann J, Neumann R, Probst O, Wörtge M (1993) Nanotech 4:143
24. Hähner G, Marti A, Spencer ND (1997) Tribol Lett 3:359
25. Magonov SN, Reneker DH (1997) Annu Rev Mater Sci 27:175
26. Frisbie CD, Rozsnyai A, Noy A, Wrighton MS, Lieber CM (1994) Science 265:2071–2074
27. Amrein M, Müller DJ (1999) Nanobio 4:229–256
28. Carrillo A, Gujraty KV, Kane RS (2004) In: Muller U, Nicolau DV (eds) Microarray technology and applications, Chap 3. Springer, Berlin Heidelberg New York
29. Hanson KL, Filipponi L, Nicolau DV (2004) In: Muller U, Nicolau DV (eds) Microarray technology and applications, Chap 2. Springer, Berlin Heidelberg New York
30. Allen MJ, Bradbury EM, Balhorn R (1997) Nucl Acids Res 25(11):2221–2226
31. Bezanilla M, Manne S, Laney DE, Lyubchenko YL, Hansma HG (1995) Langmuir 11:655–659
32. Shao Z, Mou J, Czajkowsky DM, Yang J, Yuan J-Y (1996) Adv Phys 45:1–86
33. Shlyakhtenko LS, Gall AA, Filonov A, Cerovac Z, Lushnikov A, Lyubchenko YL (2003) Ultramicroscopy 97:279–287

34. Lyubchenko Y, Shlyakhtenko L, Harrington R, Oden P, Lindsay S (1993) PNAS 90:2137–2140
35. Möller R, Csáki A, Köhler M, Fritzsche W (2000) Nucl Acids Res 28:1–5
36. Ivanova EP, Pham DK, Brack N, Pigram P, Nicolau DV (2004) Biosens Bioelectr 19:1363–1370
37. Koch T, Jacobsen N, Fensholdt J, Boas U, Fenger M, Jakobsen MH (2000) Bioconj Chem 11:474
38. Fixe F, Dufva M, Telleman P, Christensen CBV (2004) Lab on Chip 4:191
39. Kohsaka H, Taniguchi A, Richman DD, Carson DA (1993) Nucl Acids Res 21:3469
40. Running JA, Urdea MS (1990) BioTechniques 8:276
41. Beecher JE, McGall GH, Goldberg M (1997) Polym Mater Sci Eng 76:394
42. Beecher JE, McGall GH, Goldberg M (1997) Polym Mater Sci Eng 76:597
43. Matson RS, Rampal J, Pentoney SL, Anderson PD, Coassin P (1995) Anal Biochem 224:110
44. Sreekumar A, Nyati MK, Varambally S, Barrette TR, Ghosh D, Lawrence TS, Chinnaiyan AM (2001) Can Res 61:7585
45. Weiler J, Hoheisel JD (1996) Anal Biochem 243:218
46. http://www2.muw.edu/~rwhitwam/ABZDNA.html
47. http://www.ndsu.nodak.edu/instruct/mcclean/plsc731/dna/dna4.htm
48. Sinden RR, Potaman VN, Oussatcheva EA, Pearson CE, Lyubchenko YL, Shlyakhtenko LS (2002) J Biosci 27(1):53–65
49. Clausen-Schaumann H, Rief M, Tolksdorf C, Gaub HE (2000) Biophys J 78(4):1997–2007
50. Leger JF, Romano G, Sakar A, Robert J, Bourdieu L, Chatenay D, Marko JF (1999) Phys Rev Lett 83:1066–1069
51. Bouchiat C, Wang MD, Allemand JF, Strick T, Block SM, Croquette V (1999) Biophys J 76:409–413
52. Strick T, Allemand JF, Croquette V, Bensimon D (2000) Prog Biophys Mol Biol 74:115–140
53. Cherny DI, Foucade A, Svinarchuck F, Nielson PE, Malvy C, Delain E (1998) Biophys J 74:1015–1023
54. Jing J, Reed J, Huang J, Hu XH, Clarke V, Edington J, Housman D, Anantharaman TS, Huff EJ, Mishra B, Porter B, Shenker A, Wolfson E, Hiort C, Kantor R, Aston C, Shwartz DC (1998) PNAS 95:72–75
55. Seong GH, Niimi T, Yanagida Y, Kobatake E, Aizawa M (2000) Anal Chem 72:1288–1293
56. Taylor JR, Fang MM, Nie S (2000) Anal Chem 72:1979–1986
57. Alivisatos AP, Johnsson KP, Peng X, Wilson TE, Loweth CJ, Bruchez-Jr MP, Schultz PG (1996) Nature 382:609–611
58. Mirkin CA, Letsinger RL, Mucic RC, Storhoff JJ (1996) Nature 382:607–609
59. Winfree E, Liu F, Wenzler LA, Seeman NC (1998) Nature 394:539–544
60. Richter J, Mertig M, Pompe W, Monch I, Schackert HK (2001) Appl Phys Lett 78:536–538
61. Keren K, Krueger M, Gilad R, Ben-Yoseph G, Sivan U, Braun E (2002) Science 297:72–75
62. Wang J (2000) Nucl Acids Res 28(16):3011–3016
63. MacKerell-Jr AD, Lee GU (1999) Eur Biophys J 28:415–426
64. Hughes SD, Woolley AT (2003) Biomed Microdev 5(1):69–74
65. Argaman M, Golan R, Thomson NH, Hansma HG (1997) Nucl Acid Res 23(21):4379–4384

66. Drake B, Prater CB, Weisenhorn AL, Gould SA, Albrecht TR, Quate CF, Cannell DS, Hansma HG, Hansma PK (1989) Science 243:1586–1589
67. Hansma HG, Hoh JH (1994) Annu Rev Biophys Biophys Chem 23:115–139
68. Fritz M, Radmacher M, Clevelend JP, Allersma MW, Stewart RJ, Gieselmann, R, Janmey P, Schmidt CF, Hansma PK (1995) Langmuir 11:3529–3535
69. Thomson NH, Fritz M, Radmacher M, Cleveland JP, Schmidt C, Hansma PK (1996) Biophys J 70:2421–2431
70. Bezanilla M, Drake B, Nudler E, Kashlev M, Hansma PK, Hansma HG (1994) Biophys J 67:2454–2459
71. Hansma HG, Revenko I, Kim K, Laney DE (1996) Nucl Acids Res 24(4):713–720
72. Grange W, Strunz T, Schumakovitch I, Guntherodt HJ, Hegner M (2001) Single Mol 2:75–78
73. Shlyakhtenko LS, Potaman VN, Sinden RS, Gall AA, Lyubchenko YL (2000) Nucl Acid Res 28(1):3472–3477
74. Holliday R (1964) Genet Res 5:282–304
75. Ortiz-Lombardia M, Gonzalez A, Eritja R, Aymamy J, Azorin F, Coll M (1999) Nature Struct Biol 6:913–917
76. Kasas S, Thomson NH, Smith BL, Hansma HG, Zhu X, Guthold M, Bustamante C, Kool ET, Keshlev M, Hansma PK (1997) Biochem 36:461–468
77. Sinden RR (1999) Am J Hum Genet 64:346–353
78. Sinden RR (1994) DNA structure and functions. Academic, San Diego
79. Pastre D, Pietrement O, Fusil P, Landousy F, Jeusset J, David MO, Hamon C, Le Cam E, Zozime A (2003) Biophys J 85(4):2507–2518
80. Lyubchenko Y, Shlyakhtenko L (1999) Technical bulletin. BioForce Laboratory, Ames, IA
81. Shlyakhtenko L, Gall AA, Weimer JJ, Hawn DD, Lyubchenko Y (1999) Biophys J 77:568–576
82. Hansma HG, Kim KJ, Laney DE, Garcia RA, Argaman M, Allen MJ, Parsons SM (1997) J Struct Biol 119:99–108
83. Nakamura J, Walker VE, Upton PB, Chiang SY, Kow YW, Swenberg JA (1998) Cancer Res 58:222–225
84. Sun HB, Qian L, Yokota H (2001) Anal Chem 73:2229–2232
85. Bustamante C, Rivetti C, Keller DJ (1997) Curr Opin Struct Biol 7:709–716
86. Feng XZ, Bash R, Balagurumoorthy P, Lohr D, Harrington RE, Lindsay SM (2000) Nucl Acids Res 28(2):593–596
87. Metzler R, Hanke A (2005) Knots, bubbles, unwinding, and breathing: probing the topology of DNA and other biomolecules. In: Rieth M, Schommers W (eds) Handbook of theoretical and computational nanotechnology. American Scientific, California (in press)
88. Strunz T, Oroszlan K, Schafer R, Guntherodt HJ (1999) PNAS 96:11277
89. Williams MC, Rouzina I, Bloomfield VA (2002) Acc Chem Res 35:159
90. Baumann CG, Bloomfield VA, Smith SB, Bustamante C, Wang MD, Block SM (2000) Biophys J 78:1965–1978
91. Bensimon D, Simon AJ, Croquette V, Bensimon A (1995) Phys Rev Lett 74:4754–4757
92. Cluzel P, Lebrun A, Heller C, Lavery R, Viovy J-L, Chatenay D, Caron F (1996) Science 271:792–794
93. Ahsan A, Rudnick J, Bruinsma R (1998) Biophys J 74:132–137
94. Konrad MW, Bolonick JI (1996) J Am Chem Soc 118:10989–10994
95. Kosikov KM, Gorin AA, Zhurkin VB, Olson WK (1999) J Mol Biol 289:1301–1326
96. Lebrun A, Lavery R (1996) Nucl Acids Res 24:2260–2267

97. Marko JF (1997) Europhys Lett 38:183–188
98. Marko J F (1998) Phys Rev E 57:2134–2149
99. Allemand JF, Bensimon D, Lavery R, Croquette V (1998) PNAS 95:14152–14157
100. Lee GU, Chrisey LA, Colton RJ (1994) Science 266:771
101. Strick TR, Allemand JF, Bensimon D, Bensimon A, Croquette V (1996) Science 271:1835–1837
102. Strick, TR, Allemand J-F, Bensimon D, Croquette V (1998) Biophys J 74:2016–2028
103. Bockelmann U, Essevaz-Roulet B, Heslot F (1997) Phys Rev Lett 79:4489–4492
104. Nogues C, Cohen SR, Daube SS, Naaman R (2004) PCCP 6:4459–4466
105. Watanabe H, Manabe C, Shigematsu T, Shimotani K, Shimizu M (2001) Appl Phys Lett 79(15):2462–2464
106. Anselmetti D, Fritz J, Smith B, Fernandez-Busquets X (2000) D Single Mol 1:53–58
107. Ouyang JQ, Hu J, Chen SF, Sun JL, Li MQ (1997) J Vac Sci Technol B 15:1385
108. Hu J, Zhang Y, Li B, Gao HB, Hartmann U, Li MQ (2004) Surf Interface Anal 36:124–126
109. Hu J, Zhang Y, Gao HB, Li MQ, Hartmann U (2002) Nano Lett 2:55
110. Pum D, Neubauer A, Gyorvary E, Sara M, Sleytr UB (2000) Nanotech 11:100–107
111. Debabov VG (2004) Mol Biol 38(4):482–493
112. Meyer RK, Aebi U (1990) J Cell Biol 110:2013–2024
113. Taylor KA, Taylor DW (1999) J Struct Biol 128:75–81
114. Mao C, Sun W, Seeman NC (1999) J Am Chem Soc 121:5437
115. Seeman NC (2001) Nano lett 1:22
116. Mao C, LaBean T, Reif JH, Seeman NC (2000) Nature 407:493
117. Kanno T, Tanaka T, Miyoshi N, Kawai T (2000) Jpn J Appl Phys 39:L269
118. Cai L, Tabata H, Kawai T (2000) Appl Phys Lett 77:3105
119. Lenigk R, Carles M, Ip NY, Sucher NJ (2001) Langmuir 17:2497–2501
120. Boncheva M, Scheibler L, Lincoln P, Vogel H, Akerman B (1999) Langmuir 15:4317–4320
121. Demers LM, Ginger DS, Park SJ, Li Z, Chung SW, Mirkin CA (2002) Science 296:1836
122. Fang Y, Hoh JH (1998) Nucl Acids Res 26(2):588–593
123. Han WH, Lindsay SM, Dlakic M, Harington RE (1997) Nature 386:563
124. Fang Y, Spisz TS, Hoh JH (1999) Nucl Acids Res 27(8):1943–1949
125. Klein DCG, Gurevich L, Janssen JW, Kouwenhoven LP, Carbeck JD, Sohn LL (2001) Appl Phys Lett 78(16):2396
126. Vesenka J, Henderson E, Marsh T (2002) In: Fritzsche W (ed) Workshop on DNA-based molecular construction, Jena, Germany, May 2002. AIP Conf Proc 640:109–122
127. Marsh TC, Vesenka J, Henderson E (1995) Nucl Acids Res 23(4):696–700
128. Bhaumik A, Ramakanth M, Brar LK, Raychaudhuri AK, Rondelez F, Chatterji D (2004) Langmuir 20:5891–5896
129. Liu M, Amro NA, Chow CS, Liu G (2002) Nano lett 2(8):863–867
130. Danielsen S, Varum KM, Stokke BT (2004) Biomacromol 5:928–936
131. Rackstraw BJ, Martin AL, Stolnik S, Roberts CJ, Garnett MC, Davies MC, Tendler SJB (2001) Langmuir 17:3185–3193
132. Nakamura F, Mitsui K, Hara M (2001) Riken Review 37:63
133. Niemeyer CM, Adler M, Pignataro B, Lenhert S, Gao S, Chi L, Fuchs H, Blohm D (1999) Nucl Acids Res 27(23):4553–4561
134. Chen J, Seeman NC (1991) Nature 350:631
135. Seeman NC (1998) DNA Annu Rev Biophys Biomol Struct 27:225–248
136. Yang X, Wenzler L, Qi J, Li X, Seeman N (1998) J Am Chem Soc 120:9779–9786
137. Sha RJ, Liu FR, Seeman NC (2002) Biochem 41(19):5950–5955

138. Winfree E, Sun W, Seeman NC (1998) Nature 394:539–544
139. LaBean T, Yan H, Kopatsch J, Liu F, Winfree E, Reif JH, Seeman NC (2000) J Am Chem Soc 122:1848–1860
140. Liu D, Wang M, Deng Z, Walulu R, Mao C (2004) J Am Chem Soc 126(8):2324–2325
141. Yan H, Feng L, LaBean TH, Reif JH (2003) Ninth international meeting on DNA-based computers (DNA9), Madison, Wisconsin, 2–4 June 2003
142. Li Y, Tseng YD, Kwon SY, D'Espaux L, Bunch S, McEuen PL, Luo D (2004) Nature Mater 3:38
143. Reif J (ed)(2004) Foundations of nanoscience: Self-assembled architectures and devices (FNANO 2004), Snowbird, Utah, 21–23 April 2004. ScienceTechnica (http://www. cs.duke.edu/∼reif/FNANO/FNANO04/)
144. Brun Y, Gopalakrishnan M, Reishus D, Shaw B, Chelyapov N, Aldeman L (2004)In: Reif J (ed) Foundations of nanoscience: Self-assembled architectures and devices (FNANO 2004) Snowbird, Utah, 21–23 April 2004. ScienceTechnica, p 2
145. Yan H, Park SH, Finkelstein G, Reif JH, LaBean TH (2003) Science 301:1882
146. Xiao S, Liu F, Rosen AE, Hainfeld JF, Seeman NC, Musier-Forsyth K, Kiehl RA (2002) J Nanoparticle Res 4:313–317
147. Adleman L (1994) Science 266:1021–1023
148. Winfree E (1998) Algorithmic self-assembly of DNA. California Institute of Technology, PhD thesis
149. Wang H (1963) Proceedings of symposium on the mathematical theory of automata. Polytechnic, Brooklyn, NY, pp 23–55
150. Carbone A, Seeman N (2002) Circuits and programmable self-assembling DNA structures PNAS 99(20):12577–12582
151. Schulman R, Lee S, Papadakis N, Winfree E (2004) In: Proceedings DNA computers 9, Madison, 2–4 June 2003. Lect Notes Comp Sci 2943:108–125
152. Yan H, LaBean TH, Feng L, Reif JH (2003) PNAS 100(14):8103–8108
153. Schwartz PV (2001) Langmuir 17:5971–5977
154. Zhou D, Sinniah K, Abell C, Rayment T (2002) Langmuir 18:8278–8281
155. Schena M, Shalon D, Davis RW, Brown PO (1995) Science 270:467
156. Schena M, Shalon D, Heller R, Chai A, Brown PO, Davis RW (1996) PNAS 93:10614–10619
157. Garno JC, Amro NA, Wadu-Mesthrige K, Liu GY (2002) Langmuir 18(21):8186–8192
158. Hilliard LR, Zhao XJ, Tan WH (2002) Anal Chim Acta 470(1):51–56
159. Rogers YH, Jiang-Baucom P, Huang JZ, Bogdanov V, Andersen S, Boyce-Jacino MT (1999) Anal Biochem 266:23–30
160. Delpech MC, Coutinho FMB, Habibe MES (2002) Polym Test 21:411–415
161. Steel AB, Levicky RL, Herne TM, Tarlov MJ (2000) Biophys J 79:975–981
162. Casero E, Darder M, Diaz DJ, Pariente F, Martin-Gago JA, Abruna H, Lorenzo E (2003) Langmuir 19:6230
163. Sawant PD, Watson GS, Nicolau-Jr DV, Myhra S, Nicolau DV (2005) J Nanosci Nanotech 5(6):951–957
164. Mazzola LT, Frank CW, Fodor SPA, Mosher C, Lartius R, Henderson E (1999) Biophys J 76:2922–2933
165. Jin Y, Wang K, Tan W, Wu P, Wang Q, Huang H, Huang S, Tang Z, Guo Q (2004) Anal Chem 76:5721–5725
166. Nicolau DV, Pham DK, Ivanova EP, Wright JP, Lenigk R, Smekal T, Grodzinski P (2005) Small 1:610
167. Wang J, Bard AJ (2001) Anal Chem 73(10):2207
168. O'Brien JC, Stickney JT, Porter MD (2000) J Am Chem Soc 122:5004

169. O'Brien, JC, Stickney, JT, Porter, MD (2000) Langmuir 16:9559
170. Elmas B, Camli ST, Tuncel M, Senel S, Tuncel A (2001) J Biomat Sci Polym Ed 12(3):283
171. Piner RD, Zhu J, Xu F, Hong S, Mirkin CA (1999) Science 283:661–663
172. Hong SH, Mirkin CA (2000) Science 288:1808–1811
173. Hong SH, Zhu J, Mirkin CA (1999) Langmuir 15:7897–7900
174. Hong SH, Zhu J, Mirkin CA (1999) Science 286:523–525
175. Piner RP, Hong S, Mirkin CA (1999) Langmuir 15:5457–5460
176. Ivanisevic A, Mirkin CA (2001) J Am Chem Soc 123:7887–7889
177. Wilson DL, Martin R, Hong S, Cronin-Golomb M, Mirkin CA, Kaplan DL (2002) Proc Natl Acad Sci 98:13660–13664
178. Su M, Liu X, Li S-Y, Dravid VP, Mirkin CA (2002) J Am Chem Soc 124:1560–1561
179. Nicolau DV, Demers LM, Ginger D (2004) Nanoarrays. In: Muller U, Nicolau DV (eds) Microarray technology and applications, Chap 6. Springer, Berlin Heidelberg New York
180. Zhang M, Bullen D, Chung S-W, Hong S, Ryu KS, Fan Z, Mirkin CA, Liu C (2002) Nanotech 13:212–217

Top Curr Chem (2005) 260: 161–186
DOI 10.1007/128_006

Published online: 15 September 2005

Impedimetric Detection of DNA Hybridization: Towards Near-Patient DNA Diagnostics

Anthony Guiseppi-Elie (✉) · Louise Lingerfelt

Center for Bioelectronics, Biosensors, and Biochips (C3B), Department of Chemical and Life Science Engineering, Virginia Commonwealth University, 601 West Main Street, Richmond, VA 23284-3038, USA
guiseppi@vcu.edu

Abstract Immobilization strategies for the attachment of nucleotide probes to both microarrays and microfabricated interdigitated electrodes differ to address the specific requirements for optical and electrochemical detection, respectively. The DNA immobilization chemistry dictates how the probe molecule is presented to its complement during hybridization and thereby contributes significantly to the final detection signal. This chapter introduces the relevant immobilization strategies for DNA probes on both microarrays and microfabricated interdigitated microsensor electrode arrays. Specifically, we examine immobilization via electrostatic attraction and covalent coupling. The immobilization of DNA presents many challenges because of the need to promote efficient hybridization while minimizing or eliminating nonspecific adsorption to exposed areas of the device substrate. The immobilization strategies also present challenges because of the various materials and surface chemistries that may be involved, the flow characteristics during detection, and the need to perform hybridizations under specific buffer and temperature cycling conditions. This paper provides a rationale for the move towards low-density genosensors using electrochemical detection with focused example applications in human health care. Specifically, electrochemical impedance spectroscopy (EIS) is introduced and discussed as an advantageous method for DNA hybridization detection. The various immobilization strategies are discussed in reference to EIS detection. In conclusion, the advantages of impedance detection are addressed with critical assessments for the advancement of impedance detection for DNA hybridization.

Keywords DNA diagnostics · Impedimetric detection · DNA hybridization · DNA immobilization

Abbreviations

A	adenine
Ag/AgCl	silver/silver chloride
AC	alternating current
AFM	atomic force microscopy
APS	3-aminopropyltrimethoxysilane
BSA	bovine serum albumin
C	cytosine
C	capacitance
CEPs	conducting electroactive polymers
CLIA	Clinical Laboratory Improvement Amendments
CE	counter electrode
Cy3	cyanine 3
Cy5	cyanine 5
DSG	disuccinimidylglutarate
DNA	deoxyribose nucleic acid
dsDNA	double-strand DNA
EIS	electrical impedance spectroscopy
ATR-FTIR	attenuated total reflectance-Fourier transform infrared spectroscopy
G	guanine
GPS	glycidoxypropyltrimethoxysilane
i	AC current response signal
i_m	Maximum AC current response signal
IME	interdigitated microsensor electrode
MPS	3-mercaptopropyltrimethoxysilane
PAMAM	polyamidoamine
PDITC	phenylenediisothiocyanate
PDITC	phenylenediisothiocyanate
p-t-p	peak-to-peak
R	resistance
RE	reference electrode
RNA	ribonucleic acid
R_o	equivalent circuit resistance
R_s	solution resistance
SA	succinic anhydride
ssDNA	single-strand DNA
SMPB	succinimidyl 4-[malemidophenyl] butyrate
t	time
T	thymine
QCM	quartz crystal microbalance
V	voltage
V_m	maximum voltage
WE	working electrode
X	reactance
Z	impedance
Z'	imaginary component of impedance

Z''	real component of impedance
$\|Z\|$	magnitude of impedance
θ	phase shift
τ_p	time constant
ω	radial frequency

1 Introduction

The surface chemistry and immobilization strategy for DNA on an analytical device play an important role in the quality of detection, regardless of the specific detection platform employed. Immobilized DNA is important in such technologies as DNA microarrays, genosensors, and various blotting methods. The effect of the DNA immobilization strategy is significant regardless of the type of probe, be it cDNA or oligonucleotides, which is immobilized to the device surface. The immobilization of DNA dictates how the probe is presented to its complement during hybridization and thereby affects the final detection signal. The immobilization strategy also strongly influences the surface chemistry that is presented to the target environment in non-probe bearing regions and so governs nonspecific background adsorption. The plurality of surface types employed for DNA hybridization detection dictates the appropriate method or chemistry used for immobilization. Among these surface types are oxidized silicon, glass, metals such as gold and platinum, plastics such as cellulose acetate, and hydrogels. The objective of all immobilization strategies, regardless of the specific chemistry and substrate employed, is (i) high density coverage of the single-stranded or cDNA probes; (ii) improved hybridization kinetics; (iii) minimal background and nonspecific adsorption to the support or substrate; (iv) improved sensitivity; and (v) long-term stability of the DNA probe.

Currently, the most widely used method for high throughput screening of the complete genome of an organism is the DNA microarray. Microarray technology utilizes thousands of gene probes immobilized in a 2-D array on a glass slide [1], or microporous support including nitrocellulose, polyacrylamide gel, and agarose films [2–4]. Microarrays depend upon differential detection of cDNA targets obtained from sample and reference sources. Both the sample and reference cDNA are labeled using two different fluorescent dyes, typically Cy5 (red, reference) and Cy3 (green, sample). The intensities of emissions from the sample are compared to that of the reference. An ideal reference would be a source capable of producing cDNA that would equally highlight all features on the microarray. Under these conditions, fluorescence intensity correlates to greater amounts of reference or sample DNA

hybridized to the microarray. The intensity profiles generated, therefore, indicate gene expression for the sample as compared to the reference.

DNA microarray technology has fundamentally revolutionized biological assay techniques allowing the parallel assessment of multiple gene expression levels. A consequence of this rapid screening approach is the development of a diagnostic biochip that would allow more targeted and individually focused therapeutic regimens dependent on the unique genetic profile of the diseased state [5]. Future developments in gene expression technology offer the potential for improved capabilities over traditional medical diagnosis, prognosis, and treatment. The continued identification of genes associated with particular disease states is steadily rising. Furthermore, classification of diseases based on their unique genetic expression profiles is increasingly being studied as compared to more traditional methods of disease classification.

However, the current DNA microarray technology presents an impractical solution for the development of a rapid-performance DNA biochip for the diagnosis of disease states. Sample size requirements are too large and sample preparation is too time-consuming for the DNA microarray platform to achieve real-time detection of DNA hybridization [6] and classification. Additionally, data analysis for large microarray data sets requires significant statistical processing leading to the familiar "paralysis by analysis". Finally, the technology must be made clinically "hardened", that is, made robust and quantitative with the ability to withstand the scrutiny of the Clinical Laboratory Improvement Amendments (CLIA) of 1998. The key limiting issues, therefore, are speed, analytical fidelity, and clinical hardening.

An alternative implementation of the current microarray approach is the development of a DNA biochip that uses electrochemical impedance for detection of the DNA hybridization related to a select number of disease-specific genes. Other detection modalities are possible and practical. Electrochemical impedance spectroscopy (EIS) is a radio frequency technique that is widely used for the characterization of electrified interfaces and ionic solutions. The technique uses a sinusoidally varying, nonperturbating but interrogating voltage (typically 20–50 mV p-t-p) applied between a pair of opposing working and counter electrodes. The inclusion of a third or reference electrode and an appropriate potentiostat allows the sine wave to be superimposed on the quiescent potential of the working electrode. Under these circumstances the ensuing current informs on both the coupled mass transport and charge transfer kinetics of electrochemically dischargeable species and of the movement of ions under the influence of the oscillating electric field. When potentials are selected that do not electrochemically discharge redox active moieties of DNA (such as guanine), and a single frequency is used for interrogation, the technique of electrochemical impedance (EI) then measures the ability of DNA to support ionic mobility and has been demonstrated as an effective analytical technique for understanding the way in which charge migration is impeded or facilitated through an interface that is decorated

with oligonucleotides, particularly before and after its hybridization with its complement. The most convenient format for the delivery of the interrogating voltage is via a pair of co-planar interdigitated microsensor electrodes (IMEs). Co-planar interdigitated electrodes may be fabricated using state of the industry microlithography techniques; these devices create a well-defined electric field, and may be readily decorated with oligonucleoptides or cDNA using established noncontact microarraying techniques. Microfabricated devices create potential for mass production with a high degree of reproducibility at modest to low cost. These microdevices are, therefore, based on bioelectronic detection and are part of the family of microdevices that connect the chemical and electrical domains allowing chemical potential energy to be transduced into a proportionate electrical signal.

Electrochemical impedance is most useful when applied to a limited suite of genes and is not practical for a complete genome given that a set of interdigitated electrode structures must be nano- or micro-fabricated to support each probe set and interrogating electronics must be designed to independently address each pair of electrodes. Gene expression that is linked to particular disease states permits profiling using a limited number of genes and is therefore well suited for analysis by EI. Detection devices based on an EI system represents the possibility for mass production of sensing devices through microlithographic production of IME chips and the decorating of these with oligonucleotides via noncontact printing techniques such as ink-jet. Moreover, the overall cost of equipment for an EI implementation is likely smaller than that of optical techniques. Finally, its implementation will likely support a much smaller laboratory footprint and reduced overall equipment cost. Direct measurements of DNA hybridization by electrochemical detection have shown much greater sensitivity to smaller sample quantities compared to optical methods [7].

Electrochemical methods for DNA biosensors, so called genosensors, have been demonstrated using the principles of photoelectrochemistry [8], potentiometry [9–13] and amperometry applied to DNA-modified electrodes [14–16]. Oligonucleotide probes that were oriented parallel to the electrode resulted in decreased conductance compared to oligonucleotides that were oriented perpendicular to the electrode [17]. The increase in conductance is associated with increased current and hence lowered detection limits. The density of the surface coverage also affects the final detection signal. Investigation of the effect of DNA probe length for thiol-terminated linkers that comprised ethyl hexyl or phenyl to a deoxyribose or thymine residue found that high surface coverage of the DNA prevented the sample DNA from accessing the target while too low surface coverage resulted in nondetectable signal differences upon hybridization [18].

Immobilization strategies for electrochemical detection may involve physical adsorption, thiol-linking chemistries to gold electrodes, and organosilane linking chemistries to oxidized silicon or glass substrates. Immobilization

strategies may also be used to improve the detection signals by providing for electrocatalysis, redox mediation, or conduction at the surface as demonstrated by immobilization of DNA using conducting electroactive polymers.

2
Electrochemical Impedance Spectroscopy

2.1
Basic Principles

Electrochemical impedance (EI) detection occurs through the combined measurement of current, voltage, and phase angle [19]. EI is traditionally conducted as a three-electrode system arrangement of a working electrode (WE), reference electrode (RE), and counter electrode (CE). A function generation applies a sinusoidally varying and interrogating potential to the CE via a potentiostat. The potentiostat allows the applied potential to be referenced to the RE potential. The ensuing AC current is measured at the working electrode and the transfer function allows a measure of impedance. The applied EIS excitation voltage is sinusoidal and given by the equation

$$V = V_m \sin \omega t \tag{1}$$

in which ω is the radial frequency, V_m is the maximum voltage at the peak, V is the voltage at any given instant. The AC response signal (i), is characterized by both its maximum amplitude (i_m) and its phase shift (θ) with respect to the applied ac voltage, as shown below.

$$i = i_m \sin(\omega t + \theta) \tag{2}$$

The ratio of the amplitudes of the applied and the response signal (V_m/i_m) and the phase shift between these signals (θ) can be used to determine the impedance, which can be represented as a complex number. The real component of impedance is known as the resistance, R, and the imaginary component, given by X, is known as the reactance [19].

$$Z = R + jX \tag{3}$$

The reactance describes the part of the system that behaves as a capacitor or inductor while the resistance term describes the part of the system that behaves as a resistor. The magnitude of the impedance is determined by the square root of the sum of the squares for the resistance and reactance [19]:

$$|Z| = \sqrt{R^2 + X^2} \tag{4}$$

Electrochemical impedance spectroscopy (EIS) profiles, measured as a function of the interrogating frequency, can be represented on both Bode and Nyquist plots. The two-component Bode plot presents a comprehensive and

detailed representation of the frequency dependence of the impedance and presents the magnitude of the impedance, $|Z|$, and the phase shift, θ, in relation to the interrogating frequency. Specific regions of the spectrum can be linked to characteristic frequency ranges [20]. The Nyquist plot shows the relationship of the imaginary component of impedance, Z'', to the real component of the impedance, Z'. Representative Bode and Nyquist plots are shown in Fig. 1.

EIS data is generally interpreted based on defining an appropriate equivalent circuit model that best fits the acquired data. The elements of the circuit model involve a specific arrangement of resistors, capacitors, and inductors that tacitly represent the physicochemical reality of the device under test. Under these circumstances the numerical value for chemical properties of the system can be extracted by fitting the data to the equivalent circuit model. Impedance measurements are typically described by one of two models:

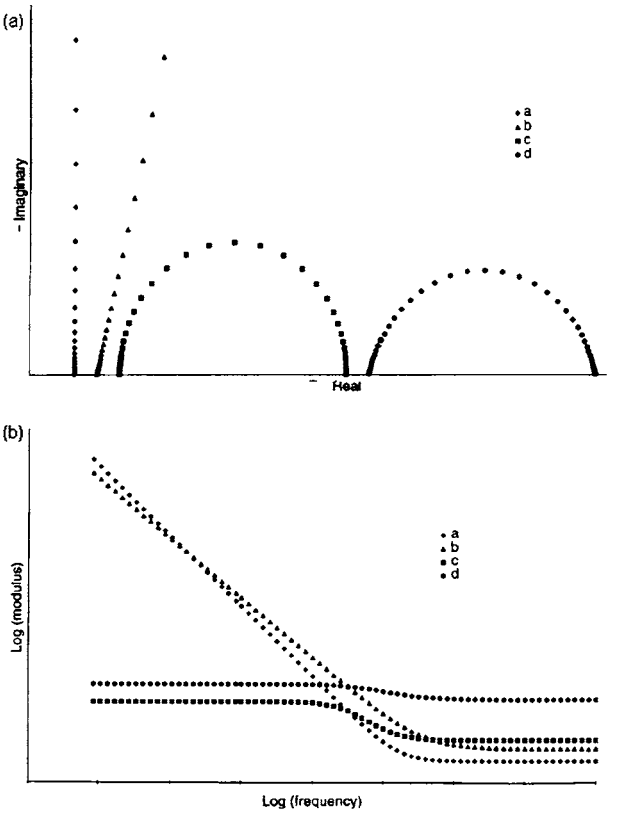

Fig. 1 Representative **a** Nyquist and **b** Bode plots from electrochemical impedance spectroscopy measurements (Hubrecht J (1998) Metals as Biomaterials, Helsen J, Breme H (eds) © John Wiley & Sons Limited. Reproduced with permission)

a combination of a resistor and a capacitor in series or parallel. The most frequently used equivalent circuit models are shown in Fig. 2. The physicochemical significance of the resulting equivalent circuit model can be understood by examination of the components of the specific electrochemical cell. Solution resistance has a profound impact on the impedance measurements. The electrolytic solution will affect the resistance based on the ionic concentration, type of ion, solution temperature, and geometry of the electrodes. For dilute solutions, impedance decreases as the ionic concentration is increased, facilitating ion transfer in the medium. Charge transfer is also affected by the development of a capacitative double layer between the electrode and the surrounding electrolyte solution. When a metal working electrode (WE) is inert with respect to the solution it contacts, as is the case for noble metals such as platinum, palladium, and gold, the system behaves purely capacitively due to the presence of the electrochemical double layer at the interface [20]. The complex expression for the impedance, Z, for such a simple capacitor model is:

$$Z = R_s + \frac{1}{j\omega C} \tag{5}$$

where R_s is the resistance of the electrolyte layer between the working and reference electrodes, and C is the capacitance of the electrochemical double layer [20]. The change in impedance based on the linear properties can be

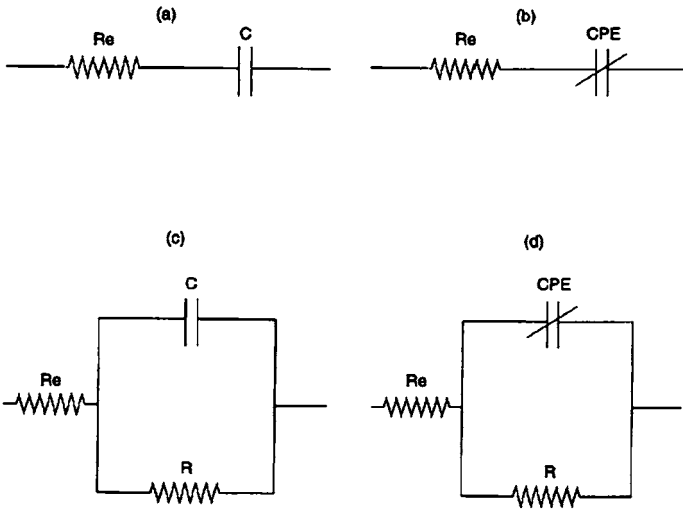

Fig. 2 Equivalent circuit models (Hubrecht J (1998) Metals as Biomaterials, Helsen J, Breme H (eds) © John Wiley & Sons Limited. Reproduced with permission)

described by the complex Cole equation:

$$Z(\omega) = R_s + \frac{R_0 - R_s}{1 + (j\omega\tau_\rho)^{1-m}} \quad 0 < m < 1 \tag{6}$$

where R_0 is the value of the equivalent circuit resistance and $R_{\text{inf}} \ll R_0$, solution resistance as ω, τ_p is the time constant, and m is a dimensionless number between 0 and 1.

Diffusive effects on impedance have led to a specific impedance profile known as the Warburg-impedance. This impedance is dependent upon the frequency of perturbation. For high frequencies, the Warburg impedance is small due to the limited distance that reactants must diffuse. The distance of travel for reactants at low frequencies is much greater, thereby increasing the Warburg-impedance. The Warburg impedance on a Nyquist plot would appear as a diagonal line with a slope of 45° and demonstrate a phase shift of 45° on a Bode plot.

2.2 Microfabricated Devices

For clinical diagnostics applications, microsensor devices based upon an array of interdigitated electrodes may be fabricated using microlithography techniques. Each element of the array consists of a pair of opposing platinized platinum electrodes of 1 mm to 3 mm digit length and of digit width and separation that may be 100 nm to 10 microns. These dimensions serve to define the serpentine length (width of the channel), the inter digit space (length of the channel) and the overall area of interdigitation. The metallization is typically 10 nm of magnetron sputter deposited titanium/tungsten (Ti/W), which serves as an adhesion-promoting layer (chromium is entirely inappropriate for the electrolytic environment), followed by 100 nm of e-gun deposited platinum. The substrate may be oxidized silicon with a minimum 100 nm of thermally grown oxide or may be a highly polished, electronics-grade, borosilicate glass. These independently addressable interdigitated elements are accompanied by a large area counter electrode of area 100 to 1000 times that of the area of each region of interdigitation. Such a counter electrode supports the electrochemical oxidation or reduction of electroconductive polymers that are cast or grown on each region of interdigitation. Finally, a reference electrode of silver/silver chloride accompanies each microsensor device. This reference electrode provides the reference potential for the electrochemical impedance determination of each multiplexed element of the array. This reference electrode, one on each chip, may be fabricated of platinum and subsequently electroplated with silver. The subtractive steps in the microlithography that serve to define the conductor pattern may be ion bean milling or lift off. Figure 3 shows the multi-element interdigitated array of the VCU Center for Bioelectronics, Biosensors and Biochips fondly referred to

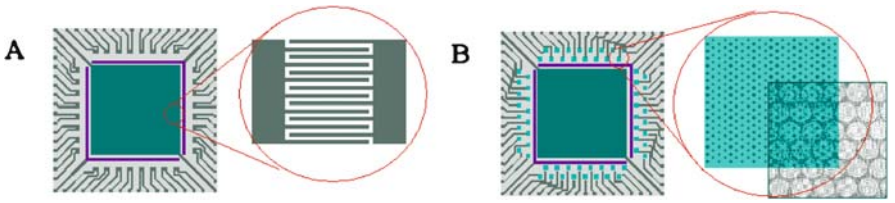

Fig. 3 Schematic illustration of a microfabricated multi-element array; **A** comprising 32 interdigitated microsensor electrodes, and **B** comprising 64 independently addressable microdisc voltametric electrodes. Each device shows the large area counter electrode (*middle*) and the reference electrode as a band around the counter electrode

as the "be64 Biochip". This impedimetric genosensor array comprises 32 interdigitated sensing elements. Single-stranded DNA probes are noncontact spotted and covalently coupled to each region of interdigitation. Hybridization measurements are taken using a multiplexing impedance analyzer to determine the change in impedance for each of the interdigitated areas before, during, and following DNA hybridization.

3 DNA Hybridization

DNA hybridization is the joining of two strands of DNA via the Watson–Crick principle of complimentary bases to form a double helix. Since any two strands of DNA will contain complementary elements (A–T, C–G), the fidelity with which the complete strands bind and the discrimination of strands that possess a single base miss-match is of great analytical significance. For detection in an electrochemical impedance platform of co-planar metallic electrodes fabricated on insulating borosilicate glass or oxidized silicon, a complete double helix would represent a single strand of probe DNA immobilized on the surface hybridizing with a single strand of target DNA. The single-stranded DNA probe may be immobilized to the surface via chemical modification of the silica surface. The immobilized single-stranded probe DNA is negatively charged and associated with counter cations that support ionic conductivity. The sample DNA is introduced into the hybridization chamber and transported to the surface with immobilized single-stranded targets by diffusive mass transfer. Upon hybridization with the target, the density of counter-cations is reduced resulting in a decrease in the overall ionic conductivity and hence an increase in the impedance in the proximal space between the electrodes. The equivalent circuit model for EIS measurements suggest that the solution resistive component and the charge transfer

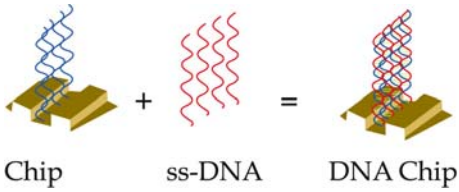

Fig. 4 A schematic illustration of the cross-sectional representation of the DNA hybridization reaction occurring between a pair of electrode digits

component of the impedance are primarily influenced by the hybridization reaction [21]. A schematic of the hybridization event is depicted in Fig. 4.

Hybridization conditions play a crucial role in ensuring an effective reaction. A challenge in detection mechanisms based on hybridization is the confounding influence of nonspecific interactions. Nonspecific interactions are contributed when a noncomplementary strand of target DNA binds or associates with the probe of interest. Nonspecific interactions are likely to occur for nucleotide sequences that share a high degree of similarity or hybridization conditions with low stringency. Altering the chemical composition of the buffer solution by adding chemicals that lower the melting temperature of hybrids [22] or increasing the ionic strength of the hybridization wash buffer [23] can control the stringency of a hybridization reaction.

Hybridization kinetics is also affected by the nature of the immobilization of probe DNA to the surface. However, immobilized DNA can result in a rate of reaction that is comparable to the reaction rate of complementary strands that are free in solution [24]. The Brownian motion and translational degrees of freedom are reduced upon immobilization. The length of the immobilized DNA strand has also been shown to have a much greater effect than the effect of immobilization on a two- or three-dimensional surface for DNA strands with lengths greater than 100 bases [25]. The hybridization rate was shown to decrease with linker lengths greater than 712 bases. In comparison, signal intensities based on optical detection continued to increase with increased length of the DNA probe [25].

3.1 Electrochemical Properties of DNA

Although the hybridization of single-stranded DNA to its complement results in detectable changes in electrochemical properties, particularly in support of non-Faradaic current, the DNA bases may also demonstrate redox behavior that gives rise to Faradaic currents. The electrochemical behavior of DNA has been studied over the past few decades. Differential pulse voltammograms show clearly defined peaks for the reduction of cytosine and adenosine. Electrochemical characterization of guanine by cyclic voltammetry has shown

that guanine produces an anodic peak on or near the point of hydrogen evolution at an oxidation potential of 1.07 V vs. a standard Ag/AgCl reference electrode. Guanine has the lowest oxidation potential of all of the nucleic acids, and the direct oxidation of guanine moieties has been explored as a potential detection method [26]. For some conditions, it is possible that the electrochemical behavior of the bases could present a confounding influence on the analytical measurement of DNA hybridization. For electrochemical impedance measurements, however, the applied potential is generally not sufficient to oxidize or reduce the bases of DNA that would cause any additional background in the detection signal.

4
Immobilization Strategies

Examples of the various methods of DNA immobilization are shown in Fig. 5. Amongst these are physical adsorption and covalent immobilization. The covalent immobilization is best exemplified by the use of organo-silane chemistries and alkanethiol chemistries.

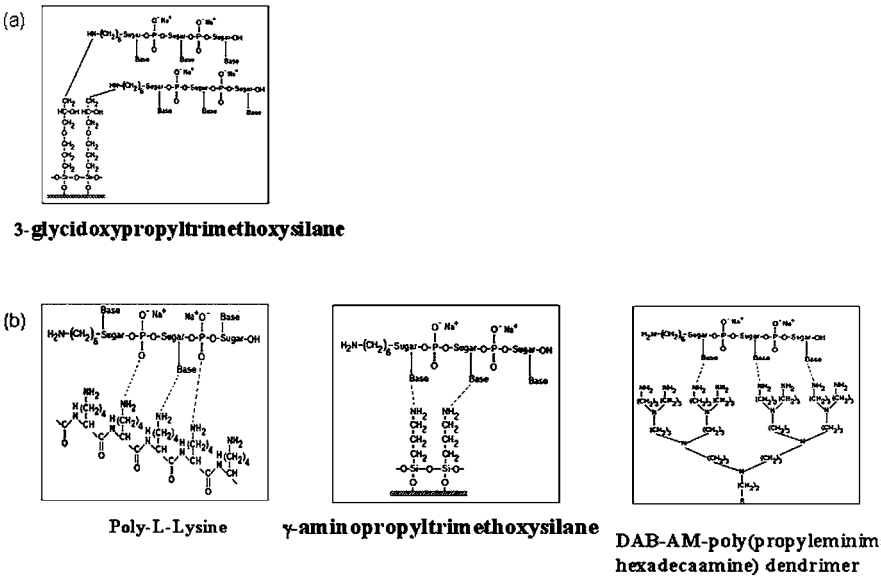

Fig. 5 Depictions of DNA immobilization by **a** covalent immobilization and **b** physical adsorption

4.1 Physical Absorption

The most straightforward method of DNA immobilization is adsorption onto a chemically modified surface. DNA adsorption is based upon dispersion and hydrogen-bonding interactions of the macromolecule with the surface but is greatly enhanced by electrostatic attractive forces between charged entities on the surface and the single-stranded DNA probe. Surfaces that have been chemically modified with an overall positive charge provide for electrostatic interactions of the negatively-charged, single-stranded DNA molecule with the surface. Specifically, surfaces modified to provide terminal amines result in electrostatic attractive forces between the positively charged amine and the negatively charged phosphate groups of the nucleic acid. The DNA strands are oriented parallel to the surface in alignment with the phosphate backbone of the probe. This orientation significantly limits the mobility of the molecule, decreasing the hybridization kinetics and overall efficiency of the reaction [27]. Immobilization of single-stranded DNA to the surface via such approaches represents a nonspecific interaction. The immobilization of the DNA is highly dependent on the density and homogeneity of charges on the surface of the substrate [28]. This lack of specificity for binding DNA has a greater potential to create interference with the binding of the single-stranded probe to its complement [1]. In addition, physical adsorption of the single-stranded DNA probe to the surface represents a modulatable type of surface attachment that may be influenced by temperature, pH, and the ionic strength (electrolytic concentration) of the medium. Electrolytic concentration has been shown to affect the degree of DNA adsorption, providing a possible mechanism for the control and optimization of probe thickness [27]. The thickness of the adsorbed layer of DNA has been shown to decrease as the salt concentration is increased [27]. DNA adsorption represents a relatively simple mechanism for the attachment of single-stranded probes to the surface. Dendrimers such as polyamidoamine (PAMAM) with a high density of terminal amino groups may be used to increase the surface coverage of physically adsorbed DNA to the surface [29].

The phosphate backbone of DNA molecules often results in undesirable electrostatic interactions with the substrate. Although the electrostatic interactions of DNA can be utilized for physical adsorption of DNA to the surface, this process can also lead to the nonspecific physical adsorption of target DNA on the surface. Rather than sample DNA hybridizing to the probe, it can adsorb to the surface and lead to interferences with the final detection call. Nonspecific adsorption effects have primarily been examined by the microarray community. Blocking strategies have been developed to prevent these nonspecific interactions. Succinic anhydride (SA) and bovine serum albumin (BSA) are two common methods to prevent nonspecific adsorption on amine modified surfaces. Blocking strategies are desired to react with or pas-

sively cover the region of the microarray surface not containing immobilized probe to create surface chemistries that have low affinity for DNA and prevent DNA adsorption. Blocking strategies were shown not to affect the raw spot intensity but BSA resulted in lower background intensities for amine-modified surfaces [29].

Carbon electrodes are advantageous for electrochemical analysis due to the wide potential range, low residual current, lack of chemical reactivity, and reduced cost [30]. The most common types of carbon electrodes are glassy carbon and carbon paste electrodes. Carbon paste electrodes are formed by mixing glassy carbon micro particles with an organic pasting liquid. Carbon paste electrodes have been shown to have more desirable electrochemical properties compared to glassy carbon electrodes [30]. DNA immobilization on glassy carbon electrodes results from electrostatic attractive forces and produces a thick film of approximately 0.1 mm that can be conditioned in an acetate buffer [31]. Wang et al. demonstrated DNA adsorption onto carbon paste electrodes with anodic polarization at + 1.7 V for several minutes as a pretreatment [32]. Surfactants have also been used to enhance DNA immobilization to carbon paste electrodes [33].

Electrochemical impedance measurements of the physical adsorption of ssDNA and dsDNA yields useful information about the kinetics and mobility of the adsorption process. Physical adsorption of DNA is a simple and inexpensive method of immobilization. The ability to detect differences between ssDNA and dsDNA by impedance could be applicable to DNA biosensor technology. EIS measurements were made of the electrical double layer of a hanging drop mercury electrode for both ssDNA and dsDNA [34]. The impedance profiles were modeled by the Debye equivalent circuit for the adsorption and desorption of both ssDNA and dsDNA. Desorption of denatured ssDNA demonstrated greater dielectric loss than desorption of dsDNA. The greater flexibility of the ssDNA compared to dsDNA was proposed to account for this difference.

Electrochemical impedance measurements using carbon electrodes have been used to study the physical immobilization of DNA by adsorption. Adsorption of DNA onto glassy carbon electrodes with an additional conditioning step of acetate buffer treatment has led to the development of a gel-like DNA layer. Impedance profiles were performed at applied potentials of 0.3, 1.0, and 1.4 V that correspond to the oxidation potential of guanine, between guanine and adenine, and after the potential for the oxidation of adenine, respectively. The EI data were modeled using two capacitors in parallel with the physical interpretation that capacitance was represented by both the capacitance at the interface without interaction from the ssDNA and from the interaction of the ssDNA at the interface. The interfacial capacity was similar for both the 0.3 V and 1.0 V impedance measurements, but showed a significant decrease at + 1.4 V, possibly as a result of solvent decomposition. As the number of scans increased, the interfacial capacity also increased, suggest-

ing that adsorption of molecules from the solution as well as changes in the configuration of molecules on the surface had occurred. The substrate surface was demonstrated to be a strong conductor as evidenced by the slight increase in the ohmic resistance of the system with the presence of the modified ss-DNA probe layer. Electrochemical characterization of DNA immobilized on carbon paste electrodes showed enhanced charge transfer rates when modified with the surfactant, cetyltrimethyl ammonium bromide. The exchange current was increased by approximately two-fold. The EIS spectrum revealed electron transfer limitations at higher frequencies indicated by a semi-circle plot and diffusive limitations at lower frequencies indicated by a linear relationship as shown on a Nyquist plot.

4.2 Organosilane Chemistry

Covalent attachment of single-stranded DNA probes to a surface allows greater control over the orientation of the immobilized probe. Well established silane chemistry has been effectively used for the immobilization of DNA probes modified with terminal amine groups. The reactive functional groups that are suitable for the covalent attachment of DNA include: amino- [35–38], mercapto- [39–41], and epoxy-groups [42–47]. Common silanizing agents include: 3-aminopropyltrimethoxysilane (APS), 3-mercaptopropyltrimethoxysilane (MPS), and 3-glycidoxypropyltrimethoxysilane (GPS) as shown in Fig. 6. These bifunctional agents create a surface layer with chemically available amino, mercapto, and epoxy functionalities, respectively and have been proven to provide linkages that are chemically stable and sufficient in length to eliminate interferences due to steric hindrance [44, 45]. These silanizing agents have been shown to be soluble in aqueous solutions and not contribute appreciably to nonspecific interactions [40].

The oligonucleotide probes must be chemically modified, usually during synthesis, to provide a functional group with the capacity to covalently

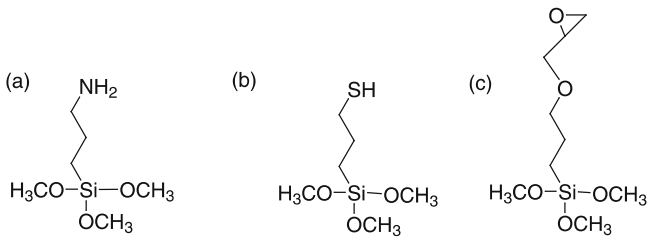

Fig. 6 Common silanizing agents to promote covalent DNA immobilization: **a** 3-aminopropyltrimethoxysilane (APS) **b** 3-mercaptopropyltrimethoxysilane (MPS) **c** 3-glycidoxypropyltrimethoxysilane (GPS)

react with the terminal functional group of the silanized surface. Amine-terminated oligonucleotides possessing suitable hydrocarbon spacers (C5, C6, or C7) have been covalently coupled to either epoxy- [42–45, 47] or amino-derivatized supports [38]. The reaction between the epoxy moiety of GPS with the 5′-amino-ssDNA probe is based on the standard nucleophilic ring opening of an epoxide by an amine, as depicted in Fig. 7. In this reaction, the nonbonded electron pair of the nitrogen on the primary amine initially attacks the acidic carbon atom of the epoxy ring (i), prompting the electrons of the C – O bond to migrate preferentially to the oxygen, thus opening the ring as represented in step (ii). The excess of negative charge on the oxygen atom attracts the nearby hydrogen atom, once bonded to nitrogen, to from a hydroxy group (iii), permitting electronic rearrangement (iv) and producing the final, neutral product [48].

When linking amino-modified probes with amino-derivatized surfaces, homobifunctional crosslinking agents such as disuccinimidylglutarate (DSG) or 1,4 phenylenediisothiocyanate (PDITC) are usually employed [35, 49]. Figure 8 depicts the reaction mechanism for the covalent attachment of amine-terminated oligonucleotides to amino-modified (APS) supports via a PDITC linker. Excess PDITC is used to convert the surface-bound primary amines to amine-reactive phenylisothiocyanate groups [38]. The subsequent immobilization of 5′ amine-modified DNA probes to the PDITC groups result in the covalent attachment of the oligonucleotides. Confirmation of the covalent coupling of the amine-modified single-stranded DNA probe to the epoxy-derivatized silane surface was verified using attenuated total reflectance-Fourier transform infrared spectroscopy (ATR-FTIR) [21].

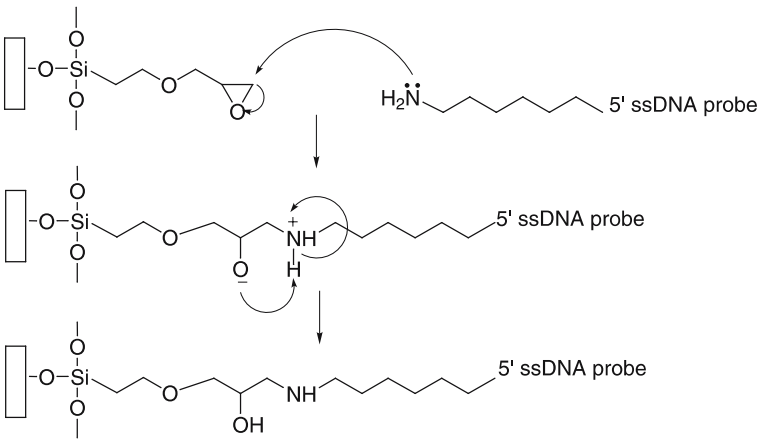

Fig. 7 Reaction of glycidoxypropyltrimethoxysilane with a 5′-amino-terminated single-strand DNA probe

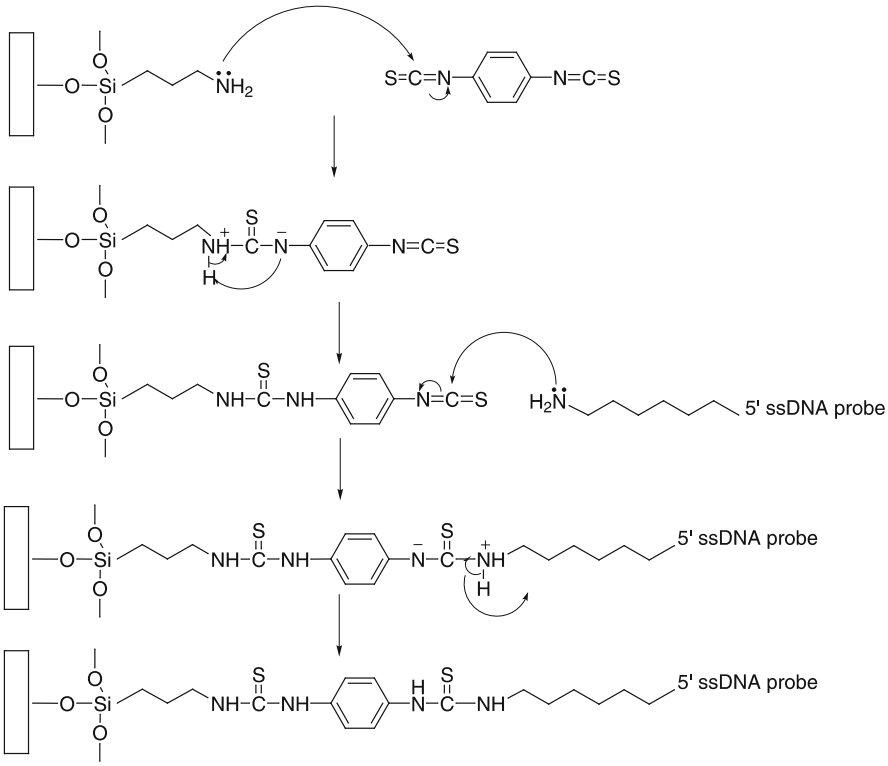

Fig. 8 Covalent attachment of amine-terminated oligonucleotides to amino-modified (APS) supports via a PDITC linker

The silanized method of DNA immobilization has shown probe spacing varies for 3-glycidoxypropyl-trimethoxysilane from one ssDNA probe per nm^2 on platinum-driving electrodes [21] to two ssDNA probes per nm^2 for gold-driving electrodes [50] based on quartz crystal microbalance studies (QCM). Radiolabeling studies have indicated lower coverage of ssDNA probe on the surface with approximately 10^{11} strands/cm^2 with 36% of these strands undergoing hybridization [51]. Polyamidoamine (PAMAM) dendrimers present a high density of terminal amino groups and have been demonstrated as an effective surface derivatizing agent for improving the stability and coverage of cDNA probes [36] and may be covalently coupled to epoxy-modified surfaces for the subsequent attachment of DNA oligomers [29].

DNA immobilized by organosilane chemistries has proven to be an effective method for measuring impedance changes upon hybridization using both gold and platinum electrodes [21, 50]. The effect of different silane chemistries creates differences in the hydrophobicity and hydration levels of the modified surface. The organosilane treatment along with the ssDNA

immobilization to the surface contribute to the capacitative component of the overall impedance network. Differences in silane chemistry alter the overall impedance network. A comparison of silanization of the interdigit space with octadecyl-trichlorosilane and 3-glycidoxypropyl-trimethoxysilane demonstrated a larger overall impedance network of the former [50]. The observed differences in impedance were likely the result of the exclusion of water molecules from the region proximal to the device surface and also within the region of highest electric field strength. Similarly, hybridization affects the density of ions surrounding the immobilized ssDNA, resulting in an overall increase in the impedance network. Upon DNA hybridization, gold-driving electrodes have shown significant changes in the impedance value for both the real and imaginary components with an 11% increase at 120 Hz and a 0.004% decrease in resonant frequency values [50]. Platinum-driving electrodes demonstrated a 0.012% decrease in resonant frequency values and 35.4% and 42.1% increase in impedance magnitude upon hybridization [21]. For both platinum and gold electrodes the effects of nonspecific interactions have been shown to result in minimal changes to the resonant frequency and impedance. Silanization chemistry is an effective method of DNA immobilization to measure electrochemical impedance changes.

4.3 Thiol Chemistry

Thiol terminated oligonucleotides can also be used for covalent coupling to a glass surface [37] but are more often used for direct attachment to gold electrodes. Heterobifunctional cross linkers such as succinimidyl 4-[malemidophenyl] butyrate (SMPB) can be used to covalently couple thiol-modified ssDNA probes [52] to amine bearing surfaces. However, homobifunctional cross-linkers such as 1,4-phenylenediisothiocyanate have demonstrated improvement in hybridization efficiency at reduced cost [37]. Figure 9 depicts the chemistry used to covalently attach thiol-modified DNA oligomers to amino-silane derivatized supports. In this particular reaction, an APS-modified substrate is treated with SMPB, whose succinimide ester moiety reacts with the primary amine of APS. The thiol-ssDNA subsequently interacts with the maleimide group of the SMPB crosslinking agent to yield the covalently immobilized oligonucleotide.

An alternative to the covalent immobilization of ssDNA to surfaces is found in the thiol/disulfide exchange reaction between disulfide-modified oligonucleotides and mercapto-modified substrates [39], as illustrated in Fig. 10. The disulfide groups on the 5′-end of the ssDNA probe reacts with the thiol functional groups of the MPS layer on the surface. Under alkaline conditions, the alcohol-based leaving group promotes the thiol to disulfide exchange reaction. This method of covalent attachment does not require an additional reduction step to generate a reactive but unstable thiol intermedi-

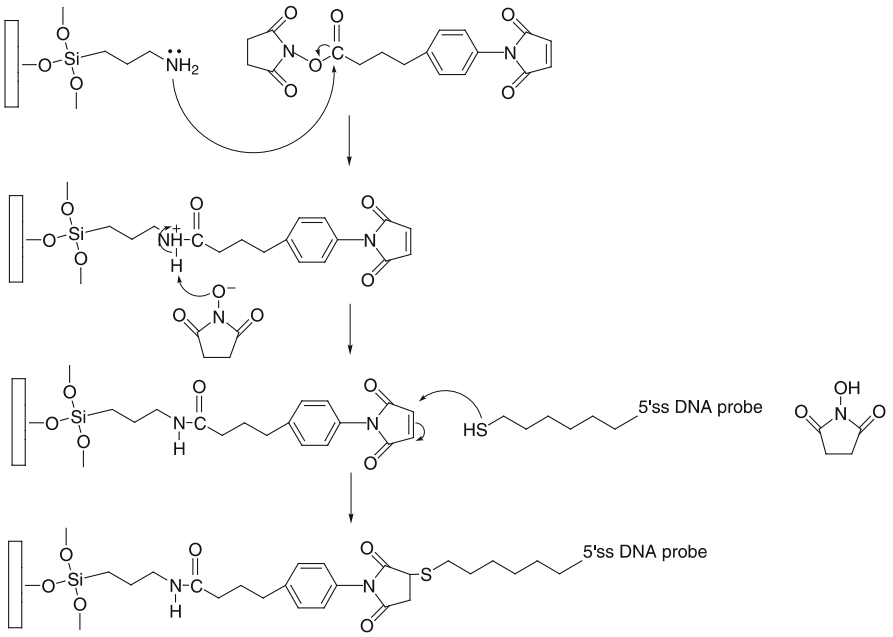

Fig. 9 Covalent attachment of thiol-modified DNA oligomers to amino-silane derivatized supports

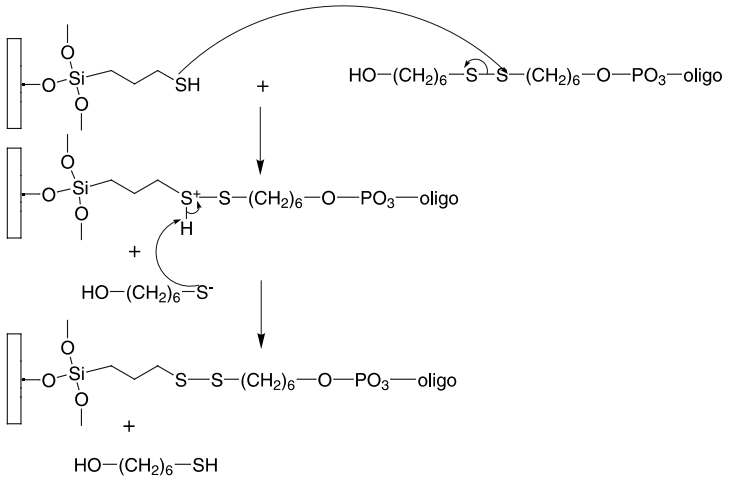

Fig. 10 Covalent immobilization of ssDNA by thiol/disulfide exchange reaction between disulfide-modified oligonucleotides and mercapto-modified substrates

ate, rather, the modified probe binds directly. Side reactions are significantly reduced as a result of the high degree of reaction specificity [39].

Thiol chemistry has also been used for DNA immobilization involving gold and silver nanoparticles immobilized onto a gold substrate electrode [53, 54]. DNA can be immobilized directly onto the gold without significant effect on the overall activity of the molecule. Gold nanoparticles improve the electrochemical signal by forming a set of closely packed conducting surfaces, thereby dramatically increasing the effective surface area of the electrode. Also, oligonucleotides modified with nanoparticles demonstrated denaturation properties that varied significantly with salt concentration resulting in the removal of mismatched targets following a wash with a buffer solution of the appropriate ionic concentration [55]. The gold electrode is silanized with 3-mercaptopropyltrimethoxysilane (MPS) and cross-linked by treatment with sodium hydroxide. The one-dimensional monolayer was then combined with a sol-gel network. The sol-gel matrix allowed a second silane layer to be formed having the effect of increasing the overall network impedance. The second silane layer was formed to expose the terminal thiol functionalities for binding with gold nanoparticles by chemisorption [53]. These modified electrodes showed strong stability as measured by continuous monitoring using cyclic voltammetry and reproducibility based on minimal impact on the peak currents after storage for one month [53]. A Randel's equivalent circuit model was chosen to fit the results. Based on modeling of the equivalent circuit, it was shown that gold nanoparticles reduced the electron transfer resistance. The system examined impedance detection before and after hybridization of different sample concentrations. Calibration curves indicated the logarithmic impedance to be linear within a concentration range of 1.0×10^{-6} M to 1.0×10^{-8} M and to possess a detection limit of 5.0×10^{-9} M. The level of sensitivity was attributed to the silanized layer remaining on the metallic digits and interdigitated space. Colloidal silver nanoparticles were also immobilized in the sol-gel matrix following a similar procedure. The silver nanoparticle system demonstrated similar properties of stability and reproducibility as that shown for gold nanoparticles [54]. Silver nanoparticles [54] showed an electron transfer resistance with a linear response in the range 8.0×10^{-9} M to 1.0×10^{-6} M and a detection limit of 4.0×10^{-9} M. Samples introduced into the chamber with noncomplementary sequences did not result in a detectable difference of the electron transfer resistance. Both the silver and gold nanoparticles increase the surface area of the electrode and thereby increase the difference in the impedance signal before and after hybridization.

4.4 Electropolymerized Electroactive Polymers

Electropolymerizable monomers that give rise to conducting electroactive polymers (CEPs) or insulating polymer thin films provide a convenient approach for the immobilization of DNA. More importantly, this method provides an easy means to achieve spatial separation of the ssDNA sequence

based on the application of a suitable electrode potential to a pattern of microfabricated conductors on the substrate. CEPs, particularly polypyrrole, have been explored for the immobilization of DNA. Pyrrole monomer may be electrochemically oxidized to produce a highly conjugated and electronically conductive polymer film in which dopant anions are incorporated to neutralize the positive bi-polaronic states of the oxidized form of the polymer backbone. The polymer film is grown on, and largely limited to, the surface of the electrode. The thickness of the film and its morphology may each be controlled by the amount of charge passed and by the conditions of the electrosynthesis. In one approach, single-stranded DNA can be associated with an electroconductive polymer thin film; first by conjugation of the ssDNA to a pyrrole monomer followed by electropolymerization [56]. In another approach, DNA polypyrrole blends have also been formed by direct incorporation of the negatively charged ssDNA into the polypyrrole backbone during electropolymerization [57]. Under these circumstances the negative charges associated with the phosphate groups of the ssDNA backbone allows DNA to be used as the single dopant macromolecular counteranion. The possibility to create DNA polypyrrole blends with both ssDNA and dsDNA has also been demonstrated [57].

Electropolymerization for specific site selection has been demonstrated using two different spotting techniques. The first method known as the electrified quill uses an electrified stainless steel pin that becomes the counter-electrode and the substrate the corresponding working electrode in a two-electrode electrochemical cell. The monomer solution, in the form of a 10 nl drop at the tip of the electrified quill, was contacted with the substrate and a voltage applied between the pin and substrate during the drop contact. The polymer film was grown in the drop contact area. A second method to direct site specificity for electropolymerization aspirates the monomer solution into a microcapillary. A drop of the monomer solution hanging from the tip of the capillary makes contact with the chip substrate. Again, during the drop contact, a voltage is applied and the electropolymerization occurs in the region of the drop contact. Polypyrrole films can be further augmented, with the specific aim of improving the detection signal upon hybridization, by doping the nucleic acid probes with carbon nanotubes. The carbon nanotubes confine the target and enhance hybridization [58].

Polypyrrole has the potential to provide an effective method for reagentless transduction by immobilization of the ssDNA probe within the polymer matrix. Significant differences in the impedance profile of ssDNA and dsDNA have been demonstrated [59]. The differences in the impedance profile are purportedly based on intercalation differences of the polymer with ssDNA compared to dsDNA. The exact mechanism for impedimetric change resulting from conducting polymer films has not been identified, although it is likely linked, much like the impedimetric response of pure DNA, to the change in ion density that accompanies the double strand compared to the

single strand. However, a decrease in the current response of polypyrrole films has been demonstrated due to the rigid structure of the polymer [60].

Polypyrrole films have also been studied in combination with carbon nanotube-modified electrodes using metallization of the DNA following hybridization [58]. The polymer film was grown using the oligonucleotide as the counteranion. The carbon nanotubes are suggested to improve charge transfer to the surface. Atomic force microscopy (AFM) analysis of the carbon nanotubes revealed a random orientation and irregular length with an average length of 180 nm. The metallization of the DNA helix was proposed to improve charge transfer and increase the capacitive charging on the double-layer surrounding the electrode. The metallization procedure was shown to not only enhance the limit of detection, but also to improve the ability of impedance detection to distinguish differences in mismatched probes.

5 Applications to Human Health

In medical applications, the primary focus for development of genosensors involves the enhanced classification of disease. Microarrays are currently being utilized to study gene expression profiles and improve class prediction for an array of different cancers including the colon [61], lung [62, 63], esophagus [64], and breast [65, 66]. Various statistical methods for improved class prediction have emerged [67–70]. Another possibility for improved medical diagnostics is the development of a brain tumor biochip. This project is being pursued by the Center for Bioelectronics, Biosensors and Biochips (C3B) to improve diagnostics and treatment of brain tumor patients. The brain tumor biochip aims to identify a targeted suite of genes that may be used to delineate the grade and stage of astrocytomas. The goal of this work would be to provide diagnostic and prognostic information to the clinician using a more rapid and objective method based on impedimetric measurements as compared to current histopathology techniques.

Although DNA-chip systems have the potential to be applied to a variety of analytically relevant questions, the potential for these technology platforms to be commercially developed and applied in clinical medicine as an aid to human health requires many new engineering solutions as well as considerable technological improvements. A complete lab-on-a-chip system not only requires a robust detection platform for DNA hybridization but the ability to perform cell sorting, DNA or RNA extraction and purification, reverse transcription of extracted RNA, and possibly include amplification of specific sequences using polymerase chain reaction. Cell sorting methods have largely relied on exploiting specific differences in cell types for the specific application of interest. Blood and bacteria components have been separated based on

application of dielectrophoresis [71]. Purification of nucleic acid products has been demonstrated by preferentially adsorbing DNA onto silica beads immobilized in a sol-gel network with a single channel configuration [72]. Proteins and other products released from the cell lysis are washed and the DNA is released from the sol-gel network using a low-ionic strength buffer. A variety of methods from improving amplication of DNA products by polymerase chain reaction have been developed. Traditional methods use a Peltier heating element below a microfabricated PCR chamber for cycling temperatures and time [73]. A more rapid method for polymerase chain reaction has been demonstrated using a continuous channel with specific temperature zones for denaturation, annealing, and extension reactions [74]. The number of cycles is determined by the number of passes of the channel over each of the heating zones. For genomic sensors to have practical utility, complete integration of each of the laboratory operations on the microfabricated device is necessary.

Integration of these components could be advantageous, from the perspective of efficiency, by coupling energy intensive processes. However, integration is a complicated process that requires additional fluidic controls for transportation of the sample as well as greater stringency to prevent sample contamination. A completely integrated genosensor based on electrochemical DNA hybridization detection has been developed by Motorola Sciences [75]. This microfluidic device contains all necessary pre-processing steps of sample preparation, mixing, and detection with dimensions of $60 \times 100 \times 2$ mm in size. The system is completely self-contained and includes thermally actuated microvalves for flow regulation with electrochemical and thermopneumatic pumps for solution transport.

Analytical fidelity and sensitivity are also issues that require further improvement before a clinically applicable device can be realized. The low level of signal generated from the DNA hybridization reaction often results in a high signal-to-background ratio. An additional engineering challenge is the development of microfabrication techniques for chemical systems; mechanical and electrical engineers pioneered the majority of current microfabrication techniques. The aqueous environment for many chemical and biological reactions requires new materials and new fabrication techniques. Finally, the necessary trade-off to improve the time-to-market, meet market demands, and address regulatory requirements must be determined [76].

Acknowledgements This work was supported by the Commonwealth of Virginia's Department of Planning Commonwealth Technologies Research Fund (CTRF grant no. SE2002-02 for Cancer Genomics and Development of Diagnostic Tools and Therapies) and the consortium of the VCU Center for Bioelectronics, Biosensors and Biochips.

References

1. Schena M (2003) Microarray Analysis. Wiley, New York
2. Livshits MA, Mirzabekov AD (1996) Biophys J 71:2795
3. Afanassiev V, Hanemann V, Wolfe S (2000) Nucleic Acids Res 28:e66
4. Stillman BA, Tonkinson JL (2000) BioTechniques 29:630
5. Guiseppi-Elie A (2003) PharmaTech 87:1
6. Vercoutere W, Akeson M (2002) Curr Opin Chem Biol 6:816
7. Popovich ND, Eckhardt AE, Mikulecky JC, Napier ME, Thomas RS (2002) Talanta 56:821
8. Qingwen L, Guan L, Jun F, Dawen C, Qi O (2000) Analyst 125:1908
9. Wang J, Jiang M, Mukherjee B (1999) Anal Chem 71:4095
10. Wang J, Kawde A-N, Sahlin E (2000) Analyst 125:5
11. Wang J, Xiaohua C, Renandes JR, Grant DH, Ozsoz M (1998) J Electroanal Chem 441:167
12. Wang J, Xiaohua C, Jonsson C, Balakrishnan M (1996) Electroanalysis 8:2
13. Wang J, Zhang X, Parrado C, Rivas G (1999) Electrochem Commun 1:197
14. Takenaka S, Uto Y, Saita H, Yokoyama M, Kondo H, Wilson WD (1998) Chemical Communications 10:1111
15. Takenaka S, Yamashita K, Takagi M, Uto Y, Kondo H (2000) Anal Chem 72:1334
16. Zhao Y-D, Pang D-W, Hu S, Wang Z-L, Cheng J-K, Dai H-P (1999) Talanta 49:751
17. Hianik T, Gajdos V, Krivanek R, Oretskaya T, Metelev V, Volkov E, Vadgama P (2001) Bioelectrochem 53:199
18. Taft B, O'Keefe M, Fourkas JT, Kelley SO (2002) Anal Chim Acta 496:81
19. Kell DB (1987) In: Turner A, Karube I, Wilson GS (eds) Biosensors: Fundamentals and Applications. Oxford University Press, Oxford, p 427
20. Hubrecht J (1998) In: Helsen JA, Breme HJ (eds) Metals as Biomaterials. Wiley, Chichester
21. Hang TC, Guiseppi-Elie A (2004) Biosens Bioelectron 19:1537
22. Xu D-K, Ma LR, Liu Y-Q, Jiang ZH, Liu ZH (1999) Analyst 124:533
23. Korkola J, Estep A, Pejavar S, DeVries S, Jensen R, Waldman F (2003) BioTechniques 35:828
24. Towery RB, Fawcett NC, Zhang P, Evans JA (2001) Biosens Bioelectron 16:1
25. Stillman BA, Tonkinson JL (2001) Anal Biochem 295:149
26. Wang J, Cai X, Fernandes DH, Ozsoz M (1997) Anal Chem 69:4056
27. Berney H, Oliver K (2005) Biosens Bioelectron (pending)
28. Pastre D, Peitrement O, Fusil S, Landousy F, Jeusset J, David M-O, Hamon L, Le Cam E, Zozime A (2003) Biophys J 85:2507
29. Taylor S, Smith S, Windle B, Guiseppi-Elie AT (2003) Nucleic Acids Res 31:e87
30. Wang J, Kirgoz UA, Mo J-W, Lu J, Kawde A-N, Muck A (2001) Electrochem Commun 2001:203
31. Brett C, Brett AM, Serrano S (1999) Electrochim Acta 44:4233
32. Wang J, Ozsoz M, Cai X, Rivas G, Shiraishi H, Grant DH, Chicharro M, Fernandes J, Palecek E (1998) Bioelectrochem Bioenerg 1998:33
33. Hu C, Hu S (2004) Electrochim Acta 49:405
34. Strasak L, Dvorak J, Hason S, Vetterl V (2002) Bioelectrochem 56:37
35. Beier M, Hoheisel JD (1999) Nucleic Acids Res 27:1970
36. Benters R, Niemeyer CM, Drutschmann D, Blohm D, Wohrle D (2002) Nucleic Acids Res 30:e10

37. Charles PT, Vora GJ, Andreadis JD, Fortney AJ, Meader CE, Dulcey CS, Stenger DA (2003) Langmuir 19:1586
38. Guo Z, Guilfoyle RA, Thiel AJ, Wang R, Smith LM (1994) Nucleic Acids Res 22:5456
39. Hilliard LR, Zhao X, Tan W (2002) Anal Chim Acta 470:51
40. Moser I, Schalkhammer T, Pittner F, Urban G (1997) Biosens Bioelectron 12:729
41. Pividori MI, Merkoci A, Alegret S (2000) Biosens Bioelectron 15:291
42. Cloarec JP, Deligianis N, Martin JR, Lawrence I, Souteyrand E, Polychronakos C, Lawrence MF (2002) Sensors and Actuators B: Chemical 58:405
43. Cloarec JP, Martin JR, Polychronakos C, Lawrence I, Lawrence MF, Souteyrand E (1999) Sens Actuators, B 58:394
44. Lamture JB, Beattie KL, Burke BE, Eggers MD, Ehrlich DJ, Fowler R, Hollis MA, Kosicki BB, Reich RK, Smith SR (1994) Nucleic Acids Res 22:2121
45. Maskos U, Southern EM (1992) Nucleic Acids Res 20:1679
46. Piunno PAE, Watterson J, Wust CC (1999) Anal Chim Acta 400:73
47. Preininger C, Sauer U (2003) Sens Actuators, B 90:98
48. Sales JAA, Prado AGS, Airoldi C (2002) Polyhedron 21:2647
49. Benters R, Niemeyer CM, Wohrle D (2001) Chem Bio Chem 2:686
50. Gheorge M, Guiseppi-Elie A (2003) Biosens Bioelectron 19:95
51. Cloarec JP, Deligianis N, Martin JR, Lawrence I, Souteyrand E, Polychronakos C, Lawrence MF (2002) Biosens Bioelectron 17:405
52. Chrisey LA, Lee GU, O'Ferrall CE (1996) Nucleic Acids Res 24:3031
53. Fu Y, Yuan R, Xu Y, Chai Y, Zhong X, Zhong X, Tang D (2005) Biochem Eng J 23:37
54. Fu Y, Yuan R, Xu L, Chai Y, Liu Y, Tang D, Zhang Y (2005) J Biochem Biophys Methods 62:163
55. Park S-J, Taton TA, Mirkin CA (2002) Science 295:1503
56. Livache T, Bazin H, Caillat P, Roget A (1998) Biosens Bioelectron 13:629
57. Gheorge M, Lei C, Guiseppi-Elie A (2000) A Proc ACS PMSE 83:550
58. Xu Y, Jiang Y, Cai H, Pin-Gang H, Yu-Zhi F (2004) Anal Chim Acta 516:19
59. Farace G, Lillie G, Hianik T, Payne P, Vadgama P (2002) Bioelectrochem 55:1
60. Korri-Youssoufi H, Garnier F, Srivtava P, Godillot P, Yassar A (1997) J Am Chem Soc 199:7388
61. Bertucci F, Salas S, Eysteries S, Nasser V, Finetti P, Ginestier C, Charafe-Jauffret E, Loriod B, Bachelart L, Montfort J, Victorero G, Viret F, Ollendorff V, Fert V, Giovaninni M, Depero J-R, Nguyen C, Viens P, Monges G, Birnbaum D, Houlgatte R (2004) Oncogene 23:1377
62. Beer DG, Kardia S, Huang C-C, Giordano TJ, Levin AM, Misek DE, Lin L, Chen G, Gharib TG, Thomas DG, Lizyness ML, Kuick R, Hayasake S, Taylor J, Iannettoni MD, Orringer MB, Hanash S (2002) Nat Med 8:816
63. Parmigiani G, Garrett-Mayer ES, Anbazhagan R, Garielson E (2004) Clin Cancer Res 10:2922
64. Brabender J, Marjoram P, Salonga D, Metzger R, Schneider PM, Park JM, Schneider S, Holscher AH, Yin J, Meltzer SJ, Danenberg KD, Danenber PV, Lord RV (2004) Oncogene 23:4780
65. Glinsky GV, Higashiyama T, Glinskii AB (2004) Clin Cancer Res 10:2272
66. Wilson CA, Dering J (2004) Breast Cancer Res 6:192
67. Lee Y, Lee C-K (2003) Bioinformatics 19:1132
68. Hastie T, Tibshirani R, Eisen MB, Alizadeh A, Levy R, Staudt L, Chan WC, Botstein D, Brown P (2000) Genome Biology 1:0003.1

69. Golub TR, Slonim DK, Tamayo P, Huard C, Gaasenbeek M, Mesirov JP, Coller H, Loh ML, Downing JR, Caligiuru MA, Bloomfield CD, Lander ES (1999) Science 286:531
70. Bijlani R, Cheng Y, Pearce DA, Brooks AI, Ogihara M (2003) Bioinformatics 19:62
71. Cheng J, Sheldon EL, Wu L, Uribe A, Gerrue LO, Carrino J, Heller MJ, O'Connell JP (1998) Nat Biotechnol 16:541
72. Breadmore MC, Wolfe KA, Arcibal IG, Leung WK, Dickson D, Giordano BC, Power ME, Ferrance JP, Feldman SH, Norris PM, Landers JP (2003) Anal Chem 75:1880
73. Khandurina J, McKnight TE, Jacobson SC, Waters LC, Foote RS, Ramsey JM (2000) Anal Chem 72:2995
74. Obeid PJ, Christapoulos TK, Crabtree HJ, Backhouse CJ (2003) Anal Chem 75:288
75. Liu R-H, Yang J, Lenigk R, Bonanno J, Grodzinski P (2003) Anal Chem 76:1824
76. Henke C (1998) IVD Technology, p 35

Author Index Volumes 251–260

The volume numbers are printed in italics

Subject Index